

**NASA  
Reference  
Publication  
1400**

1997

**Atmospheric Effects of  
Subsonic Aircraft: Interim  
Assessment Report of the  
Advanced Subsonic  
Technology Program**

**Edited by:**

**Randall R. Friedl**  
*NASA Headquarters*  
*Washington, D. C.*



National Aeronautics and  
Space Administration

**Goddard Space Flight Center**  
Greenbelt, Maryland 20771  
1997

## Contributing Authors

Dr. Randall R. Friedl  
NASA Jet Propulsion Laboratory  
Pasadena, California

Dr. Bruce E. Anderson  
NASA Langley Research Center  
Hampton, Virginia

Dr. Kuo-Nan Liou  
University of Utah  
Salt Lake City, Utah

Dr. David H. Rind  
NASA Goddard Space Flight Center  
Goddard Institute for Space Studies  
New York, New York

Dr. Hanwant B. Singh  
NASA Ames Research Center  
Moffett Field, California

Dr. Donald J. Wuebbles  
University of Illinois  
Urbana, Illinois

Dr. Steven L. Baughcum  
Boeing Company  
Seattle, Washington

Dr. John Hallett  
Desert Research Institute  
Reno, Nevada

Dr. Philip J. Rasch  
National Center for Atmospheric Research  
Boulder, Colorado

Dr. Kenneth Sassen  
University of Utah  
Salt Lake City, Utah

Dr. Leah R. Williams  
SRI International  
Menlo Park, California

This publication is available from the NASA Center for AeroSpace Information,  
800 Elkridge Landing Road, Linthicum Heights, MD 21090-2934, (301) 621-0390.

# ATMOSPHERIC EFFECTS OF SUBSONIC AIRCRAFT: INTERIM ASSESSMENT REPORT OF THE ADVANCED SUBSONIC TECHNOLOGY PROGRAM

---

## Table of Contents

EXECUTIVE SUMMARY.....	v
1. INTRODUCTION.....	1
2. AIRCRAFT EMISSIONS.....	5
2.1 Emissions Characteristics.....	5
2.1.1 Gaseous Emissions.....	5
2.1.2 Particle Emissions.....	7
2.2 Global Inventory Methodologies.....	9
2.3 1992 Emission Inventories.....	10
2.4 Uncertainties in Aircraft Emission Inventories.....	11
2.4.1 Simplifying Assumptions.....	12
2.5 Future Trends and Methodology for Constructing Long-Range Forecasts.....	14
2.6 Summary.....	15
3. UNDERSTANDING THE EFFECTS OF AIRCRAFT EMISSIONS.....	27
3.1 Near-Field Effects.....	27
3.2 Regional and Global-Scale Effects.....	29
3.2.1 Perturbations to Ambient Levels.....	29
3.2.1.1 NO <sub>x</sub> .....	29
3.2.1.2 CO <sub>2</sub> , CO, and Hydrocarbons.....	31
3.2.1.3 H <sub>2</sub> O.....	32
3.2.1.4 Soot.....	32
3.2.1.5 Sulfate.....	33
3.2.2 Ozone Chemistry.....	35
3.2.2.1 Ozone Tendencies Relative to NO <sub>x</sub> .....	35
3.2.2.2 Role of Non-Methane Hydrocarbons.....	36
3.2.2.3 Heterogeneous Chemistry.....	36
3.2.2.4 Ozone Trends.....	39
3.2.3 Radiative Forcing.....	40
3.2.3.1 Clear Sky Effects.....	41
3.2.3.2 Direct Cloud Effects of Contrails.....	41
3.2.3.3 Indirect Cloud Effects of Contrails.....	43
3.2.3.4 Cirrus Cloud Trends.....	44
3.3 Summary.....	44

4.	MODELING THE GLOBAL EFFECTS OF AIRCRAFT EMISSIONS.....	57
4.1	Global Modeling Characteristics.....	58
4.1.1	Model Types.....	59
4.1.2	Assessment Model Requirements.....	60
4.2	Effects on Atmospheric Chemistry.....	61
4.2.1	Description of Modeling Tools.....	62
4.2.1.1	IMAGES Model.....	62
4.2.1.2	Harvard/GISS Model.....	63
4.2.1.3	GMI Core Model.....	64
4.2.2	Evaluation of Models.....	65
4.2.2.1	Evaluation of Chemical Mechanisms.....	65
4.2.2.2	Rn Tracer Study: Evaluation of Rapid Vertical Transport Near the Ground.....	67
4.2.2.3	NO <sub>y</sub> Tracer Study: Evaluation of Large-Scale Transport in the Upper Troposphere.....	71
4.2.2.4	Comparison of IMAGES and Harvard Models with Observations.....	74
4.2.3	Sensitivity Studies.....	77
4.2.3.1	Description of the Experiments.....	77
4.2.3.2	Model Results and Discussion.....	78
4.3	Effects on Climate.....	82
4.3.1	Description of Modeling Tools.....	82
4.3.1.1	Description of Models.....	82
4.3.1.2	Description of Modeling Techniques.....	83
4.3.2	Climate Sensitivity Studies.....	83
4.3.2.1	Layered vs. Well-Mixed Forcing and GWP.....	83
4.3.2.2	Aircraft Water Vapor Emissions.....	84
4.3.2.3	Aircraft-Induced Ozone Changes.....	85
4.3.2.4	Aircraft Soot Emissions.....	86
4.3.2.5	Aircraft Contrail Simulations.....	86
4.3.2.6	Aircraft CO <sub>2</sub> Emissions.....	87
4.3.2.7	Aircraft NO <sub>x</sub> Emissions.....	87
4.3.2.8	Aircraft SO <sub>2</sub> Emissions.....	88
4.3.2.9	Summary.....	88
4.4	Findings and Future Needs.....	88
5.	CONCLUSIONS.....	123
5.1	Summary.....	123
5.2	Recommendations.....	125
6.	REFERENCES.....	127
APPENDICES		
A	Authors and Contributors.....	A-1
B	Acronyms and Abbreviations.....	B-1
C	Chemical Nomenclature and Formulae.....	C-1

# EXECUTIVE SUMMARY

---

## 1. What are the concerns associated with emissions from subsonic aviation?

Subsonic aircraft operate primarily in the upper troposphere and lower stratosphere. Engine exhaust emissions of gases and particles from fleets of these aircraft are potentially in sufficient amounts to affect atmospheric ozone and climate, particularly with the projected growth in air traffic.

- Important emissions include: water vapor, carbon dioxide, nitric oxide and nitrogen dioxide (collectively referred to as  $\text{NO}_x$ ), sulfur oxides, carbon monoxide, non-methane hydrocarbons, and soot.
- The impact of these emissions depends on the relative change they induce in the background atmosphere and on their role in atmospheric photochemical, dynamical, and radiative processes. Photochemical processing of these emissions can affect ozone and other important species. Climate change may result from changes in concentrations of radiatively important species (e.g., water, carbon dioxide, ozone, and particles). Formation of contrails and changes in clouds caused by aircraft emissions can also affect climate.

## 2. How well understood are emissions from current subsonic aircraft?

For engines operating at cruise conditions, a growing body of in-flight and engine chamber test data is available for gaseous and particle emissions. Detailed inventories of aviation fuel use and the emissions of  $\text{NO}_x$ , carbon monoxide, and non-methane hydrocarbons have been calculated for air traffic in 1990 and 1992.

- Calculated aviation fuel use is approximately equal to reported fuel production by refineries, within the estimated uncertainties.
- $\text{NO}_x$  emission indices (grams  $\text{NO}_x$ /kg fuel burned), readily derived from measurements taken behind commercial airliners in flight, are in good agreement with emission indices calculated for those flight conditions using the methodology developed for the emission inventories.
- Measured concentrations of volatile particles (presumed to be primarily composed of sulfuric acid) in commercial aircraft wakes are large and show significant and unexplained variability (approximately a factor of 100) between different airplanes. In some cases their production can be related to the sulfur content of the fuel.

### **3. What are the important atmospheric processes potentially affected by subsonic aviation?**

Chemical and radiative processes in the atmosphere can be affected by subsonic aircraft emissions. The concentration of tropospheric ozone, an important greenhouse gas, is determined by transport and by chemical production and loss involving reactions of  $\text{NO}_x$ , non-methane hydrocarbons, carbon monoxide, and hydrogen oxides (collectively referred to as  $\text{HO}_x$ ). The radiative balance of the atmosphere is affected by clouds, aerosols, and trace constituents such as carbon dioxide, water, and ozone. The most important ways in which these processes can be affected are:

- The ozone balance in the upper troposphere and lower stratosphere can be perturbed by increases in  $\text{NO}_x$  and, to a lesser extent, by increases in carbon monoxide, water, and non-methane hydrocarbons from aircraft. Aerosols produced from sulfur oxides, soot, and water emitted by aircraft may have an indirect effect on ozone concentrations through reactions that take place on aerosol surfaces.
- The radiative balance of the atmosphere can be affected both directly by the accumulation of carbon dioxide, water and other emissions from aircraft and indirectly through changes in ozone due to reactions involving  $\text{NO}_x$  and other emissions.
- The radiative balance of the atmosphere can be perturbed by aircraft-induced changes in aerosols and clouds. Chemical and physical processes occurring in the aircraft plume and wake produce aerosols and, under suitable conditions, rapid growth of the aerosol particles produce visible “contrail” clouds. In addition to their direct radiative effects, aircraft-derived aerosols and contrails may affect the radiative balance indirectly by increasing high cloud occurrence and/or changing cloud radiative properties.

### **4. What are the estimated impacts of subsonic aviation?**

Models used to study the impacts of subsonic aircraft must be able to represent the spatial and temporal variations in tropospheric processes, consequently, the best assessment tools are 3-D models that simulate the meteorological variability of the atmosphere. Several three-dimensional models were used in this assessment in a series of sensitivity studies to examine the impact of current and projected aircraft emissions on atmospheric chemistry and climate.

#### *Impacts on atmospheric chemistry*

- Model studies done for this assessment suggest that current aircraft emissions contribute a significant fraction of the  $\text{NO}_x$  in the upper tropospheric region between 7- and 13-km: 5 to 10%, averaged globally; up to 20%, averaged between 30°N and 60°N.
- Although subject to substantial uncertainties, model studies suggest that emissions of  $\text{NO}_x$  from current aircraft have increased upper tropospheric concentrations of ozone, by about 1%, averaged globally, and 3%, averaged between 30°N and 60°N. This corresponds to an increase in total column ozone of approximately 0.1 %, averaged globally and 0.3%, averaged between 30°N and 60°N.

- Effects on ozone from aircraft emissions have not been discerned in existing long-term observational datasets, in part because of the year-to-year variability measured in tropospheric ozone.
- Model calculations show that increases in ozone from growth in the subsonic fleet will be roughly proportional to the increased emissions of NO<sub>x</sub>.
- Current emissions of carbon monoxide and non-methane hydrocarbons do not have a significant effect on ozone in the model calculations.

#### *Impacts on climate*

- Current emissions of carbon dioxide from aircraft are 2.5% of the total emissions from fossil fuel use. Over the last 30 years, aircraft have contributed about 1.5% of the industrial increase in atmospheric carbon dioxide, or approximately 0.5 ppmv (parts per million by volume). In equilibrium this would lead to a calculated surface air temperature change of approximately 0.007°C.
- Current emissions of NO<sub>x</sub> from aircraft, through induced changes in atmospheric ozone, are estimated to have an effect on climate that is comparable to that from aircraft carbon dioxide emissions. As carbon dioxide and NO<sub>x</sub> emissions increase in the future, the climate response will increase as well.
- Direct climate effects caused by accumulation of water vapor, carbon monoxide, non-methane hydrocarbons, sulfur oxides, and soot emissions from the current and projected aircraft fleets are estimated to be small relative to aircraft carbon dioxide emissions.
- Model sensitivity studies suggest that the climate impacts of aircraft-induced increases in cloud cover are potentially significant relative to those of other aircraft emissions. In some locations, high-altitude cloud cover has been observed to increase in conjunction with aircraft contrails. However, an accurate quantification of large-scale changes in cloud cover and corresponding radiative properties is not possible currently because of limited observational data and insufficient knowledge of the physical interactions between aircraft exhaust and clouds.
- Some aircraft-induced perturbations in climate forcing, such as those from increased ozone, generally occur near the tropopause. Recent climate model studies indicate such perturbations are less effective in inducing surface air temperature changes than the same climate forcing applied to lower levels. As a result, the Global Warming Potential concept, which was developed for carbon dioxide and other well-mixed gases, may not represent as accurately the climate impact of ozone changes.

### **5. How good are current estimates of subsonic aviation impacts?**

The validity of any model predictions can only be evaluated by formal numerical tests. Such tests include both intercomparison of results from different models and comparison of model simulations with atmospheric observations. Evaluation of the accuracy of our current predictions of subsonic aircraft impacts is restricted by insufficiencies in atmospheric data and inadequate representation of some key physical and chemical processes in assessment models. Specifically, model representation of chemical, transport, radiative and cloud processes must be rigorously tested.

- Testing of models used for ozone change predictions by comparison to atmospheric observations is hindered by the lack of a suitable measurement database. Comparison to existing observations suggests significant deficiencies in the ability of models to predict the abundance of nitrogen oxides and their partitioning into active and inactive reservoirs. Models also have difficulty in reproducing seasonal and vertical distributions of upper tropospheric ozone. These identified inadequacies reduce confidence in the reported values of ozone change due to aviation.
- Where we are able to calculate aircraft perturbations to trace gas abundances (e.g., carbon dioxide and ozone), the direct radiative effects of such changes are probably understood well enough, given the small magnitudes of the predicted changes and the absence of any identified large chemical-radiative feedbacks. Indirect radiative effects of changes in aerosol abundance and composition are less well understood. The properties of cirrus clouds, such as cloud frequency, areal extent and optical properties, are not well represented in climate models, and aircraft radiative effects may be large. Climate feedbacks associated with large radiative perturbations are not well understood.
- Global chemistry models have a consistent representation of photolysis and chemical mechanisms. Limited model intercomparisons show that calculated clear-sky photolysis rates agree with each other to within 10%, and calculated ozone production and loss rates agree to within 10 to 15%. However, the different transport formulations, spatial resolutions and meteorology among current 3-D models produce a wide range in results, up to a factor of 4 in the calculated concentrations of nitrogen oxides in the upper troposphere attributed to different sources. These discrepancies worsen in the near-tropopause region.
- The conversion of  $\text{NO}_x$  emissions to nitric acid ( $\text{HNO}_3$ ) in the plumes and wakes of aircraft are both calculated and observed to be small. Sulfur dioxide ( $\text{SO}_2$ ) conversion to sulfuric acid ( $\text{H}_2\text{SO}_4$ ) and subsequent formation of volatile aerosol in aircraft plumes and wakes, as well as aerosol interaction with emitted soot, are not well understood.

## 6. What is needed to improve the assessment of the impacts of subsonic aviation?

Substantial improvements in the fundamental understanding and model treatment of upper tropospheric gas and particle sources and chemistry and transport processes are required before more credible quantitative ozone and climate predictions can be made. A number of key scientific uncertainties have been identified in this assessment, although none of these uncertainties have been quantified yet. Future efforts are expected to focus on improving the predictive capabilities of 3-D chemistry and climate models through collection of critical field and laboratory datasets and further development of model parameterizations of atmospheric processes. Some specific strategies for progressing toward more credible aircraft impact predictions are listed below in no particular order of priority:

- Quantify the increase in  $\text{NO}_x$  in the atmosphere that is due to aircraft emissions by acquiring and analyzing a comprehensive and reliable set of atmospheric observations. Of interest are measurements made both inside and outside principal aircraft routes. Additional measurements are needed to investigate the magnitudes and distributions of other sources of upper tropospheric  $\text{NO}_x$  such as lightning, stratospheric intrusions, and surface convection.

- Determine the net rate of ozone production as a function of  $\text{NO}_x$  and  $\text{HO}_x$  concentrations in the upper troposphere. Obtain suitable measurements of nitrogen and hydrogen oxides and use them to improve the understanding of nitrogen and hydrogen partitioning and chemistry, gauge the role of aqueous phase and heterogeneous reactions, and evaluate the influence of non-methane hydrocarbon chemistry.
- Obtain measurements of atmospheric species with well-understood sources and sinks and use them to test model treatments of transport processes such as convection. Intercompare model treatments of transport in the troposphere.
- Determine the fraction of aircraft exhaust emitted into the lower stratosphere by analysis of emissions as a function of altitude relative to the tropopause. Improve model treatments of near tropopause chemistry and transport.
- Characterize aerosol production in the engine exhaust, including conversion of sulfate species and production and loss of cloud-forming particles, through further aircraft wake observations and engine test cell studies.
- Develop a physical model for the formation and persistence of contrails by analysis of new datasets that address the microphysical and radiative properties of contrails and exhaust-altered cirrus, and the environmental conditions that promote ice particle growth and control the spatial distribution of contrails and high clouds. Identify contrail case studies for testing models (e.g., high-resolution mesoscale or cloud models) and satellite retrievals.
- Provide basis for improving parameterizations in global climate models by conducting two-dimensional (2-D) and 3-D mesoscale cloud model simulations of the time evolution of contrail microphysical and radiative properties. Test model predictions with available observations.



# ATMOSPHERIC EFFECTS OF SUBSONIC AIRCRAFT: INTERIM ASSESSMENT REPORT OF THE ADVANCED SUBSONIC TECHNOLOGY PROGRAM

---

## 1. INTRODUCTION

An immense and complex world transportation system has evolved that serves as the lifeblood of present national and international economies. Aviation connects distant peoples and places; as such it has become an integral part of a rapidly developing global society. Today, commercial airlines transport hundreds of millions of passengers per year over distances ranging from hundreds to thousands of miles. In terms of total passenger miles, transport by aviation represents about 10% of the total due to all forms of modern transportation. This fraction is likely to grow since aviation travel continues to increase at rates exceeding other forms of transportation. Industry forecasts predict growth in world aviation travel of 70% over the next ten years and 180% over the next twenty years [Boeing, 1996; Douglas, 1995].

The bulk of current air travel is provided by jet aircraft burning hydrocarbon-based "fossil" fuels. As with other fossil fuel transportation technologies, jet aircraft operation results in gaseous and particle combustion byproducts. Emission of these byproducts around airports during aircraft landing and take-off (LTO) cycles was recognized long-ago as a possible contributor to urban smoke problems and photochemical smog generation. In response to those concerns, the International Civil Aviation Organization (ICAO) adopted standards in 1981, based on a precautionary principle, that limited emissions of smoke, carbon monoxide (CO), unburned hydrocarbons (HC), and reactive oxides of nitrogen ( $\text{NO}_x$  = nitric oxide (NO) + nitrogen dioxide ( $\text{NO}_2$ )). In recent years, these standards have been periodically reviewed and strengthened to reflect improvements in engine design and manufacture.

Although much of the initial environmental focus on subsonic aircraft has been directed at LTO emissions, the majority of aircraft emissions are released at cruise altitudes (i.e., 9 to 13 km) where aircraft spend most of their time during flight. This region of the atmosphere, encompassing both the upper part of the troposphere (UT) and the lower part of the stratosphere (LS), differs markedly from the portion of the atmosphere near the ground (i.e., the tropospheric boundary layer) that is of interest in the LTO case. Whereas the boundary layer is typified by highly turbulent mixing and diurnally varying temperature and wind conditions, the UT/LS is subject to substantially less vertical mixing and little diurnal variation in meteorology. Only in regions with deep convection, such as frontal activity or thunderstorms, can constituents be effectively transported to the UT. For the most part, reactive gases and particles emitted in the boundary layer are mostly confined to the area of release because they frequently encounter surface loss sites, such as soil and water. As a result, only a small fraction of reactive, surface emitted species ascend into the relatively 'clean' UT/LS. By directly emitting materials into the UT/LS, commercial aircraft "bypass" these atmospheric cleansing mechanisms and thus constitute a significant fraction of the upper tropospheric burden of trace constituents and particles.

Species reaching the UT/LS, where residence times are fairly long, can be transported substantial distances before removal. As an example, for a typical westerly upper tropospheric flow pattern

found at northern mid-latitudes, air parcels traverse the globe along a latitudinal circle in ten to twenty days, time scales that are comparable to the chemical lifetimes of even moderately reactive species. Accordingly, along with helping to create a global transportation network, aviation may contribute to global scale environmental changes that reach far beyond the primary areas of aircraft operation.

The recently established links between the human-caused buildup in the atmosphere of chlorofluorocarbons (CFCs) and carbon dioxide (CO<sub>2</sub>) to stratospheric ozone depletion and global warming, respectively, have increased awareness of the potential for human activities to affect the atmosphere on a global scale. The scientific assessment of the impact of the proposed High-Speed Civil Transport (HSCT) on stratospheric ozone has become very important as interest in building such an airplane has heightened [Prather and Wesoky, 1992; Stolarski and Wesoky, 1993; Stolarski *et al.*, 1995]. While there is no evidence linking present subsonic aircraft to ozone depletion, subsonic aircraft emissions in the UT/LS are of concern in general, since they can change the local atmospheric concentrations of many trace substances. These include nitric oxide (NO), nitrogen dioxide (NO<sub>2</sub>), ozone (O<sub>3</sub>), water vapor (H<sub>2</sub>O), hydrocarbons (e.g., CH<sub>4</sub>), sulfur dioxide (SO<sub>2</sub>), and particles (soot, sulfates), all of which can directly or indirectly lead to changes in the global radiation balance and result in climate change. In addition, subsonic aviation currently accounts for ~3% of the world fossil fuel usage, and is therefore an obvious, if small, contributor to the buildup of global CO<sub>2</sub> levels.

While the effects of increased CO<sub>2</sub> are well defined, the details of the effects of the other mentioned subsonic aircraft emissions are less well understood, and are the primary focus of this assessment.

The magnitudes of atmospheric changes due to aviation depend, in large part, on the amount of aircraft emissions relative to corresponding natural and other anthropogenic emissions. In this context aircraft emissions must be quantified relative to the fraction of surface emissions that are lifted to the UT/LS, the fraction of upper stratospheric air that descends into the UT/LS, and, in the case of NO<sub>x</sub>, the amount created by lightning. In theory, the various sources can be differentiated by direct observations of atmospheric composition, provided that each source possesses a unique signature. Unfortunately, this separation has proven difficult in practice. For instance, aircraft emission features largely resemble those of urban ground emissions.

Because of the complexities inherent in differentiating various chemical sources, the primary method for quantifying aircraft impacts on the global-scale atmosphere is the use of mathematical models. The physics and chemistry contained in any credible model are developed from, and tested against, relevant laboratory findings and atmospheric observations. Modeling tools used in global atmospheric assessments range from zero-dimensional box model calculations to full three-dimensional (3-D) treatments of the dynamical and chemical features of the atmosphere. The choice of modeling tool depends on the degree to which some of the physical and chemical complexities can be neglected and others can be treated with simplified or approximate mathematical expressions. The appropriateness of a particular choice of model tool can only be established through comparison with other models and with atmospheric and laboratory data.

The Subsonic Assessment (SASS) component of NASA's Advanced Subsonic Technology Program is designed to assess the atmospheric effects of cruise emissions from the existing world fleet of subsonic jet aircraft and the potential effects of a likely larger future subsonic fleet. The sought after assessment will be comprised of numerical predictions of regional and global scale

impacts and quantitative appraisals of the uncertainties associated with such predictions (see Figure 1-1). The SASS project is planned for an eight-year duration (1994 to 2001). Over that period, SASS is aimed at improving a number of atmospheric science assessment tools. In particular the project seeks to accelerate 3-D chemistry transport model (CTM) and general circulation model (GCM) development, formulate rigorous benchmarks and tests of model performance, and collect and analyze atmospheric and laboratory data in a few areas of critical conceptual uncertainty. A detailed description of SASS plans can be found in the First Report of the SASS Project [Thompson *et al.*, 1996].

This first interim assessment of the SASS project attempts to summarize concisely the status of our knowledge concerning the impacts of present and future subsonic aircraft fleets. It also highlights the major areas of scientific uncertainty, through review of existing databases and model-based sensitivity studies. In view of the need for substantial improvements in both model formulations and experimental databases, this interim assessment cannot provide confident numerical predictions of aviation impacts. However, a number of quantitative estimates are presented which provide some guidance to policy-makers.

The interim assessment is organized into six chapters. In Chapter 2, we summarize the development of detailed fleet emission scenarios on 3-D grids suitable for input into CTMs and GCMs. Emission indices (EIs) for individual species are discussed and folded into global inventories for 1990 and 1992. The resulting emission databases include scheduled and charter airlines and military aviation. The databases reflect the complete flight cycle, including takeoff, climb, descent, and landing. Uncertainties in the databases are discussed as well as methodologies for predicting future fleet emissions.

Chapter 3 reviews the progress made in qualitatively understanding the effects of aircraft emissions on UT/LS gas and particle levels and the consequences of such perturbations on chemical and radiation processes related to ozone and climate. Chemistry effects discussed include ozone tendencies in response to NO<sub>x</sub> and hydrocarbon perturbations, increased polar stratospheric cloud catalyzed chemistry due to H<sub>2</sub>O injections, and possible tropospheric heterogeneous chemistry due to aircraft particle emissions. Climate effects are discussed in terms of direct and indirect changes to the average net radiation at the top of the troposphere. Changes of this sort, defined as “radiative forcings,” are related to a number of processes, including clear sky and cloud impacts of gaseous and particulate emissions.

Chapter 4 summarizes progress in realistically incorporating our understanding of the chemical, dynamical, and radiative processes in models that can be used to predict subsonic aircraft fleet impacts. The focus in this interim assessment is on evaluating the strengths and weaknesses of some existing CTMs and GCMs in their application to the aviation issue. As part of this evaluation, model test results are compared with selected data from existing observational datasets. Both the quality of the model results and observational datasets are discussed. The results of this evaluation are intended to serve as a guide for planning future model and observational database development efforts.

Due to existing inadequacies in both assessment models and databases, it is important to delineate methodologies and approaches which will facilitate future improvements in the model assessment capabilities. One assessment tool envisioned for the future is a “core” 3-D chemical transport model which would bring together models and submodels from independent researchers on a

common computing platform. The intended value of this tool would be to enable far greater levels of model evaluation than can be applied presently to individual models. Progress towards the development of this tool has been pursued within the Global Modeling Initiative (GMI) component of the SASS project and some tests of the NASA-sponsored core model are reported in Chapter 4.

Chapter 5 summarizes the conclusions of the preceding chapters and evaluates the progress that has been made on understanding the atmospheric impacts of each aircraft exhaust species. Most importantly it identifies the science areas where increased emphasis over the next three years will most benefit the next assessment effort.

Chapter 6 lists the literature references. The attached appendices provide listings of report authors and contributors, acronyms and abbreviations, and chemical nomenclature and formulae.

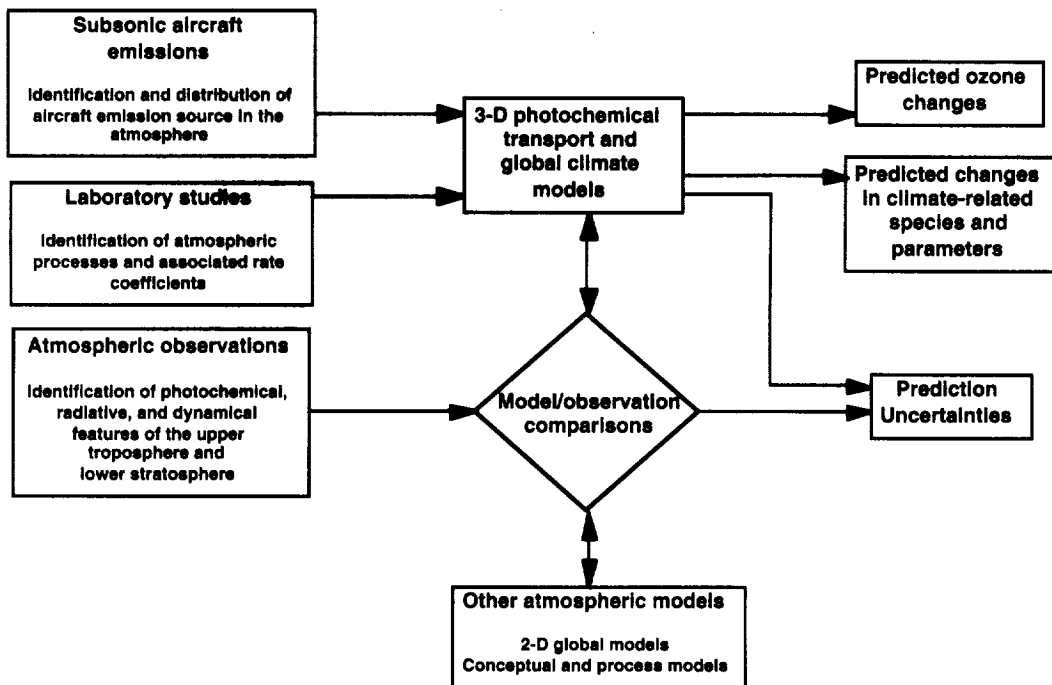


Figure 1-1. Schematic of the Subsonic Scientific Assessment Process.

## 2. AIRCRAFT EMISSIONS

### 2.1 Emissions Characteristics

Combustion of jet fuel produces both gaseous products (e.g., CO<sub>2</sub>, H<sub>2</sub>O, NO<sub>x</sub>, CO, hydrocarbons) and particles (e.g., soot, sulfate). These emissions are initially produced in the combustor, undergo some chemical changes in the turbine and nozzle of the engine, and then are emitted to the atmosphere at the nozzle exit. Further chemical processing occurs in the plume behind the aircraft as the emissions are entrained in the wing-tip induced vortices (e.g., conversion of NO → NO<sub>2</sub> → HNO<sub>3</sub> (nitric acid)/PAN (peroxyacetyl nitrate)/HNO<sub>4</sub> (peroxynitric acid), SO<sub>2</sub> → SO<sub>3</sub> (sulfur trioxide) → H<sub>2</sub>SO<sub>4</sub> (sulfuric acid)). Also in this plume region, conversion of sulfur oxides (SO<sub>x</sub>) to (H<sub>2</sub>SO<sub>4</sub>) leads to the production of H<sub>2</sub>SO<sub>4</sub> aerosols with subsequent aggregation and conglomeration of soot and sulfate aerosols. On a longer time scale, the aircraft plumes disperse and contribute to processes occurring in the background atmosphere.

In this section, the characteristics of aircraft emissions at or near the nozzle exit are discussed. The 3-D global inventories of aircraft emissions that are used as input to the modeling calculations are also described. More detailed discussions of plume and wake processing of aircraft emissions are presented in Section 3.1.

#### 2.1.1 GASEOUS EMISSIONS

The primary emissions from aircraft engines are CO<sub>2</sub> and H<sub>2</sub>O produced by the combustion of jet fuel. The emission levels are determined by the fuel consumption, combustion efficiency and the fraction of hydrogen and carbon in the fuel. Similarly, emission of SO<sub>x</sub> from aircraft engines is determined by the level of sulfur in the jet fuel. Jet fuel specifications require sulfur levels below 0.3% but levels are typically much lower than this. Measurements of fuel samples from a number of international airports yielded an average sulfur content of 0.042% (by weight) with 90% of the samples below 0.1% [Hadaller and Momeny, 1989]. Future sulfur levels are projected to drop to about 0.02% [Hadaller and Momeny, 1993] because of changes in refinery technology and the use of hydrotreating to reduce the aromatic content of refinery products.

The emissions are characterized in terms of an emission index (EI) in units of grams of emission per kilogram of fuel burned. Current and projected EIs are summarized in Table 2-1, based on the analyses of Hadaller and Momeny for commercial Jet A fuel [Baughcum *et al.*, 1996a].

Emissions of NO<sub>x</sub>, CO, and hydrocarbons (HCs) vary in quantity according to the combustor conditions and design. Nitrogen oxides are produced in the high temperature regions of the combustor primarily through the oxidation of molecular nitrogen. Thus, the amount of NO<sub>x</sub> produced by an aircraft engine is sensitive to the pressure, temperature, flow rate, and geometry of the combustor. The combustor conditions, and hence the NO<sub>x</sub> emissions, vary with the power setting of the engine, being highest at high-thrust conditions. By contrast, carbon monoxide and hydrocarbon emissions are highest at low power settings where the temperature and pressure of the engine is low and combustion is less efficient. Nitrogen oxide emissions at the nozzle exit consist of about 90% NO and 10% NO<sub>2</sub> by mass. For NO<sub>x</sub>, the EI<sub>NO<sub>x</sub></sub> is given as gram equivalent NO<sub>2</sub> to avoid ambiguity.

Total hydrocarbon emissions are measured with a flame ionization detector as part of the engine certification tests. Data on hydrocarbon speciation are much more limited. Spicer *et al.* [1992] measured methane as the dominant hydrocarbon in the exhaust but at concentrations lower than in ambient air indicating that aircraft are a net sink for methane in the atmosphere. Emissions of a number of aliphatic and aromatic compounds were measured in tests of two military engines [Spicer *et al.*, 1992] and from two engines used on transport aircraft [Spicer *et al.*, 1994]. Alkanes were the most significant hydrocarbons at all power levels. Alkene, aldehyde and ketone concentrations were much lower at higher power settings than at idle conditions.

As part of the certification process for each engine type for commercial aircraft,  $\text{NO}_x$ , HC, and CO emissions are measured on engine test stands and corrected to standard day, sea level conditions. Measurements are made at power settings of 7% (idle), 30% (approach), 85% (climb out), and 100% (take-off). These measurements have been developed to evaluate aircraft emissions in the vicinity of airports, rather than for cruise altitude conditions. They do, however, provide a comprehensive database for interpolation to cruise conditions. Boeing has developed an empirical fuel flow correlation method to calculate emissions at different flight conditions using the emissions indices from the certification measurements [see Appendices C and D of Baughcum *et al.*, 1996a]. This method includes corrections for ambient temperature, pressure, relative humidity, and installation effects. Installation effects include corrections for the extraction of cabin bleed air in flight, nominal power extraction in flight, and differences between the engine inlet used in the static test and on the aircraft.

The dependence of the emission levels on the fuel flow rate is shown in Figure 2-1 for the engine used on the NASA DC-8 research aircraft. The points for sea-level static conditions (solid line) are extracted from the ICAO database [ICAO, 1995].  $\text{EI}_{\text{NO}_x}$  and smoke emissions (discussed later) increase with increasing fuel flow rate while the  $\text{EI}_{\text{HC}}$  and  $\text{EI}_{\text{CO}}$  decrease by one to two orders of magnitude. For cruise conditions (dotted line), corrections for both installation effects and ambient conditions must be included [Lyon *et al.*, 1979, 1980]. As a reference point, the DC-8 on a 3000-nautical mile (nmi) mission begins cruise at 35 kft with a fuel flow of about  $0.37 \text{ kg s}^{-1}$  ( $\text{EI}_{\text{NO}_x} = 11.2$ ) and ends cruise at 39 kft with a fuel flow of about  $0.29 \text{ kg s}^{-1}$  ( $\text{EI}_{\text{NO}_x} = 9.7$ ). Assuming the aircraft flies an optimum flight profile, as it burned fuel it would fly higher and the fuel flow rate would decrease as it became lighter.

Representative effective emission indices for a number of aircraft types are summarized in Table 2-2. The results are shown for two altitude bands: 0- to 9-km (corresponding to takeoff, climb, descent, landing, and taxi operations) and 9- to 13-km (corresponding to cruise and, in some cases, a portion of the initial climb to start of cruise). These effective EIs were obtained by calculating individual emission inventories for each aircraft type as it was used in April 1992 and then analyzing the fuel burned and emissions in the two altitude bands. Calculations were done for the different engines used by that aircraft type and then totaled. For each aircraft type, the daily fuel use and that aircraft's fraction of the total by all scheduled aircraft also are shown. More detailed results are provided in Baughcum *et al.* [1996a]. Emission indices at any point in an individual flight will depend on the engine type, fuel burn rate, and ambient temperature and pressure.

The efficiency of a combustor can be calculated directly from the EIs of CO and unburned hydrocarbons. As combustors have become more efficient, the EIs for CO and hydrocarbons have decreased. EIs for  $\text{NO}_x$  have generally increased with the higher temperatures of more efficient

combustors. For example, a comparison of the emission indices at cruise altitudes for the Boeing 707, 727, and 757 (see Table 2-2) illustrates this trend. Increases in  $EI_{NO_x}$  have been balanced by improvements in aircraft/engine performance that have reduced the fuel use per passenger mile as new generations of aircraft have been developed. Thus, while some aircraft types have similar EIs, their fuel use per passenger mile may vary.

Recently extensive measurements have been made of emissions at the exit plane of engines in altitude chambers. As part of the Impact of  $NO_x$  Emissions from Aircraft upon the Atmosphere (AERONOX) program, measurements were made behind RB211 (used on L1011 and some B747, B757 aircraft) and PW305 (used on long range business jets) combustors [Schumann, 1995]. Similar measurements have just been completed behind a commercial-type bypass jet engine at the US Air Force Arnold Engineering Development Center (AEDC) [Howard, 1996]. These measurements have characterized the emissions over a wide range of ambient conditions and will be used to evaluate the methods used to predict emission levels at altitude. The AEDC measurements include a comparison of the conventional certification methods with other measurement techniques such as tunable diode laser (TDL) absorption [Wormhoudt *et al.*, 1996]. The results are in good agreement indicating that it may be feasible to make measurements of other species in the exhaust using the TDL technique. The AERONOX results have been used to evaluate some of the different methods used to predict  $EI_{NO_x}$ . The AERONOX report concluded that the variability in  $NO_x$  predictions can be reduced to  $\pm 18\%$  by referencing all prediction equations to ground-level  $NO_x$  certification data. They also concluded that the uncertainty in calculating emission indices is typically  $\leq \pm 15$  to 20%. The AERONOX study comparison was made to an older version of the fuel-flow correlation method used in the NASA studies. That method was later updated to be more accurate at cruise altitudes. The newer method [Baughcum *et al.*, 1996a] was used in the calculation of the emission inventories given in this assessment. Its predictions have not yet been compared with the AERONOX altitude chamber measurements.

*In situ* measurements of aircraft emissions have been made behind commercial subsonic airliners [Arnold *et al.*, 1992; Schulte and Schlager, 1996; Schulte *et al.*, 1996], behind the NASA ER-2 high-altitude aircraft [Fahey *et al.*, 1995a] and behind the Concorde [Fahey *et al.*, 1995b]. By measuring changes in  $CO_2$  and  $NO_x$  concentrations both within and outside of the aircraft plume,  $EI_{NO_x}$  values are obtained. The  $EI_{NO_x}$  measurements behind the Concorde were in good agreement with previous altitude chamber measurements. The measurements behind the Concorde and the ER-2 included a number of other species that provide insight into the chemical and physical processes occurring in the plume. Observations of particles will be discussed in Section 2.1.2. As part of the European Pollution from Aircraft Emissions in the North Atlantic Flight Corridor (POLINAT) program, simultaneous measurements of  $NO$  and  $CO_2$  have been made behind commercial aircraft. The measurements have been made behind both smaller aircraft (MD80, 727, 707, 737) [Schulte and Schlager, 1996] and larger aircraft (747, DC10, A340) [Schulte *et al.*, 1996]. They conclude that within the present uncertainties, the measurements are in general agreement with predictions based on ground-based test data. Measurements and analyses continue.

### 2.1.2 PARTICLE EMISSIONS

Particle emissions from aircraft appear to arise from two causes: soot produced directly in the combustor and sulfuric acid aerosols produced indirectly by the oxidation of sulfur dioxide in the

near-field behind the aircraft. A third cause, namely sulfur trioxide ( $\text{SO}_3$ ) generation in the combustor followed by sulfate generation in the near-field, has been suggested recently by some atmospheric observations, but remains to be fully investigated. In this section we will focus on engine-derived soot emissions and defer discussion of sulfate generation to Section 3.1.

The certification measurements on aircraft engines include smoke emissions. In these measurements, the emissions are sampled and particles collected on a filter. The smoke number is then determined from opacity measurements [SAE, 1991]. A typical dependence of smoke number with fuel flow at sea-level static conditions is shown in the bottom right panel of Figure 2-1. While these measurements provide some guide to the mass of particle emissions and their dependence on thrust setting, they do not address the issues of most concern for an atmospheric assessment (e.g., particle densities, size distributions, surface areas). It is not clear how to relate the smoke numbers measured at sea-level static conditions to the particle size distribution emitted at cruise altitudes. Accordingly, global emission inventories have not been constructed yet for soot.

Several efforts have been made recently to understand connections between smoke number and soot characteristics. Altitude chamber measurements of smoke [Schumann, 1995] and of particles [Howard, 1996] recently have been made from selected engines. The particle measurements made at AEDC on an unspecified commercial-type bypass jet engine determined a soot emission index of  $2.2 \pm 0.7 \times 10^{13}$  particles  $\text{kg}^{-1}$  fuel burned or  $0.012 \pm 0.001$  grams soot  $\text{kg}^{-1}$  fuel burned [Howard, 1996]. The size distribution was found to be a log-normal distribution (i.e., the number of particles is a normal distribution of the logarithm of the particle diameter). The total number of particles was the lowest of any engine characterized to date. Their measurements show only very small, if any, correlation with fuel/air ratio, altitude or combustor inlet pressure, or temperature. By contrast, measured smoke numbers vary with power setting [ICAO, 1995] (Figure 2-1). It is not yet clear how to interpret this result, but it should be noted that the engine studied has a very low smoke number and very low number of particles. In a separate study on the altitude dependence of the particle emissions from a J85-GE-5L engine, Rickey [1995] concluded that engine particle data taken at sea-level static test conditions do not adequately represent particle data at higher altitudes. She also noted that there were differences in particle sizes and number densities when comparing results taken on a combustor to measurements on the full engine.

Ground-based [Hagen *et al.*, 1992; Lilenfeld *et al.*, 1995], laboratory [Whitefield *et al.*, 1993] and simulated cruise [Howard, 1996] studies of hot jet exhausts indicate that subsonic jet engines emit large numbers of nonvolatile particles <200 nanometers (nm) in diameter in a single-mode size distribution (Figure 2-2) peaked at 30 to 60 nm. The low solubility of these particles suggests that they are primarily composed of soot and perhaps small amounts of  $\text{H}_2\text{SO}_4$  formed via the oxidation of sulfur compounds within the fuel [Lilenfeld *et al.*, 1995]. Soot EI values ranging from 0.03 to 0.4 g soot  $\text{kg}^{-1}$  have been reported by Lilenfeld *et al.* [1995] for a GE404 engine (used on an F-18 fighter), calculated from exhaust-plane particle size distributions and number density measurements and engine fuel/air ratios, where the lowest values correspond to typical cruise-altitude power settings. In addition, B. Anderson [personal communication], Schumann [1996], Whitefield *et al.* [1996], and Hagen *et al.* [1996] report nonvolatile (presumably soot) particle EIs ranging from 0.2 to  $10 \times 10^{15}$  particles  $\text{kg}^{-1}$  burned for several aircraft sampled in-flight under typical cruise conditions (see Figure 2-3). Assuming the particles lie within a relatively narrow size distribution peaked at 40 nm, these values imply particle mass EIs on the order of 0.01 to 0.08 g soot  $\text{kg}^{-1}$ , which is also consistent with the EI values of Lilenfeld *et al.*

[1995] for aircraft at cruise altitude and Howard [1996] for measurement under simulated cruise conditions.

A set of *in situ* and ground-based measurements have also been conducted on the supersonic Concorde aircraft. High number densities of non-volatile (presumably soot) particles were observed in both sampling tests ( $5 \times 10^{16}$  particles  $\text{kg}^{-1}$   $< EI_{\text{non-volatile}} < 10^{18}$  particles  $\text{kg}^{-1}$ ), although concentrations were consistently higher in the ground-based sea level static test [Fahey *et al.*, 1995a, b; Lilienfeld *et al.*, 1996].

Soot particle characterization remains an area of great uncertainty. Measurements behind the relatively old and inefficient Concorde Olympus engine show much higher particle emissions than from more modern commercial aircraft or the commercial-type bypass jet engine used in the AEDC tests. Questions of how to relate smoke measurements made near the exhaust plane of the engine nozzle to in-flight soot emissions remain unanswered.

## 2.2 Global Inventory Methodologies

Three-dimensional inventories of aircraft emissions have been developed recently by several groups. In earlier NASA work, detailed inventories of emissions (fuel burned,  $\text{NO}_x$ , CO, and hydrocarbons) were calculated including scheduled, military, and non-scheduled (charter, former USSR (Union of Soviet Socialist Republics), and China) air traffic for 1990 and projected to 2015 [Baughcum *et al.*, 1993a, 1994; Landau *et al.*, 1994]. More recent studies have focused on calculating emission inventories for each month of 1992 to account for seasonal variation in air traffic [Baughcum *et al.*, 1996a; Metwally, 1995]. These studies have taken a “bottom-up” approach in which aircraft schedules are utilized, aircraft/engine combinations identified, and then detailed calculations of fuel burned and emissions are done along each flight path. Other studies have used a mixture of a “bottom-up” approach to account for scheduled air traffic and a “top-down” approach to account for military and non-scheduled traffic [McInnes and Walker, 1992; Schumann, 1995]. The top-down approach starts with the assumption that you know the total global fuel burned. It then calculates part of the inventory and treats the military and the non-scheduled traffic as the difference between the total fuel use reported by the Organization for Economic Cooperation and Development (OECD) and the calculated fuel use by scheduled air traffic.

The Abatement of Nuisance Caused by Air Traffic (ANCAT) database [Schumann, 1995] predicted higher fuel use and much higher  $\text{NO}_x$  emissions for 1991-92 than was calculated in the NASA inventory for 1990. Subsequent analysis as part of the ICAO Committee on Aviation Environmental Protection (CAEP) Working Group 3 (WG3) activities concluded that the ANCAT database used an EI methodology that overpredicted  $EI_{\text{NO}_x}$  and included some double counts of flights. The ANCAT database is being updated and will be released later in 1996 [R. Gardner, personal communication]. An extensive comparison is planned between the new ANCAT database and the 1992 emission inventories developed as part of the NASA project.

The methodology used in developing aircraft emission inventories for both scheduled [Baughcum *et al.*, 1994; Baughcum *et al.*, 1996a] and non-scheduled [Landau *et al.*, 1994; Metwally, 1995] air traffic has been described extensively in earlier work and will not be repeated in detail here. The basic approach used for the calculation of emissions from scheduled air traffic is shown in Figure 2-4. A similar process is used for the calculation of non-scheduled and military emissions.

1. A schedule of aircraft frequencies between cities (i.e., city pair) for each aircraft type is extracted from flight schedules (e.g., the Official Airline Guide (OAG)). Specifying the exact aircraft/engine combination for a given flight involves matching the OAG aircraft code with the aircraft models and engines used by that airline. It also requires eliminating duplicate flights for the same airline and adjusting for code sharing of flights between two airlines (shown as two flight numbers but with only one flight).
2. The aircraft/engine combinations used by the airlines are matched to a list of aircraft for which detailed performance data is available. This performance database relates fuel burn and optimum flight altitude to weight of the aircraft. Typically, the available performance dataset is a much smaller subset of the total number of aircraft/engine combinations in use by the airline. For the latest NASA analyses, approximately 230 aircraft/engine combinations in use by the airlines were matched to a performance dataset consisting of 78 aircraft/engine combinations.
3. For each engine type considered in the dataset, a file of emission indices as a function of fuel flow is obtained from the ICAO Engine Exhaust Emissions Databank [ICAO, 1995].
4. For each flight, the takeoff gross weight of the aircraft is calculated from the flight distance (assuming great circle routing), including fuel reserves and an assumed 70% passenger load factor. The altitude as a function of distance is determined from the gross aircraft weight for the mission. The fuel burn rate is calculated from the performance data as a function of distance. From the fuel burn rate, the emission indices are calculated using an emission fuel flow methodology [Baughcum *et al.*, 1996a], with corrections for ambient conditions. The mission profile is then projected onto a 3-D grid (e.g., 1° latitude x 1° longitude x 1 km altitude resolution).
5. Step (4) is repeated for all flights (approximately 55,000 departures/day).

### **2.3 1992 Emission Inventories**

The emission inventories used in this assessment are based on air traffic in 1992. For each month, emission inventories of fuel burned, NO<sub>x</sub>, CO, and hydrocarbons were calculated for both scheduled [Baughcum *et al.*, 1996a] and non-scheduled [Metwally, 1995] air traffic. Scheduled traffic was defined as air traffic listed in the OAG and includes passenger jet airliners, freighters, and turboprop aircraft. The non-scheduled traffic includes flights within the former Soviet Union and China which were not included in the OAG, charter traffic, and estimates of military air traffic. The emission inventories were generated on a 1° latitude x 1° longitude x 1 km pressure altitude grid. For these calculations, improvements on the earlier methods were made to further eliminate flight duplications, additional older aircraft/engine combinations were added to the database, and an improved fuel flow correlation method was used to calculate emissions from scheduled air traffic. The effect of these improvements on emissions calculated previously for scheduled air traffic in May 1990 [Baughcum *et al.*, 1994] was to decrease calculated global fuel use by 3.5%, decrease global NO<sub>x</sub> by 1.3%, increase hydrocarbon emissions by 51%, and decrease CO emissions by 5.6% [Baughcum *et al.*, 1996a]. The significant increase in hydrocarbons is thought to be primarily due to the inclusion of additional older technology airplane/engine combinations to the performance/emissions database in preparation for the calculation of historical emission inventories [Baughcum *et al.*, 1996b].

The results calculated for 1992 are summarized in Table 2-3 for each month and for the annual total. The global fuel and NO<sub>x</sub> calculated for 1992 increased slightly, 1.5% and 4.0% respectively from that reported earlier for 1990 based on May 1990 as representative of the annual average [Baughcum *et al.*, 1993a].

The spatial distribution of the emissions is shown in Figure 2-5. The majority of the emissions occur at cruise altitudes (see Figure 2-6) and at northern mid-latitudes. Approximately 17% of the emissions are released in the stratosphere [Baughcum, 1996b]. The distribution of fuel use and NO<sub>x</sub> emissions in major geographical regions is summarized in Table 2-4. Approximately 94% of the global fuel use and NO<sub>x</sub> emissions occurs in the Northern Hemisphere. Approximately 60% of the fuel use and 55% of the NO<sub>x</sub> emissions occur in the 9- to 13-kilometer altitude band in the Northern Hemisphere.

The seasonal variation in NO<sub>x</sub> emissions in the 9- to 13-kilometer altitude band is shown in Figure 2-7 for four major geographical regions (North America, Europe, North Atlantic and North Pacific) (as defined in Table 2-4). These four regions account for 64% of the global NO<sub>x</sub> emissions. The top panel shows the total NO<sub>x</sub> emissions deposited in each region in the 9- to 13-kilometer altitude band as a function of month. The bottom panel shows the fractional deviation from the annual average. The largest seasonal variation occurs in the North Atlantic with increases of about 18% in the summer compared to the annual average. Similar seasonal variation is seen for the other three regions but with smaller amplitude.

The relative NO<sub>x</sub> contributions of the different air traffic components are summarized in Table 2-5. Scheduled commercial air traffic (including cargo) is calculated to account for about 70% of the fuel use by aircraft and 74% of NO<sub>x</sub> emissions. Although not shown in Table 2-5, military air traffic is calculated to account for a disproportionately large (>30%) fraction of the hydrocarbon and carbon monoxide emissions from air traffic owing to the fuel rich operation of the engines. However, further work on uncertainties in the military database is required.

## **2.4 Uncertainties in Aircraft Emission Inventories**

The calculated total jet fuel use in 1992 was 136 million metric tons (metric ton = 1000 kg). Reported apparent jet fuel consumption (distillate identified as jet fuel at the refinery) for 1992 was 171 million metric tons [DOE, 1995]. Thus, the calculated jet fuel use was 80% of that identified as jet fuel at the refinery. Work is now underway to understand this difference. Several factors may contribute to this:

1. Simplifying approximations are used to calculate the emission inventories and thus are expected to lead to some systematic errors in calculating the fuel use. These are discussed below in more detail but in general would lead to an underprediction of calculated fuel use.
2. Schedules for air traffic not listed in the OAG must be estimated and this is clearly one area of uncertainty. Similarly, military schedules and flight profiles must be estimated.
3. General aviation is not included in the emission inventory calculation. For 1990, jet fuel use by general aviation was estimated to be 3.5 million metric tons [Balashov and Smith, 1992]. This would correspond to 2% of reported jet fuel production. The recent general aviation analysis conducted by McDonnell Douglas has indicated that the fuel consumption of this fleet

is about 6%. This data has not been documented formally. The emission inventories of this report also do not account for either military or domestic helicopter flights.

4. The reported jet fuel production numbers are not the ideal reference since they do not necessarily represent jet fuel delivered to airports. Jet fuel is a fungible product and can be reclassified and sold as kerosene or mixed with fuel oils and diesel fuels depending on market requirements (e.g., when a low freezing point fuel is needed in the winter). Also, some other distillate fuels from the refinery may satisfy jet fuel requirements and ultimately be purchased and used as jet fuel. As a consequence, the reported jet fuel does not provide a rigorous upper limit to jet fuel use. It is a convenient compilation of reports from different countries but its accuracy has not been evaluated and may vary for different regions.

#### **2.4.1 SIMPLIFYING ASSUMPTIONS**

The development of aircraft emission inventories requires some simplifications, some of which are done in order to make the calculations tractable (e.g., fuel flow methodologies for calculating EIs). Others are simplifications due to the lack of more detailed data (e.g., exactly what aircraft/engine combination was used on a specific flight). The major simplifications used in the calculations of the NASA emission inventories are as follows:

##### **(a) Scheduled Aircraft**

- Aircraft are assumed to fly according to manufacturer's design performance specifications, with fuel consumption and flight altitude determined by aircraft gross weight. Flight profiles are calculated as cruise climb rather than step climbs constrained by air traffic control.
- Aircraft fly great circle routes between cities.
- The effect of winds is averaged by having flights in both directions (zero prevailing winds).
- Standard day temperatures are assumed for all flights.
- Aircraft fly with the correct amount of fuel for the mission plus safety reserves. No fuel tankering occurs. Tankering is the practice of carrying enough fuel so that several flights are made without refueling, in order to save time and money.
- Airports are treated as point sources with flights taking off and landing in the direction of their destination. No special procedures are considered for different airports; all are treated alike.
- Congestion, both on the ground and in the air, is not considered. Weather effects are not included. Air traffic delays and holding patterns are not considered.
- Fuel use by auxiliary power units is not considered.

All aircraft are assumed to fly with the same 70% load factor and no cargo other than passenger luggage.

##### **(b) Military, Unscheduled and Charter Aircraft**

Some of the simplifications listed in (a) above are relevant to the unscheduled and charter databases. In addition, the following simplifications and assumptions have been used in the military database.

- Military centers were set up around the world and the emissions were dispersed in a starburst fashion from the centers.
- Some transport aircraft flow was assumed between world regions.
- The cruise power settings and operational altitudes of the aircraft were based on available technical specifications but have not been validated.
- The fleet sizes and mixes for the individual countries were obtained from a variety of informational sources. Assumptions are required regarding utilization of specific aircraft types by given countries and could lead to significant errors in the inventories.

Since some of these simplifying assumptions may lead to systematic errors, a series of parametric studies are underway to evaluate their importance [Baughcum *et al.*, 1996a]. Some of the results are summarized below:

1. *Wind and temperature effects:* The calculations assume a standard atmosphere temperature profile and that for a round trip flight wind effects will effectively average to zero. Meteorological effects are evaluated using a database of monthly means and standard deviations of winds and temperatures derived from daily National Meteorological Center (NMC) analyses between July 1976 and June 1985. This database is incorporated into the Boeing WINDTEMP program for use by both airline route planners and design engineers to calculate winds and temperatures enroute between two selected cities. The code is integrated with Boeing's performance analyses so that the effect of winds and temperatures on fuel consumption on a given route can be calculated explicitly for different months of the year and for different reliabilities. Using this database, it was found that the simplifying assumptions about wind and temperature lead to a 1.4-2.3% underprediction of fuel use on East-West flights and a 1% underprediction on North-South flights. In actual airline operation, where air traffic control permits, aircraft will be routed to minimize fuel usage by taking advantage of the winds. The underprediction caused by the zero wind assumption is therefore likely to be less than the percentages stated above.
2. *Payload variation:* Heavier aircraft burn fuel at a higher rate than do lighter weight aircraft. Thus, the actual fuel usage for a flight is sensitive to the distance flown, the passenger load, the cargo load, and any extra fuel carried. This increased fuel burn rate for a given mission will result in higher  $EI_{NO_x}$  as well. As an example, fuel use per nautical mile (nmi) at cruise conditions for a 747 increases from approximately 36.5 pounds  $nmi^{-1}$  for a 2000-nmi mission to 44 pounds  $nmi^{-1}$  for a 7000-nmi mission. Increasing the load factor from 70% to 75% resulted in an increase in fuel use of 0.8% for a B747 (Los Angeles to Tokyo route) and 2.5% for a B737 (Los Angeles to San Francisco). For a B747 flying the Los Angeles to Tokyo mission, the fuel use would increase by 13% if the aircraft was carrying the maximum weight cargo and 7.7% if it was carrying a more typical cargo density (10 pounds  $ft^{-3}$ ) and was full. Increasing the average passenger weight allowance (passenger + baggage = 200 pounds) to 230 pounds increased mission fuel use by 1.1%. Since most aircraft do not have the cargo capacity of a 747, work is still underway to evaluate how this result should be extended to the global inventory.

3. *Tankering*: To evaluate the effects of fuel tankering, a B737 was modeled on flights between Los Angeles and San Francisco. For this 293 nautical mile flight, the aircraft can carry enough fuel for four flights. Assuming the aircraft fueled for all 4 flights, the average increase in fuel use per flight was calculated to be 4%. This is an extreme case since most aircraft fly much longer distances and tankering is less important.

To better quantify the uncertainties, a systematic analysis is underway to compare calculated fuel use with data reported by US certificated airlines to the US Department of Transportation (DOT) on DOT Form 41. This database provides total departures, total fuel use, and total miles flown for each airline and for each aircraft type used by that airline. Data is reported separately for both domestic and international travel. Thus, the comparison should help identify the magnitude of systematic errors for different aircraft types and for different types of aircraft operations (e.g., long-range international flights vs. domestic).

## **2.5 Future Trends and Methodology for Constructing Long-Range Forecasts**

An important goal of the subsonic assessment effort is to predict the atmospheric impacts of future (i.e., up to 100 years) aviation. Air traffic has grown steadily and is projected to continue to grow at approximately 5.1%/year over the 1996 to 2015 time period with some regions (e.g., Asia-Pacific and China) growing faster than that [Boeing, 1996]. Aircraft emissions due to subsonic air traffic were projected to the year 2015 as part of the assessment of the ozone impact of a fleet of HSCTs. These forecasts included scheduled [Baughcum *et al.*, 1994] and non-scheduled (military, charter, former USSR/China) [Landau *et al.*, 1994] air traffic. In that study, passenger demand was projected based on an average of forecasts by Boeing and McDonnell Douglas using economic models. Aircraft performance and emissions characteristics for future aircraft were projected and emission inventories were then calculated.

Since the earlier projections were intended only to provide a reference atmosphere for the assessment of the effect of the HSCT on the stratosphere, the projections were done simply (e.g., all aircraft types were assumed to improve at a constant rate relative to the 1992 “state of the art”). For the assessment of subsonic aircraft effects in the troposphere, a more detailed projection to 2015 is now underway [S. C. Henderson, personal communication]. In parallel with this work, the European ANCAT project is also forecasting aircraft emission inventories to 2015 [R. Gardner, personal communication].

Most industry market outlook projections of future air traffic are only made 10- to 15-years into the future. Longer range forecasts of aircraft emissions, similar to those projected as part of the IPCC assessments, have not yet been developed by the aviation industry. Two long-range forecasts of total fleet burden have been made which consider different growth and technology assumptions [Vedantham and Oppenheimer, 1994; ICAO CAEP WG3, 1995].

Long-range forecasts involve projections of global and regional economics, fuel prices, changes in aircraft size, technology and fuel efficiency, and changes in engine technology, efficiency, and emission characteristics. The interplay between air transportation and other forms of transportation (e.g., rail) and communications (e.g., videoconferencing) must be considered. Approximately half of air travel is business-related. Thus, sociological questions of how people will do business and how they will use their leisure time in the future also impact future travel projections. As such,

long-range forecasts can attempt to bound the problem by considering a range of simplifying assumptions and projections. Certainly, any long-range forecasts will be subject to great uncertainty. For instance, it is doubtful that the current air traffic and emissions would have been well predicted in 1946. Nevertheless, the SASS project must develop a credible methodology for forecasting future aviation emissions in order to assist technology and policy decision-makers.

## 2.6 Summary

Studies of aircraft emissions have demonstrated that global emission inventories of  $\text{NO}_x$ , CO, and hydrocarbons can be constructed for the current subsonic fleet using reasonable assumptions, although some of the current fleet inventories are not yet complete, awaiting further improvements on military, former USSR, charter, and general aviation contributions. Recent progress in constructing emission inventories is highlighted by the resolution of most earlier differences identified between the NASA and ANCAT emission databases and by the relatively good agreement between the jet fuel reported to be produced at refineries and that calculated in the emission inventories. In addition, the calculation of  $\text{NO}_x$  cruise emissions from engine certification data has received substantial verification by comparison to a growing body of *in situ* measurements of aircraft  $\text{NO}_x$ .

A number of the more subtle features of the gaseous emission inventories have been scrutinized recently. For instance, seasonal variations in aircraft emissions have been characterized and have been found to be of relatively small amplitude in all regions except the North Atlantic where summer emissions are up to 35% larger than winter emissions. In addition, approximately 17% of subsonic aircraft emissions are estimated to be released in the lowermost stratosphere, where gas residence times are potentially much longer than in the upper troposphere. In order to improve the estimate of the stratospheric release a more accurate treatment of tropopause heights is required, however.

Global inventories for soot particle emissions remain to be constructed. Large differences in soot emissions between older and newer engine technologies are observed and need to be reflected in the global inventory. At first glance, smoke number certification measurements appear to provide a reasonable basis for constructing a cruise soot emission inventory; however, the precise relation between smoke measurements and in-flight soot emissions is not straightforward and relatively little data now exist with which to construct a methodology.

**Table 2-1.** Emission indices in units of grams emission/kilogram fuel for 1992 and 2015.

<b>Emission</b>	<b>1992</b>	<b>2015</b>
Carbon Dioxide (CO <sub>2</sub> )	3155	3155
Water (H <sub>2</sub> O)	1237	1237
Sulfur Oxides (as sulfur dioxide, SO <sub>2</sub> )	0.8	0.4

**Table 2-2.** Summary of calculated fuel burned and effective emission indices for commercial aircraft types (based on April 1992 scheduled air traffic) [from Baughcum et al., 1996a].

Airplane Type	Fuel (1000 kg day <sup>-1</sup> )	% of Global Fuel Burned by Scheduled Traffic	0-9 km Altitude Band (g kg <sup>-1</sup> fuel)			9-13 km Altitude Band (g kg <sup>-1</sup> fuel)		
			EI (NO <sub>x</sub> )	EI (CO)	EI (HC)	EI (NO <sub>x</sub> )	EI (CO)	EI (HC)
Boeing 747-200	26,359	10.40%	22.8	22.8	12.8	14.2	1.4	0.8
Boeing 747-100	22,519	8.88%	23.4	22.2	12.1	13.9	0.4	0.6
Boeing 727-200	21,478	8.47%	11.6	5.0	0.8	8.7	2.4	0.5
DC-10	19,140	7.55%	21.0	17.6	6.5	13.2	2.0	1.3
MD-80	16,122	6.36%	14.3	5.3	1.5	10.6	3.3	1.2
Boeing 737-200	15,563	6.14%	10.2	6.5	1.4	7.7	2.9	0.6
Boeing 747-400	14,779	5.83%	25.8	8.9	1.6	13.9	1.0	0.4
Boeing 767-200	10,084	3.98%	19.6	6.1	1.3	12.2	2.6	0.6
Boeing 737-300	9,827	3.88%	12.2	15.6	1.3	9.6	2.9	0.2
Airbus A300	9,745	3.84%	20.6	18.9	7.0	14.4	1.2	0.9
DC-9	9,035	3.56%	9.5	9.6	2.7	8.1	2.3	0.5
Lockheed 1011	8,843	3.49%	20.1	19.2	13.5	15.0	1.9	0.7
Boeing 757-200	8,052	3.18%	17.3	10.4	0.9	12.6	2.0	0.2
Boeing 747-300	5,772	2.28%	24.4	15.5	9.6	14.5	1.9	0.5
Tupolev 154	5,610	2.21%	11.8	4.7	0.7	8.7	2.2	0.5
Airbus A310	4,682	1.85%	19.6	6.7	1.4	13.6	2.0	0.5
Boeing 767-300	4,536	1.79%	18.0	11.7	3.0	13.4	2.3	0.6
DC-8	4,397	1.73%	7.5	43.5	37.2	5.6	7.0	2.0
Airbus A320	3,653	1.44%	16.1	6.8	0.5	12.1	2.0	0.4
Boeing 727-100	3,107	1.23%	10.9	7.4	2.2	7.7	3.7	1.1
Small Turboprops	2,975	1.17%	8.1	4.0	0.2	Not Applicable		
MD-11	2,841	1.12%	19.6	9.7	1.5	12.4	1.6	0.2
Boeing 747-SP	2,573	1.01%	23.2	30.6	19.9	14.4	1.1	0.8
Large Turboprops	2,126	0.84%	13.0	4.3	0.0	Not Applicable		
Boeing 707	2,101	0.83%	15.1	39.1	44.7	5.9	8.0	7.9
Ilyushin 62	1,974	0.78%	14.6	34.2	39.5	5.9	5.9	6.0
Medium Turboprops	1,944	0.77%	11.8	5.1	0.6			
Boeing 737-400	1,787	0.70%	12.2	15.0	1.1	9.6	3.5	0.2
Fokker 28	1,680	0.66%	10.5	6.0	0.5	8.5	1.5	0.4
BAE-146	1,548	0.61%	8.8	8.1	0.8	7.7	0.2	0.0
Airbus A300-600	1,539	0.61%	18.9	10.9	2.0	13.2	2.0	0.4
Boeing 737-500	1,497	0.59%	11.4	12.9	0.8	9.4	3.8	0.2
Ilyushin 86	1,264	0.50%	15.1	38.8	44.7	5.8	8.1	8.0
Fokker 100	1,003	0.40%	9.5	25.9	2.5	6.4	11.5	1.6
Tupolev 134	846	0.33%	9.4	9.3	2.9	8.0	2.1	0.5
Boeing 747-SR	673	0.27%	18.6	19.3	11.1	14.0	2.7	2.7
BAC111	544	0.21%	11.4	13.4	2.3	9.3	2.7	0.6
YAK 42	460	0.18%	10.8	7.4	2.2	7.6	3.8	1.1
Concorde	404	0.16%	10.4	27.9	5.4	10.0	26.0	1.8
Ilyushin 72	248	0.10%	15.1	38.7	44.5	5.8	8.0	7.9

**Table 2-3.** Calculated fuel burned and NO<sub>x</sub> emissions as a function of month for 1992.

<b>Month</b>	<b>Fuel</b> <b>(10<sup>8</sup> kg day<sup>-1</sup>)</b>	<b>NO<sub>x</sub></b> <b>(10<sup>6</sup> kg day<sup>-1</sup>)</b>
January	3.46	4.20
February	3.59	4.36
March	3.61	4.39
April	3.65	4.45
May	3.73	4.54
June	3.84	4.69
July	3.91	4.79
August	3.92	4.79
September	3.82	4.66
October	3.72	4.54
November	3.73	4.55
December	3.70	4.51
<b>Total</b>	1.36 x 10 <sup>11</sup> kg year <sup>-1</sup>	1.66 x 10 <sup>9</sup> kg year <sup>-1</sup> 0.51 Tg (N) year <sup>-1</sup>

**Table 2-4.** Fuel burned and NO<sub>x</sub> emissions deposited in different geographical regions, considering all altitudes and the 9- to 13-kilometer altitude band.

Geographical Region	Latitude Range (degrees)	Longitude Range (degrees)	Percent of global emissions occurring within altitude band			
			All Altitudes		9 to 13 kilometers	
			Fuel	NO <sub>x</sub>	Fuel	NO <sub>x</sub>
Northern Hemisphere	0-90N	180W-180E	94	94	60	57
Southern Hemisphere	90S-0	180W-180E	6	6	4	4
Continental US	25N-49N	125W-70W	28	28	15	13
Europe	37N-70N	10W-25E	17	17	9	8
North America	25N-70N	125W-70W	30	29	16	15
North Atlantic	30N-70N	70W-10W	7	7	6	7
North Pacific	30N-65N	120E-125W	9	10	6	7

**Table 2-5.** Calculated contribution of NO<sub>x</sub> emissions from different air traffic components, considering all altitudes and the 9- to 13-kilometer altitude band. (Percentages are based on the fuel burned and emissions calculated.)

	Fuel	NO <sub>x</sub>
<b>All Altitudes</b>		
Charter	4.9%	5.1%
Military	19.0%	15.8%
Non-Scheduled (former Soviet Union and China)	6.5%	4.9%
Scheduled	69.6%	74.3%
<b>9- to 13-Kilometer Altitudes</b>		
Charter	4.6%	5.2%
Military	15.5%	13.9%
Non-Scheduled (former Soviet Union and China)	9.3%	7.2%
Scheduled	70.6%	73.7%

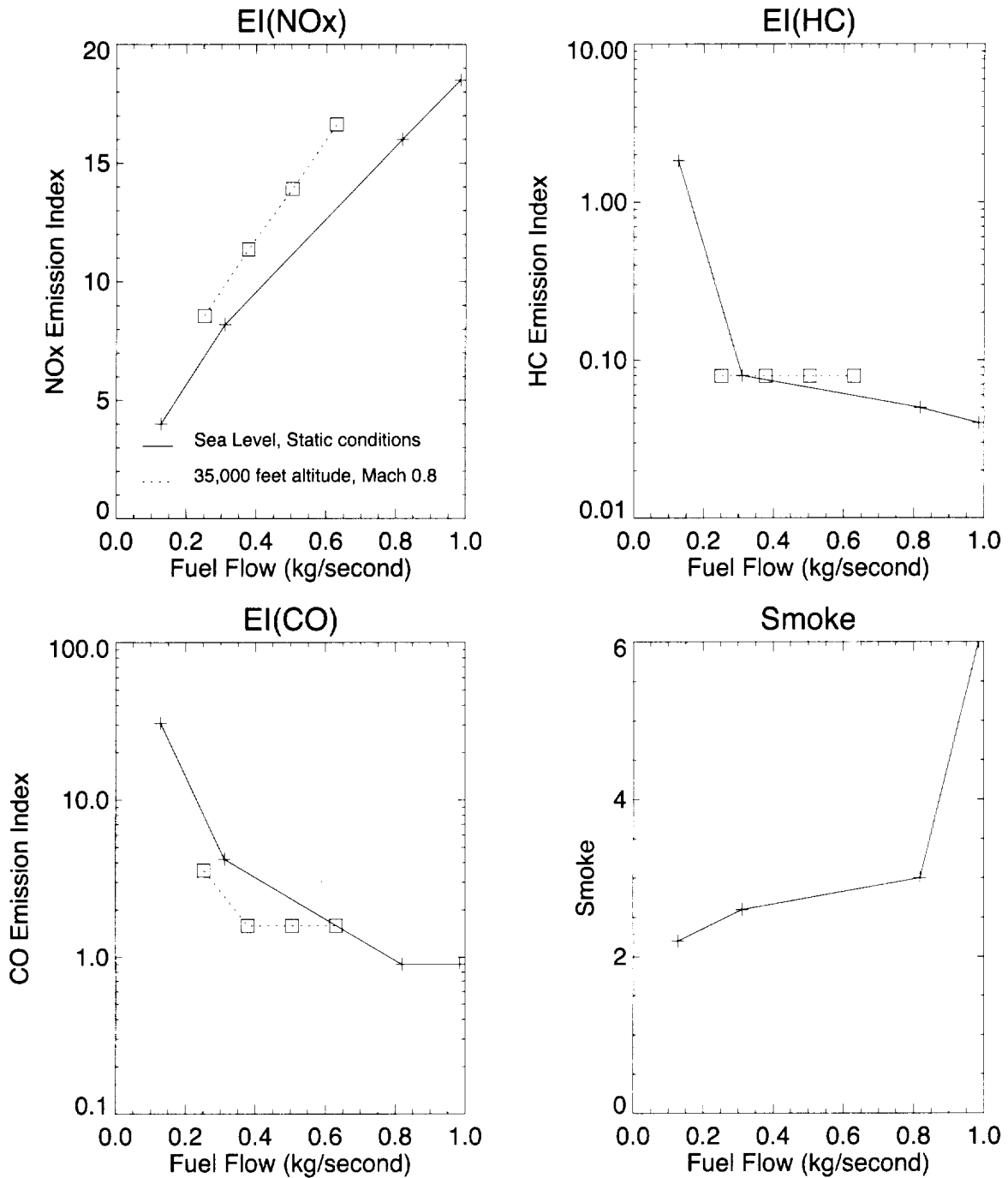


**Figure 2-1.** Emission indices and smoke number as a function of fuel flow for a CFM56-2-C5 combustor. The points on the solid line identify measurements at sea-level static conditions. The points on the dotted line were calculated for an altitude of 35,000 feet and a speed of Mach 0.8 using the sea-level static measurements corrected for installation effects and ambient conditions. (The lines are shown for visualization only.)

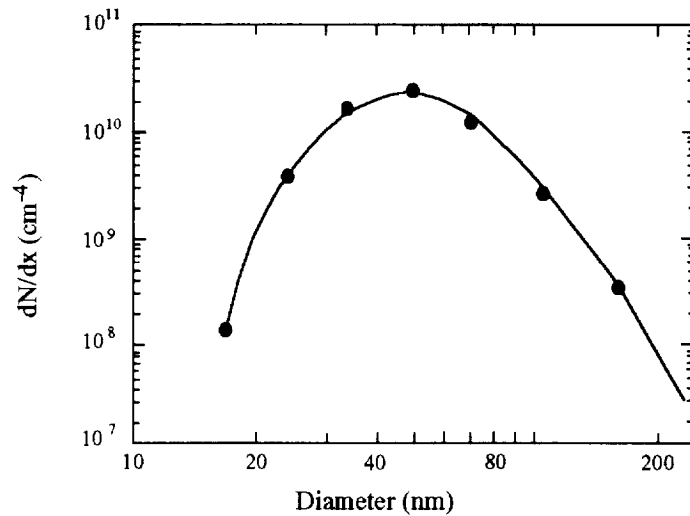


**Figure 2-2.** Particle size distribution measured in an altitude chamber immediately behind a test engine under cruise conditions at altitude 9.1 km [Howard et al., 1996]. Open circles represent particle concentrations (number per cm<sup>3</sup>) divided by particle diameter.

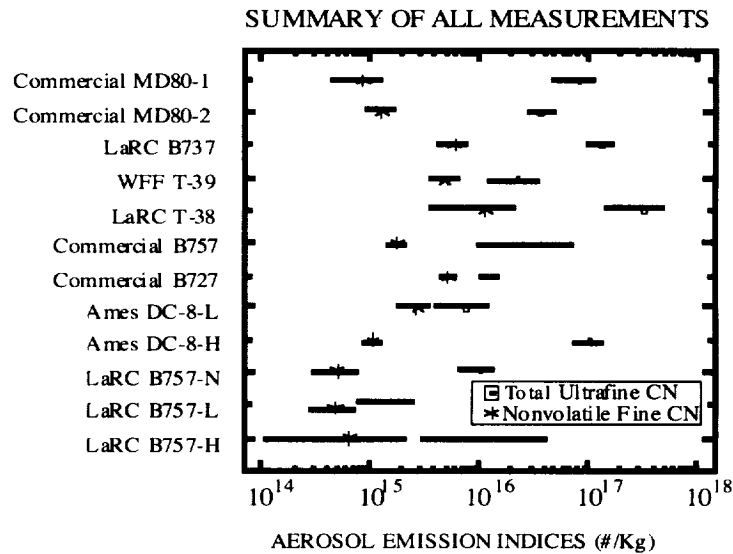


**Figure 2-3.** Aerosol emission indices for a number of subsonic aircraft as measured in the wakes of these aircraft by instrumentation aboard the NASA T-39. Data are given for two commercially operated MD80 aircraft (MD80-1 and MD80-2); the NASA Langley B737 (LaRC B737); the NASA Wallops Flight Facility Sabreliner (WFF T-39); the NASA Langley T-38 trainer jet (LaRC T-38); B757 and B727 commercial carriers; the NASA Ames DC-8 while burning 70 and 500 ppm S fuel (-L and -H, respectively); and the NASA Langley B757 while burning 500, 70, and 700 ppm S fuel (-N, -L, and -H, respectively). The nonvolatile particles represent aerosols > 20 nm in diameter and nonvolatile at temperatures < 190 C. Ultrafine particles are defined as all aerosols > 4 nm in diameter [B. Anderson, personal communication].

## Global Emissions Database Calculation Schematic

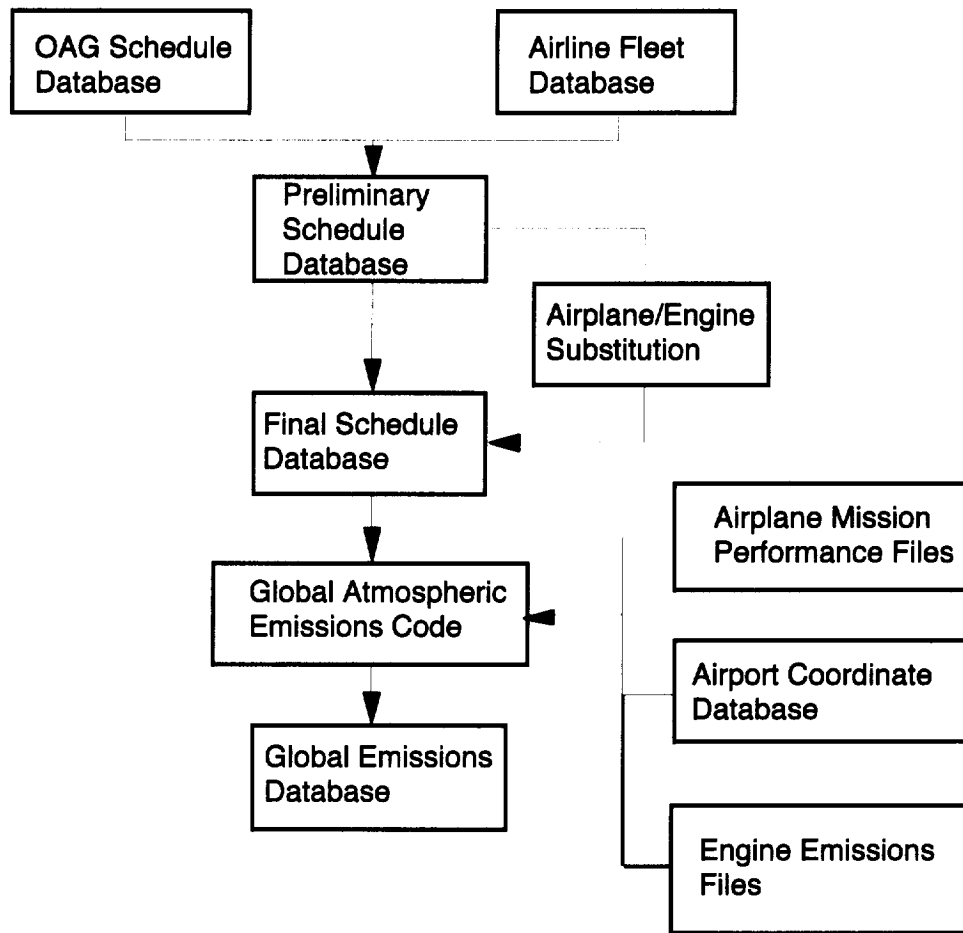


**Figure 2-4.** Schematic of emission inventory calculation.

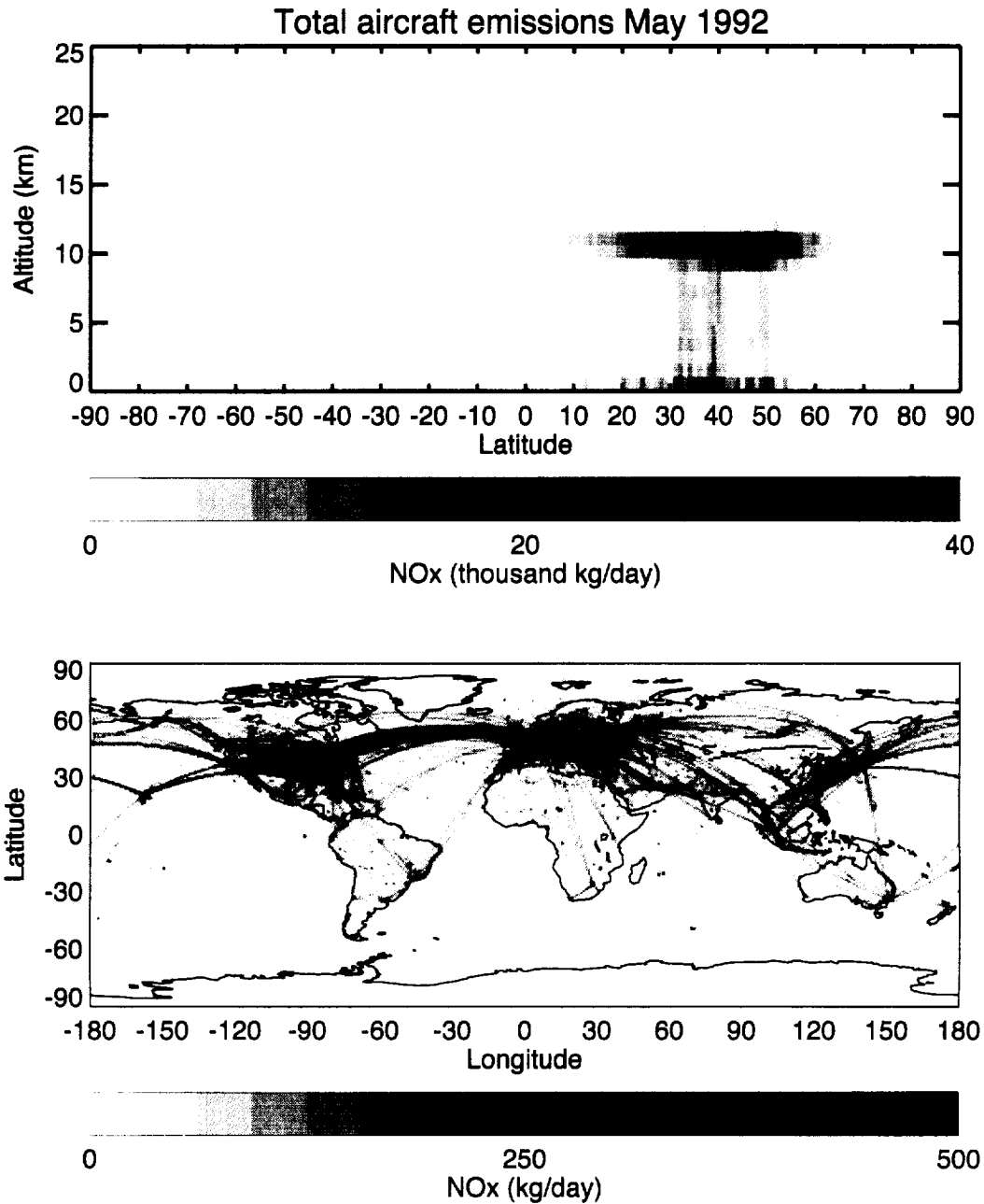


**Figure 2-5.** Calculated NO<sub>x</sub> emissions for all aircraft traffic in May 1992 as a function of altitude and latitude, summed over longitude (top panel), and as a function of latitude and longitude, summed over altitude (bottom panel). Values greater than maximum are plotted as black.

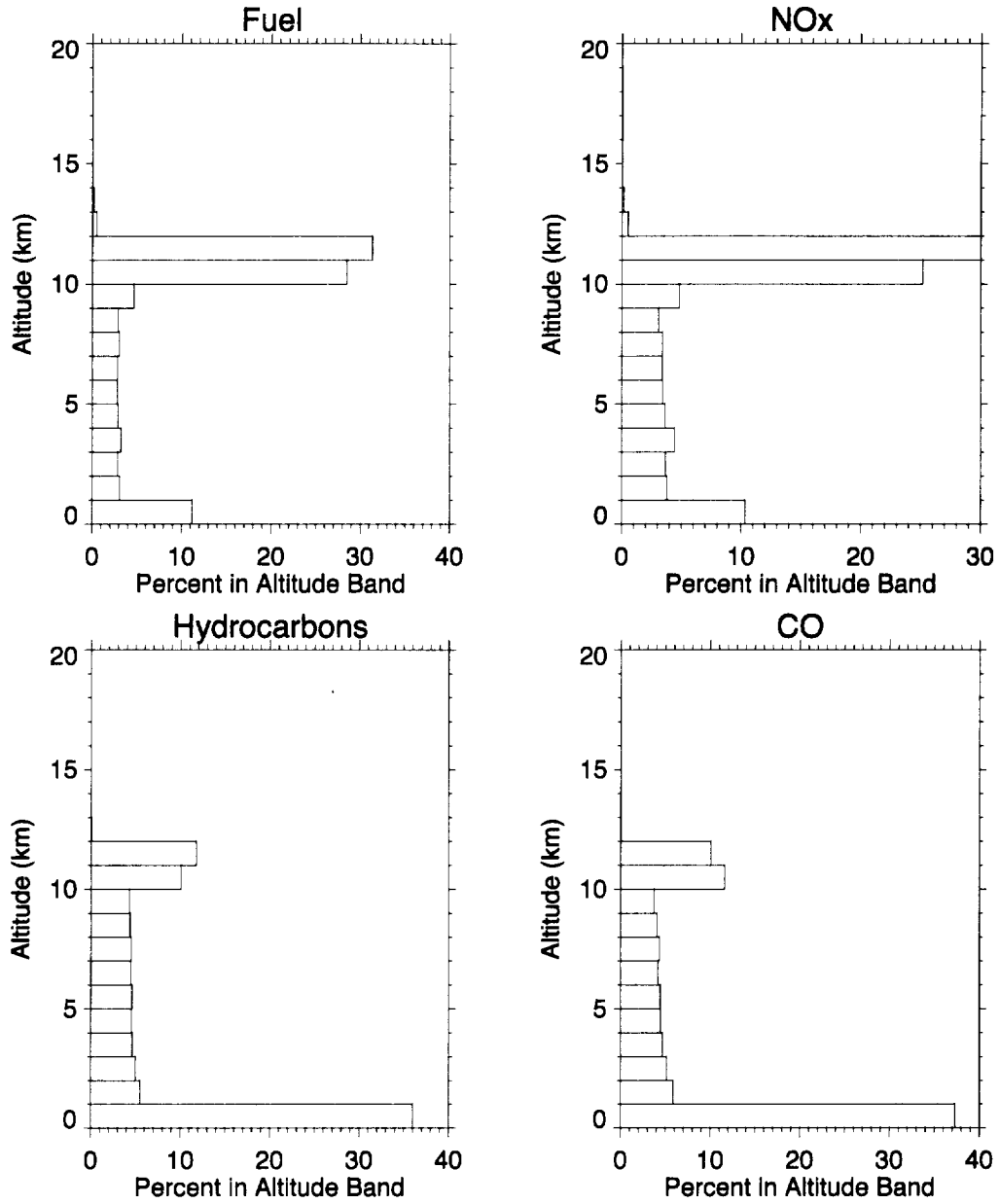


**Figure 2-6.** Fraction of emissions in each altitude band calculated for May 1992 air traffic.

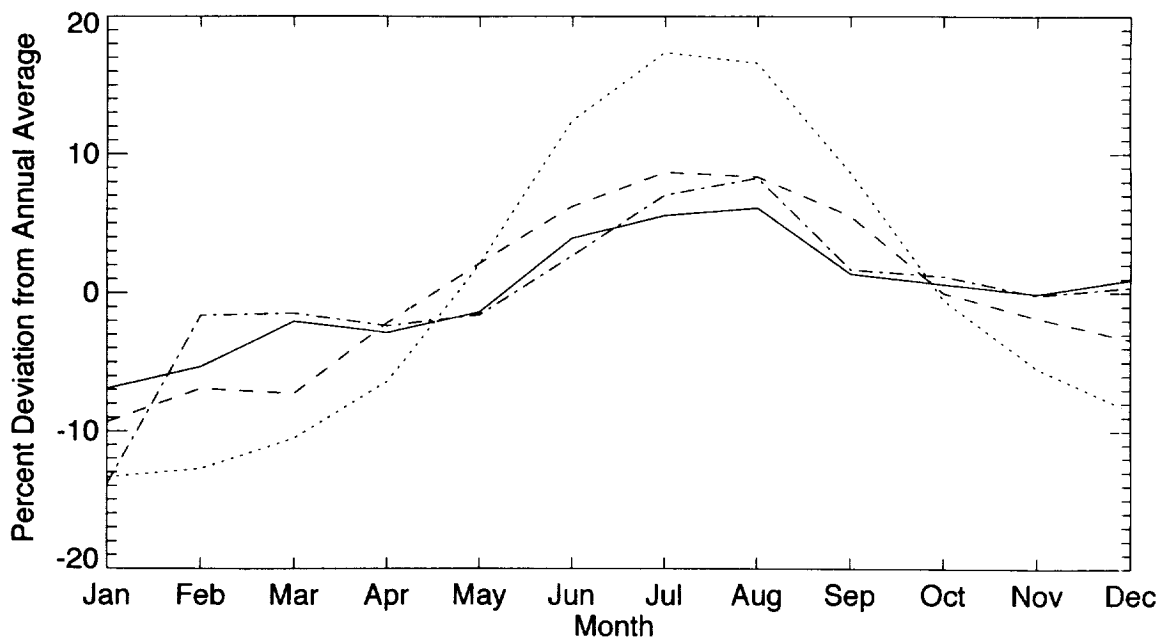
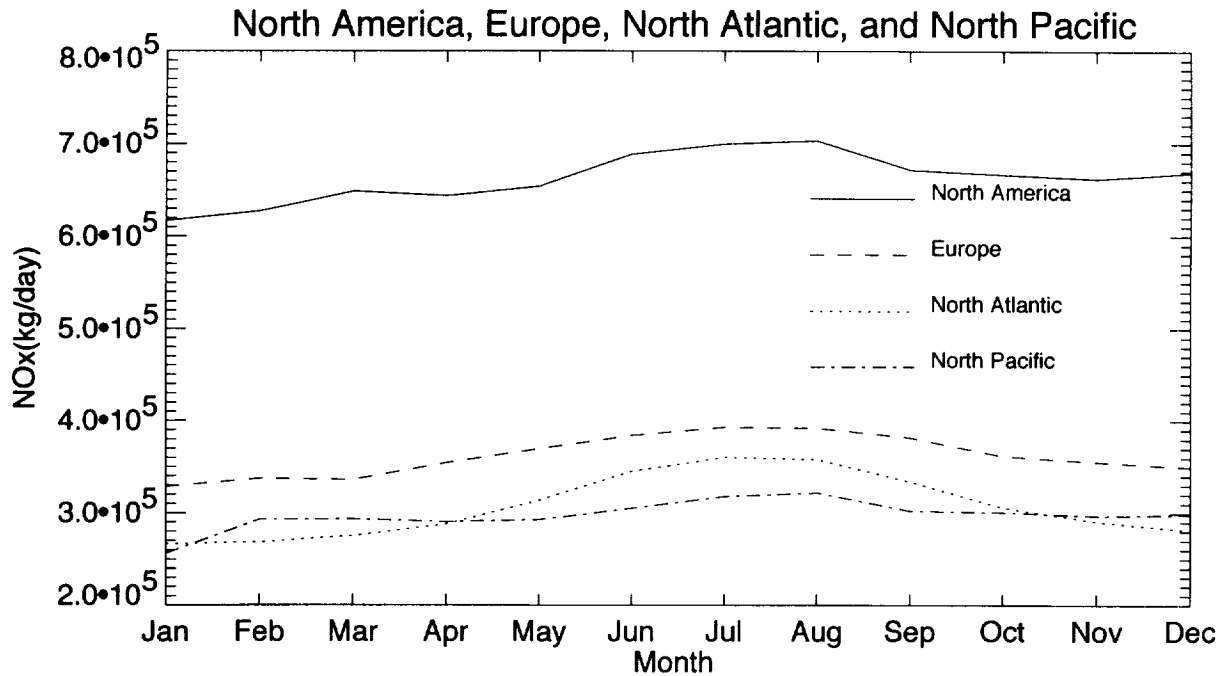


**Figure 2-7.** NO<sub>x</sub> emitted in the 9- to 13-km altitude band for all air traffic for North America (solid line), Europe (dashed line), the North Atlantic (dotted line), and the North Pacific (dash-dot line) for each month of 1992.

### 3. UNDERSTANDING THE EFFECTS OF AIRCRAFT EMISSIONS

The aircraft emission inventories presented in the preceding chapter must be added to and compared with other sources of gases and particles in the atmosphere in order to accurately assess aircraft impacts. In addition, a relatively complete understanding of the physical and chemical processes linking various emitted species with ozone and climate needs to be developed as the foundation for numerical prediction efforts. In this chapter we summarize the progress made in understanding the effects of aircraft emissions both in terms of perturbations to ambient levels of gases and particles and in terms of impacts on specific atmospheric processes. Table 3-1 summarizes the estimated range of perturbations from the subsonic fleet in areas of heavy traffic. The foundations for these estimates are detailed in the following sections.

#### 3.1 Near-Field Effects

Emissions from individual aircraft are initially highly localized within the aircraft's exhaust plume and wake. Concentrations of combustion products in plume/wakes are typically much greater than the corresponding ambient concentrations. These high concentrations do not persist very long, however, since plume/wakes rapidly expand and mix with the surrounding atmosphere on time scales of minutes to hours. Plume/wake dispersion time scales are substantially less than typical atmospheric lifetimes of exhaust species, which are on the order of days to weeks. Accordingly, the chemical and climatic effects of aircraft exhaust are expected to be manifest primarily during the time period following plume/wake breakup. Based on this expectation, aircraft emission inventories, as described in Chapter 2, have been constructed by simple dilution of the aircraft plume at the altitude of injection, with no chemical changes taking place, into a 1° longitude by 1° latitude by 1 km altitude grid.

The potential for important chemical changes to take place in short-lived aircraft plume/wakes has been actively investigated. Interest in this area is driven by recognition of the fact that a number of non-linear chemical and microphysical processes, which do not typically proceed under the low concentration conditions of the background atmosphere, may occur in species-rich plume/wakes. Such plume/wake processes may lead to global-scale effects if they result in irreversible changes (at least on the order of days to weeks) in exhaust composition. The three plume/wake processes that have attracted the most attention are conversion of  $\text{NO}_x$  to inactive forms of nitrogen, formation of large numbers of small diameter aerosol particles, and formation of ice and droplets.

Conversion of emitted  $\text{NO}_x$  to less reactive nitrogen oxides in the plume can potentially reduce the effect of these emissions on ozone. The near-field region has been modeled with  $\text{NO}_x/\text{SO}_x/\text{HO}_x$  chemistry coupled to fluid mechanical calculations of the exhaust mixing and dynamics [Miake-Lye *et al.*, 1993, 1994; Quackenbush *et al.*, 1993; Kärcher, 1995; Danilin *et al.*, 1994]. Such calculations indicate that relatively small amounts of  $\text{NO}_y$  deposited at the point of wake break-up are in the form of nitrous acid ( $\text{HNO}_2$ ) or nitric acid ( $\text{HNO}_3$ ), the bulk remaining in the form of  $\text{NO}_x$  as emitted. Measurements in the wake of the ER-2 [Fahey *et al.*, 1995b], the Concorde [Fahey *et al.*, 1995a], and several commercial subsonic airliners [Arnold *et al.*, 1992; Zheng *et al.*, 1994] provide field experimental support for the modest conversion of emitted  $\text{NO}_x$  to other species.

Unlike the NO<sub>x</sub> conversion case, where minimal conversion is found in the near-field, the fate of sulfur compounds is significantly affected by near-field processes. Plume/wake model results have shown that a large number of small particles can form via binary homogeneous nucleation of sulfur compounds [Miake-Lye *et al.*, 1994; Kärcher, 1995; Zhao and Turco, 1995; Brown *et al.*, 1995]. This has been confirmed by measurements in the Concorde plume and in a number of subsonic aircraft plumes, which show that large numbers of small, persistent particles are rapidly formed in the engine or in the plume [Fahey *et al.*, 1995a, b; Anderson [personal communication]; Schumann, 1996; Whitefield *et al.*, 1996]. The creation of numerous small particles, rather than condensation of aircraft-emitted SO<sub>2</sub> onto existing large particles, will result in greater ambient aerosol surface area for catalyzing heterogeneous chemistry. In order to quantify the surface area of the aircraft-derived aerosol, a rather complete understanding of the sulfur oxidation, gas/particle condensation, and particle coagulation and agglomeration processes is required. The dynamical details of the wake break-up dictated by wind shear and ambient turbulence, as exemplified by Lewellen and Lewellen [1996], may be expected to have a strong influence on the impact of the various competing microphysical processes.

Currently, a major difficulty exists in understanding quantitatively the process of plume sulfur oxidation. In particular, relating inferred particle mass of the small particles to percentages of oxidized fuel sulfur remains problematic; a number of measurements indicate that greater than 10% of the fuel sulfur is converted to sulfate while plume models predict that only 1 to 2% of the sulfur should be oxidized in the plume/wake. Large sulfate conversions have been observed behind the Concorde [Fahey *et al.*, 1995a, b] and behind a number of subsonic aircraft sampled during the recent SUBsonic aircraft: Contrail Cloud Effects Special Study (SUCCESS) mission [Miake-Lye, personal communication]; Anderson, personal communication]. Work is underway to identify the mechanism for rapid sulfate production. The possibilities include heterogeneous oxidation on particles in the plume and SO<sub>3</sub> production in the engine. The global-scale implications of the higher levels of sulfur conversion are discussed in Section 3.2.1.5.

Regardless of their initial size, particles produced in aircraft plumes may serve as nucleation sites for water and ice clouds, which in turn affect the Earth's radiation budget. The frequent occurrence of visible contrails attests to the importance of near-field nucleation processes. Furthermore, clear differences are observed in exhaust emission particle size distributions, particularly in the small size regime, between those measured immediately behind the engine exhaust nozzle and those measured *in situ* several kilometers back in the plume [Hagen *et al.*, 1994; Hagen and Whitefield, 1996]. However, relating the genesis of cloud droplets to specific exhaust species has proven to be challenging because exhaust particles have varying abilities to form droplets when exposed to increasing relative humidity. Particles that form droplets at high water supersaturation are classified generally as condensation nuclei (CN), however, under typical upper troposphere conditions it is the small subset of particles that can deliquesce (i.e., become liquid by absorbing moisture from the air) at humidities with respect to water that are less than unity, termed cloud condensation nuclei (CCN), that play a critical role in cloud formation. Another subset of particles called ice nuclei (IN), on which vapor may be deposited directly in the solid form or which nucleate ice in supercooled droplets, may play an important role in cirrus cloud formation under some temperature and humidity conditions.

In general, soot is hydrophobic and a poor candidate for cloud or ice nucleation. However, aviation fuel contains varying amounts of sulfur, which is oxidized to form H<sub>2</sub>SO<sub>4</sub>. Laboratory

studies show that this acid can be adsorbed onto the soot particles to increase their hydration potential [Rogaski *et al.*, 1996a; Wyslouzil *et al.*, 1994]. In support of this notion, Hagen *et al.* [1992] report that, in ground sampling of exhaust from turbo-prop engines on a King Air aircraft, particles selected from the peak of the soot distribution (34 nm) contained about 10% soluble mass fraction indicating significant soot hydration. The same researchers report similar soluble mass fractions for aerosols sampled in aircraft plumes at cruise altitudes [Schumann, 1995]. This is consistent with laboratory measurements made by the same group [Whitefield *et al.*, 1993], but at odds with *in situ* observations by others. For example, the Whitefield *et al.* [1993] laboratory flame experiments indicate that about 35% of jet exhaust particles have sufficient hydration properties to be effective CCN at 1% supersaturation. In contrast, for similar supersaturations, Hudson *et al.* [1991], found CCN/CN ratios of <1% in smoke from open combustion of JP-4 fuel and Pitchford *et al.* [1991] measured a ratio of about 1% in the near-field exhaust plume of a Sabreliner aircraft at 2600 m altitude. Likewise, Busen and Schumann [1995] observed no visible difference between the contrails of two engines burning low (2 ppmv) and normal (250 ppmv) levels of sulfur. These observational differences may be due to variations in sampling technique/instruments or flame/engine operating conditions (i.e., ambient vs. high pressures), but could also arise from differences in meteorological conditions and/or in fuel sulfur content [Whitefield *et al.*, 1993], which would affect the formulation of sulfuric acid particles from homogeneous binary nucleation. Uncertainties in the understanding of near-field nucleation processes likely translate to uncertainties in the climatic effects of aircraft exhaust on clouds. Discussion of these larger-scale radiative forcing effects is presented in Section 3.2.3.

## 3.2 Regional and Global-Scale Effects

Following dispersal of an aircraft plume and wake, the exhaust species act to enhance ambient levels of gases and particles and contribute to, or modify, ongoing chemical and radiative transfer processes. The degree to which aircraft exhaust can exert an influence on the atmosphere is largely determined by the magnitude of the perturbations to ambient levels and the effects of those perturbations on critical chemical and/or climatic processes. Specific locations of aircraft emissions are also important as indicated by the significant difference in residence time between the upper troposphere and lower stratosphere (a few weeks vs. a year or more). In the following subsections we examine the current understanding of aircraft effects on the regional and global-scale. Unless otherwise stated, the effect is from simple dilution of the aircraft exhaust to the global (or model grid) scale assuming that no chemical conversion has taken place in the wake.

### 3.2.1 PERTURBATIONS TO AMBIENT LEVELS

#### 3.2.1.1 NO<sub>x</sub>

The primary form of the nitrogen oxides emitted to the atmosphere is NO. NO is an important exhaust product from all forms of combustion including fossil fuel and biomass and is generated from bacteria in soils as well as by electrical activity in the atmosphere. Once in the atmosphere NO undergoes rapid interconversion with NO<sub>2</sub>; the sum of these two species is referred to as NO<sub>x</sub> (NO<sub>x</sub> = NO + NO<sub>2</sub>). The photochemical balance between NO and NO<sub>2</sub> favors NO during the daytime and NO<sub>2</sub> during the nighttime. Although other forms of nitrogen are also released from the earth's surface (e.g., N<sub>2</sub>O, HCN, NH<sub>3</sub>), it is primarily NO<sub>x</sub> that impacts ozone in the

troposphere [Haagen-Smit, 1951; Crutzen, 1979; Davis *et al.*, 1996]. Since  $\text{NO}_x$  is a key constituent in ozone formation, it is imperative that its atmospheric sources, fate and chemistry be well understood. This has been a difficult task because of the extreme variety of its sources and the intricacies of chemical reactions that describe its fate. For example,  $\text{NO}_x$  emitted to the atmosphere is slowly converted to species such as PAN,  $\text{HNO}_3$ , peroxyntic acid ( $\text{HNO}_4$ ),  $\text{N}_2\text{O}_5$ ,  $\text{RNO}_3$ , organic pernitrate ( $\text{RNO}_4$ ), and aerosol nitrate [Singh, 1987; Roberts, 1995]. A full understanding is made further difficult by the fact that many of these products are hard to measure, have varying lifetimes, and under certain conditions can act as reservoirs that provide secondary sources of  $\text{NO}_x$ .

Table 3-2 provides a compilation of source strength estimates for  $\text{NO}_x$ . Of the total of about 45 Tg  $\text{N yr}^{-1}$  (1 Tg =  $10^9$  kg) injected into the atmosphere, some 85% is injected near the surface of the earth. Because of rather active chemistry and fast removal in this region, only a small fraction of the surface emissions make it into the upper troposphere (UT). The major direct sources of UT  $\text{NO}_x$  are from lightning and aircraft emissions. Aircraft emissions of  $\text{NO}_x$  are reasonably well characterized, while the amount of  $\text{NO}_x$  produced by lightning is poorly defined. Approximately 44% of all  $\text{NO}_x$  emissions from aircraft occur in the 40 to 60°N latitude band. Emissions between 9- to 13-km altitudes in this latitude band account for 27% of global  $\text{NO}_x$  emissions from aircraft.

As is evident from Table 3-2, one of the most uncertain sources of  $\text{NO}_x$  is from electrical discharges (lightning) with recent estimates (since 1989) ranging from 1 to 220 Tg  $\text{N yr}^{-1}$ . Recent reanalyses of old data and new satellite flash count information have been used to conclude that the magnitude of this source is likely to be between 2 to 12 Tg  $\text{N yr}^{-1}$  but cannot be better quantified at this time [Price *et al.*, 1996; Price and Rind, 1992a, Kumar *et al.*, 1995; Levy *et al.*, 1996; Bradshaw *et al.*, 1996]. Any study of the  $\text{NO}_x$  injection into the UT from aircraft must be able to describe this seasonally and geographically highly variable source with reasonable accuracy. While there are significant uncertainties in the statistics of lightning flashes, the energies dissipated during cloud to cloud and cloud to ground discharges, and the  $\text{NO}_x$  produced per unit energy dissipated, it is likely that a large fraction of  $\text{NO}_x$  from lightning is injected in the middle to upper region of the troposphere. The overall understanding of the lightning source is further confounded by the fact that large lightning/cloud systems are typically associated with high vertical velocities resulting in the convective movement of surface emissions upwards to the middle and upper troposphere. Despite major uncertainties, it is likely that the lightning source of  $\text{NO}_x$  in the UT is 2 to 8 times as large as the aircraft source. However, much of lightning generated  $\text{NO}_x$  is distributed around the tropics with minimal impacts at mid-latitudes (except in summer), where the aircraft emissions are most pronounced. In summary, lightning, aircraft emissions, and deep convection provide significant sources of UT  $\text{NO}_x$ . Their amounts, and seasonal and geographical distributions are, however, subject to much uncertainty.

Observational attempts to identify and quantify sources of active nitrogen species in the troposphere nominally collect data on a large number of nitrogen-containing species such as NO,  $\text{NO}_2$ ,  $\text{HNO}_3$ , PAN,  $\text{NO}_y$ , and aerosol nitrate. Of all these species, NO is perhaps the most critical in ozone formation and the best measured [Davis *et al.*, 1996; Crosley, 1996]. In the UT  $\text{NO}_x$  is present mainly as NO ( $\text{NO} \approx 0.7 \times \text{NO}_x$  at 10 km) during the daytime. Other reactive nitrogen species play roles as sinks and reservoirs; in the latter role they sometimes can recycle active nitrogen [Singh and Hanst, 1981; Singh, 1987; Moxim *et al.*, 1996]. Figures 3-1 and 3-2 show some typical examples of NO vertical distributions measured in the troposphere, where NO mixing

ratios increase with altitude. It is also evident from these figures that NO abundance is extremely variable throughout the troposphere, but the variability is most pronounced just below the tropopause. A latitudinal distribution measured during the Pacific Exploratory Mission (PEM-West A) suggests that this phenomenon of higher NO aloft to be true throughout the troposphere (Figure 3-3). In one experiment (Figure 3-2), where cloudy conditions caused lightning as well as convection, somewhat higher but similarly distributed mean NO concentrations were observed [Ridley *et al.*, 1994]. Based on results from a number of NASA-sponsored missions, typical median NO concentrations in the UT are in the range of 50-200 parts per trillion by volume (pptv) [Bradshaw, 1996; Emmons *et al.*, 1996]. Larger NO concentrations have been observed in several instances, most notably during winter at high latitudes by a European-sponsored effort [Wahner *et al.*, 1994]. Identifying the causes of the high variability in UT NO levels is an important area of research. Certainly, episodic and inhomogeneous sources of NO such as lightning and large-scale convection of surface emissions deserve substantial scrutiny in this regard.

The relatively high concentrations of NO<sub>x</sub> in the UT compared to the lower troposphere are maintained as a result of a combination of factors including direct free tropospheric sources such as lightning, and the slow removal of NO<sub>x</sub>, resulting in a relatively long lifetime (3 to 10 days). Data from PEM-West A and Transport and Atmospheric Chemistry near the Equator-Atlantic (TRACE-A) demonstrate that the large surface source is not always the major contributor to UT NO<sub>x</sub> concentrations. This conclusion is based on comparison of species with differing atmospheric lifetimes. Figure 3-4 shows a plot of the NO<sub>x</sub>/propane (C<sub>3</sub>H<sub>8</sub>) ratio as a function of air mass age, indicated by the acetylene (C<sub>2</sub>H<sub>2</sub>)/CO ratio, with data segregated by altitude for the PEM-West A [Singh *et al.*, 1996]. C<sub>3</sub>H<sub>8</sub> has an essentially exclusive surface source (the aircraft source is insignificant by comparison) and a well defined lifetime that is always longer than that of NO<sub>x</sub>. In general, the NO<sub>x</sub>/C<sub>3</sub>H<sub>8</sub> ratio should be at its highest near the surface source regions and decline with time (and altitude) because of the shorter lifetime of NO<sub>x</sub>. Figure 3-4 shows that exactly the opposite is the case in the upper troposphere (7- to 12-km) in the Eastern Pacific during the PEM-West A where NO<sub>x</sub>/C<sub>3</sub>H<sub>8</sub> ratios are the largest. This is only possible if large amounts of NO<sub>x</sub> are being directly added into the upper troposphere from sources such as lightning, aircraft, or the stratosphere.

### 3.2.1.2 CO<sub>2</sub>, CO, and Hydrocarbons

Several carbon-containing gaseous species, namely, CO<sub>2</sub>, CO, and hydrocarbons (HC), are emitted from aircraft. Among these, the hydrocarbons and CO are the ones most likely to have an impact on O<sub>3</sub>/NO<sub>x</sub> chemistry, while CO<sub>2</sub> will contribute to positive changes in radiative forcing. The contribution of aircraft emissions to background levels of CO<sub>2</sub> is readily estimated because jet fuel usage is approximately 3% of total fossil fuel usage. The overall impact of anthropogenic activities on atmospheric levels of CO<sub>2</sub> has been identified through long-term records of atmospheric CO<sub>2</sub> concentrations [IPCC, 1994]. According to the data, atmospheric CO<sub>2</sub> has been increasing at approximately 1.2 ppm/year over the last 35 years. At this rate of increase, the atmospheric CO<sub>2</sub> concentration is expected to double relative to preindustrial levels by the year 2100 [IPCC, 1994]. The subsonic aircraft fleet is responsible for roughly 1.5% of the currently observed growth and figures to make a larger contribution over the coming decades.

CO and HC aircraft emissions are estimated to be 0.7 Tg yr<sup>-1</sup>, and 0.3 Tg yr<sup>-1</sup>, respectively, assuming that the military, charter, and former Soviet Union aircraft have emission indices at

cruise conditions similar to those of scheduled aircraft (as given in Chapter 2). Engine exhaust studies show that a predominant fraction of the HC emissions are in the form of non-methane hydrocarbons (NMHC) (engines appear to be net sinks of ambient CH<sub>4</sub>). Emission fluxes of NMHCs and CO from other sources have been estimated to be of order 600 Tg C yr<sup>-1</sup> and 2500 Tg C yr<sup>-1</sup>, respectively [WMO, 1995]. Compared to the other sources, aircraft emissions could perturb the UT air composition by <1 ppbv CO, and <0.1 ppbv NMHC. The perturbation to the background of CO is small, but may be significant for specific NMHCs depending upon the partitioning of emissions. Spicer *et al.* [1994] have shown, for a few engines, that a wide variety of NMHCs are produced. Unfortunately, there are very little data on either engine NMHC emission speciation or source strengths of higher molecular weight (>C<sub>3</sub>) species on which to base estimates.

### 3.2.1.3 H<sub>2</sub>O

Aircraft release 1.25 kg of water vapor for every kg of fuel burned [Lee *et al.*, 1994]. Given that 1.36 x 10<sup>11</sup> kg of fuel were burned in 1992 (see Table 2-3), aircraft are emitting 1.67 x 10<sup>11</sup> kg of water each year. This can be compared to the tropospheric background water vapor mass of about 10<sup>16</sup> kg, or the background water vapor at the height of maximum aircraft emissions (12 km) of about 10<sup>14</sup> kg. Because the water vapor loading due to aircraft is small, the direct radiative effects are expected to be small (see Section 4.3.2.2). However, as described in Section 3.1 and further in Section 3.2.3.2, local enhancements of water vapor in the wake and plume can be sufficient to achieve ice or liquid water saturation and initiate cloud formation. It is these perturbations of cloud cover that may have the greatest potential for affecting the atmosphere.

### 3.2.1.4 Soot

As discussed in Section 2.1.2, aircraft emit large numbers of soot-containing particles. Using the 1992 aviation emission statistics given in Chapter 2, and assuming that aircraft engines produce between 0.03 g and 0.4 g of soot per kg of fuel burned, we calculate that aviation sources are responsible for introducing 0.4 to 5.4 x 10<sup>7</sup> kg per year soot to the atmosphere. In terms of the global budget, recent estimates derive values between 10 and 15 Tg for emissions of black carbon in the form of soot and charcoal emitted into the atmosphere each year by charring of organic matter during combustion or by condensation from the gas phase in reducing flames [Andreae, 1995; Cooke and Wilson, 1996; Lioussé *et al.*, 1996]. Thus, in the worst case, aircraft are only responsible for <0.5 % of the total global soot emissions. However, the majority of carbonaceous aerosol sources (e.g., biomass burning, coal burning, and diesel fuel use) are surface based and may not contribute effectively to upper troposphere/lower stratosphere aerosol burdens. For example, smoke from the Kuwaiti oil fires did not present a global pollution problem because most of the particulate matter was removed regionally from the plumes by gravitational settling and precipitation scavenging [Hudson and Clarke, 1992; Limaye *et al.*, 1992]. Aircraft soot emissions, on the other hand, are concentrated at altitudes >9 km and are expected to be much longer lived, indeed, possibly >1 year for stratospheric release. Based on these long residence times, Pueschel *et al.* [1992] estimated that all the black carbon aerosol (BCA) present in the stratosphere can be accounted for by aircraft emissions, assuming a soot EI of 0.1 g kg<sup>-1</sup> fuel burned and 10% of all commercial aircraft mileage is accumulated above the tropopause. Blake and Kato [1995] reported black carbon aerosol concentrations in the upper troposphere and lower

stratosphere from 90°N to 45°S. Measured soot concentrations were found to be strongly correlated with latitude vs. altitude aircraft fuel consumption data [Baughcum *et al.*, 1993b] and ranged from a high of 3.35 ng m<sup>-3</sup> in the North Atlantic air corridor to <0.15 ng m<sup>-3</sup> in the South Pacific. BCA residence times in the stratosphere were calculated to be between 4 months and 1 year. If this estimate is valid, stratospheric burdens can be expected to increase in direct proportion to the amount of air traffic routed above the tropopause. However, because carbonaceous aerosol presently accounts for about 0.01% of stratospheric aerosol loading [Pueschel *et al.*, 1992], doubling of emissions should not significantly effect heterogeneous chemical processing within the region, though it may, as discussed later, have some measurable impact upon radiative budgets, and perhaps on the probability of freezing of the stratospheric sulfate aerosol.

Based upon *in situ* measurements, Anderson [personal communication]; Schumann [1995]; and Whitefield *et al.*, [1996] report that commercial airliners emit from 0.2 to 5 x 10<sup>15</sup> nonvolatile (presumably soot) particles per kg of fuel burned. Using the 1992 aviation fuel consumption statistics (Table 2-3) and assuming that 50% of the fuel is burned within the 9- to 12-km height regime (i.e., where cirrus cloud typically form), we calculate that aviation is responsible for injecting from 0.4 to 9 x 10<sup>23</sup> soot particles into the upper troposphere each day. Assuming that the particles have a 10-day lifetime at these elevations and that one-third of them become coated with sulfuric acid to form active CCN (i.e., particles that will become liquid by absorbing moisture from the air at humidities with respect to water that are less than unity), we find that aviation emissions enhance upper tropospheric CCN concentrations by globally-averaged amounts of 0.1 to 2.0 cm<sup>-3</sup>. Because background CCN concentrations are typically on the order of a hundred per cubic centimeter [Clarke, 1993; Hofmann, 1993], the aircraft enhanced values, in general, represent only a small fraction of the CCN present within the upper troposphere. However, because background aerosols as well as aircraft routes are not uniformly distributed in space, aircraft emissions may approach levels that are locally significant. For example, Hoinka *et al.* [1993] estimate that between 1989 and 1991, aircraft burned an average of 16.6 x 10<sup>6</sup> kg fuel day<sup>-1</sup> in the upper troposphere/lower stratosphere over the North Atlantic within a box defined by 45°N to 65°N latitude and 10°W to 60°W longitude. Adopting the statistics and assumptions provided above, this translates to aviation-related enhancements in CCN densities within the 9 to 12 km altitude regime of the region of 0.7 to 14 cm<sup>-3</sup>, which is 7 times our estimate of the global average. A doubling of air traffic within this corridor may thus have some quantifiable impact upon cloud processes. *In situ* measurements in and around the North Atlantic flight corridor provide clear evidence of this non-uniformity of aircraft emission distributions [Schumann, 1996].

### 3.2.1.5 Sulfate

In addition to coating the soot particles, the H<sub>2</sub>SO<sub>4</sub>(v) produced from jet fuel combustion can, because the atmosphere is generally saturated with respect to this species, undergo binary homogeneous nucleation with water to form new particles [Reiner and Arnold, 1993]. Indeed, model calculations suggest that this process is energetically favored over the heterogeneous condensation of H<sub>2</sub>SO<sub>4</sub> upon existing soot particles [Miake-Lye *et al.*, 1994]. Moreover, aircraft exhaust particle size distributions recorded at cruise altitudes and after the emissions have cooled to near ambient temperature generally show copious numbers of fine and ultrafine aerosols filling in the distribution at sizes below the reported soot peak of 30 to 60 nm (Figure 3-5). These aerosols are volatile at <300°C (as are sulfuric acid particles), are 10 to 100 times more abundant than the

nonvolatile (soot) exhaust particles and their size appears to be highly dependent upon ambient temperature and humidity, all of which suggests they are likely composed of H<sub>2</sub>SO<sub>4</sub> [Schumann *et al.*, 1996; Miake-Lye, personal communication; Anderson, personal communication]. Further evidence for this argument are the observations by Schuman *et al.* [1996] and Miake-Lye [personal communication] that the number density of volatile particles in aircraft exhaust vary proportionally with the fraction of sulfur contaminant contained in the fuel (Figure 3-6).

Although most of the SO<sub>2</sub> released by aircraft combustion is eventually removed from the atmosphere by heterogeneous processes, it is difficult to quantify the fraction of fuel sulfur immediately sequestered into particles during the jet exhaust/wake vortex regime. Aviation turbine fuel specifications [ASTM, 1996] allow Jet-A fuel to contain up to 3000 ppm by mass of sulfur. Prather *et al.* [1992] surveyed fuels from a number of sources and found the sulfur contents to range from 100 to 2000 ppm and to contain an average of 420 ppm, which represents an EI of 0.42 g (S) kg<sup>-1</sup> fuel burned. Model studies suggest a maximum of 1% of the SO<sub>2</sub> produced in jet combustion reacts with OH in the jet exhaust/wake regime to form H<sub>2</sub>SO<sub>4</sub>. If this vapor immediately condenses to form—based on the size constraints placed on the particles by the measurements of Fahey *et al.* [1995a, b]—nominal 16 nm diameter particles of 70% weight fraction H<sub>2</sub>SO<sub>4</sub>, we estimate that aircraft should produce an average of 3.6 x 10<sup>15</sup> particles kg<sup>-1</sup> fuel burned. By comparison, emission indices of 5 to 500 x 10<sup>15</sup> volatile (presumably sulfuric acid) particles kg<sup>-1</sup> fuel have been observed in aircraft plumes within the upper troposphere and lower stratosphere [Fahey *et al.*, 1995a, b; Miake-Lye, personal communication; Anderson, personal communication] (e.g., Figure 2-3). Clearly, the models are missing some relevant details regarding the oxidation of fuel sulfur in jet engines.

The effect of aircraft sulfate aerosol emissions upon atmospheric processes (e.g., cloud processes, heterogeneous chemistry, and radiation transfer) depends upon the equilibrium size and number density of the particles. For the newly formed, small diameter, exhaust particles the direct extinction of solar radiation is expected to be negligible in comparison to that of contrails (see Section 3.2.3). And, although the presumed 16 nm diameter particles observed by Fahey *et al.* [1995a, b] and others [Miake-Lye personal communication; Anderson, personal communication] in young aircraft plumes represent a fairly large total surface area and may influence heterogeneous processes in the upper troposphere and lower stratosphere (see Section 3.2.2.3), they are, in general, too small to affect cloud formation and microphysical processes. However, *in situ* observations suggest that as jet engine emissions age, the volatile CN coagulate to form particles as much as twice as large [Hagen *et al.*, 1996] which are, in turn, much more effective CCN.

Doubling the particles' size to produce CCN effectively reduces their number by eight-fold. Thus, the observed emission indices of 5 to 500 by 10<sup>15</sup> CN kg<sup>-1</sup> fuel burned [Fahey *et al.*, 1995a, b; Miake-Lye, personal communication; Anderson, personal communication] translate into 0.6 to 60 x 10<sup>15</sup> CCN kg<sup>-1</sup> fuel burned. Following the same arguments as presented above for soot particles, we estimate that aircraft introduce 0.1 - 10 x 10<sup>24</sup> new particles into the 9- to 13-km height band each day, which, assuming a 10 day atmospheric lifetime, results in a globally averaged CCN enrichment of 0.8 - 77 cm<sup>-3</sup>. An enhancement of 5 to 500 cm<sup>-3</sup> is calculated for the North Atlantic region described above. Because background CN/CCN concentrations are typically several hundred to a few thousand cm<sup>-3</sup> [Clarke, 1993; Hofmann, 1993] these enhancements could have a significant impact on cloud microphysics and heterogeneous chemistry in the upper troposphere/lower stratospheric region.

The above estimates of aircraft particle emissions and their impact upon atmospheric properties is highly speculative due to the scarcity of data regarding, for example, aerosol size distributions and emission indices under typical flight conditions, the fraction of aircraft exhaust soot particles which become active as CCN, and the relative loading of CN and CCN in the background air due to other processes. Clearly, focused research is needed to reduce these uncertainties and to improve our understanding of heterogeneous chemistry and aerosol physical processes in the atmosphere.

### 3.2.2 OZONE CHEMISTRY

#### 3.2.2.1 Ozone Tendencies Relative to NO<sub>x</sub>

The photochemistry of ozone in the troposphere is initiated by the ultraviolet (UV) photolysis of ozone at wavelengths <315 nm via the formation of a highly reactive photofragment O(<sup>1</sup>D). Most of the O(<sup>1</sup>D) is collisionally deactivated by molecular nitrogen (N<sub>2</sub>) and/or molecular oxygen (O<sub>2</sub>) to its ground state (O(<sup>3</sup>P)) and subsequently reconverted to ozone.



A very small fraction of the O(<sup>1</sup>D), however, reacts with water vapor to generate hydroxyl radical (OH), an important oxidizing species in the atmosphere. In the presence of sufficient levels of NO OH readily reacts through a series of reactions involving HCs to produce peroxyradicals (HO<sub>2</sub>, RO<sub>2</sub> where R = alkyl group). The resulting peroxyradicals react further to form NO<sub>2</sub> via:



NO<sub>2</sub> is then rapidly photolyzed to form O(<sup>3</sup>P) which readily converts to ozone. In the presence of HCs and CO more than one peroxyradical can be generated for each primary OH and an accumulation of ozone can take place via this amplification. There are also processes that destroy ozone and peroxyradicals and these can become dominant under NO-poor conditions.



Based on the above chemistry, the net rate of ozone production (P(O<sub>3</sub>)) can be expressed as a difference between its formation and destruction rates, depending on the relative sizes of the formation and destruction mechanisms.

$$P(O_3) = \{k_5[HO_2] + k_6[RO_2]\}[NO] - \{k_2[O(^1D)][H_2O] + k_7[HO_2][O_3] + k_8[OH][O_3]\} \quad (A)$$

It is clear from equation (A) that NO is a primary species in the formation of ozone and the net rate of ozone production can be positive or negative.

Figure 3-7 is used to illustrate this point for the region of 50°N in July at 10 km altitude (note: a similar calculation is performed in Section 4.2.2.1 as a test of model treatments of chemical mechanisms). The Y-axis shows the net ozone production rate [P(O<sub>3</sub>)] as a function of NO<sub>x</sub> under a variety of assumed conditions stated in the legend. Below a certain NO<sub>x</sub> threshold (150 to 300

pptv), P(O<sub>3</sub>) increases with increasing NO<sub>x</sub>; a minimum of about 15 pptv NO<sub>x</sub> is required for net ozone production to occur. After reaching a peak, P(O<sub>3</sub>) declines as NO<sub>x</sub> further increases. This decline is largely precipitated by the fact that NO<sub>x</sub> itself becomes an effective sink of free radicals and odd oxygen via reactions such as



Figure 3-7 is derived from a model using constant background conditions. In reality changes in NO<sub>x</sub> concentration are associated with changes in other species (e.g., NMHC, H<sub>2</sub>O, PAN) that have an effect on ozone production. Figure 3-8 shows a plot of instantaneous P(O<sub>3</sub>) vs. NO<sub>x</sub> for the actual field conditions observed over the Pacific during PEM-West A (September/October 1992). The data in Figure 3-8 are restricted to 30-40°N latitude, 10- to 12-km altitude and a solar zenith angle of 30 to 60° (peak daytime). Although the data are limited, it appears that P(O<sub>3</sub>) continues to increase up to the highest levels of NO<sub>x</sub> measured (i.e., 400 pptv).

As shown in Figures 3-1 and 3-2, NO<sub>x</sub> mixing ratios typically rise with altitude in the troposphere with mean mixing ratios of 100 to 200 pptv occurring in the upper troposphere (10- to 12-km). However, larger abundances are frequently encountered. These higher levels are often associated with lightning or lofting of pollutants from the surface during periods of convection. For example, the upper altitude mixing ratios exceeding 1 ppbv of NO that are shown in Figure 3-2 were due to lightning activity. To the extent that the background UT is poorly characterized and studied, it is hard to predict the sign of ozone response to an addition of UT NO<sub>x</sub> from subsonic aircraft. It is likely, however, that the background tropospheric NO<sub>x</sub> levels are generally low enough that addition of NO<sub>x</sub> would tend to enhance the net production rate of ozone. One consequence of the non-linear ozone response to NO is that 2-D models that zonally average the NO<sub>x</sub> concentrations may have difficulty predicting the correct ozone response. Further discussion of model capabilities is given in Chapter 4.

### 3.2.2.2 Role of Non-Methane Hydrocarbons

As illustrated in the last section, the ozone response to NO<sub>x</sub> perturbations is linked to alkylperoxy (RO<sub>2</sub>) and hydroperoxy (HO<sub>2</sub>) radical reactions. Aircraft exhaust is known to contain a large number of C<sub>2</sub> to C<sub>17</sub> species, although the relative amounts are not well established [Spicer *et al.*, 1994]. Depending on their abundances, highly reactive aircraft NMHCs could suppress OH concentrations and sequester NO<sub>x</sub> in the form of organic nitrates and pernitrates (RNO<sub>3</sub>, RNO<sub>4</sub>, RCO<sub>3</sub>NO<sub>2</sub>) thereby influencing the NO<sub>x</sub>/HO<sub>x</sub> chemistry of the UT [Singh and Hanst, 1981; Roberts, 1995]. Although the impact of NMHCs from subsonic aircraft emissions is likely to be small, no serious effort to accurately simulate these effects has been undertaken to date. A model sensitivity study on NMHC chemistry is included in Section 4.2.3.2.

### 3.2.2.3 Heterogeneous Chemistry

Heterogeneous interactions of gas-phase species with aerosol and cloud particles can modify the partitioning of chemical families and affect the removal of soluble species. In addition, aircraft emissions, such as H<sub>2</sub>O, SO<sub>x</sub> and NO<sub>x</sub>, may change the composition and surface area of existing

aerosol and cloud particles or provide new kinds of surfaces, such as soot, that might support heterogeneous reactions.

Because  $\text{NO}_x$  injection from aircraft is potentially a large chemical perturbation to the upper troposphere, heterogeneous reactions that repartition the nitrogen family will play a role in determining the overall impact. The hydrolysis of  $\text{N}_2\text{O}_5$ ,



which has been characterized in the laboratory, converts an easily photolyzed  $\text{NO}_x$  reservoir species into a more stable species that is subject to wet removal processes. Calculations by Dentener and Crutzen [1993] showed that including the hydrolysis of  $\text{N}_2\text{O}_5$  on tropospheric aerosol particles significantly decreases the concentration of  $\text{NO}_x$ , by as much as 50% on a yearly global average basis. This brings the calculated  $\text{NO}_x$  concentrations and nitrate wet deposition amounts into better agreement with observations. The current assessment models include the hydrolysis of  $\text{N}_2\text{O}_5$ . As discussed in Section 4.2.3.2, Case 5, including this reaction slightly increases the sensitivity of the ozone response to aircraft emissions by reducing the background concentration of  $\text{NO}_x$ .

Lack of knowledge about the composition of upper tropospheric aerosols and about whether composition effects heterogeneous reaction rates introduces some uncertainty into the assessment of subsonic aircraft impacts. Particles collected on wire impactors in the upper troposphere are predominately (91-94%) sulfur-containing [Pueschel *et al.*, 1994; Sheridan *et al.*, 1994], and mostly (>70%) volatile [Hofmann, 1993; Clarke, 1993]. Sulfate aerosol in the troposphere is partially neutralized by ammonium; the degree of neutralization decreases with altitude because ammonium sources are mainly ground-based. Volatility measurements on upper tropospheric aerosol have been utilized to provide an estimate of the  $\text{NH}_4^+/\text{SO}_4^-$  molar ratio of 0.1 to 0.3 (0 indicates sulfuric acid and 1 indicates ammonium bisulfate,  $\text{NH}_4\text{HSO}_4$ ) [Clarke, 1993]. In the lower free troposphere, chemical analysis indicates a molar ratio closer to 1 [Huebert and Lazrus, 1980].

The Dentener and Crutzen model [1993] assumes that all tropospheric aerosol is ammonium bisulfate and uses an uptake coefficient for the hydrolysis of  $\text{N}_2\text{O}_5$  of 0.1, independent of temperature. This uptake coefficient is based on laboratory measurements taken on cold, concentrated sulfuric acid solutions representative of stratospheric sulfate aerosol. Recent laboratory work suggests that the uptake coefficient is in the range of 0.02 to 0.04 at room temperatures on ammonium sulfate and dilute sulfuric acid surfaces representative of boundary layer tropospheric aerosols [Hu *et al.*, 1996]. Presumably, the uptake coefficient on upper tropospheric aerosols lies between these limits. However, this may represent a minor adjustment to model calculations. A sensitivity analysis conducted by Dentener and Crutzen [1993] using an uptake coefficient of 0.01 produced only small changes to the calculated  $\text{NO}_x$  concentrations.

Ice particles in cirrus clouds may provide a substrate for heterogeneous reactions, such as the hydrolysis of  $\text{N}_2\text{O}_5$  or the reactions that activate chlorine on polar stratospheric cloud (PSC) particles. They may also provide a sink for  $\text{NO}_y$  species such as  $\text{HNO}_3$  and  $\text{HNO}_4$  [Li *et al.*, 1996]. Whether the chlorine reactions play a role in the upper troposphere depends on the availability of the stratospheric chlorine reservoirs hydrogen chloride (HCl) and chlorine nitrate ( $\text{ClONO}_2$ ) which in turn depends on the exchange of air between the stratosphere and troposphere, a poorly understood atmospheric process. Heterogeneous reactions on cirrus cloud particles are not

included in models because the surface area of cirrus clouds is not well known. In addition, increasing cirrus cloud coverage due to aircraft is poorly quantified (see Section 3.2.3.4), making the assessment of this particular aircraft impact difficult.

Other heterogeneous reactions besides the hydrolysis of  $\text{N}_2\text{O}_5$  may affect the chemistry of the upper troposphere but are not well enough characterized to be included in models. In particular, inorganic free radicals, such as nitrogen trioxide ( $\text{NO}_3$ ) and  $\text{OH}$ , are important oxidants in the aqueous phase.  $\text{NO}_3$  reacts quickly with  $\text{Cl}^-$ ,  $\text{OH}^-$ , and  $\text{HSO}_3^-$  in solution, and these reactions may affect  $\text{HO}_x$  levels and sulfur conversion [Exner *et al.*, 1992]. The mass accommodation coefficients for  $\text{OH}$  and  $\text{HO}_2$  on sulfuric acid solutions have been measured to be large ( $>0.2$ ) and this uptake may promote condensed phase chemistry as well as providing a sink for gas-phase  $\text{HO}_x$  [Cooper and Abbatt, 1996; Hanson *et al.*, 1992]. Experiments on reactions of  $\text{SO}_4^-$  have shown that the reaction rate increases rapidly with increasing ionic strength, and these results have been explained with an ion-pair model [Bao and Barker, 1996]. Although concentrations of  $\text{SO}_4^-$  are low in the atmospheric condensed phase, the effect of high ionic strength on reaction rates may need to be considered.

The direct injection of soot particles by aircraft into the upper troposphere and lower stratosphere provides surfaces that may catalyze heterogeneous reactions both in the near-field and in the atmosphere at large. In the near-field, the observation of visible contrails implies that some fraction of soot particles serve as nucleation sites for water-based aerosols [Kärcher *et al.*, 1996]. The mechanism for activation of the initially hydrophobic soot surface for water uptake is not yet understood. Laboratory experiments have shown that the adsorption of  $\text{H}_2\text{SO}_4$  on soot allows hydration to occur [Wyslouzil *et al.*, 1994; Rogaski *et al.*, 1996a]. But, the calculated gas-phase concentration of  $\text{H}_2\text{SO}_4$  in the near-field is not high enough to yield the requisite soluble mass fraction [Kärcher *et al.*, 1996], although field measurements indicate that the plume models underestimate  $\text{SO}_2$  to  $\text{H}_2\text{SO}_4$  conversion [Anderson, personal communication]. Other suggestions of soot activation by heterogeneous interactions with  $\text{SO}_2$  or  $\text{HNO}_3$  [Kärcher *et al.*, 1996] are not consistent with laboratory measurements of low uptake coefficients [Rogaski *et al.*, 1996a].

In the laboratory, the reaction of  $\text{HNO}_3$  on soot has been observed to produce  $\text{NO}$  and  $\text{NO}_2$  [Rogaski *et al.*, 1996b] and possibly provides a heterogeneous mechanism for converting  $\text{NO}_y$  back into  $\text{NO}_x$ . This reaction, along with the reaction of  $\text{NO}_2$  on soot to produce  $\text{NO}$  [Tabor *et al.*, 1993; Rogaski *et al.*, 1996a], has been suggested to significantly increase ambient  $\text{NO}_x$  [Lary *et al.*, 1997]. These reactions counteract the hydrolysis of  $\text{N}_2\text{O}_5$  and may increase the impact of  $\text{NO}_x$  injection by aircraft. However, one important issue needs to be resolved. Soot particles in the atmosphere collide with gas-phase species and undergo coagulation with aerosol particles and may not support the heterogeneous chemistry observed on clean soot surfaces in the laboratory. For example, soot particles collected on wire impactors in the lower stratosphere tend to have sulfate coatings, although soot collected in the upper troposphere does not [Sheridan *et al.*, 1994].

A small percentage of subsonic aircraft emissions, on the order of 17% [Baughcum, 1996b], are injected directly into the lower stratosphere. One issue is whether  $\text{NO}_x$  and  $\text{SO}_x$  emitted from aircraft can enhance the activation of stratospheric chlorine. Laboratory studies have found that the reaction of  $\text{HCl}$  and  $\text{HNO}_2$  on sulfate aerosols may provide a significant chlorine activation mechanism [Zhang *et al.*, 1996]. However, a quantitative evaluation of this mechanism requires a detailed understanding of the plume evolution of  $\text{HNO}_2$  and sulfate particles.

Another issue is whether the direct injection of water vapor,  $\text{NO}_x$ , and particles by aircraft into the lower stratosphere will increase the temporal and geographical extent of PSC formation or the fraction of PSCs with NAT or ternary composition, thus increasing the surface area available for or rates of heterogeneous activation of ozone destroying species. Because the microphysics of PSC formation is not well understood, and because 2-D representations do not easily accommodate zonally variable effects such as clouds, assessment models for the supersonic fleet are only just starting to include PSCs [Consideine *et al.*, 1996]. Sensitivity studies with simplified PSC parameterizations based on temperature thresholds show that HSCT emissions increase the surface area and time duration of PSCs [Stolarski *et al.*, 1995]. 2-D models which include microphysical representations of PSC formation also show increases in PSC surface area, for example, by as much as 40% in the winter Northern Hemisphere [Pitari *et al.*, 1993; De Rudder *et al.*, 1996; Tie *et al.*, 1996]. Increased PSC surface area leads to more chlorine-catalyzed ozone destruction in polar regions, but also reduces the sensitivity of ozone levels to HSCT perturbations by removing  $\text{NO}_y$  [Stolarski *et al.*, 1995]. Further modeling work on PSC microphysics will reduce the uncertainty in these predictions.

Some of the difficulty in parameterizing PSCs arises from the numerous open questions in understanding PSC microphysics. Even the composition of Type I (non-water ice) PSCs is currently a subject of debate. Originally thought to be nitric acid trihydrate (NAT), observational evidence suggests that some Type I PSCs may be ternary  $\text{H}_2\text{SO}_4/\text{HNO}_3/\text{H}_2\text{O}$  solutions [Dye *et al.*, 1992; Toon and Tolbert, 1995]. In addition, although NAT is the thermodynamically favored composition, nitric acid dihydrate has a lower activation energy for homogeneous nucleation and may be more likely to form in the stratosphere [Worsnop *et al.*, 1993; Dasselkamp *et al.*, 1996]. The composition of Type I PSCs determines their vapor pressure and thus affects modeling of the partitioning between gas and condensed phase for species such as  $\text{HNO}_3$  and  $\text{H}_2\text{O}$ . Moreover, real atmosphere PSCs are likely complicated non-equilibrium phenomena containing a number of  $\text{HNO}_3$  -  $\text{H}_2\text{O}$  -  $\text{H}_2\text{SO}_4$  mixtures.

The mechanism of PSC formation is also a topic of laboratory research. Type I PSCs were formerly thought to condense on frozen sulfate aerosol particles. However, laboratory experiments have shown that neither sulfuric acid solutions nor ternary solutions are likely to freeze under Type I PSC conditions [Anthony *et al.*, 1995, 1996; Beyer *et al.*, 1994; Koop *et al.*, 1995; Carleton *et al.*, 1996], and that, if frozen, sulfuric acid does not nucleate NAT [Iraci *et al.*, 1995]. The issue of crystalline PSC formation remains unresolved and suggests that microphysical models may need to be modified in the future. Although the specific mechanism of PSC formation is important for gas/condensed phase partitioning, it may not be critical for chlorine activation.

#### 3.2.2.4 Ozone Trends

Although models have been extensively used to estimate the perturbation to UT  $\text{NO}_x$  and  $\text{O}_3$  from subsonic emissions, little direct evidence of  $\text{NO}_x$  or  $\text{O}_3$  increases from past and current aircraft fleets is available. Long-term records are not available for  $\text{NO}_x$  except in polluted locations but measurements of tropospheric ozone have been made since the late 1960s. Information on trends in ozone near the tropopause is available from ozonesonde stations, the majority of which are located at middle and high latitudes of the Northern Hemisphere. Measurements from Stratospheric Aerosol and Gas Experiments (SAGE) I and II provide trend information only above

15 km for mid-latitudes and above 18 km for the tropics [McCormick *et al.*, 1992; Wang *et al.*, 1996]. Trends derived from the sonde data are discussed in Logan [1994], Miller *et al.*, [1995], and Tarasick *et al.* [1995] and are reviewed in WMO [1995].

Figures 3-9 and 3-10 show O<sub>3</sub> trends as observed from long term surface and sonde data respectively. Detailed comparison of these datasets reveals substantial differences. For instance, large increases are found for two stations in Europe (~2% year<sup>-1</sup> throughout the troposphere for 1970-91), while there appears to be no long-term trend over Canada and only a small (<1% year<sup>-1</sup>) increase over the east coast of the United States in summer. In addition, increases are found only below 6 km at the Japanese stations. Most stations observe a trend shift since 1980. In particular, ozone values over Germany have leveled off since the early 1980s, there is no increase over the eastern United States since 1980, and the Canadian stations all show decreases in tropospheric ozone since 1980. These conclusions are unchanged with the inclusion of data up to December 1995 in the trend analysis [Logan, personal communication]. In summary, the following observations can be made:

- The sonde stations at middle and high latitudes show a decrease in ozone in the lower stratosphere, with a maximum trend of -0.8 to -1.2% year<sup>-1</sup> near 90 mbar from the early 1970s to 1991. The ozone decreases extend from about 30 mbar down to the tropopause.
- There are significant station to station variations in the trends in the troposphere. In the lower troposphere, there are indications of ozone increases over the past 25 years in parts of northern mid-latitudes, but the increase appears to have leveled off since the mid-1980s over Europe and the United States.
- During the period of 1970 to 1991, there are no systematic indications of ozone changes near the tropopause level (≈200 mbar) in the upper troposphere. The natural variability of ozone is highest near the tropopause leading to substantial uncertainty in the derived trends.

The lack of a discernible trend in UT ozone places a limit on the possible impact of aircraft emissions assuming no other sources of a trend in UT ozone. From the trend data alone an approximate limit of ≤1% year<sup>-1</sup> can be placed on the potential size of the aircraft impact on UT ozone. Given that the likely trend due to subsonic emissions is in the range of 0.05% per year (see Table 4-6), it appears that the uncertainty associated with the trend data is too large to effectively constrain the model predictions.

### 3.2.3 RADIATIVE FORCING

There are a number of mechanisms by which aircraft emissions can potentially alter climate, and essentially these can be divided into direct and indirect effects. Direct effects include the radiative perturbations produced by the ice crystals comprising the contrails in the UT, and by radiatively active combustion gaseous species and aerosols, such as carbon dioxide and soot particles, respectively. Indirect effects can also be considered in two categories: microphysical modifications to natural cirrus through the conditioning of the upper troposphere with water vapor and cloud-forming nuclei (potentially both CCN and ice nuclei (IN)), and changes in atmospheric ozone chemistry processes due to NO<sub>x</sub> injection. The relative importance of direct and indirect radiative effects is discussed below.

### 3.2.3.1 Clear Sky Effects

Aircraft gaseous emissions can influence climate directly by effecting both solar and terrestrial radiation. H<sub>2</sub>O, CO<sub>2</sub>, NO<sub>x</sub>, and SO<sub>2</sub> all have longwave absorption bands, and H<sub>2</sub>O, NO<sub>2</sub>, and SO<sub>2</sub> absorb short-wave radiation as well. Indirect radiative changes may result from modifications to the ozone balance in the UT caused by NO<sub>x</sub> injections. Consideration of the indirect effects is complicated by the feedbacks between chemistry and climate. For instance, O<sub>3</sub> chemistry is sensitive to UV flux [Clarke 1993], which, in turn, is dependent on ozone abundance.

Observing the climatic effects of these aircraft emissions is difficult for two reasons: the radiative forcing associated with these emissions is relatively small, and the aircraft contribution compared to the natural or other anthropogenic sources for these gases is also small, in general. Specific calculations of aircraft climate effects are described in Chapter 4.

### 3.2.3.2 Direct Cloud Effects of Contrails

The formation of cirrus clouds derived from contrails, even if persisting only momentarily, is the most obvious impact of jet traffic, and represents one of the potentially important climate impacts. From a radiative transfer standpoint, however, it is by no means certain whether the net impact (effect) of contrail cirrus will be to contribute to the cooling (albedo) or warming (greenhouse) of the earth/atmosphere system. Cirrus cloud radiative simulations have established that both the magnitude and sign of the forcing associated with clouds in the UT depends critically on their locations and microphysical properties, such as ice crystal size, shape, and concentration, which are controlled mainly by the cloud layer structure and temperature [Stephens *et al.*, 1990; Takano *et al.*, 1992; Ou and Liou, 1995]. The overall radiative effect is also determined by the time of day when the contrail or cirrus forms, how much area it covers, how long it persists, and the albedo and temperature of the underlying surface.

In general, natural cirrus (with the exception of thunderstorm anvil-cirrus) formation takes place from the top-down through the precipitation of ice crystals nucleated near the cloud layer top. (However, the precipitation process may thermodynamically alter the underlying atmosphere, leading to altered dynamics and new particle generating zones, [see Starr and Cox 1985]). The cloud layer top position is critical because during adiabatic ascent, either on convective or synoptic scales, it represents the region of coldest temperatures where conditions are most favorable to the homogeneous freezing of haze particles. In contrast, contrail formation is a binary occurrence: either the ambient temperatures and humidities at the aircraft flight level are suitable for condensation to occur, or they are not and no contrail is formed as the exhaust plume mixes out with the environment. Contrail persistence requires, according to our current state of knowledge, that the condensed droplets, or the growing haze particles that preceded them, grow and exist long enough for homogeneous freezing to occur. Since the UT is always subsaturated with respect to water as a consequence of the thermodynamic barrier imposed by cirrus cloud formation processes in which ice crystals grow at the expense of liquid water, all liquid droplets formed in a contrail will eventually evaporate. Consequently, it is the transience of the liquid phase coupled with mixed air temperatures colder than about -40°C that allows ice contrails to persist. (The creation of IN in the exhaust plume could be a factor under warmer conditions where homogeneous nucleation rates are relatively slow, but large numbers of such particles would probably be needed to produce a visible contrail.) Similarly, unless the ambient environment is at least saturated with respect to

ice at the aircraft altitude, the ice particle contrail will also eventually evaporate. The fact that contrails are often observed to persist in cloud-free air, however, demonstrates that they can pioneer an environment that is not quite suitable for the formation of natural cirrus clouds, which require an ice-supersaturated environment at all temperatures and near-water saturation at temperatures warmer than about  $-40^{\circ}\text{C}$  in the UT [Sassen and Dodd, 1989].

The manner in which contrails are produced has important microphysical and radiative consequences. The rapid expansion and mixing of the exhaust plume behind the aircraft has the potential to create an exceptionally large number of minute ice crystals of  $\sim 5$  to 10 microns in diameter, which tend to remain small because of the strong competition for the available water vapor supply; if this is so the particles would consequently have negligible rates of fall. Clouds composed of such particles would likely have solar albedo effects that dominate over their infrared (“greenhouse”) effects on radiative transfer in the UT, because of the relatively low absorption efficiencies for small particles in the infrared. However, continued contrail ice particle growth will eventually lead to a balance between these two effects, or to the dominance of the greenhouse effect. The balance of these effects also depends on the time of day, season, and latitude. Ice (sphere) diameters larger than 20 to 30 microns are required for the particles to approach a mid-infrared (10-micron wavelength) absorption efficiency of unity, but other factors such as low solar zenith angle, multiple scattering, and contrail height may still favor solar albedo effects. Thus, understanding the evolution of persisting contrail microstructure is critical to assessing their climatic impact, stressing the need for combined *in situ*, remote sensing, and theoretical investigations of effects of contrail particle size to help settle the question of the solar albedo versus greenhouse competition.

As an example of the unusual structure of persisting contrails, we present in Figure 3-11 a lidar backscatter height-versus-time display collected during a recent field campaign at high spatial (1.5 m height by 0.1 s time) resolution. This example shows a pair of intersecting contrails produced by commercial air traffic, both approximately 45-min old according to visual inspection. Clearly, observations of persisting contrails at this scale contain a wealth of information regarding contrail fine structure which can help illuminate fundamental properties related to radiative impacts. As is typical, these contrails display a cellular structure, which could result either from the original vortex structures or from induced convection. It is important to note, however, that despite their ages, the vertical extents of the contrails are limited to at most a few hundred meters, and are often only 50-m. This implies that contrail ice crystal fallspeeds, and sizes, can remain relatively small for extended periods, probably on the order of the 10- to 30- $\mu\text{m}$  diameter indicated by contrail corona observations [Sassen, 1991]. Thus this type of remote sensing information indicates that persisting contrails may contain relatively minute ice particles for extended periods, supporting the possibility that they may tend to cool the surface through the dominance of the solar-scattering albedo effect.

Contrail growth and persistence determine the large-scale radiative effects of contrails. These characteristics are best monitored through satellite remote sensing. Figure 3-13 shows an example of the development of a cirrus cloud from a contrail during SUCCESS. In this case, the condensation trail formed from the exhaust of the NASA DC-8 as it flew in a racetrack pattern (Figure 3-13A) off the coast of California. The next 4-km-resolution infrared image from GOES-9 (Geostationary Operational Environmental Satellite) shows the development of an oval-shaped contrail in the location of the DC-8 flight track at an altitude of approximately 10 km corresponding

to a temperature of  $-43^{\circ}\text{C}$ . Only 2 hours after the DC-8 completed its final racetrack pattern, the contrail is several pixels wide, more than 10 km across. Other contrails, presumably from commercial trans-Pacific flights, are also evident in the vicinity of the DC-8 flight area (Figure 3-13B). In the subsequent images (Figure 3-13C-N), the oval contrail continues to grow and fill in as it passes over the coast, across the Sacramento Valley, and over the Sierra Nevada. At its maximum size, this contrail cirrus covers an area of  $\sim 4000\text{ km}^2$  before dissipating over Nevada. During this period, no other cirrus formed around the contrail indicating that the cloud would not have formed without the aircraft exhaust. Thus, there was a significant net increase in cloud cover over this area due to just one plane. The contrail initially formed during the late afternoon over bright low clouds. When it passed over the clear sky, inland, the sun was almost down. Therefore, this contrail had minimal impact on the solar albedo. Its infrared warming, however, was significant, increasing as it passed over the land and reaching a maximum over the Sierra when it was thickest and most widespread.

This example demonstrates the complexity of assessing large-scale contrail radiative effects. Other examples have also been studied in detail by Palikonda *et al.*, [1996]. Most old contrails do not have easily recognizable shapes like ovals. The irregularity and width of older, linear contrails obscure their anthropogenic origins. Ground observers can typically identify a contrail only in its early stages before it grows wider than a few kilometers. At greater widths or later in its lifetime, a contrail cloud will be indistinguishable from a natural cirrus. To date, direct evaluation of contrail radiative effects have relied on surface or high-resolution satellite observations of young contrails. It is clear from Figure 3-13 that such assessments can only provide a lower bound on the contrail radiative impact. Investigations to determine more representative statistics of contrail growth and lifetime are continuing under SASS.

### 3.2.3.3 Indirect Cloud Effects of Contrails

Aircraft engine exhaust that does not form contrails, and contrails that persist and then evaporate, leave behind enhanced aerosol and moisture fields in the UT that have the potential to alter the formation and content of future cirrus clouds. (Whether there are significant differences in aerosol production associated with the dry and wet exhaust chemistries remains to be determined.) It is clear that the abundant sulfate species aerosols created in the wake of aircraft, composed either of sulfuric acid, ammonium sulfate, or an admixture with soot, would serve as effective CCN to create the haze particles that are the precursors of cirrus ice crystals (following their homogeneous freezing). The question is whether their cloud particle-forming activity, in relation to the background aerosol in the UT, is of enough significance to alter cirrus cloud content in a radiative sense. Certainly, the UT is not rich in CCN. If the contrail sulfate aerosol particles are comparatively large, then radiatively significant alterations to cirrus are possible. This follows from 1-D model simulations of growing cirrus clouds, which indicate that the CCN size spectrum can be quite important during the crucial early moments of the haze particle freezing sequence in an updraft. Since water vapor competition ultimately determines the number concentration (and subsequent size distribution) of the ice cloud, large CCN-induced early nucleation events both increase initial ice particle sizes, and decrease their concentrations. The same argument would apply if relatively effective artificial IN (perhaps from engine metal fragments) were to affect the cirrus cloud particle nucleation sequence. Such IN could be of importance in relatively weak

(several cm/s) updrafts. Primarily, it is the relative effectiveness of the aircraft-produced cirrus cloud particle-forming nuclei that must be understood.

The argument for the effects of water vapor emissions depends critically on the evolution of contrail ice particle sizes. Simply put, if crystals grow large enough to undergo significant fallout, then persisting contrails will dehydrate the UT by removing not only the emitted water vapor but also the excess taken from the (ice-supersaturated) environment during contrail development. Conversely, if only relatively minor vertical contrail depths are characteristic, or non-contrail-producing water vapor emissions are more significant, then a humidification of the UT must occur.

#### **3.2.3.4 Cirrus Cloud Trends**

Various statistical studies [Machta and Carpenter, 1971; Changnon, 1981; Liou *et al.*, 1990] have indicated a significant correlation between jet fuel consumption and routine National Weather Service (NWS) reports of high cloud frequencies. A related increase in average surface air temperatures has also been suggested, even though the sign of the possible climate perturbation induced by increased cirrus cloud amounts is ambiguous (depending on the assumed cloud composition model), and the effects of other possible causes like greenhouse-gas warming must also be taken into consideration. It is noteworthy that the NWS high cloud data that appear to show some of the strongest correlations have come from Salt Lake City (SLC), Utah [Machta and Carpenter, 1971; Liou *et al.*, 1990]. Figure 3-12 [from Liou *et al.*, 1990; personal communication] depicts the analysis of SLC high cloud frequency over the period from 1948 to 1993, compared with the total domestic consumption of jet fuels. The results for SLC appear to support the connection between increasing jet aircraft operations in the UT and regional climate change, particularly in the mid-1960s when a sharp increase in domestic air traffic occurred.

A more recent SASS analysis using Air Force surface-based contrail observations [Minnis *et al.*, 1996a] and the May 1990 fuel usage assessment [Baughcum, 1996] shows a high correlation between contrail occurrence and fuel usage between 7- and 22-km (Figure 3-14), although most of the fuel is consumed between 9- and 12-km. Given the clear link between contrails and the growth of aircraft-induced cirrus (e.g., Figure 3-13), the apparent relationship between fuel usage and high cloud cover (Figure 3-12), and the dependence of contrail occurrence on fuel usage, it is fair to conclude that increasing the fuel consumption at high altitudes will lead to additional high cloud cover. Among the consequences will be changes in the radiation budget, especially over areas with dense air traffic [Minnis *et al.*, 1996b]. The overall direct and indirect impacts will be fully assessed as the SASS investigations continue.

### **3.3 Summary**

A substantial foundation of physical and chemical information is available for qualitatively understanding the atmospheric effects of aircraft emissions. Perturbations to ambient concentrations of CO<sub>2</sub>, H<sub>2</sub>O, NO<sub>x</sub>, and SO<sub>x</sub> in aircraft wakes are large, have been readily observed, and form a basis for estimating the large-scale changes induced by aircraft. Aircraft contributions to upper troposphere NO<sub>x</sub> are likely significant albeit highly uncertain, while those of CO<sub>2</sub>, H<sub>2</sub>O, CO, hydrocarbons, sulfur, and soot are relatively small. However, because aerosol and cloud formation are highly non-linear processes with respect to environmental conditions and species

concentrations, even small perturbations of H<sub>2</sub>O, sulfur, and soot may carry significant atmospheric implications.

Process-level studies conducted in the laboratory and in intensive field campaigns have demonstrated that upper tropospheric levels of NO<sub>x</sub> are set by a number of sources and that the effect of aircraft NO<sub>x</sub> on ozone is a complex function of background gas levels. Because of the plethora of chemical species present in the atmosphere, there remains substantial uncertainty in the gas-phase and aerosol-phase chemistry of nitrogen oxides in the upper troposphere. Currently there are only a limited number of atmospheric datasets with which to understand upper troposphere NO<sub>x</sub> distributions and related photochemical processes. In addition, long-term ozone trend data do not well constrain the aircraft impact due to the measured year to year variability in tropospheric ozone.

Climate impacts of aviation are divided into direct and indirect effects. Direct effects arising from the accumulation of gas-phase species are likely to be small and amenable to realistic model predictions. The direct effect of particle injections, in the form of aircraft contrails, is much more difficult to predict; the magnitude and sign of the effect is uncertain and depends critically on the locations and the microphysical properties of the contrails.

Indirect climate effects of potential importance are related to ozone changes in response to aircraft NO<sub>x</sub> injections and alteration of the formation and content of future high clouds by aircraft particle injections. The magnitudes of both effects are highly uncertain. In some locations, such as Salt Lake City, Utah, high-altitude cloud cover has been observed to increase in conjunction with aircraft fuel usage and/or contrail occurrence. However, in order to use physically based models to quantify such climate effects it is important to define the number of CCN and IN formed in or behind jet engines. Initial attempts to characterize aircraft particle emissions have found substantial, and unexplained, airplane to airplane variability in volatile aerosol production.

**Table 3-1.** Catalog of potential upper troposphere/lower stratosphere perturbations by existing subsonic fleet.

<b>Emittant</b>	<b>Projected Peak Perturbation</b>	<b>Potential Atmospheric Interactions</b>
<b>Ozone Effects</b>		
NO <sub>x</sub>	2 to 50% increase	Ozone production by NO <sub>x</sub> -CO-hydrocarbon (RO <sub>x</sub> ) chemistry, ozone loss by NO <sub>x</sub> catalysis
H <sub>2</sub> O	0.001 to 0.01% increase	HO <sub>x</sub> formation and ozone production (or destruction)
		NAT/ice condensation, denitrification in polar vortex, increased ClO <sub>x</sub> catalysis
Sulfur	0.3 to 2% increase	Increased aerosol surface area and sequestering of NO <sub>x</sub> , decreased ozone production
Soot	Uncertain - up to 10% increase	Additional nucleation sites for aerosols, increased surface area-changes in chemical reactivity of aerosols
Hydrocarbons	0.1% increase relative to ambient CH <sub>4</sub>	Source of CO, HO <sub>x</sub> , and H <sub>2</sub> O, interactions with aerosol chemistry
CO	0.5 to 2% increase	Modification of catalysis by HO <sub>x</sub> and NO <sub>x</sub>
<b>Radiative Forcing Effects</b>		
CO <sub>2</sub>	Currently ≈3% of CO <sub>2</sub> from fossil fuel	Direct change in IR radiative forcing
H <sub>2</sub> O	0.001-0.01% increase	NAT/ice condensation, cirrus cloud formation, direct and indirect change in radiative forcing
Sulfur	0.3 to 2% increase	Increased aerosol mass loading, direct and indirect change in radiative forcing
Soot	Uncertain - up to 10% increase	Additional nucleation sites for aerosols, increased surface-area, direct and indirect change in radiative forcing
NO <sub>x</sub>	2 to 50% increase	Ozone production, change in radiative forcing

**Table 3-2.** Global sources of NO<sub>x</sub> and compilation of source strength estimates.

Source	Estimated strength (Tg N yr <sup>-1</sup> )	Reference
Fossil Fuel	22	Hameed and Dignon [1988]
	21.2	Levy and Moxim [1989]
	22.2	Benkovitz <i>et al.</i> [1996]
	21.4	Levy <i>et al.</i> [1996]
Subsonic Aircraft	1	Beck <i>et al.</i> [1992]
	0.46	Wuebbles <i>et al.</i> [1993a, b] Baughcum <i>et al.</i> [1996]
Stratosphere	0.64	Kasibhatla <i>et al.</i> [1991]
Biomass Burning	~6	Hao <i>et al.</i> [1989]
	8.5	Levy <i>et al.</i> [1991]
	5.8	Penner <i>et al.</i> [1991]
Soil Biogenic Emissions	~5	Dignon <i>et al.</i> [1992]
	4.7	Müller [1992]
	5.5	Yienger and Levy [1995]
Lightning	2.1	Hameed <i>et al.</i> [1981]
	19.1 - 152	Liaw <i>et al.</i> [1990]
	3 - 10	Penner <i>et al.</i> [1991]
	220	Franzblau and Popp [1989]
	1 - 8	Lawrence <i>et al.</i> [1995]
	2 - 6	Levy <i>et al.</i> [1996]
	4	Price and Rind [1994]

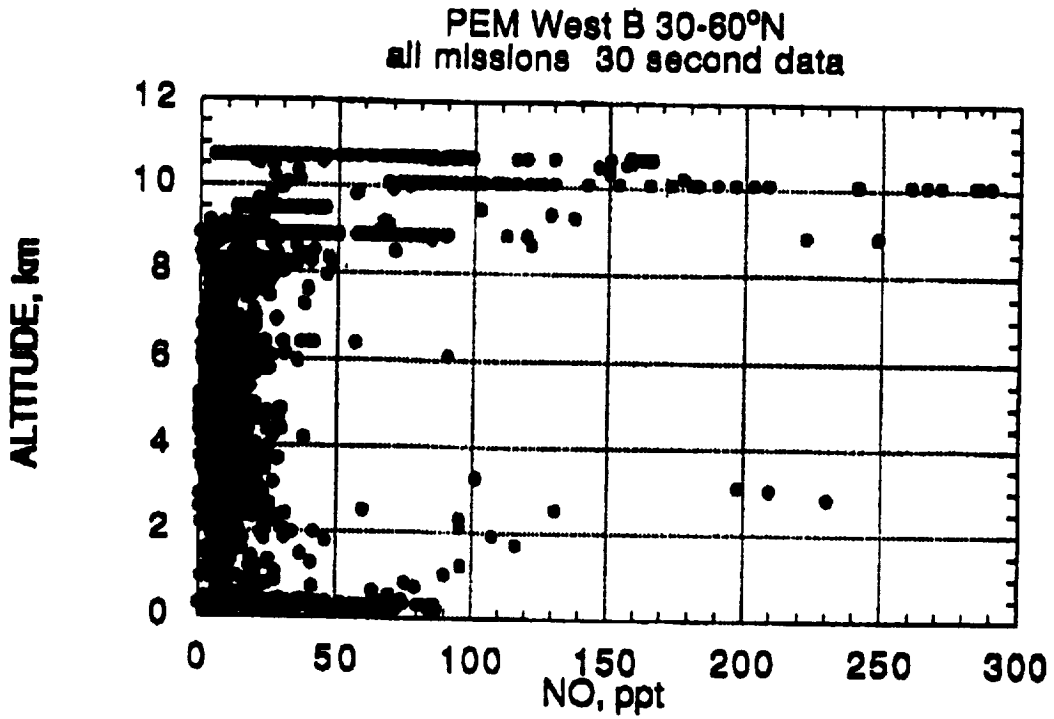


**Figure 3-1.** Vertical distribution of NO over the Pacific during winter/spring as measured in PEM-B (February/March 1994).

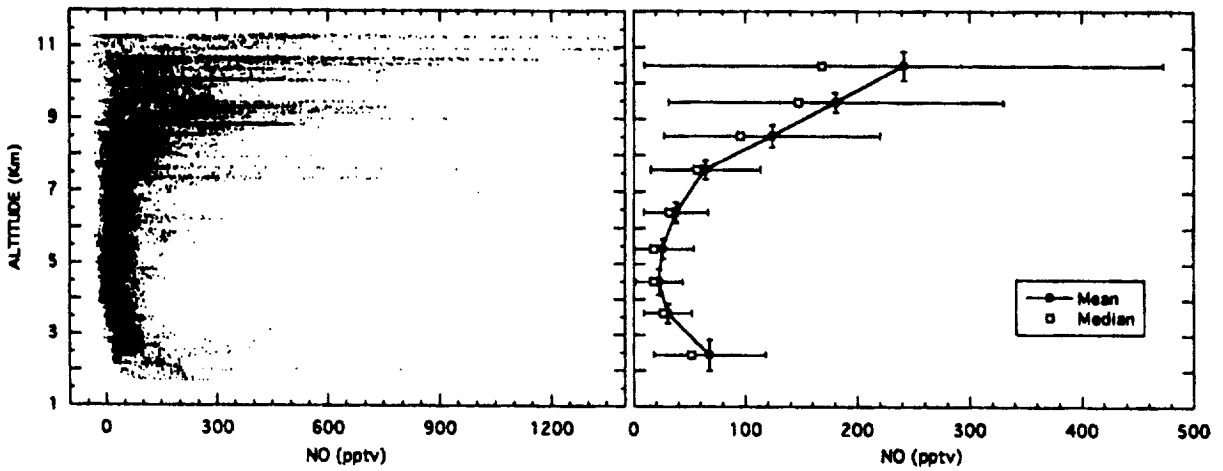


**Figure 3-2.** NO distribution over New Mexico. Data are for July/August 1989 during the summer monsoon season [from Ridley *et al.*, 1994].

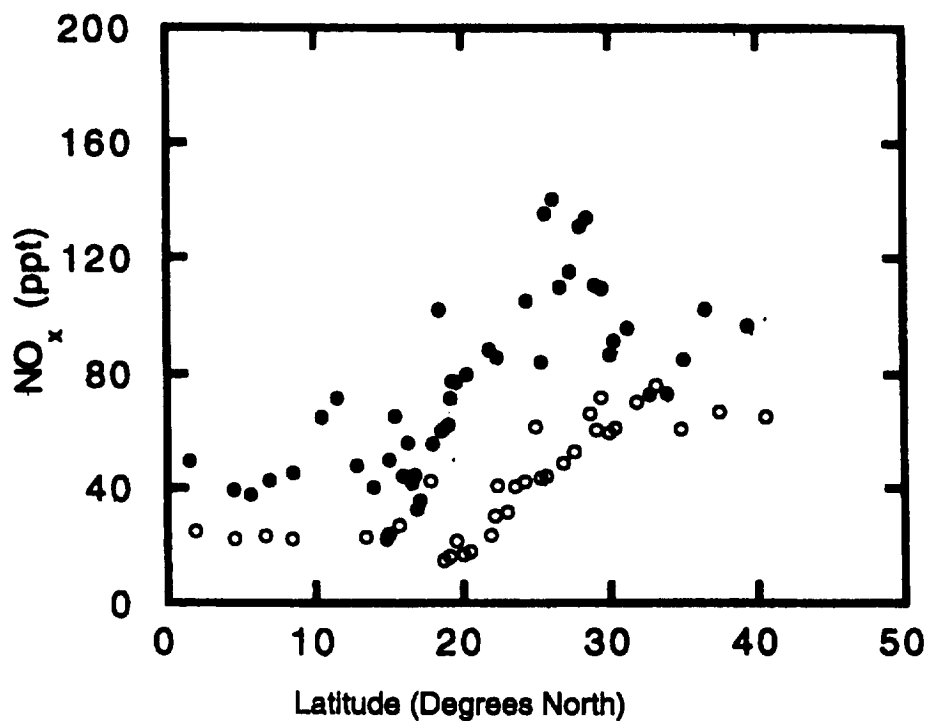


**Figure 3-3.** Latitudinal distribution of  $\text{NO}_x$  over the Pacific. Open circles are for altitude bins of 3- to 7-km; solid circles represent 7- to 12-km bins.

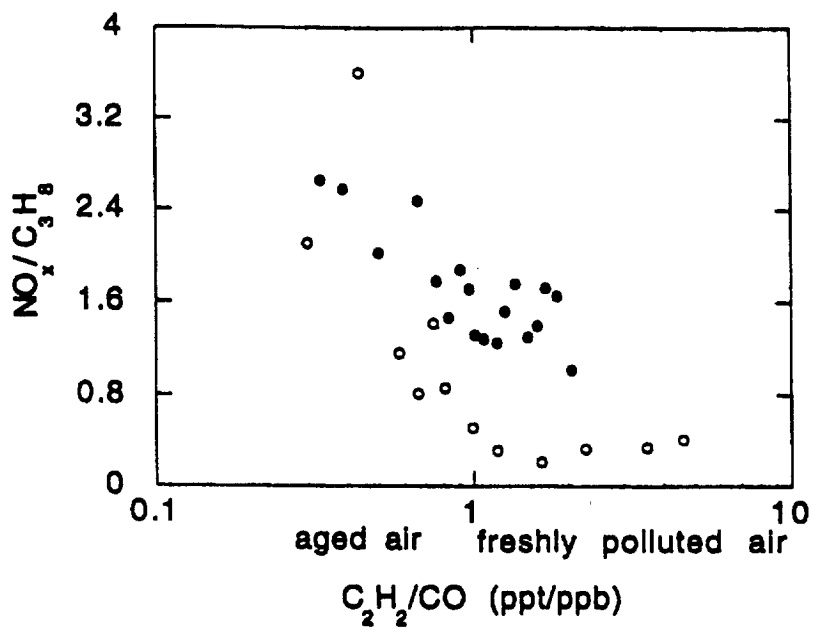


**Figure 3-4.**  $\text{NO}_x/\text{C}_3\text{H}_8$  ratios as a function of air mass age. Open circles represent 0- to 3-km; solid circles represent 7- to 12-km.

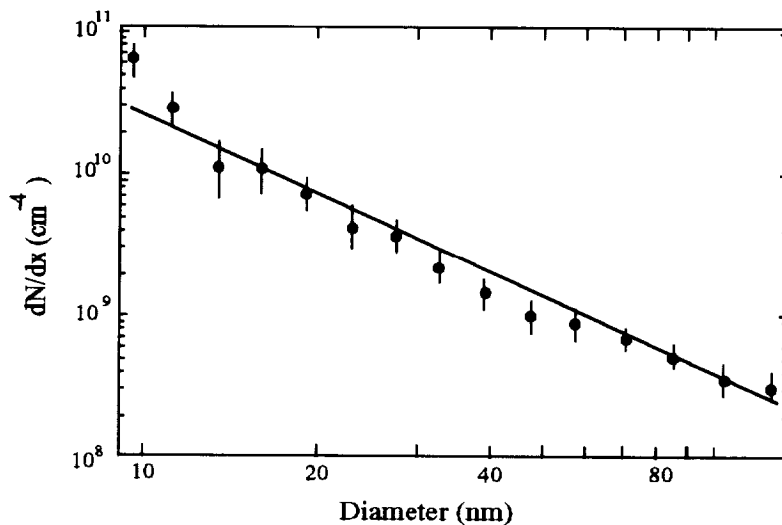


**Figure 3-5.** Particle size distribution measured during inflight sampling of a Boeing 737-S aircraft [Lilenfeld *et al.*, 1995].

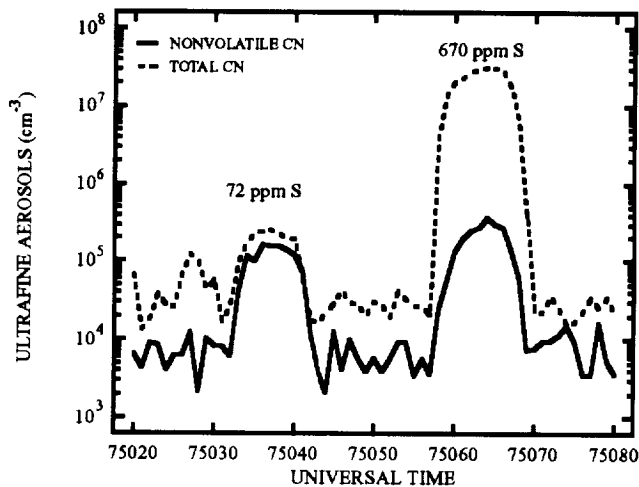


**Figure 3-6.** Time series of total and nonvolatile (at 290°C) ultrafine aerosol (>4 nm in diameter) number densities recorded during exhaust plume crossings behind a B757 aircraft simultaneously burning fuels of different sulfur content in its left and right engines [Miake-Lye, personal communication].

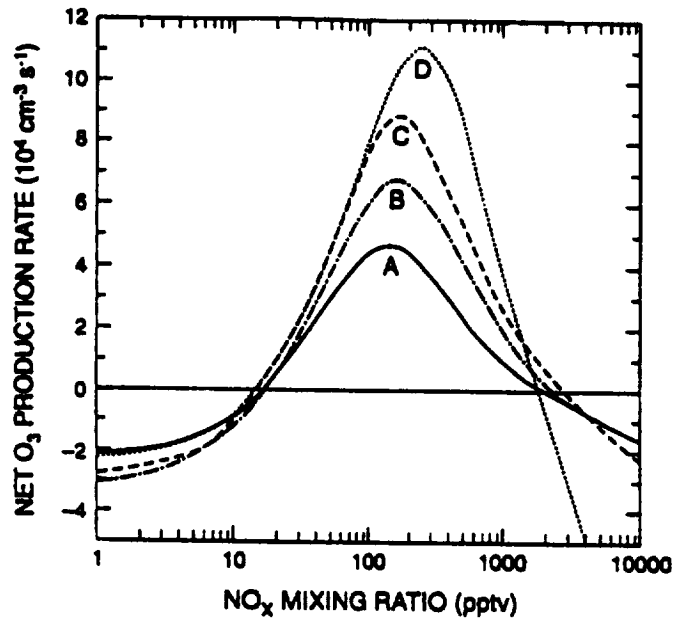


**Figure 3-7.** Net ozone production rate calculated as a function of the atmospheric  $\text{NO}_x$  mixing ratio at  $50^\circ\text{N}$  at 10-km altitude in July for clear-sky conditions. In all cases 84 ppbv of ozone, 73 ppbv of  $\text{CO}$  and 1.6 ppmv of  $\text{CH}_4$  are used. (a)  $\text{H}_2\text{O} = 50$  ppmv; (b)  $\text{H}_2\text{O} = 100$  ppmv, (c) includes NMHC as well as  $\text{H}_2\text{O} = 100$  ppmv; and (d) includes diurnal cycle in model calculations. [Source: Brasseur *et al.*, 1996].

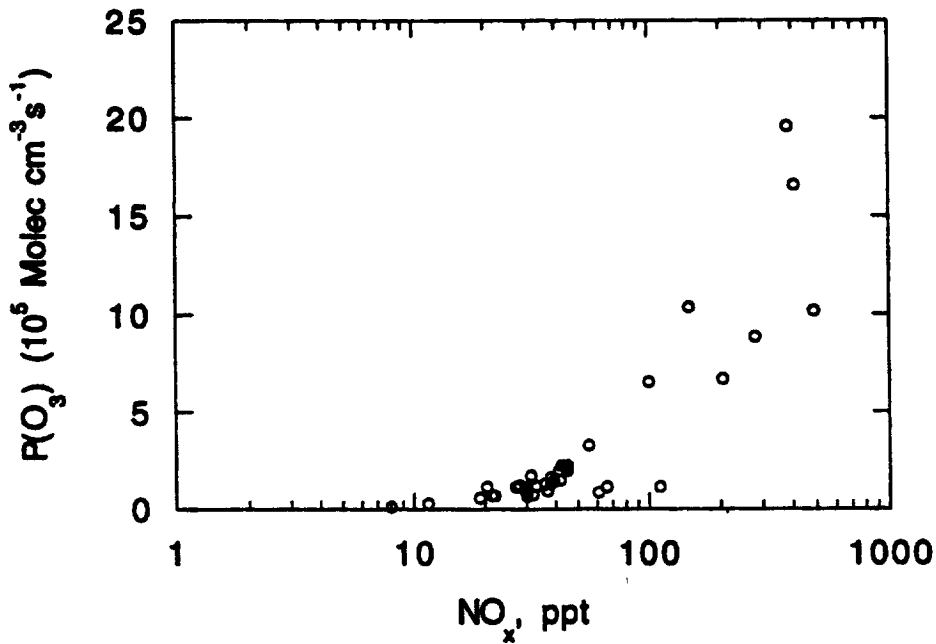


**Figure 3-8.** Instantaneous production rate of ozone ( $P(\text{O}_3)$ ) in the upper troposphere (10- to 12-km) over the Pacific ( $30$  to  $40^\circ\text{N}$ ). These PEM-West A (September/October 1992) data are for daytime restricted to those cases where the solar zenith angle was in the range from  $30$  to  $60^\circ$ .

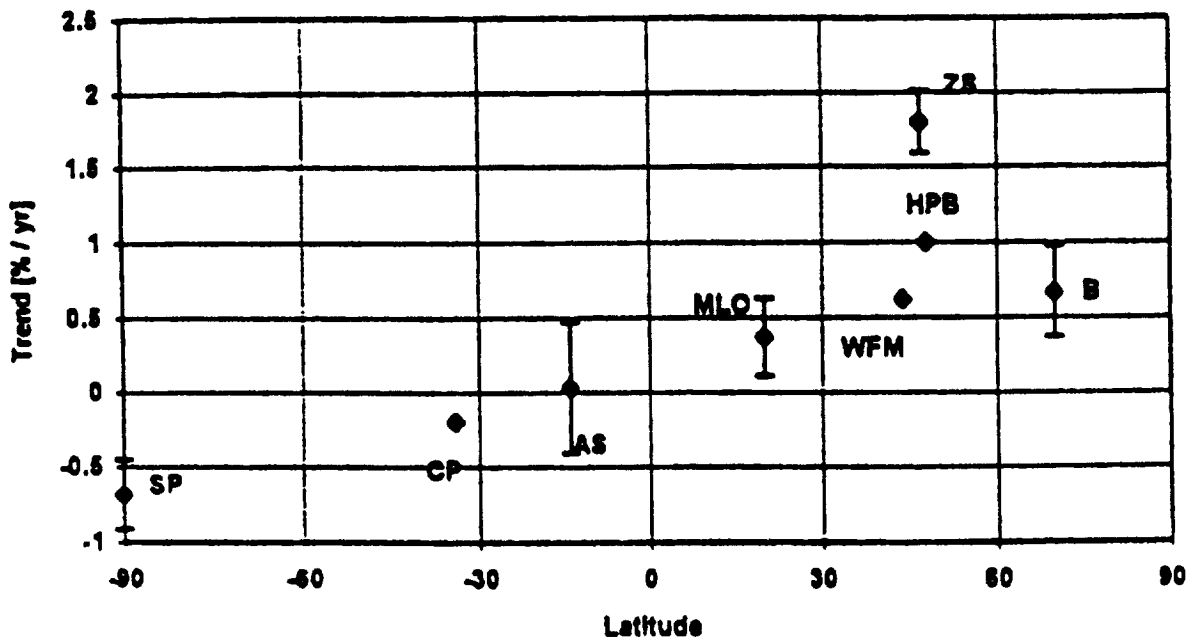


**Figure 3-9.** Trends in boundary layer tropospheric ozone observed at different latitudes, including only coastal and high-altitude sites [after Volz-Thomas, 1993]. AS: American Samoa, 14°S; B: Barrow, 70°N [Oltmans and Levy, 1994]; CP: Cape Point, 34°S [Scheel *et al.*, 1990]; HPB: Hohenpeissenberg, 48°N, 1000m [Wege *et al.*, 1989]; MLO: Mauna Loa, 20°N, 3400m; SP: South Pole, 90°S, 2800m ASL; WFM: Whiteface Mountain, 43°N, 1600m [Kley *et al.*, 1994]; ZS: Zugspitze, 47°N, 3000m.

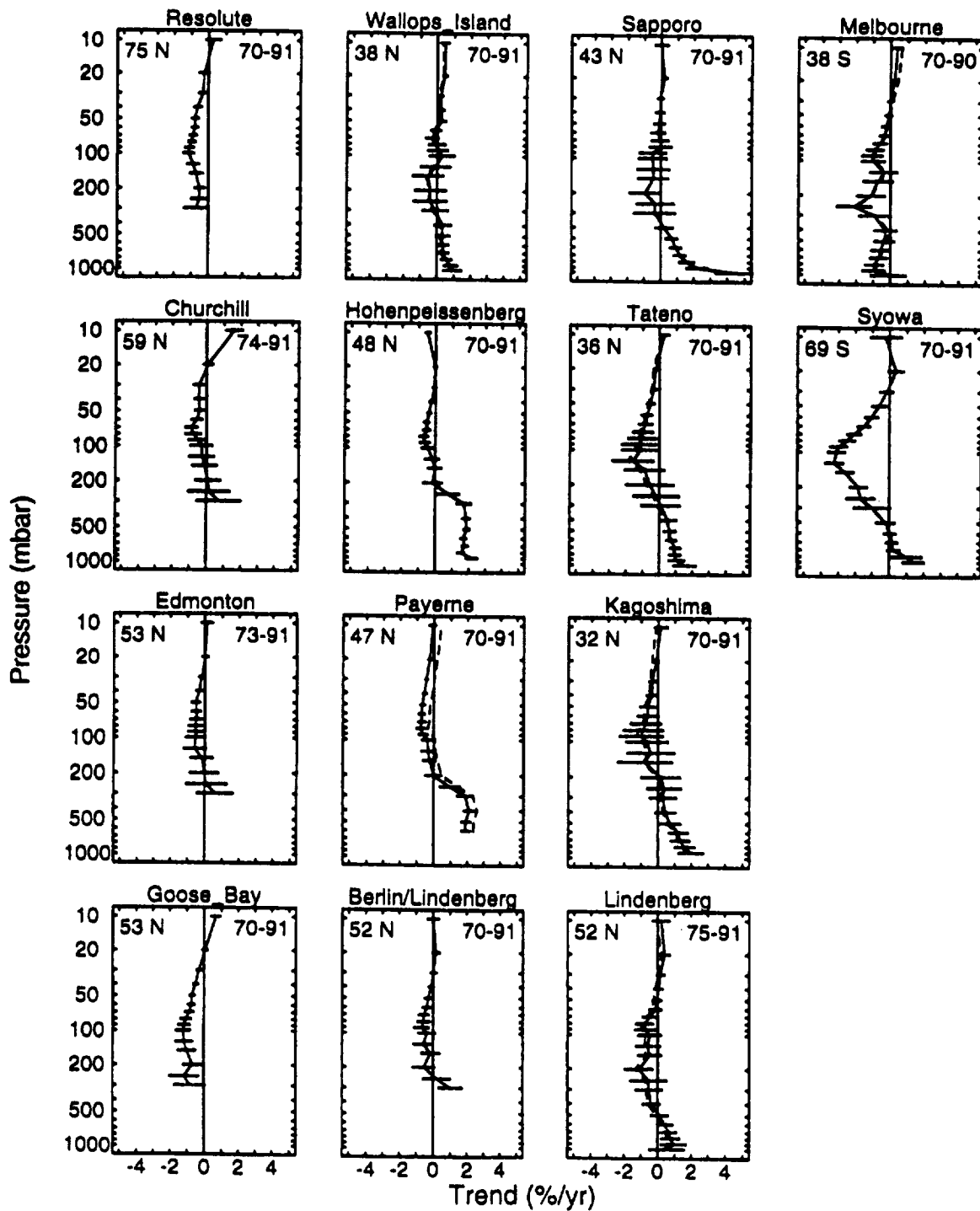


**Figure 3-10.** Trends for the periods shown in the ozonesonde measurements at different altitudes. 95% confidence limits are shown [adapted from Logan, 1994].

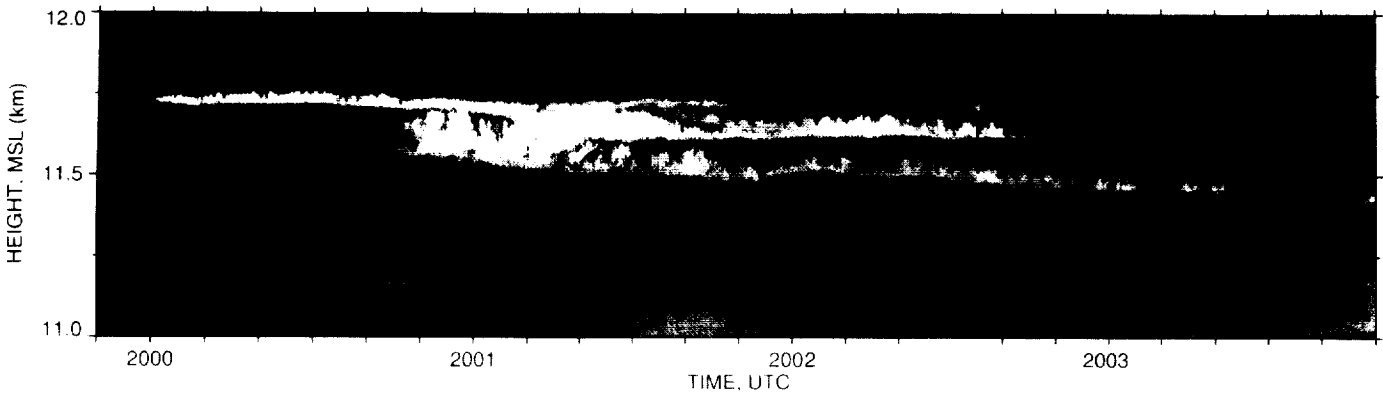


**Figure 3-11.** High-resolution (1.5 m by 0.1 s) height-time display of 1.06-micron laser backscattering from two ~45-minute-old overlapping contrails produced by commercial jet air traffic in a corridor to the north of the DOE Southern Great Plains Clouds and Radiation Testbed (CART) site, collected during the SUCCESS field campaign on 2 May 1996 by the University of Utah Polarization Diversity Lidar.

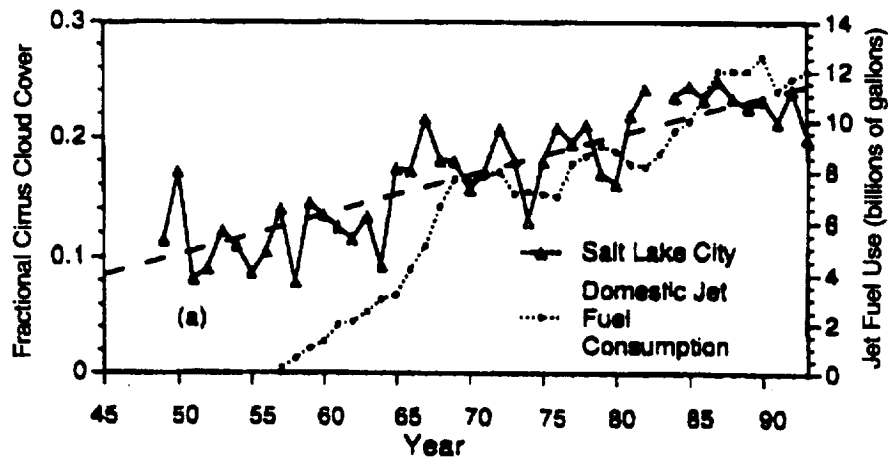


**Figure 3-12.** Observed mean annual fractional cirrus cloud cover over Salt Lake City, Utah, from 1948 to 1993 [Liou *et al.*, 1990; Liou, personal communication]. The dashed line represents a statistical fit to the cloud cover data for the entire period. Domestic jet fuel consumption, beginning in 1957, (filled with circles) is provided for comparison.

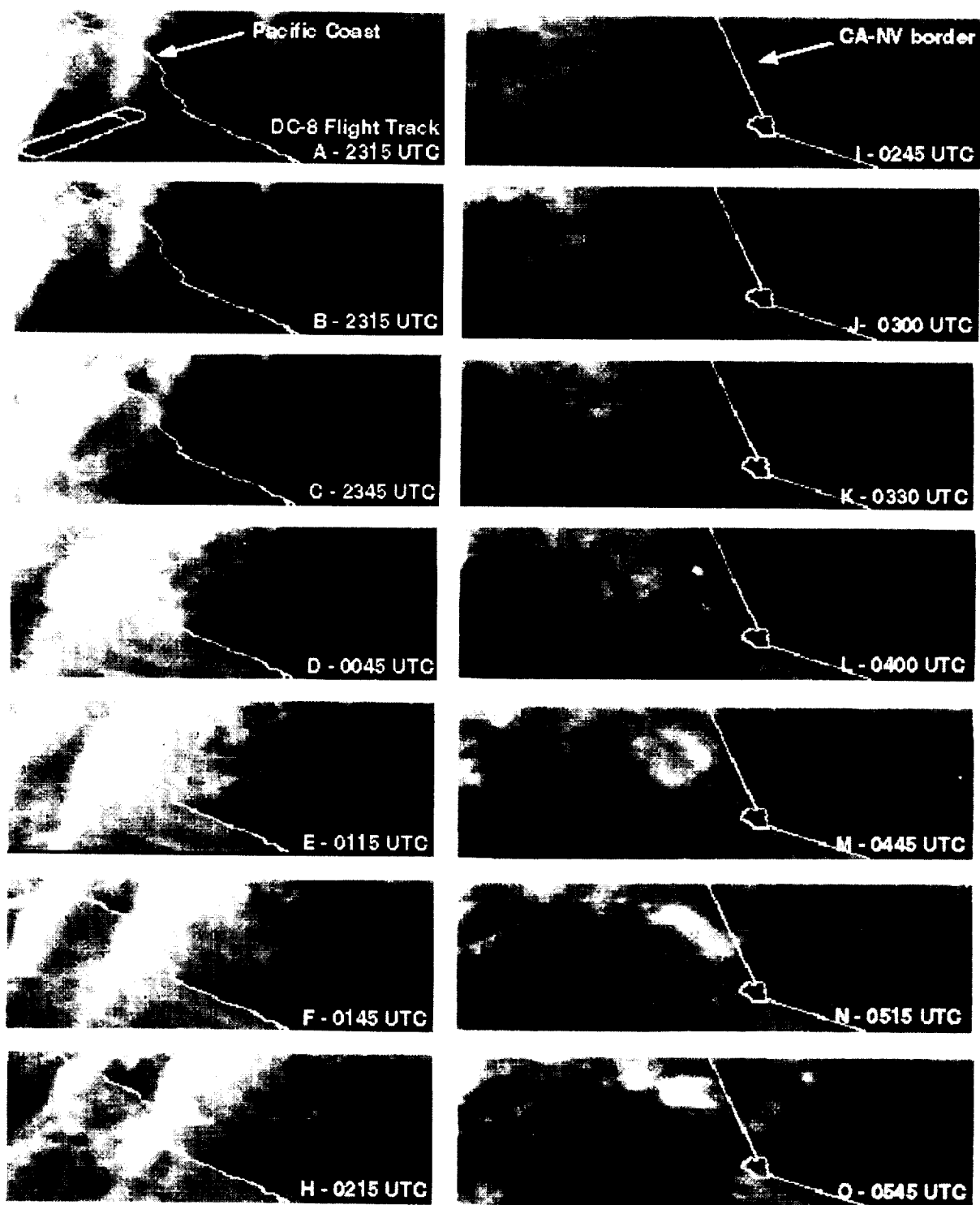


**Figure 3-13.** Cloud development from a DC-8 contrail during SUCCESS off northern California to Nevada border, 12-13 May 1996.

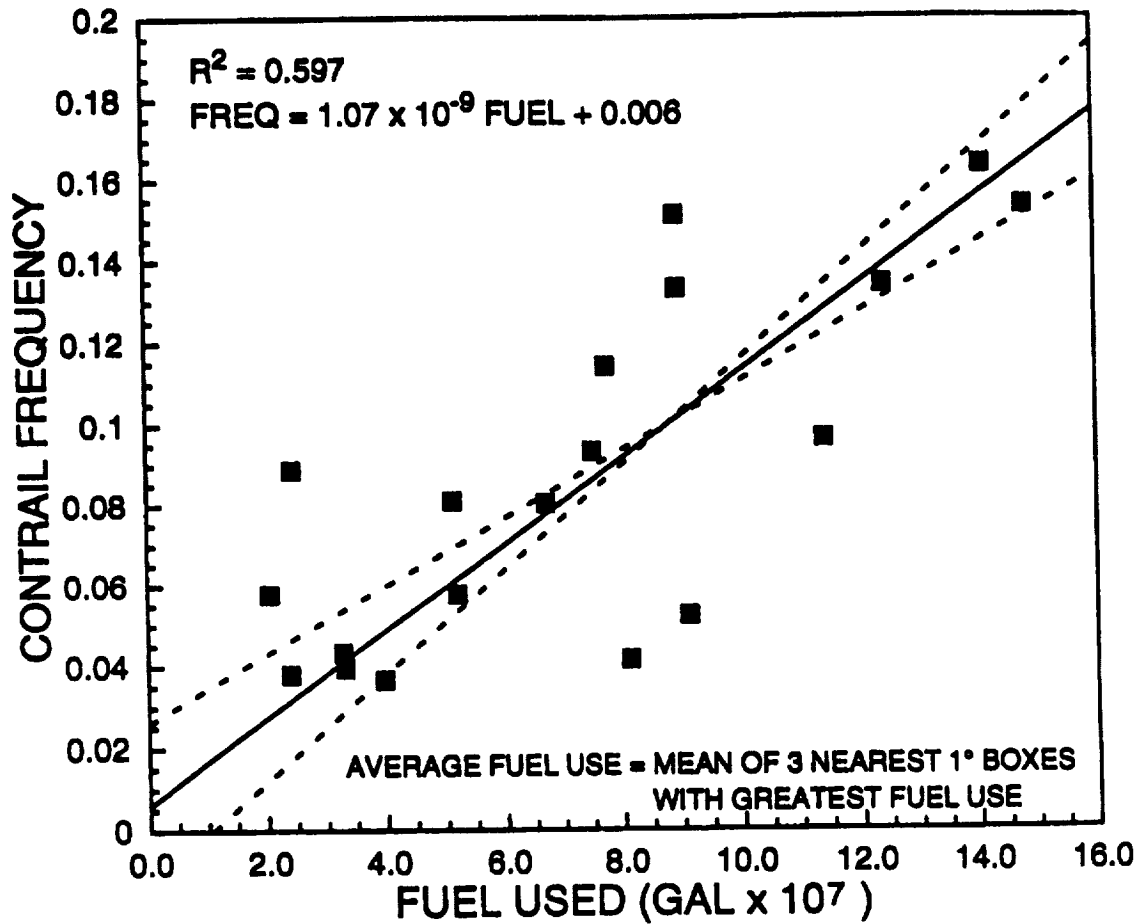


**Figure 3-14.** Correlation of a mean annual contrail frequency and estimated May 1990 aircraft fuel usage between 7- and 22-km altitudes. Contrail frequencies based on 1993 to 1994 hourly surface observations from 19 US Air Force bases.

## 4. MODELING THE GLOBAL EFFECTS OF AIRCRAFT EMISSIONS

Attempts to quantitatively predict regional and global scale impacts of subsonic aviation must focus, at a minimum, on the following key aircraft emissions/atmospheric processes:

1. Chemical perturbations to the upper troposphere and lower stratosphere; in particular, increases in ambient  $\text{NO}_x$  due to aircraft emissions leading to changes in ozone in an altitude region (9- to 13-km) where ozone is an efficient greenhouse gas.
2. Soot and sulfate aerosols resulting from aircraft emissions can reflect/absorb solar and infrared (IR) radiation and affect the tropospheric radiative budget.
3. Contrails formed by aircraft could reflect/absorb solar and IR radiation and lead to modifications in the tropospheric radiative budget.
4. Gas and particle emissions from aircraft that increase the concentration of CCNs and, consequently, cirrus cloud occurrence, leading to perturbations in the radiative balance.

Past modeling studies have focused primarily on the impacts related to chemical perturbations (#1 above). These studies, done primarily with zonally-averaged, two-dimensional models and a few three-dimensional models, suggest that current aircraft may have caused an increase of as much as 5 to 7% in upper tropospheric ozone at northern mid-latitudes [e.g., Wuebbles and Kinnison, 1990; Johnson *et al.*, 1992; Hauglustaine *et al.*, 1994; Wauben *et al.*, 1995; Jones *et al.*, 1996; Brasseur *et al.*, 1996]. The amount and location of  $\text{NO}_x$  injected into the stratosphere suggests that the impact of aircraft emissions on the stratospheric ozone layer is smaller, although larger effects could occur if future fleets flew at higher altitudes. Careful analysis of the capabilities and limitations of current atmospheric models in determining the global environmental effects from subsonic aircraft has not been accomplished yet and is pursued in this assessment.

Modeling the impacts of aircraft-derived aerosols and particulates (#2-4, above) has received much less attention so far. Consequently, global model treatments of the particle effects are in a relatively rudimentary state. The aims of this assessment are to gauge the magnitudes of potential climatic effects of aircraft emissions through model sensitivity studies and to identify the areas of model development requiring increased emphasis.

The complexities of the tropospheric processes to be incorporated into assessment models requires use of three-dimensional assessment models. Although we have not established confidence at the assessment level in current CTMs for tropospheric  $\text{O}_3$  prediction, we do have published examples of individual groups' calculations. We begin in this report to establish a standard process of model evaluation. We believe that this process should include: a) testing and intercomparison of algorithms and parameterizations used in large-scale models; b) model simulations to determine the sensitivity of model results to existing uncertainties in model input and formulation; c) review and compilation of a database of laboratory and atmospheric measurements which can meaningfully constrain and test different model components; and d) comparison of model results to atmospheric observations to reduce existing uncertainties. This chapter outlines efforts in the above areas.

The organization of the chapter is as follows: we first give a brief description of the types of models used in the past for quantitative predictions and their associated treatments of chemical and climate processes. In subsequent sections of the chapter we describe the results of a number of model calculations and tests performed on several specific advanced global models. For

atmospheric chemistry, the specific models employed were IMAGES, Harvard/GISS, and the modular code being developed by NASA's Global Modeling Initiative (GMI); for climate impacts, we used the GISS climate model. As will be demonstrated in the following sections, none of these models are sufficiently developed to be able to provide credible predictions of aviation impacts. The purpose of this interim assessment effort is to denote the requirements for a reliable assessment model and apply these requirements to the existing global models in order to identify directions for future model development. We also envision that the modular structure and science team approach of the GMI will facilitate future model development and assessment capabilities.

#### **4.1 Global Model Characteristics**

A variety of model types have been developed that are useful in the assessment of the effects of aircraft on the atmosphere. A fundamental difficulty that has strongly influenced the evolution of assessment models concerns the spatial and temporal resolution of important atmospheric processes. Clearly, aircraft emissions may affect processes spanning orders of magnitude in spatial and temporal scale. On the smaller scale one needs to worry about the chemistry and dynamics important to a description of the plume over a temporal scale of a few seconds and spatial scale of a few meters following emissions from an aircraft engine. At the larger scale one needs to be concerned with the potential of emissions to influence the Earth's climate on time scales of years or longer, and on global spatial scales by changing, for example, the distribution of ozone in the troposphere and stratosphere.

It is impossible to treat in detail with a single model all the important processes that operate over these temporal and spatial scales. The computational complexity of such a model far exceeds our current (or near future) capabilities. It is thus desirable to treat some processes crudely and others more elaborately, based on their relative importance to the scientific questions being addressed. In addition, in attempts to understand a complex process, it is generally advantageous to isolate one component of the system and simplify those other components that are peripheral to the area of focus. These constraints have strongly controlled the evolution of assessment models, and it is possible to categorize the models in a variety of ways.

One way of categorizing these models is by spatial scale. At the smallest temporal and spatial scales are several types of models, including those attempting to examine the processes in the emission plume. These models treat small scale phenomena, and ignore processes that operate on larger time and space scales (i.e., those processes with scale greater than a km, or longer than a few hours). Another example of small scale models are "box models" which essentially ignore the role of transport and focus primarily on the chemical constituent evolution in a small volume of air. We will loosely call these models "small scale," or "process" models throughout the rest of this section.

At the other end of the spectrum are models that attempt to represent the large spatial (e.g., greater than 1000 km in the horizontal, or 1 km in the vertical) scales and ignore, or attempt to represent very crudely those processes such as clouds that operate on smaller scales. We will loosely call these type of models "global" models, although "mesoscale" or "regional" models might also fall into this category.

### 4.1.1 MODEL TYPES

Amongst global models, a means of categorization is by which “processes” are treated explicitly, and which are treated implicitly or approximately. For example, most of the global models used here attempt to assess the role of emissions on only the chemical composition of the atmosphere. They typically use a prescribed dynamical component (i.e., the winds, temperature, clouds, etc.), and calculate the chemical evolution of the atmosphere and its response to changing emissions. By prescribing the dynamical component they eliminate any feedbacks (interactions) that can take place between changing atmospheric trace constituents and dynamics. These models are typically identified as chemistry-transport models (CTMs). They have formed the backbone of the assessment effort to date, and are still a very important component today. The level of complexity of the transport representation can vary from 2-D (latitude, height) prescriptions of the transport circulation [e.g., Jackman, 1991] to more realistic three-dimensional prescriptions (such as the CTMs used in this assessment).

Because of their computational efficiency 2-D models have commonly been used for assessment studies of potential ozone changes in the atmosphere, particularly for the stratosphere. However, we are reaching the point where the known complexity in the chemistry and transport processes limit the utility of these models. In 2-D models, transport is typically represented by a combination of a residual mean circulation to account for large-scale processes and eddy diffusivity to account for transient and unresolved mixing processes. The 2-D models seem to generally do quite a reasonable job of representing the transport circulation in the stratosphere away from the tropopause. However in these models the processes that act to control trace species distributions in the vicinity of the tropopause and below are particularly difficult to handle in a realistic fashion, and this is a region of special importance to assessments of both subsonic and supersonic aircraft. An example of processes that are exceedingly difficult to represent in these models are clouds (such as polar stratospheric clouds or tropospheric convective clouds) formation and evaporation which cannot be readily predicted using zonal mean quantities. The errors associated with the simplification of the transport circulation inherent in 2-D formulations have been of some concern to the assessment community. Several studies [e.g., Rasch *et al.*, 1994, Douglass *et al.*, 1993] have used 3-D models, which include reasonably realistic specifications of the winds and highly simplified chemistry, in an effort to understand differences between 2-D and 3-D representations of transport processes in the upper troposphere and stratosphere. The next level of complexity involves the three-dimensional CTMs like the Intermediate Model for the Annual and Global Evolution of Interactive Systems (IMAGES) model [Müller *et al.*, 1995], used in this interim assessment and described elsewhere in this chapter, which attempt to treat many more processes of importance in the troposphere, and much more elaborate chemistry and emissions, but use statistical parameterizations (discussed below) of many of those processes.

Another major difficulty with 2-D models in the troposphere is their zonal-averaged treatment of the chemistry and transport processes involving short-lived gases and aerosols. Sources for many of the short-lived constituents of interest are primarily over land, resulting in chemical interactions that are clearly non-zonal. Nonlinear dependencies on the concentrations of these constituents further add to the difficulty of treating global tropospheric chemistry with a 2-D model.

Another class of model prescribes the chemical composition of the atmosphere, and predicts the dynamical behavior using an explicit description of the physics of the atmosphere. The

atmospheric motions are driven by heating associated with absorption of solar radiation, the absorption and emission of long-wave radiation, and through heating associated with phase changes of water, and exchanges of heat with other components of the climate system (i.e., oceans, cryosphere, biosphere). This type of model is typically identified as a “dynamical model.” More elaborate versions are generally known as “general circulation models” (GCMs). By changing the prescription of the chemical composition of the atmosphere, one can examine changes in the model atmosphere and use the model to assess the influence of these changes on the Earth’s climate (such as the Goddard Institute for Space Studies (GISS) model used in this assessment).

A third type of global model is actually a combination of the first two. Predictive equations for both the chemistry and dynamics are used within the model. The changing chemical composition can affect the radiative and hydrologic processes in the model, which will, in turn, feed back on the chemistry through a dynamical response. Comprehensive 3-D versions of this type of model have not yet reached a point where they are useful in the assessment effort, but it is an area of active research [e.g., Austin *et al.*, 1992, Rasch *et al.*, 1996]. Crude versions of this type of model do exist, in which the model dynamics and chemistry are allowed to interact, but the interactions are severely simplified when compared to how those processes operate in the real world. Examples of this type of model are the 2-D models, which attempt to use simplified diabatic circulations to represent the actual 3-D atmospheric flows [Brasseur *et al.*, 1990]. They do allow feedbacks between chemical composition and radiative forcing, but are thought to be more effective for stratospheric assessments because of the simplifications made in treating tropospheric processes.

#### **4.1.2 ASSESSMENT MODEL REQUIREMENTS**

The need for treating some kinds of processes from first-principle physics, and other processes approximately has introduced the concept of “parameterization” into the lexicon of modeling. Physical processes are “parameterized” when they are treated in a way in which one attempts to capture the qualitative behavior of a process correctly, but not necessarily to express the process in terms of a fundamental physical law, derived from first principles. For example, an expression for the fraction of air occupied by clouds within a volume of air could be used at each point of a global model. Since there is a strong empirical correlation between relative humidity and cloudiness, the cloud fraction is often represented as a quasi-linear function of relative humidity, and the coefficients of the function are adjusted to provide a reasonable cloud fraction when compared to observations. The concept of parameterization provides an explicit link between “process models,” “box models,” etc., and large-scale models. It is sometimes possible to use these process models to construct parameterizations or evaluate the properties of the parameterization.

All of the types of models discussed above, and their incorporated parameterizations, continue to evolve as the understanding of important atmospheric processes improves. Currently, uncertainties in both the basic understanding of important processes and in the treatment of some of the chemical and physical processes in models significantly affect the ability to represent the atmosphere in general, and limit the accuracy of the model predicted changes in atmospheric chemistry or climate from aircraft emissions. For example, major uncertainties in the effect of lightning on background levels of tropospheric nitrogen oxides lead to uncertainties in the calculated effects of additional nitrogen oxides on concentrations of tropospheric ozone. Likewise, uncertainties in potential feedbacks between various climate system components limit the accuracy of GCM simulations. Many climate processes and their feedbacks are non-linear leading to

potentially large predictive errors. As a specific example, current GCMs calculate polar temperatures which are too low [Boer *et al.*, 1992]. As a consequence, fully coupled chemistry/ climate models can not yet be expected to predict accurately the effects of emissions on PSC-catalyzed ozone chemistry.

A reliable assessment must be carried out with models that fulfill the following conditions:

- The chemical mechanisms in the model are accurately solved, and give a realistic representation of atmospheric chemistry. Although current stratospheric chemical mechanisms seem to have reached the point at which they accurately describe stratospheric concentrations, the same cannot be said of the troposphere. Different assumptions regarding photolysis rates, heterogeneous/aqueous chemistry, and hydrocarbon chemistry can lead to different results. Tropospheric chemical mechanisms must be intercompared and tested against simultaneous observations of different constituents.
- The model incorporates an accurate representation of the transport mechanisms, both large-scale (such as advection) and subgrid (convection). The appropriateness of these schemes depends on: (i) whether the models incorporate accurate numerical algorithms for solution of the advective and convective mass fluxes, and (ii) whether the incorporated meteorology accurately represents the long-term average climatology of the troposphere. Thus these models are tested by: (a) intercomparison of model results utilizing different winds/transport schemes; and (b) comparison of model results to atmospheric observations of constituents that are particularly sensitive to a given transport mechanism (for example, radon-222 ( $^{222}\text{Rn}$ ) as a diagnostic of convection).
- The model must give distributions of trace species sensitive to both chemistry and transport that compare well to observations. In particular, since the primary goal is predicting changes in  $\text{O}_3$  from changes in  $\text{NO}_x$ , agreement with available observations of ozone and  $\text{NO}_x$  must be established to the greatest extent possible.

## 4.2 Effects on Atmospheric Chemistry

The present effort constitutes a first attempt to address the above requirements by testing different aspects of assessment models. Thus, we emphasize the model intercomparison and sensitivity, rather than the final “predictions,” because we are still in the process of improving current models. This effort includes the following components:

1. Intercomparison of chemical mechanisms used in CTMs for treatment of tropospheric chemistry.
2. Three-dimensional simulations of a reactive nitrogen ( $\text{NO}_y$ )-like tracer and  $^{222}\text{Rn}$  in CTMs to examine the treatment of transport processes in these models.
3. Identification of atmospheric observations needed to test different aspects of current CTMs and a limited comparison of available data with the models used in this assessment.
4. Sensitivity tests with current CTMs to investigate the effects of several major uncertainties on the tropospheric impact of aircraft emissions.

In this section, these components are used to examine the abilities and limitations of several representative models of tropospheric processes and to examine the sensitivity of ozone and climate in these models to current and potential future aircraft emissions. The next subsection gives a short description of the 3-D chemical transport models used in this assessment before proceeding with the analyses of these models and sensitivity analyses of effects on ozone.

#### **4.2.1 DESCRIPTION OF MODELING TOOLS**

This section describes the 3-D CTMs used in this interim assessment. Because they were employed in the sensitivity analyses, the IMAGES and Harvard/GISS models are examined in detail. However, initial results from the new GMI modeling capability are also provided in the sections examining atmospheric tracers. Table 4-1 describes the spatial and temporal resolution used in these models, while Figure 4-1 depicts the vertical resolution from the ground to 100 mbar in each of these models. The IMAGES model has a much finer vertical resolution, and also extends to higher altitudes, than the Harvard/GISS model.

##### **4.2.1.1 IMAGES Model**

The IMAGES model is a 3-D CTM with a weather-less, monthly mean description of tropospheric transport. It calculates the monthly averaged distributions of 56 chemical species, including ozone, hydrogen oxides, nitrogen oxides, sulfur oxides, methane, and several non-methane hydrocarbons. Its horizontal resolution is 5° in latitude and in longitude. In the vertical, the model has 25 layers extending between the Earth's surface and the lower stratosphere (50 mbar) [Müller and Brasseur, 1995; Pham *et al.*, 1995].

The transport of the species is solved by a semi-Lagrangian scheme [Smolarkiewicz and Rasch, 1991] which calculates the advection using monthly averaged winds. The winds, temperatures, and water vapor concentrations are an average of 1985 to 1989 taken from an analysis of the European Center for Medium-Range Weather Forecasts (ECMWF). Note, however, the existence of problems with ECMWF and other analyses near the tropopause concerning the actual strength of the jets [c.f., Tenenbaum, 1991; 1996]. The impact of wind variability at time scales smaller than one month is taken into account by the introduction of a diffusion term in the continuity equation. The diffusion coefficients are estimated from the ECMWF wind variances. Vertical mixing in the planetary boundary layer is also represented as diffusion. The effect of deep convection on vertical transport is parameterized following the scheme of Costen *et al.* [1988]. Cloud updrafts are parameterized using the deep convective cloud coverage and cloud top altitudes estimated by the International Satellite Cloud Climatology Project (ISCCP) [Rossow and Schiffer, 1991]. Convection intensity is adjusted so that the model reproduces the observations for radon (Rn) at mid-latitudes in summer [Liu *et al.*, 1984].

The chemical scheme includes more than 150 reactions, including simplified oxidation schemes for ethane, propylene, propane, isoprene, etc. The photodissociation rates are interpolated from a look-up table. This table contains J values for discrete values of the zenith angle, altitude, ozone column, albedo, and 500 mbar and 200 mbar temperatures. The table was calculated using the 8-stream discrete ordinates radiative model. The effect of clouds in the model is parameterized following Chang *et al.* [1987] and using the cloud cover and optical depth estimated by ISCCP.

The surface emissions and deposition velocities used in IMAGES are based on an inventory of the sources by Müller [1992] (see also Müller and Brasseur [1995]), with several modifications. The biomass burning emissions are based on a newer inventory by Granier *et al.* [1996]. The ocean source of CO has been reduced to 20 Tg yr<sup>-1</sup>, whereas the motor vehicle exhaust emissions of CO and hydrocarbons have been increased.

The production of NO by lightning discharges in the basic model is 5 Tg N yr<sup>-1</sup> globally, distributed in accordance with the satellite-derived flash frequencies of Turman and Edgar [1982]. The emission is assumed to be constant with altitude between the surface and the top altitude of the deep convective clouds. The washout scheme is based on the ISCCP cloud dataset and climatological precipitation rates. The conversion of N<sub>2</sub>O<sub>5</sub> to HNO<sub>3</sub> on aerosols is parameterized using the model-calculated sulfate distribution.

The integration time step is 6 hours except during 3 days at the beginning of each month of simulation. These 3 days are calculated using a time step of half an hour and diurnally varying photolysis rates. The diurnal behavior of the concentrations is saved and used afterwards to correct the chemical reaction rates, in order to estimate the effect of the diurnal cycle.

In prior studies, the IMAGES model has been used to investigate the budget of important tropospheric species and their evolution since pre-industrial times [Müller and Brasseur, 1995], the sulfur cycle [Pham *et al.*, 1995, 1996], the impact of biomass burning [Granier *et al.*, 1996], and an earlier look at the impact of subsonic aircraft [Brasseur *et al.*, 1996].

#### 4.2.1.2 Harvard/GISS Model

The Harvard/GISS CTM has a spatial resolution of 4° x 5°, with 9 vertical layers in sigma coordinates, extending from the surface to 10 mbar. Meteorological fields are from the NASA GISS GCM II [Hansen *et al.*, 1983], and are updated every 4 hours. A mass-conserving second-order moment scheme [Prather, 1986] is used in tracer advection. Dry and wet convection fluxes in the model are consistent with the GCM [Prather *et al.*, 1987]. Dry deposition is computed with a resistance-in-series scheme similar to that of Gao and Wesely [1995]. Wet deposition of soluble tracers is computed with the scheme of Balkanski *et al.* [1993]. The CTM has been applied previously to a number of atmospheric chemistry problems [Prather *et al.*, 1987; Jacob *et al.*, 1987; Spivakovsky *et al.*, 1990a; Balkanski *et al.*, 1993; and Jacob *et al.*, 1993].

The present version of the model transports 15 reactive chemical tracers: odd oxygen (O<sub>x</sub> = O<sub>3</sub> + O + NO<sub>2</sub> + HNO<sub>4</sub> + 2 x NO<sub>3</sub> + 3 x N<sub>2</sub>O<sub>5</sub>), NO<sub>x</sub> (NO + NO<sub>2</sub> + NO<sub>3</sub> + nitrous acid (HNO<sub>2</sub>)), N<sub>2</sub>O<sub>5</sub>, HNO<sub>4</sub>, PANs (peroxyacetyl nitrate and its homologues), alkylnitrates (≥C<sub>4</sub> lumped as butylnitrate), HNO<sub>3</sub>, CO, ethane, higher alkanes (≥C<sub>4</sub> lumped as butane), alkenes (≥C<sub>3</sub> lumped as propene), isoprene, acetone, higher ketones (≥C<sub>2</sub> lumped as methylethyl ketone), and H<sub>2</sub>O<sub>2</sub>. The chemical mechanism is based on recent compilations including Paulson and Seinfeld [1992], Atkinson *et al.* [1992], and DeMore *et al.* [1994]. The quantum yields of O(<sup>1</sup>D) from ozone photolysis have been updated following Michelsen *et al.* [1994]. The termolecular reaction rate constant of OH + NO<sub>2</sub> is based on a new recommendation by Donahue *et al.* [1996], and is 15 to 20% slower than that by DeMore *et al.* [1994] under tropospheric conditions. Hydrolysis of N<sub>2</sub>O<sub>5</sub> to HNO<sub>3</sub> on aerosol surfaces is included with a reaction probability of 0.1 [DeMore *et al.*, 1994]. Aerosol surface areas are derived from a CTM simulation of sulfate [Chin *et al.*, 1996]. Following

the procedure described by Spivakovsky *et al.* [1990b], the chemical mechanism is parameterized for rapid computation.

Global sources of NO<sub>x</sub> in the model include: 21 Tg N from fossil fuel combustion [Benkovitz *et al.*, 1996], 0.46 Tg N from the 1992 subsonic aircraft NO<sub>x</sub> emissions inventory [Baughcum *et al.*, 1996a, and Metwally 1995], 11.6 Tg N from biomass burning based on a preliminary CO emissions inventory by J. Logan, and 6.6 Tg N from soils following the scheme by Yienger and Levy [1995]. A lightning source of 4 Tg yr<sup>-1</sup> is apportioned over convective regions, following Price and Rind [1994]. The amount of NO<sub>y</sub> transported from the stratosphere is 0.5 Tg N yr<sup>-1</sup>. In sum, the total NO<sub>y</sub> source in the troposphere is 44 Tg N yr<sup>-1</sup>.

HC emissions from fossil fuel combustion are based on Piccot *et al.* [1992], with the emission ratios from Middleton *et al.* [1990] and light alkane ratios derived from measurements at Harvard Forest [Goldstein *et al.*, 1995]. Biomass burning sources are scaled to the CO source based on observed emission ratios [Lobert *et al.*, 1991; Laursen *et al.*, 1992; Nance *et al.*, 1993; Hurst *et al.*, 1994; and Andreae, 1996]. Isoprene emissions are computed based on the scheme by Guenther *et al.* [1995].

#### 4.2.1.3 GMI Core Model

The NASA AEAP GMI is a new approach towards integration of a 3-D chemical transport model for assessment purposes. The initiative brings together algorithms, databases, and process models from different investigators, and integrates them into a common shell, the so-called "core model." This core model is able to carry out simulations on both sequential/conventional type supercomputers as well as massively parallel machines. This structure allows for testing a matrix of possible numerical algorithms and physical parameterizations for simulating atmospheric physical and chemical processes, and intercomparing results using different approaches. The GMI Science Team has been constituted to put this model together and analyze the results. The development is still underway.

The simulations carried out by the core model for this report use 2 different sources for the input meteorological fields and 2 different transport schemes. These two fields are derived from climate model outputs (i.e., GCMs); one being the National Center for Atmospheric Research (NCAR) developed Community Climate Model version 2 (CCM2) and the other being the NASA GISS climate model in coordination with University of California at Irvine (UCI). NCAR meteorological data are saved every 6 hours and NASA GISS GCM data every 8 hours. Details of each transport scheme follow.

The GCM derived data of the NCAR CCM2 extend into the stratosphere (to 0.025 mbar) having 44 layers with horizontal resolution of approximately 3° by 5°. Advection and convection in the NCAR CCM2 are based on the semi-Lagrangian algorithm [Rasch and Williamson, 1990] and Hack convection algorithm [Hack, 1994]. Vertical diffusion in the boundary layer is represented by typical down gradient diffusion throughout the depth of the atmosphere plus a non-local term within the convective boundary layer [Holtslag and Boville, 1993].

The GCM derived data of the NASA GISS/UCI model has a resolution of 7.8° in latitude by 10° in longitude, with 21 vertical layers extending to 0.02 mbar. The NASA GISS model uses a second

order moment algorithm [Prather, 1986] for advection while convection is based on Rind *et al.* [1988].

Although no calculations of chemistry effects from aircraft are yet available from GMI, this report does include results from Rn and NO<sub>y</sub> tracer studies done with the GMI/CCM2 and GMI/UCI versions of these meteorological datasets. The GMI is also incorporating the winds and advection algorithm from the Data Assimilation Office (DAO) at NASA's Goddard Space Flight Center [Schubert *et al.*, 1995]. Results utilizing these winds/advection algorithms will appear in future reports.

## **4.2.2 EVALUATION OF MODELS**

### **4.2.2.1 Evaluation of Chemical Mechanisms**

In this section, several chemical reaction mechanisms and radiation codes for generating photolysis rate coefficients are compared in order to ascertain the level of agreement or identify discrepancies in our current understanding of atmospheric chemical processes. As discussed below, simulations of ozone formation in the upper troposphere agree to within 2 to 15% among tropospheric chemical models using NO<sub>x</sub>-catalyzed chemistry. The model comparison exercise included the IMAGES and Harvard models, described in Section 4.2.1, as well as some other current CTMs. Table 4-2 lists the participants of this comparison exercise and provides a brief description of their models (including literature reference).

Several research groups have compiled chemical reaction schemes derived from field and laboratory measurements, and have devised numerical techniques for calculating the production and destruction rates of reactive atmospheric constituents. In addition, photolysis rates are calculated using radiative transfer models employing various assumptions and parameterizations of radiative processes. These chemistry and radiation mechanisms must balance requirements for numerical accuracy against limitations of computational speed and memory, and different degrees of extrapolation are employed to account for the chemistry of important but poorly measured constituents and processes. Therefore, various research groups employ different species categories, reaction groupings, and reaction sequences in order to optimize their chemical reaction mechanisms to individual research objectives. Differences between calculated rates of chemical reactions provide a crude estimate of the current understanding of these processes, and also provide an estimate of the confidence with which these processes can be simulated in the troposphere.

#### *Comparison of Chemical Mechanisms*

For this comparison, we emphasize model calculations of ozone production and loss in the upper troposphere. All models were initialized with identical upper tropospheric chemical and meteorological conditions, according to specifications in a protocol document (available through Chris Walcek, SUNY Albany). Each group calculated photolysis rates from a specified ozone column under clear sky, no aerosol, no surface albedo conditions. Nine simulations were performed under a range of reactive nitrogen concentrations (10 pptv - 10 ppbv), and each group provided concentrations of several constituents at 12-hour intervals during each 10-day simulation. No emissions or non-chemical removal processes were considered in this comparison.

Figure 4-2 shows the calculated concentrations of  $\text{NO}_x$  and ozone during one 10-day integration according to six participating models for 3 ppbv total  $\text{NO}_y$ , initially present only as NO. During the 10-day period, highly reactive radicals reach a diurnally-varying, short-term steady-state, while total reactive nitrogen approaches a chemical steady-state within a time constant of several days. Ozone and hydrogen peroxide ( $\text{H}_2\text{O}_2$ ) slowly accumulate, never reaching a chemical balance, reflecting their relatively long chemical lifetimes in this region of the atmosphere. The total concentration of reactive nitrogen ( $\text{NO}_y = \text{NO} + \text{NO}_2 + \text{HNO}_3 + \text{HNO}_4 + \text{PAN} + \text{NO}_3 + 2\text{N}_2\text{O}_5$ ) remains essentially constant during the integrations, although some models include a relatively minor source of  $\text{NO}_x$  from nitrous oxide ( $\text{N}_2\text{O}$ ) reactions. All models initially show diurnal fluctuations in ozone concentration, which disappears after a few days as  $\text{NO}_x$  concentrations decrease, and the sunlight-induced  $\text{NO-NO}_2\text{-O}_3$  photostationary fluctuations diminish.

Figure 4-3 shows ozone formation rates averaged over the last five days of each 10-day integration calculated by the six models. The models agree to within 5 to 15% under most  $\text{NO}_y$  concentrations. The absolute agreement is within less than a few tenths of a ppbv per day for most mechanisms, although both the relative and absolute differences between models increase at  $\text{NO}_y$  concentrations greater than a few ppbv. At 10 ppbv  $\text{NO}_y$ , a concentration that is rarely observed in the upper troposphere, the calculated ozone formation rates disagree by about 50%.

The trends shown in Figures 4-2 and 4-3 are extremely sensitive to the precise time integration period, the hydrocarbon mix, pressure, temperature, photolysis rates, ozone and water vapor concentrations, among other factors. For this comparison, “typical” or “representative” values were specified for each of these parameters. The calculations shown here cannot be used to make generalized conclusions about the chemistry of reactive pollutants in the upper troposphere, since many additional nonchemical factors influence ozone and  $\text{NO}_y$  concentrations in the upper troposphere. The main purpose of the calculations shown here is to highlight the discrepancies in our ability to quantify the chemical reactivity of various pollutants in the upper troposphere.

Differences among the model results arise from differences in mechanism formulations, numerical techniques, photolysis rates and other factors. Deviations in calculated ozone chemical tendencies were not significantly correlated with deviations in numerous other model diagnostic parameters such as photolysis rates, concentrations of individual reactive nitrogen species, and calculated concentrations of OH and  $\text{HO}_2$  radicals. In addition, relative model discrepancies are different at different  $\text{NO}_y$  concentrations. Therefore, it is difficult to unambiguously identify the reasons for the differences among the various mechanisms. Figure 4-4 shows the relative root mean square deviations among models for numerous calculated parameters. The magnitude of the disagreement in ozone chemical tendencies is comparable to the differences among several other diagnostic parameters. Some of the largest differences in chemistry or photolysis rate calculations occur in those areas where rate coefficient recommendations are undergoing revisions based on recent measurements and evaluations. In particular, rate coefficients for PAN formation and ozone photolysis to give  $\text{O}(\text{D})$  are undergoing substantial revisions, resulting in corresponding deviations among modeling groups for these factors. In addition, the relatively large discrepancies in calculated PAN concentrations are misleading, since PAN accounts for only 1 to 3% of the total reactive nitrogen, and small differences in absolute concentration become large in a relative sense.

### *Comparison of Photolysis Rates*

Figure 4-5 shows scatter diagrams correlating two key photolysis rates and corresponding ozone formation rate calculations. All modeling groups calculated photolysis rates for 40°N, 21 June, clear-sky, no aerosol and zero surface albedo conditions. In addition, all groups used the identical vertical distribution of ozone and total ozone column (320 Dobson units). NO<sub>2</sub> photolysis rates are fairly consistently calculated, with a relative rms deviation of 6%. However, there were ±10% deviations in the calculated ozone photolysis rate. These deviations in part reflect recent suggested updates and controversies about the wavelength dependence of O(<sup>1</sup>D) quantum yields from ozone photolysis. Many of these updates have not been incorporated into standardized summaries of photolysis information.

In summary, several chemical reaction mechanisms and radiation codes used around the world for estimating ozone formation in the upper troposphere are compared. Among the mechanisms considered, calculated ozone formation rates from NO<sub>x</sub>-catalyzed reactions in the upper troposphere agree to within 2-15%. Differences between calculated ozone formation rates are comparable to the discrepancies in photolysis rates, nitrogen speciation, and free-radical concentrations calculated by the various models. The largest differences in chemistry or photolysis rate calculations occur in areas where rate coefficient recommendations are undergoing revisions based on new measurements and ongoing evaluations. In particular, rate coefficients for ozone photolysis (O(<sup>1</sup>D)) and PAN formation are undergoing substantial revisions, resulting in corresponding deviations among modeling groups for these factors.

#### **4.2.2.2 Rn Tracer Study: Evaluation of Rapid Vertical Transport Near the Ground**

##### *Description of the Experiment*

Radon (Rn) is chemically inert, has a 5.5-day e-folding in the atmosphere due to radioactive decay, and has generally well understood sources from radium decay in soils. For these reasons, it provides a useful tracer of rapid transport processes in models of the atmosphere. Rn was recently used in two model intercomparison workshops sponsored by the World Climate Research Program (WCRP) [Jacob *et al.*, 1996a (hereafter referred to as WCRP93); Rasch *et al.*, 1996 (hereafter WCRP95)] as part of its evaluation of transport processes in the atmosphere. Areas remote from radon sources (i.e., oceanic regions or the upper troposphere) are typically characterized by low values of radon unless there is a mechanism like convection which can move it rapidly into that region. High values of radon thus provide an indication of where those rapid transport mechanisms are important. The observational data used to compare to the models discussed below is described in more detail in Jacob *et al.* [1996b]. In the following paragraphs we describe briefly some conclusions arising from a comparison of observations with the IMAGES simulations of Rn, and the GMI model driven by meteorology archived from the NCAR CCM2 and GISS/UCI models. A version of the Harvard/GISS model was included in the earlier WCRP inter-comparisons.

The modeling of atmospheric trace species has evolved very rapidly over the last five years. Our understanding of the processes controlling trace species distribution and the representation of those processes in models has changed substantially. Models are also occasionally adjusted to be

optimal for treating a particular type of problem. For example, it is important to resolve vertical structures in the vicinity of the tropopause for problems in which stratosphere-troposphere exchange is critical. This would not be important for studying the controlling influences of a species with an origin at the Earth's surface if the area of focus was the middle troposphere. To minimize the computational burden, tradeoffs in resolution and process detail are balanced, and a reasonable compromise is chosen. For this reason, a variety of model configurations have been adopted by the groups participating in this assessment, and the model configurations have been changing as more is learned about the controlling processes for the problem of interest. The models used in the assessment reflect a variety of optimization strategies.

The CCM2 and GISS/UCI meteorological datasets used here have lower horizontal resolution and higher vertical resolution than the configurations typically used for tropospheric simulations, in order to provide resolutions more suited for simulations of stratosphere-troposphere exchange (STE) processes and trace species distributions in the stratosphere used by the Stratospheric Tracers of Atmospheric Transport (STRAT) Mission Science Team. More recent configurations of the NCAR and GISS climate models, with improved physical parameterizations and resolutions more suited for the troposphere, were used in the WCRP93 and WCRP95 workshops. The differences in parameterizations and resolution have a significant impact on the Rn simulation, and we will occasionally comment on this and contrast it with the WCRP simulations. We also note that the GMI model can be used with the NASA DAO analyses for the driving meteorological data. Rn simulations with these data are described in Allen *et al.* [1996].

Only monthly averages were reported by the GMI model and the IMAGES model has only monthly average meteorology and thus does not produce any variability to be compared with observations. This means that we cannot comment on higher frequency phenomena in the simulations, and thus we concentrate on seasonal phenomena.

The simulations used the scenario proposed for the WCRP95 intercomparisons. Rn was assumed to be emitted from all land surfaces except Greenland and Antarctica (no emissions poleward of 60°S and 70°N). Emissions were assumed to be uniform in space and time over this region, with a source strength of about 1 atom cm<sup>-2</sup> s<sup>-1</sup> between 60°N and 60°S and 0.5 atom cm<sup>-2</sup> s<sup>-1</sup> between 60°N and 70°N (1 atom cm<sup>-2</sup> s<sup>-1</sup> corresponds to 3.69 x 10<sup>-21</sup> kg m<sup>-2</sup> s<sup>-1</sup>). Each model renormalized the basic emission rate slightly to provide a global value of 15 kg yr<sup>-1</sup> after compensating for differing land masks. The decay rate for Rn was set to provide a half-life of 3.83 days corresponding to an e-folding lifetime (i.e., time to reach 1/e = 1/2.72 of initial value) of 5.52 days.

The models were started with zero atmospheric distributions and were integrated until an equilibrium between sources and sinks was reached. The models were then evaluated over a subsequent one year simulation.

### *Model Results*

Figure 4-6 shows the zonally averaged December, January, February (hereafter DJF) composite distribution for Rn for the three models. The contours are approximately logarithmic in scale. High values dominate near the surface, decreasing towards the tropopause, reflecting the rapid decay occurring as Rn moves from its source region. Relatively high Rn concentrations are evident in the tropical upper troposphere in all models, with maxima concentrated in the region of

outflow from convective regions. The higher emissions in the Northern Hemisphere (NH) associated with the dominance of land there is also evident. The DJF figures are consistent with models participating in the WCRP intercomparisons, although the GMI/UCI model tends to have higher values at 100 mbar than most of the WCRP participants.

The high values in the upper troposphere stand out even more strongly during June, July, and August (JJA), particularly in the GMI/UCI model which has a maximum value of order  $10 \times 10^{-21}$  (volume mixing ratio units) at 300 mbar in the NH. This equatorial maximum was also evident in the related GISS model in the WCRP intercomparison.

A region of discontinuity indicated by “kinks” in the contours at 100 mbar is evident during both seasons in IMAGES at the tropical tropopause where the contours are nearly horizontal and cluster very closely. The discontinuity is thought to be directly connected to a lack of temporal variability in its convection scheme and the use of climatological, monthly mean cloud statistics. The GMI/CCM2 model shows substantially more mixing in the upper polar troposphere than either of the two other models. IMAGES transports significantly less  $R_n$  into the middle and upper troposphere in the south polar regions than most other CTMs.

A composite observational profile over the western US (115 to 100°E, 35 to 45°N) is shown in Figure 4-7 for summer (JJA, panel a) and winter (DJF, panel b). The observational profiles are comprised of a subset of observed profiles from Liu *et al.* [1984]. The models provide reasonable simulations for both seasons. During the winter season, the GMI/UCI model shows the strongest venting to the upper troposphere and stratosphere, a bias also seen in the companion GISS and Harvard datasets used in the earlier intercomparisons. The IMAGES model has the highest surface values and the strongest gradient near the surface where it also has the highest vertical resolution (about twice that of the CCM2 and three times that of the UCI model in the lower troposphere). All models tend to overestimate the  $R_n$  concentrations during summer at 10 km. The GMI/CCM2 model has the lowest concentrations in the upper troposphere and lower stratosphere where it has the highest vertical resolution of the 3 models. A hint of a problem with the seasonal cycle over the western US can be seen in Figure 4-7, panels a and b. While the observations suggest a maximum at the surface in the winter months and minimum in summer (consistent in a physical sense with the idea of a trapping of boundary layer air during the winter, and the convective venting of boundary layer air in summer), the variation in the IMAGES model is much weaker. The physically intuitive seasonal cycle is seen at some sites, e.g., Socorro, New Mexico (not shown), although it is substantially weaker in that model than the observations.

Perhaps the most comprehensive set of vertical profiles assembled for one region are the those gathered by M. Kritz [personal communication] in the summer of 1994 in a series of flights originating in the San Francisco area and extending over the region 125 to 114°W longitude, 34 to 41°N latitude. A comparison of the composite summer profile for the models and observations can be seen in Figure 4-7, panel c. All models have difficulty in capturing the “C” shape profile (i.e., mixing ratios increasing in the upper troposphere) seen in the San Francisco observations.

A rigorous test of the simulation of transport to remote regions of the world is provided at Mauna Loa (Figure 4-8, panel a), where measurements are made at about 600 mbar and sampled during downslope conditions. The measurements thus provide a useful measurement of the free troposphere from a surface site. The models significantly underestimate the  $R_n$  amount there, as do all other models we are aware of. Kasibhatla and Mahowald [personal communication] have

suggested that this error is due to a significant underestimate of the emission over the Asian plateau. The models capture the seasonal cycle of transport of continental air off the coast of the US well at Bermuda (Figure 4-8, panel b), demonstrating their ability to treat resolved scale transport accurately, at least over relatively short distances in areas with well characterized meteorology (like the eastern US and adjacent Atlantic). The GMI/CCM2 model tends to overestimate transport here during winter months, although this is not seen in the WCRP95 simulations using improved model physical parameterizations and horizontal resolution.

The IMAGES simulation at Cape Grim (Tasmania, Figure 4-8, panel c) shows the right seasonal cycle, although it is a factor of two to three higher than the corresponding observations. The GMI/CCM2 and GMI/UCI models are close in amplitude but lack the appropriate seasonal cycle. Again, their simulations in the WCRP95 intercomparison were considerably better, presumably because of improved parameterizations and resolution. Because only one year of observations was available, one cannot discount natural variability as an explanation for model/observation discrepancies there.

There are on the other hand more than 10 years of observations for the French islands of Crozet, Kerguelen and New Amsterdam located in the South Indian Ocean [Lambert, Polian, Ardouin and Balkanski, personal communication] and at Dumont d'Urville (Antarctica), and each model (particularly IMAGES) significantly overestimates the measured values in these regions. This problem is demonstrated for two of the stations in Figure 4-8, panel d. These simulations are significantly less accurate in the Southern Hemisphere (SH) than the simulations obtained in WCRP95 using the meteorology from the CCM2 or GISS/UCI models.

### *Conclusions*

These models generate simulations of Rn transport that are of comparable quality to other CTMs. They are not the best, nor the worst when evaluated in the context of the WCRP intercomparison. It is important to be aware of the following IMAGES and GMI model behavior:

- Very strong and rapid transport from the surface to the upper troposphere during NH summer by GMI/UCI.
- The IMAGES and GMI/UCI models show a much more isolated summer polar region than does the GMI/CCM2 model. There is also substantially stronger mixing into the lower stratosphere in the tropics in IMAGES and the GMI/UCI models than that seen in the GMI/CCM2 model although it is difficult to see in the Figure 4-6 plots.
- There is a suggestion of excess diffusive transport to the remote extratropics for the IMAGES model, as seen by the Cape Grim and Dumont d'Urville comparisons with observations.
- There is a suggestion of the wrong seasonality of boundary layer fluxes over the western US in IMAGES.
- There is a suggestion of excessive vertical transport to the upper troposphere in the GMI/UCI model, at least over the western US.

These characteristics of the models are important to the assessment, because they indicate areas where model uncertainties may influence our ability to correctly interpret model results. For example, overly rapid cross tropopause transport of NO<sub>x</sub> into the lower stratosphere could

certainly affect our interpretation of the models response to airplane emissions. Similarly, overly rapid transport by convection from the surface could affect our perception of the relative importance of surface emission of  $\text{NO}_x$  to that of aircraft.

Later versions of the transport models from GISS/Harvard/UCI and NCAR (documented in the WCRP intercomparisons) show noticeable improvements in the Rn simulation, when compared to the simulations described here, which use earlier, less accurate meteorology to drive the CTM. An obvious improvement to the GMI modeling effort would be to utilize these more recent datasets for tropospheric simulations. This update to the more recent model datasets is in progress.

#### **4.2.2.3 $\text{NO}_y$ Tracer Study: Evaluation of Large-Scale Transport in the Upper Troposphere**

##### *Description of the Experiment*

The  $\text{NO}_y$  tracer study was designed to identify some important modeling issues that need to be addressed in simulations of subsonic aircraft effects on ozone. Like the Rn study, this study is designed to compare the effects of transport processes, but in this case focusing on the processes affecting the amount of odd-nitrogen in the upper troposphere. The chemical family  $\text{NO}_y$  (sum of  $\text{NO}_x$  and its oxidation products) is conserved with the exception of precipitation and surface-deposition of soluble or sticky components such as  $\text{HNO}_3$ . By focusing on  $\text{NO}_y$ , we avoid uncertainties associated with transformation between  $\text{NO}_x$  and  $\text{NO}_y$ .  $\text{NO}_y$  is emitted by aircraft, lightning, and surface sources (combustion, soils), and is also transported down from the stratosphere to the troposphere. For the present simulations we defined each source as follows:

- *Aircraft Emissions:* A source of  $0.46 \text{ Tg N yr}^{-1}$  was specified on a  $1^\circ$  latitude x  $1^\circ$  longitude x 1 km altitude grid with monthly resolution for 1992. This source is described in detail in Chapter 2; it includes emissions from both scheduled aircraft [Baughcum *et al.*, 1996a] and military and non-scheduled aircraft [Metwally, 1995]. An error was subsequently discovered in the way that  $\text{NO}_x$  from military and non-scheduled aircraft was calculated. Table 2-3 reflects the corrected  $\text{NO}_x$  values.
- *Stratospheric Source:* Seasonally invariant flux of  $0.45 \text{ Tg N yr}^{-1}$  was assumed across the tropopause [Ko *et al.*, 1991]. This flux was specified in IMAGES by imposing a fixed concentration in the top model level (50 mbar) and scaling the resulting tropospheric  $\text{NO}_y$  concentrations by the ratio of the calculated cross-tropopause flux to  $0.45 \text{ Tg N yr}^{-1}$ . In the other models, the cross-tropopause flux was imposed by a spatially uniform, time-independent source of  $\text{NO}_y$  in the middle stratosphere.
- *Lightning Source:* A global lightning source of  $5 \text{ Tg N yr}^{-1}$  was assumed with monthly temporal resolution. This source was distributed geographically using the ISCCP convective cloud top data for 1983 to 1991 [Rossow and Schiffer, 1991] and the parameterization of Price and Rind [1992a, b; 1993] relating lightning flash frequency to cloud top height. C-shaped vertical distributions of  $\text{NO}_x$  emissions from lightning (shown in Table 4-3) were assumed on the basis of cloud-ensemble model [Tao and Simpson, 1993] calculations by K. Pickering [1996].

- *Surface Source:* Three types of surface emissions were included: emissions from fossil fuel combustion (21.0 Tg N yr<sup>-1</sup>), biomass burning (4.9 Tg N yr<sup>-1</sup>), and soils (5.5 Tg N yr<sup>-1</sup>). Emissions from fossil fuel combustion [Benkovitz *et al.*, 1996] were specified as a time-independent source with 1° x 1° resolution. The biomass burning source and the soil source [Yienger and Levy, 1995] were specified with 1° x 1° spatial resolution and monthly temporal resolution based on the Global Emissions Inventories Activity (GEIA) inventory.

Removal of NO<sub>y</sub> from the atmosphere by deposition was parameterized as a first-order loss dependent only on altitude. The lifetimes of NO<sub>y</sub> against deposition were interpolated from the following values [Logan *et al.*, 1981]:

Ground to 800 mbar	1 day
600 mbar	5 days
500 mbar	10 days
400 mbar	18 days
300 mbar	38 days
200 mbar	no loss

This representation of NO<sub>y</sub> deposition is greatly oversimplified in that it does not account for the sensitivity of NO<sub>y</sub> deposition to the chemical partitioning of NO<sub>y</sub> (HNO<sub>3</sub> is the main depositing component of NO<sub>y</sub>) or to the geographical distribution of precipitation. As a result we may expect to overestimate the contribution of surface sources to NO<sub>y</sub> in the upper troposphere, because the coupling between upward motions and scavenging is not accounted for [Rodhe, 1983; Giorgi and Chameides, 1986; Balkanski *et al.*, 1993]. Aircraft contributions to NO<sub>y</sub> in the upper troposphere should be less affected by this problem because the removal of NO<sub>y</sub> from the upper troposphere is controlled more by large-scale subsidence (resolved by the models) than by precipitation scavenging.

The models participating in the NO<sub>y</sub> tracer study were IMAGES, Harvard/GISS, GISS GCM 2' (new version of the NASA GISS GCM [Rind and Lerner, 1996]), and GMI with two different sets of meteorological fields (CCM2 and UCI). Descriptions of these models, with exception of the new GISS GCM, are given in Section 4.2.1. Each model conducted four separate simulations covering the different NO<sub>y</sub> sources listed above. The simulations were conducted for two years, except for the stratospheric source simulation which was conducted for 3 to 5 years. The first year (or two) was used for initialization, and results were archived from the last year.

### *Model Results and Discussion*

Figure 4-9 compares the concentrations of aircraft NO<sub>y</sub> simulated by the different models at 250 mbar. 50% of total aircraft emissions are released in a narrow altitude band between 200 and 270 mbar (10- to 12-km) [Baughcum *et al.*, 1996a]. The highest concentrations in Figure 4-9 are found at northern mid-latitudes where the emissions are concentrated. In this region, the NO<sub>y</sub> concentrations differ by a factor of 5 among models. Some of the difference appears to reflect the coarse vertical gridding of the models; interpolation of the aircraft source on the model grid induces numerical diffusion and also aliases the actual altitude of emission. This point is illustrated in Figure 4-10 with the zonal mean concentrations of aircraft NO<sub>y</sub> in the different models given as a function of altitude and latitude (model gridpoint altitudes are also shown on the Figure). In the GISS models (Harvard, GISS 2', GMI/UCI), which have vertical resolutions coarser than 100

mbar, the vertical distribution of aircraft  $\text{NO}_y$  in the upper troposphere is defined to a large extent by the model gridding. In comparison with other models, Figure 4-10 suggests that the 50-mbar resolution of the IMAGES model may be more adequate to capture the vertical structure of aircraft emissions.

The zonal mean concentration maxima of aircraft  $\text{NO}_y$  simulated by the different models are located at 300 to 200 mbar in the northern extratropical latitudes, and range from 40 to 200 pptv depending on the model (Figure 4-10). These values are found to be similar to those in the AERONOX simulations by the ECMWF model, Hamburg version (ECHAM3) and GISS models [Sausen *et al.*, 1995], after correcting for the higher aircraft source used in AERONOX ( $0.85 \text{ Tg N yr}^{-1}$  vs.  $0.46 \text{ Tg N yr}^{-1}$ ). The earlier global model study by Kasibhatla [1993], which used a global source similar to ours ( $0.45 \text{ Tg N yr}^{-1}$ ) indicates a maximum zonal mean  $\text{NO}_y$  contribution from aircraft of about 500 pptv at 190 mbar, much higher than is found here. A possible explanation is that most of the emissions in the Kasibhatla [1993] study were released at 190 mbar (the next-lower gridpoint in that model was at 315 mbar), where vertical mixing is slower because of its location in or near the stratosphere. In the same way, the relatively high  $\text{NO}_y$  maximum found in Figure 4-10 for the GISS 2' model ( $>200$  pptv) could reflect the high altitude of that maximum (200 mbar).

Despite the large variations among models in the simulation of  $\text{NO}_y$  in the upper troposphere, there is close similarity in the simulated large-scale vertical gradients between the upper and lower troposphere (Figure 4-10). For example, the aircraft contribution to  $\text{NO}_y$  concentrations in surface air at northern mid-latitudes is only 2 to 5 pptv in all models. Such similarity between models in the computed large-scale subsidence rates had been noted previously in the WCRP93 intercomparison of short-lived tracers in global models [Jacob *et al.*, 1996a]. Meridional transport of aircraft  $\text{NO}_y$  from mid-latitudes to the tropics and across the equator in the upper troposphere varies greatly, however, among models. GMI/CCM2 has the most extensive meridional transport, with concentrations of 5 to 10 pptv in the upper troposphere at southern mid-latitudes; Harvard and GMI/UCI have the slowest, with concentrations of 1 to 2 pptv in the same region. The new GISS meteorology, (2') used in the GMI model shows more extensive mixing into the upper troposphere of the southern tropics. IMAGES appears to have anomalously high interhemispheric transport in the lower stratosphere. Large differences among global 3-D models in the simulation of meridional transport in the upper troposphere had also been noted in the previously cited WCRP intercomparison.

Zonal mean concentrations of  $\text{NO}_y$  originating from different sources are shown for July in Figure 4-11 for the GMI/CCM2 model. In this and the other models, we find that the zonal mean contribution of aircraft to total  $\text{NO}_y$  in the upper troposphere at northern mid-latitudes is about 10% in summer and 15% in winter. Most of the  $\text{NO}_y$  in the upper troposphere at northern mid-latitudes is from surface sources and lightning; the contribution from the stratosphere is small and comparable to the aircraft contribution, although it increases rapidly above 200 mbar. The AERONOX model simulations indicated a 30-50% relative contribution of aircraft to zonal mean  $\text{NO}_y$  levels in the upper troposphere at northern mid-latitudes [Sausen *et al.*, 1995], much higher than is found here. The discrepancy is due in part to differences in the magnitude of the aircraft source, and also more interestingly to differences in the influence of the lightning source. In the AERONOX simulations, lightning accounts for only ~10% of  $\text{NO}_y$  in the upper troposphere at northern mid-latitudes in summer; whereas in our simulations it accounts for 30-50%. There may be significant differences between AERONOX and the present simulations in the specification of

lightning  $\text{NO}_x$  emissions at northern mid-latitudes. Also, the AERONOX simulations assumed that lightning emissions are released uniformly in the convective column, whereas we assume a C-shaped distribution (Table 4-3) which would enhance the influence of lightning  $\text{NO}_x$  in the upper troposphere.

The models presented here and the AERONOX studies both indicate a major contribution of surface sources to  $\text{NO}_y$  in the upper troposphere. We have, however, little confidence in our ability to represent this source because of the crudeness of the parameterized  $\text{NO}_y$  removal. Since  $\text{HNO}_3$  is the principal depositing component of  $\text{NO}_y$ , it is critical to resolve the chemical partitioning of  $\text{NO}_y$ . Another critical issue is quantification of the fraction of  $\text{HNO}_3$  scavenged during wet convective transport.

### *Conclusions and Recommendations*

- The vertical grid resolution of the model is likely a critical issue when simulating the effect of subsonic aircraft emissions on  $\text{NO}_x$  concentrations in the upper troposphere. A vertical resolution of at least 1-km between 8- and 14-km altitude may be necessary to resolve the vertical distribution of aircraft emissions and the resulting chemical perturbations.
- The relative perturbation of aircraft emissions to  $\text{NO}_x$  in the upper troposphere depends on the relative contributions of lightning and surface sources to the  $\text{NO}_x$  budget. Quantifying the influence of these two sources on  $\text{NO}_x$  levels in the upper troposphere is an integral part of a subsonic aircraft assessment.
- Our results suggest that aircraft make a much lower contribution to  $\text{NO}_y$  levels in the upper troposphere than was previously concluded by AERONOX. The difference is due in part to lower aircraft emissions in our simulations ( $0.46 \text{ Tg N yr}^{-1}$  vs.  $0.85 \text{ Tg N yr}^{-1}$ ), and also to differences in the contribution of the lightning source. There is considerable uncertainty regarding the magnitude and spatial distribution (vertical and horizontal) of  $\text{NO}_x$  emission from lightning. Narrowing down this uncertainty should be a top research priority.
- Both our simulations and those of AERONOX indicate a major contribution of surface sources to  $\text{NO}_y$  levels in the upper troposphere at northern mid-latitudes. This source may be overestimated in both studies due to inadequate accounting of the efficient scavenging of  $\text{HNO}_3$  in wet convective updrafts. Critical uncertainties that need to be addressed are the chemical partitioning of  $\text{NO}_y$  (particularly in the boundary layer, where  $\text{HNO}_3$  is prone to deposition) and the efficacy of  $\text{HNO}_3$  scavenging in wet convective systems.

#### **4.2.2.4 Comparison of IMAGES and Harvard Models with Observations**

Evaluation of the ability of a model to reproduce observed features of the atmosphere is a prerequisite for use of the model in an assessment mode. We describe here evaluation of the IMAGES model and the Harvard model. An earlier version of IMAGES was evaluated with a variety of atmospheric observations in Müller and Brasseur [1995]. The version of IMAGES used for this assessment had been somewhat modified relative to the older version, and there are considerably more data available now for model evaluation. The Harvard model is a global version of the model described in Jacob *et al.* [1993] with updated chemistry, and will be described in detail in a later publication [Wang, personal communication]. The models were evaluated with the

same data: (1) the methylchloroform lifetime; (2) surface data for carbon monoxide from about 30 sites [P. Novelli, personal communication]; (3) ozone profiles for 18 sites [J. Logan, personal communication] and surface data from about 25 sites [Oltmans and Levy, 1994; J. Logan, personal communication]; and (4) aircraft data for NO, HNO<sub>3</sub>, and PAN, provided on a grid on 5° in latitude and longitude, and 1 km in altitude [J. Bradshaw, personal communication]. The data for CO and ozone are generally based on several years of measurement, and should represent climatological means. The observations of NO species are from campaigns, and cluster in particular seasons and regions of the globe as shown in Figure 4-12. Vertical profiles were derived from 15 regions for June-October, and 9 regions for December to March (Figure 4-12); the profiles cannot be considered climatological means. Many of the campaigns were large scale surveys, so that many regions with data have extremely limited sampling. The profiles extend to only 7 km for data from Canada, Alaska, and the Amazon, and to about 11 km for the US, western Pacific, Brazil, and south tropical Atlantic.

### IMAGES

- *OH and CO:* The lifetime for methylchloroform due to reaction with OH is 4.2 years in IMAGES (for 200 to 1000 mbar). Prinn *et al.* [1995] derived a lifetime due to OH of  $4.9 \pm 0.2$  years (for 200 to 1000 mbar), based on an analysis of observations of methylchloroform and allowing for an ocean sink; their combined lifetime (OH + ocean) was  $4.6 \pm 0.2$  years. The analysis of Prinn *et al.* [1995] implies that the mean OH concentrations in IMAGES are too high by about 10%. IMAGES systematically underestimates CO, by as much as 20% in the NH. The seasonality of CO is reproduced reasonably well, but the winter-spring maximum is 1 to 2 months early in the NH.
- *NO, HNO<sub>3</sub> and PAN:* Several general conclusions emerge from the comparison of IMAGES with nitrogen oxide observation. The model is in reasonable agreement with NO profiles from northern mid-latitudes and from the western Pacific below 7 km, except for an overestimate of near-surface continental values. The model overestimates HNO<sub>3</sub> for the western US, and Canada. Concentrations of PAN are in good agreement with the data for the South Atlantic, Canada, and Alaska, but are too high in the upper troposphere off Asia. It tends to underestimate NO above 8 km off the Asian Coast in March, but not in October (refer to Figure 4-13). The model also underestimates NO above 8 km over the southern tropical Atlantic, by as much as a factor of 2, while it agrees well with the data below 6 km; the model overestimates HNO<sub>3</sub> above 6 km in this region, so the NO/HNO<sub>3</sub> ratio is much too low (Figure 4-13, dashed lines show IMAGES results). The ratio is too low also off the coast of Japan and Hong Kong. Difficulties in simulating observations of the NO/HNO<sub>3</sub> ratio using current photochemical schemes were also discussed in Chapter 3.
- *Ozone:* A major characteristic of the distribution of tropospheric ozone is the seasonal pattern; for northern mid-latitudes there is a broad maximum in ozone in the middle troposphere extending from May to August. This changes to a spring maximum in the upper troposphere, and at lower latitudes [e.g., Logan, 1985]. IMAGES appears to have about the correct annual mean amount of ozone for northern mid-latitudes. However, for 30-75°N below 400 mbar, the model tends to be too high for December to March, and too low from about May to August (e.g., Figure 4-14). The discrepancies are about 10 to 20 ppbv out of 40 to 60 ppbv. The model's seasonal cycle above 800 mbar peaks in early spring, 2 to 3 months earlier than the

data. Comparisons with data from surface sites at several altitudes in southern Germany show that the model has a summer maximum in the boundary layer, but a spring maximum by 700 mbar. The model reproduces the seasonal cycle in surface ozone quite well at most of the northern remote sites, with a tendency for the spring maximum to be 1 to 2 months early. The model significantly underestimates ozone at 200 mbar in winter and spring for latitudes above 45°N.

In the northern sub-tropics, the model is much too high in December to April, primarily above 600 mbar, with discrepancies of a factor of 2 at 200 mbar; the model is too low in May and September below 400 mbar, but in reasonable agreement for the rest of the year. In the southern tropics, the model is too low most of the year at Natal below 300 mbar, with largest discrepancies (~20 ppbv) in September to February (Figure 4-14); it is also too low at Samoa below about 400 mbar for October to June. The model tropopause appears to be too low over Samoa. The model is in excellent agreement with the stations at southern mid-latitudes, but is too low below 600 mbar over the Antarctic.

### *Harvard*

- *OH and CO:* The lifetime for methylchloroform is 5.5 years, indicating that the globally averaged OH is about 10% too low. The model underestimates CO in winter and spring at middle and high latitudes of the NH, but matches the late summer minimum reasonably well; it reproduces the data from the sub-tropics and tropics, but systematically overestimates CO at southern mid-latitudes.
- *NO, HNO<sub>3</sub> and PAN:* The agreement for the Harvard model for NO is about the same as that for IMAGES, as shown in Figure 4-13. The major difference between the model profiles is that the Harvard model has much lower NO in winter at latitudes above 45°N. HNO<sub>3</sub> is too high almost everywhere, except the lower troposphere over the south tropical Atlantic, and near the surface over the continents. The Harvard model also predicts ratios of NO/HNO<sub>3</sub> in the upper troposphere that are too low. The model profiles are quite different for HNO<sub>3</sub>, however, likely a consequence of the treatment of rainout of soluble gases. The Harvard model generally has higher concentrations than IMAGES in the lower half of the troposphere, while IMAGES has higher concentrations in the upper troposphere (Figure 4-13). PAN concentrations are in reasonable agreement for profiles at northern mid-latitudes, except that the model is too high in the boundary layer for Alaska and Canada. The model overpredicts PAN in the upper troposphere over Hawaii and the US, and for the whole troposphere off the coast of Asia in fall; it underpredicts PAN at about 6- to 10-km over the region of Ascension Island, but matches the low values in the marine boundary layer. The model captures the low values of PAN in the more tropical regions off the coast of Asia in the fall.
- *Ozone:* The Harvard model reproduces the distribution of ozone in the middle troposphere of the NH rather well, as shown for two stations in Figure 4-14; it captures the broad summer maximum at middle and high latitudes, and the shift to a spring maximum at the Hilo Pacific site. The model underpredicts, by 10 to 20 ppbv, the amount of ozone for 500 mbar in the middle of the year for the stations with the highest concentrations, Wallops Island, Hohenpeissenberg, and Sapporo. It also fails to capture the summer minimum in the lower troposphere at the more southerly Japanese stations. The major deficiency of the Harvard

model with respect to the ozone distribution is that the model tropopause is too high outside of the tropics, a consequence of the low vertical resolution of the model (see Figure 4-1). The model layer at ~200 mbar is in the troposphere all year, with correspondingly low values of ozone (Figure 4-14). Consequently the model grossly underestimates the amount of ozone at 200 mbar for latitudes higher than 35°, and underestimates ozone at 300 mbar for most stations at latitudes higher than 40°. Another result of the low vertical resolution of the model is that vertical profiles for ozone are often too uniform, with little increase in ozone at the higher altitudes.

The model underpredicts the amount of ozone above 6 km over Natal, particularly in August to December (e.g., Figure 4-14). The discrepancy is as much as 20 to 25 ppbv out of 75 ppbv. The model is as much as 10 to 15 ppbv too high below 2 km. The model is more successful in reproducing the low values of ozone over Samoa, but it underpredicts ozone in the upper troposphere, by 5 to 15 ppbv out of 40 ppbv in October to January. The model overestimates the amount of ozone at the surface for all the tropical stations, by as much as 10 to 20 ppbv. The model seriously underpredicts ozone at Pretoria above 4 km, but matches the data from southern mid-latitudes quite well, except in the upper troposphere.

In conclusion, both the IMAGES and Harvard chemical transport models have difficulties with representing the limited amount of data available for nitrogen oxides in the upper troposphere. IMAGES does not get the correct seasonal cycle nor the near-tropopause values for ozone. As will be discussed further in Section 4.4, the disagreements with observations suggest strong reservations about the capabilities of these models to accurately represent the effects on tropospheric chemistry from aircraft emissions.

### **4.2.3 SENSITIVITY STUDIES**

#### **4.2.3.1 Description of the Experiments**

A series of sensitivity studies has been designed to examine the effects of uncertainties in our knowledge of tropospheric processes on the ozone changes calculated from aircraft emissions. These studies primarily use the IMAGES chemical transport model, although a subset of these studies has also been calculated with the Harvard/GISS model. In these studies, the baseline calculation for the current atmosphere is based on the standard version of each model, i.e., there was no attempt to standardize the chemistry or treatments of input parameters. These calculations stress sensitivity to uncertainties rather than absolute values of the environmental effects.

Table 4-4 describes sensitivity cases examined by the two models. Particular emphasis is given to the significant uncertainties associated with the lightning production of nitrogen oxides and the effect of convection on upper tropospheric concentrations. The lightning source is poorly known, with a likely value ranging from approximately 2 to as much as 12 Tg N yr<sup>-1</sup>. Cases 3A through D examine a range of 2 to 10 Tg N yr<sup>-1</sup> under two different assumptions of the spatial distribution of NO<sub>x</sub> production (based on Turman and Edgar [1982] and on an updated version of Price and Rind [1994], as discussed in Section 4.2.2.3). In their baseline calculations, the IMAGES model assumes lightning production of 5 Tg N yr<sup>-1</sup> based on Turman and Edgar [1982], while Harvard uses 4 Tg N yr<sup>-1</sup> based on Price and Rind [1994].

Several other significant differences between the baseline models should be noted relative to the model descriptions given earlier (Section 4.2.1). Meaningful information from the Harvard model is restricted to altitudes below 150 mbar (about 14 km) while the IMAGES model extends to 50 mbar (about 20 km). The baseline version of the IMAGES model uses the NASA 1990 emissions database [Wuebbles *et al.*, 1993a, b; Baughcum *et al.*, 1993a] while the Harvard model uses the more recent 1992 emissions database [Chapter 2, Baughcum *et al.*, 1996]. Although the database for 1992 includes seasonal variations and many improvements over the earlier database, there are only minor differences in the globally integrated amount of nitrogen oxides produced from aircraft ( $0.46 \text{ Tg N yr}^{-1}$  for the 1992 database compared to  $0.44 \text{ Tg N yr}^{-1}$  for the 1990 database). In Case 2, both IMAGES and Harvard use the 1992 database. With the exception of Case 8 (1992 emissions increased by a factor of five), all other sensitivity calculations with the IMAGES model are based on the 1990 emissions database.

The large uncertainties in model treatment of convection processes are partially captured by two cases (4A and 4B) that increase and decrease, respectively, the rate for convection to the upper troposphere by a factor of two.

Heterogeneous chemistry in the troposphere, in particular the reaction of  $\text{N}_2\text{O}_5$  with water to form  $\text{HNO}_3$ , is examined in Case 5. The effect of incompletely representing hydrocarbon chemistry in the model is examined in Case 6, largely motivated by the fact that some of the earlier published studies of aircraft effects did not include NMHCs. The effect of reactions that increase cycling of nitrogen oxides is examined in the IMAGES model by increasing the photolysis rate of nitric acid by a factor of three.

In order to examine potential nonlinearities associated with future increases in global emissions of nitrogen oxides from aircraft, Case 8 examines the effect of increasing the 1992 emissions by a factor of five. There was no attempt in this assessment to examine more realistic representations of future emissions.

#### 4.2.3.2 Model Results and Discussion

*Effects of Sensitivity Analyses on Derived Background Atmosphere:* Figures 4-15 and 4-16 compare distributions at the corresponding latitudes and longitudes from the sensitivity studies using IMAGES with the observations at Ascension Island and the eastern US, respectively. Comparisons with the  $\text{NO}$  distribution are generally better with the larger lightning source of  $\text{NO}_x$ , but the comparison with the  $\text{HNO}_3$  data becomes even worse. Reducing convection or increasing  $\text{NO}_x$  recycling also improves the comparison in the upper troposphere with  $\text{NO}$ , but with no meaningful impact on the poor comparison with the  $\text{HNO}_3$  data at Ascension Island. The sensitivity studies have a minor effect on the distribution of ozone at mid-latitudes, with only a small variation, as shown in Figure 4-17. The model results are always low compared with the data at Wallops Island, but do show a better comparison with data at Natal when more lightning or reduced convection are used. It should be noted that these are examples of the effects of model sensitivity and are not in any way conclusive statements about what is needed to better explain observed distributions. In addition, the representativeness of the existing measurements remains to be verified.

Figures 4-18 through 4-22 compare derived distributions of  $\text{NO}_x$  and ozone from the IMAGES and Harvard models for Case 2 using the 1992 aircraft emissions. There are many similarities in

the derived distributions of  $\text{NO}_x$  in the two models. Notable differences occur outside North America, where the Harvard model derives larger peak amounts of  $\text{NO}_x$  at 300 mbar than the IMAGES model. The zonally averaged distributions for  $\text{NO}_x$  are similar within the constraint of the low upper boundary in the Harvard model. As mentioned earlier, the Harvard model has much less variation in concentrations of ozone in both the 300 mbar latitude and longitude contours and in the zonally-averaged distribution.

Further discussion on the effect of individual sensitivity studies on the background atmosphere are also given in the next section.

*Sensitivity Analyses of Aircraft Effects on  $\text{NO}_x$  and Ozone:* Table 4-5 gives the changes in ozone in January and July at altitudes from the ground to 150 mbar from the IMAGES model for each of the sensitivity studies. Shown are calculated changes in ozone due to aircraft at mid-latitudes in the NH, the changes averaged over each hemisphere, and the changes averaged globally. For the cases also calculated with the Harvard model, Table 4-6 shows the globally averaged changes in nitrogen oxides ( $\text{NO}_x = \text{NO} + \text{NO}_2$ ) and ozone from both models for July. Table 4-6 gives the changes in  $\text{NO}_x$  and changes in ozone in percent change (part a) and in absolute changes in mass (part b). Also given in Table 4-6 are the changes from 400 to 150 mbar (in parentheses) as well as the changes from the ground to 150 mbar. The results for each of the sensitivity analyses are examined below.

*Cases 1 and 2 Baseline Models:* The IMAGES calculations for the 1992 emissions case shown in Table 4-5 indicate zonally averaged changes at mid-latitudes of 2.1% and a globally averaged change of about 1.15% for altitudes below 150 mbar, with the largest changes occurring in the summer. Assuming no changes in ozone from aircraft emissions above the top altitude of the IMAGES model would imply a total column change of only 0.13%. As expected, the 1992 emissions give a slightly larger effect on ozone in the IMAGES model than the 1990 emissions.

As seen in Table 4-6, the IMAGES and Harvard models have quite different responses to the 1992 aircraft emissions. Although the globally integrated changes in ozone are similar, the corresponding changes in nitrogen oxides are quite different, with the Harvard model giving less change (2.2% in July) than the IMAGES model (4.3%). As seen in the figures described below, the changes in  $\text{NO}_x$  and ozone are also quite different spatially. Table 4-6 and these figures also indicate that the largest increases in  $\text{NO}_x$  and ozone do occur in the upper troposphere, where maximum emissions occur, as expected.

Figures 4-22 and 4-23 show the changes in  $\text{NO}_x$  from the IMAGES and Harvard models for the effects from 1992 aircraft emissions, while Figures 4-24 and 4-25 show analogous results for the change in ozone. The results from the Harvard model in general show much smaller gradients and the effects on ozone are more dispersed than the IMAGES model. Differences in the treatment of convection and other transport processes may explain much of this, but the low resolution of the Harvard model in the upper troposphere also affects this.

Many aspects of the calculated effects of aircraft emissions are in strong agreement with earlier published studies. The calculated effects on nitrogen oxides and ozone are much larger in the NH than the SH, at latitudes corresponding to the bulk of the aircraft emissions. For the 1992 aircraft emissions, IMAGES calculates a maximum change in  $\text{NO}_x$  of more than 80% (about 40% zonally averaged) at 250 mbar and mid-latitudes of the NH, while the Harvard model gives about a 100%

increase. The largest effects on ozone are in the upper troposphere at subsonic aircraft cruise altitudes (about 5.5% increase at 250 mbar in the IMAGES model for the 1992 emissions).

The overall sensitivity of the IMAGES model to aircraft is larger (about 5% maximum ozone change in the upper troposphere in this study compared with about 4.5%) than in their previously published analyses [Brasseur *et al.*, 1996]. Several changes have been made to the model (including a different representation of lightning) since those calculations were done.

Changes in the tropospheric inventory of  $\text{NO}_x$  and ozone from the two models are much smaller than those determined from the 2-D and 3-D models used in the AERONOX assessment in Europe [Schumann, 1995]. However, the emissions used here are appreciably smaller than emissions used in that study. The IMAGES model gives an integrated change in nitrogen oxides and ozone of 3.6 Gg N and 3.77 Tg  $\text{O}_3$  due to the 1992 aircraft emissions, respectively, while the Harvard model gives 2.3 Gg N and 2.8 Tg  $\text{O}_3$  (integrated over the entire grid of each model). Also, as discussed earlier, the background atmospheres, including the assumed  $\text{NO}_x$  production from lightning, are quite different from the AERONOX studies.

*Case 3 Effects of Lightning:* The effect of uncertainties in lightning  $\text{NO}_x$  production on upper tropospheric  $\text{NO}_x$  are the same as or greater in magnitude than the aircraft impact on  $\text{NO}_x$  in this region. In the tropics, the uncertainty due to lightning is much larger than that from aircraft.

The uncertainties in representing lightning production of  $\text{NO}_x$  assumed in Cases 3A-3D have a significant effect on the background atmospheres and on the derived effects from aircraft. For example, in the NH summer with the reduced lightning scenario (Case 3A) in IMAGES,  $\text{NO}_x$  in the upper troposphere decreases by 10 to 15% over much of North America and the North Atlantic, and by <10% over Europe. Some portions of the tropics show around 50% reduction in  $\text{NO}_x$ . In January, the  $\text{NO}_x$  reduction is 5 to 10% in the upper troposphere over North America and Europe and as much as 50 to 60% in the tropics. There is also a small impact on the background levels of ozone.

When the lightning source is doubled (Case 3B), zonal mean values of  $\text{NO}_x$  in the NH mid-latitude upper troposphere increase by 20% with a corresponding ozone increase of 6 to 8%, which is slightly greater than the aircraft impact. In January,  $\text{NO}_x$  in this region increases by 0 to 10% and ozone increases by 2 to 4%, which is about twice the aircraft impact. In the tropics  $\text{NO}_x$  increases in this scenario up to 90%, with corresponding ozone increases of up to 24%.

The IMAGES model sensitivity runs were performed using the Turman and Edgar lightning emission scenario that maintains constant  $\text{NO}_x$  injection with altitude. Recent analyses suggest that a C-shaped  $\text{NO}_x$  profile is more likely, at least over the continents, where downdrafts are more vigorous. If such profiles were used instead, the sensitivity results would likely show greater changes in  $\text{NO}_x$  and ozone in the upper and lower troposphere and lesser changes in the middle troposphere than are seen in the baseline IMAGES simulations. Case 3C is a sensitivity simulation run with the Price and Rind lightning parameterization, including the use of a C-shape vertical profile. In this run it is difficult to determine how much of the changes are due to the different parameterization and how much are due to the use of the different vertical profile. In this simulation large increases (>100%) in upper tropospheric  $\text{NO}_x$  are seen in the tropics. As much as a 70 to 80% increase at 60 to 70°N results with this formulation in summer. Decreased  $\text{NO}_x$  is seen in the lower and middle troposphere in the tropics and in the mid-latitudes of the SH. This scenario yields a maximum of about 10% increase in ozone in the tropical upper troposphere and

about the same increase in the NH mid-latitude flight corridor region in summer. This uncertainty is about twice the ozone impact of aircraft emissions.

The effects of aircraft emissions are increased by about 20% (from 0.84% global averaged change in tropospheric ozone to 1.01%) when the lightning source is reduced in the IMAGES model (Case 3A). In contrast, the effect of aircraft emissions is decreased by about 20% in IMAGES and 27% in the Harvard model when the lightning source is doubled (Case 3B in IMAGES, 3D in Harvard). Results shown in Table 4-6 indicate large differences in model sensitivity to aircraft still remain when both models use the same lightning source.

*Case 4 Effects of Convection:* Two sensitivity studies were conducted with the IMAGES model by halving (Case 4A) and by doubling (Case 4B) the rate of convective transport in the model. Case 4B was also evaluated with the Harvard model. Convection appears to be a process that must be simulated as accurately as possible in the assessment model. The results of this sensitivity test show that changes of a factor of two in convective transport over major air traffic corridors of the NH in summer cause changes in upper tropospheric ozone greater than the perturbation in ozone due solely to aircraft emissions. In NH summer (July) convection reduced by a factor of two caused more than a 25% increase in NO<sub>x</sub> at 250 mbar over broad areas of the remote troposphere. This result is likely due to less downward transport of NO<sub>x</sub> from the upper troposphere in the reduced convection scenario. This increase in NO<sub>x</sub> in the upper troposphere causes greater photochemical ozone production, which along with reduced downward transport of ozone, causes ozone mixing ratios in the upper troposphere to increase by as much as 30% in the tropics (15% in the zonal mean) and by 5 to 10% in the NH mid-latitudes (refer to Figure 4-17). In contrast, the maximum ozone perturbation in the upper troposphere due to aircraft emissions is 4 to 5%.

In January, NO<sub>x</sub> increased by >30% in the upper troposphere over the major areas of large-scale subsidence west of the continents of South America, southern Africa, and Australia (areas of no deep convection). Apparently the upper troposphere throughout the SH contains more NO<sub>x</sub> under the reduced convection scenario because of less downward convective transport. The net result appears to be most evident in these major subsidence regions. In these same regions ozone mixing ratios increased >20%. Over NH air traffic corridors ozone increases by about 5% in the reduced convection scenario compared with a maximum of 1.5% increase due to aircraft emissions, again demonstrating the importance of correctly computing convective transport.

While having a significant effect on the background atmospheric levels of NO<sub>x</sub> reducing or increasing convection has a smaller effect on the derived changes in nitrogen oxides and ozone resulting from aircraft emissions. Reducing convection increased the effect on tropospheric nitrogen oxides and ozone (altitudes less than 150 mbar) by about 8.7% and 8%, respectively, in the IMAGES model. Doubling the convection reduced the effects on NO<sub>x</sub> and ozone by similar amounts in both the IMAGES and Harvard models.

*Case 5 Effect of Heterogeneous Chemistry:* Removing the N<sub>2</sub>O<sub>5</sub> + H<sub>2</sub>O heterogeneous reaction in the IMAGES model has a significant effect on NO<sub>x</sub> concentrations, particularly in the winter hemisphere. The sign and magnitude of the calculated changes in background atmosphere concentrations are in agreement with earlier studies [Dentener and Crutzen, 1993]. The effect of neglecting this reaction relative to the aircraft perturbation is to reduce the sensitivity of atmospheric composition to aircraft emissions. The change in ozone is reduced by about 10% (from a 0.97% change, globally averaged, to 0.87%), with greater effect in winter than in summer.

*Case 6 Effect of Hydrocarbon Chemistry:* Although aircraft hydrocarbon emissions are minor relative to other sources, inclusion of hydrocarbon chemistry is important in determining the effect of NO<sub>x</sub> emissions on O<sub>3</sub> (see Section 3.2.2.2). Leaving NMHC chemistry out of the IMAGES model has a significant effect on the levels of nitrogen oxides in the background atmosphere, resulting in more NO<sub>x</sub> in the lower troposphere and less in the upper troposphere (due to creation of PAN and other organic nitrates). At 250 mbar, NO<sub>x</sub> concentrations are lower by 30 to 40% at mid-latitudes and up to 80% in the tropics. Removing hydrocarbon chemistry from the model reduces the sensitivity of ozone to aircraft NO<sub>x</sub> emissions appreciably (from 0.97% to 0.61% globally and annually averaged).

*Case 7 Effect of Increased NO<sub>x</sub> Recycling:* The fraction of UT NO<sub>x</sub> that is due to aircraft depends, in part, on the rate of removal of NO<sub>x</sub> in that region. Processes which recycle NO<sub>x</sub> will decrease the effective removal rate and influence the overall UT NO<sub>x</sub> budget. Observations from a number of field missions suggest that current models are missing some important NO<sub>x</sub> recycling processes. In an attempt to introduce a recycling mechanism we have increased the photolysis rate of nitric acid by a factor of 3 in IMAGES. This change is seen to have a large impact on NO<sub>x</sub> in the upper troposphere and lower stratosphere. NO<sub>x</sub> levels more than double in the lower stratosphere and increase by 30 to 70% in the upper troposphere. The sensitivity to aircraft emissions is reduced giving a change in globally averaged tropospheric ozone of 0.78% (compared to 0.97% in the baseline case).

*Case 8 Effect of 5 Times the 1992 Emissions:* Increasing the 1992 emissions by a factor of 5 results in a proportionately larger change in nitrogen oxides arising from the aircraft emissions but less than a proportional change in the ozone. NO<sub>x</sub> increases by 23.4%, globally averaged for July, in the IMAGES model (compared to 4.3% in the baseline 1992 emissions case) and by 10.9% in the Harvard model (compared to 2.2% in the baseline model). Globally averaged ozone increases by 4.4% in the IMAGES model and 3.9% in the Harvard model. Integrated changes in absolute amounts of NO<sub>x</sub> and ozone are 20.2 Gg N and 15.0 Tg O<sub>3</sub>, respectively, from the IMAGES model in July and 10.9 Gg N and 12.0 Tg O<sub>3</sub> from the Harvard model, indicating that the large difference in the NO<sub>x</sub> perturbation is not due simply to having significantly different levels of background NO<sub>x</sub>.

The IMAGES model gives more than a 400% increase in NO<sub>x</sub> in the upper troposphere relative to the baseline case while the Harvard model gives over a 700% increase. The effect of the aircraft emission is to increase upper tropospheric ozone by as much as 14% in the IMAGES model and by as much as 17% in the Harvard model.

## **4.3 EFFECTS ON CLIMATE**

### **4.3.1 DESCRIPTION OF MODELING TOOLS**

#### **4.3.1.1 Description of Models**

For this assessment, two computations were made: the radiative forcing at the tropopause associated with the different aircraft emissions, and the climatic response to those radiative forcings. The GISS GCM(s) and radiation code were the particular modeling tools involved. The GISS GCMs include the 9-layer model which extends from the surface into the lower stratosphere

(10 mbar) [Hansen *et al.* 1983], and the 23-layer Global Climate Middle Atmosphere Model (GCMAM) which extends from the surface into the mesosphere (0.004 mb or 85 km) [Rind *et al.*, 1988]. The models were used at  $8^\circ \times 10^\circ$  horizontal resolution; both include a complete set of surface and atmospheric responses, including variable sea ice, cloud cover, etc. The ocean is characterized by a 65m mixed layer with specified ocean heat transports [Hansen *et al.*, 1984]. Both versions use the same radiation code, which has been tested in an inter-model comparison, and performed well compared to line by line calculations and other radiation models being used in GCMs [Cess *et al.*, 1993].

The GISS GCM predicts a  $4.2^\circ\text{C}$  surface temperature rise for doubled atmospheric  $\text{CO}_2$ , which translates to a forcing of  $4.4 \text{ W m}^{-2}$  at the tropopause. This is at the high end of the IPCC [1992] estimate of likely atmospheric sensitivity, given as a range of  $1.5^\circ\text{C}$  to  $4.5^\circ\text{C}$ ; however, it is near the average of the 10-15 GCMs used for climate change studies [IPCC 1990; 1992]. The GISS models have considerable tropical sensitivity, such that the high latitude/low latitude amplification is only about a factor of two for doubled  $\text{CO}_2$ , less than the result from some models (e.g., the Geophysical Fluid Dynamics Laboratory (GFDL) model), but similar to others (e.g., United Kingdom Meteorological Office (UKMO)) [Rind, 1987]. The model also produces maximum doubled  $\text{CO}_2$  warming in the tropical upper troposphere [Hansen *et al.*, 1984], a result which is absent in simulations with reduced tropical surface warming [IPCC, 1990]. The proper tropical sensitivity is unknown [Rind, 1995].

#### **4.3.1.2 Description of Modeling Techniques**

To calculate the radiative forcing at the tropopause, the GISS GCM is run with altered atmospheric composition for one year, to allow for seasonally and diurnally changing solar zenith angle. Tropospheric temperatures are kept fixed, but stratospheric temperatures are allowed to change; the radiative forcing calculated at the tropopause is therefore the value adjusted for radiative response in the stratosphere. Given the rapid response time in the stratosphere, it is felt that this is the more appropriate value for the purpose of assessing tropospheric sensitivity.

To calculate the climate response, the GCM or GCMAM is run for 50 to 75 years, for both a control run with current atmospheric composition, and for experiments with an estimated aircraft-induced change in composition. The long run guarantees that the sea surface temperatures have adjusted to the imposed radiation imbalance. The result is therefore an equilibrium response to aircraft forcing and is not meant to provide a forecast for any particular year.

### **4.3.2 CLIMATE SENSITIVITY STUDIES**

#### **4.3.2.1 Layered Versus Well-Mixed Forcing and GWP**

Aircraft-induced radiative forcings differ from the more canonical perturbations such as altered  $\text{CO}_2$  or solar constant in that they are not well-mixed throughout the depth of the atmosphere. Aircraft-induced changes in stratospheric ozone, aerosols or water vapor produce a radiative perturbation at the tropopause by affecting specific atmospheric levels. In so doing, they alter the temperature lapse rate in the vertical, and affect clouds at high altitudes. Since the normal procedure in calculating the tropospheric response to radiative forcing in radiative-convective models (RCMs) is to assume an unchanging lapse rate, layered forcings violate this basic

assumption. They therefore produce a different sensitivity of surface temperature response to tropopause radiative imbalance than do the well-mixed forcings. The commonality of this response to forcing in RCMs has led to the concept of the “global warming potential” (GWP) of different gases which can be characterized by simply noting the radiative forcing at the tropopause; layered forcings would appear to contradict this simple approach, and their surface temperature response may have to be calculated for each particular case.

Hansen *et al.* [1993] used a “ghost” forcing of  $4 \text{ W m}^{-2}$  applied at different levels in the atmosphere to determine how the surface responded. Their results indicated that forcing (warming) in the lower stratosphere produced only 20% of the sensitivity of forcing applied directly to the surface. Rind and Lonergan [1995] found that increased stratospheric water vapor produced only about 20% of the surface temperature response expected from the resulting radiation imbalance at the tropopause. In both cases, changes in vertical lapse rate, and cloud response at high altitudes, reduced the climate sensitivity. Given that model cloud cover parameterizations are uncertain, it is possible that the model result will differ from the true atmospheric sensitivity, and will vary between models.

Forcings induced in the upper troposphere, as would be the case for most of the subsonic aircraft emissions, are more problematic; they are layered in initial input, but they are within the relatively well-mixed domain of the troposphere. In an experiment with reduced ozone in both the upper troposphere and lower stratosphere, Rind and Lonergan [1995] found that the surface temperature response was about 50% of that expected from the tropopause radiation imbalance, implying a surface sensitivity in-between that of stratospheric and well-mixed forcings. The sensitivity experiments discussed below test the model response to various specific aircraft perturbations in the troposphere.

There are additional problems associated with defining GWPs for aircraft emissions. The GWP is “currently inapplicable to gases and aerosols that are very unevenly distributed, as is the case for tropospheric ozone and aerosols and their precursors” [IPCC, 1994, 1996]. The short lifetime of  $\text{NO}_x$ , for example, can lead to large regional inconsistencies in its effect on ozone concentrations, making its indirect GWP practically impossible to calculate with confidence. The same is true for aircraft aerosol emissions. Carbon dioxide emissions from aircraft have a GWP of 1.0 (since everything else is relative to  $\text{CO}_2$ ) by definition. Carbon dioxide emissions from aircraft amount to 2.4% of fossil fuel emissions. Water vapor is emitted by aircraft, but it has not historically been included in GWP calculations. Its GWP would be as problematic as that for other aircraft emissions, due to its short lifetime and large regional heterogeneity. This would be true as well for aircraft effects such as generation of contrails or alteration of cirrus clouds.

#### **4.3.2.2 Aircraft Water Vapor Emissions**

Aircraft release 1.17 kg of water vapor for every kg of fuel burned [Lee *et al.*, 1994]. In 1990,  $1.34 \times 10^{11}$  kg of fuel were burned [Wuebbles *et al.*, 1993a, b]; hence about  $1.67 \times 10^{11}$  kg of water vapor were released. With expected passenger demand and aircraft increases in mileage, it is estimated that  $3.8 \times 10^{11}$  kg of water vapor will be released annually by the year 2015 [Baughcum *et al.*, 1993a].

Experiments with the GISS GCMAM were performed in which water vapor was released along flight paths in the upper troposphere [Rind *et al.*, 1996], occurring predominantly in the NH.

Various water vapor amounts were released, ranging from 1.5 times the 2015 value to 300 times its value. The results showed that observable climate effects were noticed only when releases were some 15 times the 2015 estimates (Figure 4-26); with that magnitude, the surface air temperature response was a few tenths °C. Compared to natural variability the predicted temperature rise would be observable in the troposphere [Shah *et al.*, 1996].

With enhanced emissions, the aircraft signature (compared to increased atmospheric CO<sub>2</sub>) consisted of greater increases in NH extratropical cloud cover, relative humidity and specific humidity in the upper troposphere. The specific humidity increase however did not maximize at upper tropospheric levels; as the climate warmed, evaporation increased, and the maximum in additional water vapor occurred at low altitudes in the tropics. The total enhancement in atmospheric water vapor resulted primarily from this climate feedback, emphasizing that the total climate response can be very different from the input forcing. A similar experiment without allowing for surface temperature feedback performed by Ponater *et al.* [1996] did not produce the tropical water vapor response.

Because of this interaction, it is not possible to calculate what the true climate forcing was in these experiments. However, by comparison with CO<sub>2</sub>-induced temperature changes of similar magnitude, it appears as if the aircraft forcing had less effect on surface processes, particularly sea ice. Increased CO<sub>2</sub> therefore produced a greater high latitude surface temperature response, associated with decreased sea ice, than did the aircraft forcing, even though aircraft forcing was predominantly at high latitudes in the NH. This result illustrates that upper tropospheric, layered forcing is comparatively less effective in influencing surface responses. Although there was considerable longitudinal variation in the input water vapor release, there was little in the way of longitudinal signature in response, due to the homogenizing effect of advective processes. The results therefore also emphasize that the latitude and location of the applied forcing does not necessarily dictate the location of the response.

#### **4.3.2.3 Aircraft-Induced Ozone Changes**

The 1992 aircraft-induced ozone change, as calculated by the IMAGES model (Figure 4-25a) was input into the GISS 9-layer GCM and integrated for 50 years. The zonal average peak ozone perturbation, on the order of 10 ppbv in the Northern Hemisphere extratropical upper troposphere, is a change of only about 3-5% of background values. Hence the radiative forcing is extremely small (0.0095 W m<sup>-2</sup>), and the temperature response, a global annual average change of 0.01°C, was less than the model's natural variability. Therefore, there was essentially no model discernible impact associated with the ozone changes as specified.

An additional experiment was performed using the ozone changes induced by 5x 1992 aircraft emissions, as calculated by the IMAGES model. The zonal ozone changes in this run peak at about 10%, and on the global average, the ozone change was 3.46 times larger than for the 1992 emissions. The radiative forcing was approximately 0.033 W m<sup>-2</sup> and the global annual average temperature response was a warming of 0.09°C. This is on the order of the model's interannual variability, and therefore its significance is somewhat questionable; if real, it would imply a large climate sensitivity (3°C W<sup>-1</sup> m<sup>2</sup>). The results are for the last 25 years of 75 year simulations (for both experiment and control), during which time the experiment was consistently warmer, a result

that did not happen in the 1992 aircraft ozone experiment, and would seem to be unlikely to occur by chance.

Figure 4-26 shows the annual-average temperature changes produced for the 15x present subsonic water vapor releases (top) and the 5x 1992 aircraft ozone changes (bottom). There are similarities between the results of the two experiments. The warming maximizes in the polar regions of both hemispheres, especially near the surface; contributing to this effect is the sea-ice albedo feedback. The surface response is therefore dominated by system feedbacks, not by the location of the aircraft forcing which is predominantly in NH middle latitudes. There is cooling aloft, associated with the greater thermal emissions from increased water vapor or ozone; only in the specified ozone change experiment does this have a clear Northern Hemisphere bias, as the system responds by further altering the water vapor distribution.

#### 4.3.2.4 Aircraft Soot Emissions

The aircraft emissions were calculated by Wuebbles, Rahmes and Omar [personal communication], for an emission index of 0.02 g soot/kg fuel (based on recommendations from aircraft industry by H. Lilienfeld and others). Hence about  $2.7 \times 10^{10}$  g of soot were released by aircraft in 1990. The particles are small, with diameters on the order of 0.01 to 0.05 microns; their single scattering albedo in the visible range is also quite small, on the order of 0.02 or less, which implies that they do little scattering, and are basically absorbing. Their impact on the net radiation budget would therefore be positive. However, the calculated optical thickness is extremely small, with column-integrated values peaking at about  $4 \times 10^{-7}$  for a diameters of 0.03 microns at 50 to 65°N. As calculated by the CCM3 GCM radiation code, this produces a peak response of close to 0.0025 W m<sup>-2</sup>. In the GISS GCM, assuming the sensitivity for well-mixed forcings, this would produce a surface temperature response of a few hundredths °C, less than the model's interannual variability.

#### 4.3.2.5 Aircraft Contrail Simulations

Limited numerical experiments have been performed to understand possible climatic effects of contrail cirrus on regional or global climate. Hansen *et al.* [1981] used a one-dimensional radiative-convective model and found that a 2% global increase in high clouds would lead to a 1 K surface temperature increase, which represents about one-third of the sensitivity produced by the doubling of CO<sub>2</sub> in the same model. Liou *et al.* [1990], using a two-dimensional cloud and climate model, found that a surface temperature increase of about 1°C was possible if contrail-cirrus increased the total amount of high cloud by 5% (from 20-25%) from 20° to 70°N. Schumann [1994], using a regional scale model, determined that a linear increase in surface temperature of about 0.05°C occurred due to an increase of 0.4% in high clouds associated with contrails, although these calculations omitted a number of global feedback processes included in Liou *et al.* [1990]. Ponater *et al.* [1996], using the ECHAM GCM, increased cirrus cloud cover by 2%, 5% and 10% along aircraft flight paths, and found surface air temperature changes ranging from 1°C to 4°C in the experiments. Keeping the “contrails” present all the time undoubtedly exaggerated the results, although not allowing sea surface temperatures to adjust likely minimized the surface temperature response.

It is important to recognize that our ability to satisfactorily treat contrails in large-scale model cloud-radiation schemes is still in a rudimentary state, for several reasons. Detailed knowledge of the time evolution in contrail particle size distributions, which is crucial to greenhouse versus albedo radiative forcing predictions, is largely lacking; the linear spatial structure of persisting contrails represents a very inhomogeneous cloud feature; and the geographic distribution of contrails varies significantly over regional and global scales. Mesoscale cloud models capable of treating microphysics and radiation explicitly would be most suitable for providing parameterizations needed by the global climate models.

#### 4.3.2.6 Aircraft CO<sub>2</sub> Emissions

Aircraft release 3.15 kg of CO<sub>2</sub> per kg of fuel burned. With approximately  $1.34 \times 10^{11}$  kg of fuel burned in 1990, aircraft were therefore releasing  $4.22 \times 10^{11}$  kg of CO<sub>2</sub>, which is 0.42 Gt of CO<sub>2</sub>; this equals 0.11 Gt of carbon. Over the past 30 years, assuming aircraft fuel-burning increased at a rate of 4.6% year<sup>-1</sup> (literally true for 1976-1992; probably an overestimate for the prior 15 years), aircraft can be estimated to have produced about 2 Gt of carbon. In comparison, over the same time period, industrial processes are estimated to have produced approximately 150 Gt of carbon [IPCC 1990, 1992, 1994, 1996]. The aircraft contribution has therefore been approximately 1.5%.

The release of 2 Gt of carbon is approximately equal to 1 ppmv of CO<sub>2</sub> over the past 30 years, or 0.033 ppmv year<sup>-1</sup>. Over the same time period, industrial production has increased atmospheric CO<sub>2</sub> 2.4 ppmv year<sup>-1</sup>. The observed atmospheric increase is about one-half that amount, 1.2 ppmv year<sup>-1</sup>, reduced from the emission value due to uptake by the oceans and perhaps the biosphere. Assuming the same residence time for aircraft and other CO<sub>2</sub> releases, we estimate that aircraft have been associated with an atmospheric CO<sub>2</sub> increase of  $0.033/2 = 0.0165$  ppmv CO<sub>2</sub> year<sup>-1</sup>, over the last 30 years, for a total increase of 0.5 ppmv (in contrast to other aircraft releases, which have short lifetimes, aircraft CO<sub>2</sub> would accumulate). Using the same reasoning, in 1992, aircraft emissions were increasing CO<sub>2</sub> by about 0.05 ppmv year<sup>-1</sup>.

In the GISS GCM, an addition of 300 ppm CO<sub>2</sub> results in a radiative forcing of  $4 \text{ W m}^{-2}$ , and a surface temperature response of about 4.2°C in equilibrium. Using this relationship, the 1992 aircraft CO<sub>2</sub> release produced radiative forcing on the order of  $3 \times 10^{-4} \text{ W m}^{-2}$ , and an equilibrium temperature response of similar magnitude. Over the past 30 years, an aircraft-induced increase of 0.5 ppmv would have produced radiative forcing of approximately  $0.0067 \text{ W m}^{-2}$ , and therefore an equilibrium surface air temperature response on the order of 0.007°C. Given the range of climate sensitivity from different models noted in IPCC [1990, 1992, 1994, 1996], this number might be as small as 0.0025°C, or as large as 0.009°C.

#### 4.3.2.7 Aircraft NO<sub>x</sub> Emissions

The primary influence of aircraft NO<sub>2</sub> is its influence on ozone. NO<sub>x</sub>, in the form of NO<sub>2</sub>, absorbs in the visible and near infrared; the total short-wave absorption (including both tropospheric and stratospheric concentrations) is on the order of  $10^{-1} \text{ W m}^{-2}$ . The contribution from the region of maximum subsonic aircraft release, from 200 to 300 mb, is about 1%, hence short-wave absorption here is on the order of  $10^{-3} \text{ W m}^{-2}$ . Therefore, were aircraft to increase NO<sub>2</sub> by 50% in the upper troposphere, they would contribute a forcing of the same order ( $10^{-3} \text{ W m}^{-2}$ ) as CO<sub>2</sub>.

NO<sub>2</sub> also absorbs in the infrared, at around 6 microns, and in the 11- to 15-micron region, but the effect is of less importance than its short-wave absorption.

NO<sub>x</sub> is also associated with production of nitrate aerosols. According to IPCC [1994], natural nitrates from NO<sub>x</sub> have an optical depth of  $1 \times 10^{-3}$ , while anthropogenic nitrates from NO<sub>x</sub> have an optical depth of  $2 \times 10^{-3}$ . (These represent about 2% of both the natural and anthropogenic total aerosol optical thicknesses.) A 3% NO<sub>x</sub> increase for the whole troposphere due to current aircraft emissions would therefore increase the nitrate aerosol optical depth by approximately  $10^{-4}$ , which is equivalent to a short-wave forcing of  $2.7 \times 10^{-3} \text{ W m}^{-2}$ . A potential further effect of these aerosols on natural cloud properties is currently uncertain.

#### **4.3.2.8 Aircraft SO<sub>2</sub> Emissions**

Aircraft emit approximately 1 g of SO<sub>2</sub> for each kg of fuel burned. In 1990, approximately  $1.3 \times 10^{11}$  g of SO<sub>2</sub> were emitted. This can be compared to  $2.4 \times 10^{14}$  g emitted each year by natural and other anthropogenic sources [IPCC, 1996]. SO<sub>2</sub> absorbs in the infrared somewhat better than NO<sub>2</sub>, but its primary climate impact is associated with sulfate aerosol production. Natural and anthropogenic sulfate aerosols produce an estimated global mean optical depth of  $3.3 \times 10^{-2}$ ; the contribution from aircraft can therefore be crudely estimated as  $1.5 \times 10^{-5}$ . This is equivalent to a short-wave forcing of approximately  $4 \times 10^{-4} \text{ W m}^{-2}$ . Again, the possible additional effect of sulfate aerosols on natural cloud properties cannot yet be determined.

#### **4.3.2.9 Summary**

The results from the climate impact experiments performed for this assessment and estimates from other work are shown in Table 4.7. As noted above, the radiative forcing actually induced by the water vapor release is difficult to ascertain. The realistic aircraft gaseous radiative forcings examined here are all extremely small, resulting in surface temperature responses that are not significantly different from the model's natural variability. The exaggerated forcing experiments do suggest that the "aircraft footprint" will be more likely found at altitude, since the surface response is dominated by the system feedbacks to the original forcing. Major uncertainties exist in estimating the aircraft contrail forcing.

### **4.4 Findings and Future Needs**

The tracer studies (Rn and NO<sub>y</sub> model calculations) and the model comparisons with available observations of chemical constituents indicate that major uncertainties remain in current model representations of tropospheric processes. The NO<sub>y</sub> tracer calculations suggest that the vertical resolution is an important factor in accurately representing the upper tropospheric chemistry, indicating that the resolution should be at least 1 km in the upper troposphere. The IMAGES model used in the sensitivity studies possesses resolution on this order, but the Harvard model is coarser than this.

Additional problems have been discussed regarding the chemical-transport models used in this assessment. Many, if not most, of these problems also apply to every other existing 3-D model of tropospheric processes that have been used to investigate the chemical effects of subsonic aircraft emissions. For example, the use of monthly averaged winds in the IMAGES model restricts its

ability to accurately represent transport of trace constituents in the troposphere. Also, both of the models used in this assessment have extremely limited representations of the stratosphere, including essentially an invariant stratospheric source of nitrogen oxides into the upper troposphere. The studies with these models can tell us little about the effects of subsonic aircraft emissions into the stratosphere and effects of subsonic aircraft on stratospheric chemistry. These also do not address resulting changes in the transport of nitrogen oxides and other constituents between the lower stratosphere and upper troposphere.

There is extremely limited data for NO for northern middle and high latitudes with which to test models. Unfortunately, this means we cannot really assess how well the models are doing for the NO<sub>y</sub> family north of 45°N in the upper troposphere. However, the IMAGES and Harvard models were found to have difficulties calculating the observed partitioning of NO<sub>y</sub> among NO, HNO<sub>3</sub>, and PAN, in the regions where data is available for comparison purposes. Also, IMAGES does not get the correct seasonal cycle for ozone. Since the Harvard model contains a simplified upper troposphere, it appears inappropriate for aircraft assessments for latitudes greater than 45°. Given the problems with IMAGES and the Harvard model in the upper troposphere and lower stratosphere (in the 300 to 200 mbar region) the use of these models in assessing the effects of aircraft emissions is questionable.

Despite these problems with the models, the results are in agreement with prior studies and suggest that aircraft do have an effect on concentrations of upper tropospheric nitrogen oxides and ozone. Although these effects, as calculated by the models, may be large enough to be measurable, the current sets of observational measurement data (as discussed in Chapter 3) do not clearly indicate any effects on nitrogen oxide and ozone levels due to aircraft. Effects on the total column of ozone from aircraft appear to be relatively small.

As with earlier published modeling studies, all of the results presented here, including the range of sensitivity studies investigating several major uncertainties in model treatments of important processes, suggest that emissions from aircraft increase ozone in the upper troposphere. How well is this relationship established? Existing measurements of NO<sub>x</sub> and ozone indicate that such a relationship is to be expected for the level of nitrogen oxides determined in the models. Unfortunately, there are insufficient global-scale data to define the background atmosphere and variability for concentrations of nitrogen oxides, limiting our ability to draw a strong conclusion about the expected ozone response.

A number of processes are still poorly represented or are missing in the tropospheric models used here. For example, effects of production of NO<sub>x</sub> from galactic cosmic rays [Jackman, 1991, 1993; Vitt and Jackman, 1996] are not included in the models used here and could have as much as a 2 to 10% effect on upper tropospheric NO<sub>x</sub>. Major uncertainties still exist about the representation of effects from lightning and convection in the models. At this point, however, recognized uncertainties do not appear to be sufficient to change the sign of the effects on ozone from subsonic aircraft emissions.

The modeling studies indicate that additional measurements for NO and other NO<sub>y</sub> gases are badly needed in the upper troposphere (>6 km), in general throughout the globe but particularly at mid-latitudes in the NH. Questions about the relative amounts of NO<sub>y</sub> species also need to be resolved.

Large differences were found in the IMAGES and Harvard models in the maximum effects on ozone from the 5x 1992 emissions case; however, much smaller differences existed in the change

in ozone integrated over the entire troposphere. Both models were nonlinear in their effects on ozone relative to the 1992 emissions case, giving more than a linear effect on ozone. With approximately a doubling in emissions expected for 2015 relative to 1992, the model results suggest that the effects on ozone should be slightly more than double the effects for 1992. The differences between the maximum effects in models for the 5x 1992 case still need to be explained but likely relate to the large differences in model domain, grid structure, and treatment of the tropopause.

The GMI model is expected to be the primary tool for the future assessments of chemistry effects from subsonic aircraft emissions. Improved representations, including higher resolution, of dynamics from DAO, NCAR, and GISS/UCI are expected to be incorporated during the next year. Chemistry is being tested and will be added to the model. Development of improved understanding and representation of lightning and convection processes for the model will be extremely important to reducing the uncertainties of aircraft effects on ozone.

The impact studies conducted so far suggest that current and expected levels of subsonic aircraft emissions (through 2015) should have at most only a small impact on surface climate (individually on the order of 0.1°C or less, globally), especially when compared with projections for total fossil fuel emission effects. The most likely exception to this conclusion concerns aircraft particle emissions and their effect on contrails. Future studies should emphasize understanding this forcing, as well as the potential for aircraft gaseous and particle emissions to ultimately affect natural cirrus cloud radiative properties.

**Table 4-1.** Basic description of global three-dimensional chemistry-transport models participating in this assessment.

MODEL	HORIZONTAL RESOLUTION (lat x long)	#VERTICAL LAYERS		TEMPORAL RESOLUTION (i.e., altitudes < 12 km)
		Total	p >200 mbar	
IMAGES	5° x 5°	25	21	1 month
HARVARD / GISS	4° x 5°	9	7	4 hours
GMI / CCM2	3° x 5°	44	12	6 hours
GMI / UCI	8° x 10°	21	8	8 hours

**Table 4-2.** Chemical model comparison participants.

Model Identifier	Contributor & Affiliation	Description/Reference
Colorado	<u>Jana Milford &amp; Madhurima Das</u> University of Colorado	Stockwell <i>et al.</i> , [1990]; Gear integrator
Harvard	<u>Daniel Jacob</u> , Harvard University	Jacob <i>et al.</i> , [1996a]
IMAGES	<u>Jean-Francois Müller</u> Belgian Institute for Space Aeronomy	Müller & Brasseur [1995]
MEDIANTE	<u>Richard Ramarosan</u> ONERA	Ramarosan & Brasseur [1996]
Stanford	<u>Mark Jacobson</u> Stanford University	Atkinson <i>et al.</i> , [1992]; DeMore <i>et al.</i> , [1994]; Gery <i>et al.</i> , [1989]
SUNY	<u>Chris Walcek</u> State University of New York at Albany	Stockwell <i>et al.</i> , [1990]; Euler integrator; updated DeMore <i>et al.</i> [1994] kinetics

**Table 4-3.** Percentage of mass of NO<sub>x</sub> produced by lightning as a function of altitude for deep convective clouds in 3 regimes [Pickering et al., 1996].

<b>Altitude (km)</b>	<b>Tropical Marine</b>	<b>Tropical Continental</b>	<b>Mid-Latitude Continental</b>
0-1	0.7	3.39	21.9
1-2	0.5	1.44	4.4
2-3	0.7	1.53	1.2
3-4	0.7	1.63	1.8
4-5	0.6	1.1	3.5
5-6	0.7	1.3	4.4
6-7	1.3	1.6	3.9
7-8	4.8	2.8	4.7
8-9	12.1	4.6	5.9
9-10	19.2	6.5	7.8
10-11	20.8	8.4	10.3
11-12	19.7	11.0	10.8
12-13	11.5	14.8	9.3
13-14	4.1	17.2	6.6
14-15	1.3	13.6	2.7
15-16	0.5	6.4	0.6
16-17	0.3	2.1	0.1
17-18	0.3	0.6	0.0
18-19	0.2	0.1	0.0
19-20	0.2	0.0	0.0

**Table 4-4.** Sensitivity studies evaluated with the IMAGES and Harvard CTMs (each case calculated with and without aircraft emissions).

Case		IMAGES	Harvard
1	Baseline model, 1990 emissions	X	
2	Baseline model, 1992 emissions	X	X
3	Effects of lightning		
	A. Turman and Edgar, 2 Tg N yr <sup>-1</sup>	X	
	B. Turman and Edgar, 10 Tg N yr <sup>-1</sup>	X	
	C. Price and Rind, 5 Tg N yr <sup>-1</sup>	X	X
	D. Price and Rind, 10 Tg N yr <sup>-1</sup>		X
4	Effects of convection		
	A. Decrease by factor of 2	X	
	B. Increase by factor of 2	X	X
5	Effect of heterogeneous chemistry (no N <sub>2</sub> O <sub>5</sub> + H <sub>2</sub> O)	X	
6	Effect of hydrocarbons (no NMHCs)	X	
7	Effect of increased recycling (increase J (HNO <sub>3</sub> ) by factor of 3)	X	
8	Effect of increased aircraft emissions (NASA 1992 x factor of 5)	X	X

**Table 4-5a.** Calculated changes in ozone below 150 mb for January and July from the IMAGES CTM for the sensitivity studies.

**Changes in Ozone due to aircraft (%)**  
**January** **July**

<b>Case</b>	<b>30-50°N</b>	<b>NH</b>	<b>SH</b>	<b>Global</b>	<b>30-50°N</b>	<b>NH</b>	<b>SH</b>	<b>Global</b>
1 Standard Model, 1990 aircraft	1.28	1.21	0.19	0.84	1.99	1.91	0.30	1.07
2 1992 emissions	1.32	1.27	0.21	0.89	2.12	2.04	0.33	1.15
3A Lightning to 2 Tg N yr <sup>-1</sup>	1.43	1.39	0.29	1.01	2.41	2.38	0.41	1.35
3B Lightning to 10 Tg N yr <sup>-1</sup>	1.08	1.00	0.11	0.66	1.49	1.40	0.20	0.78
3C Price and Rind Lightning	1.01	0.95	0.17	0.67	1.38	1.35	0.22	0.77
4A Convection/2	1.38	1.30	0.22	0.90	2.21	2.11	0.33	1.15
4B Convection x 2	1.14	1.09	0.16	0.76	1.66	1.62	0.23	0.91
5 No Hetero. Chem.	0.90	0.92	0.20	0.68	1.85	1.78	0.31	1.01
6 No NMHC	0.76	0.77	0.14	0.53	1.22	1.17	0.21	0.66
7 J(HNO <sub>3</sub> x 3)	1.01	0.97	0.16	0.67	1.58	1.54	0.26	0.88
8 5 x 1992 emissions	4.77	4.76	1.01	3.40	7.62	7.39	1.59	4.36

**Table 4-5b.** Calculated changes in NO<sub>x</sub> below 150 mb for January and July from the IMAGES CTM for the sensitivity studies.

**Changes in NO<sub>x</sub> due to aircraft (%)**  
**January** **July**

<b>Case</b>	<b>30-50°N</b>	<b>NH</b>	<b>SH</b>	<b>Global</b>	<b>30-50°N</b>	<b>NH</b>	<b>SH</b>	<b>Global</b>
1 Standard Model, 1990 aircraft	4.26	3.87	0.44	2.79	5.49	5.37	1.08	3.87
2 1992 emissions	4.00	3.70	0.49	2.68	6.04	5.94	1.19	4.28
3A Lightning to 2 TgN/year	4.18	3.91	0.62	3.03	5.86	6.03	1.20	4.34
3B Lightning to 10 TgN/year	4.36	3.79	0.29	2.47	5.00	4.61	0.95	3.32
3C Price and Rind Lightning	4.51	3.86	0.38	2.68	4.75	4.61	1.02	3.42
4A Convection/2	4.51	4.01	0.51	2.84	6.33	6.10	1.30	4.35
4B Convection x 2	4.08	3.78	0.35	2.76	4.62	4.59	0.81	3.31
5 No Hetero. Chem.	4.20	3.66	0.47	3.19	5.75	5.64	1.03	3.64
6 No NMHC	4.95	4.47	0.34	3.01	5.95	5.60	1.17	4.08
7 J(HNO <sub>3</sub> x 3)	4.12	3.70	0.33	2.53	5.58	5.79	0.83	3.86
8 5 x 1992 emissions	23.83	21.33	2.26	15.29	32.51	32.71	6.06	23.39

**Table 4-6.** Global changes in NO<sub>x</sub> and ozone during July due to aircraft emissions from the IMAGES and the Harvard models for altitudes from ground to 150 mb and from 400 - 150 mb (in parentheses).

(a) Percent Change

Case		$\Delta\text{NO}_x$ (%)		$\Delta\text{O}_3$ (%)	
		IMAGES	Harvard	IMAGES	Harvard
2	1992 emissions	4.28 (9.65)	2.19 (5.55)	1.15 (1.42)	0.91 (1.04)
3C	lightning (5 Tg N, Price and Rind)	3.42 (6.22)	2.08 (5.02)	0.77 (0.87)	0.80 (0.96)
3B,3D	lightning, 10 Tg N yr <sup>-1</sup>	3.32 (6.67)	1.70 (3.41)	0.78 (0.96)	0.61 (0.71)
4B	2 x convection	3.31 (7.77)	1.98 (5.05)	0.91 (1.10)	0.77 (0.91)
8	5 x 1992 emissions	23.39 (53.00)	10.87 (27.60)	4.36 (4.88)	3.92 (4.55)

(b) Absolute Change

Case		$\Delta\text{NO}_x$ (Gg N)		$\Delta\text{O}_3$ (Tg)	
		IMAGES	Harvard	IMAGES	Harvard
2	1992 emissions	3.69 (3.42)	2.20 (1.78)	3.96 (2.43)	2.66 (1.03)
3C	lightning (5 Tg N, Price and Rind)	3.58 (3.32)	2.18 (1.78)	2.78 (1.58)	2.52 (0.97)
3B,3D	lightning, 10 Tg N yr <sup>-1</sup>	3.42 (3.18)	2.14 (1.75)	2.88 (1.75)	2.09 (0.78)
4B	2 x convection	2.78 (2.56)	1.93 (1.56)	3.00 (1.76)	2.23 (0.83)
8	5 x 1992 emissions	20.19 (18.79)	10.94 (8.87)	15.03 (8.37)	12.02 (4.5)

**Table 4-7. Radiative forcing and global annual average surface temperature response for selected aircraft releases.**

<b>Perturbation</b>	<b>Radiative Forcing</b>	<b>Surf Temp Response</b>
300x 2015 Aircraft Water Vapor	NA	+1.03°C
15x 2015 Aircraft Water Vapor	NA	+0.24°C
1.5x 2015 Aircraft Water Vapor	NA	Less than model variability
1992 Subsonic Aircraft Ozone	0.01 W m <sup>-2</sup>	Less than model variability (0.01°C)
5x1992 Subsonic Aircraft Ozone	0.033 W m <sup>-2</sup>	0.09°C
1992 Subsonic Aircraft Soot	~(10 <sup>-3</sup> ) W m <sup>-2</sup>	Less than model variability (0.02°C)
1992 CO <sub>2</sub> Emissions	0.0003 W m <sup>-2</sup> ; (over last 30 years 0.0067 W m <sup>-2</sup> )	Less than model variability (0.007°C)
1992 NO <sub>x</sub> Emissions	10 <sup>-3</sup> W m <sup>-2</sup> Locally	Less than model variability
1992 SO <sub>2</sub> Emissions	10 <sup>-4</sup> W m <sup>-2</sup> Locally	Less than model variability

### Vertical Resolution of participating models

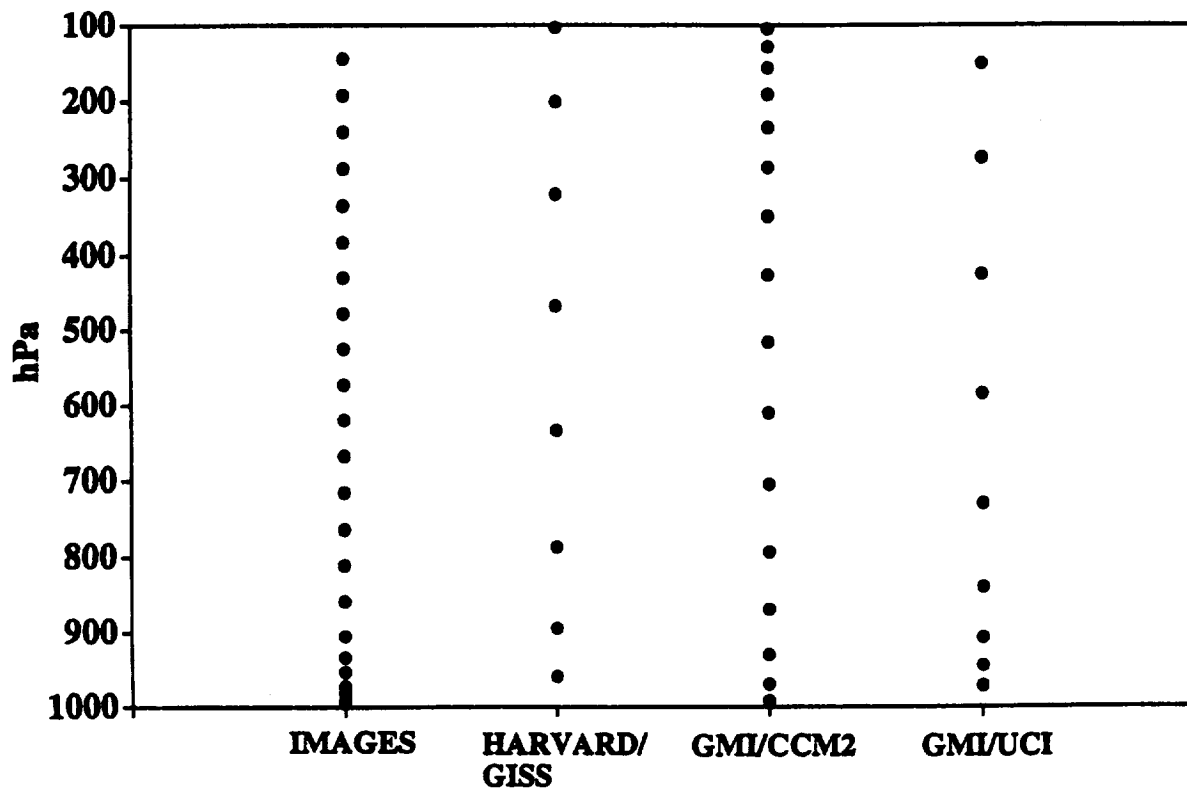


**Figure 4-1.** Vertical resolution from 1000 to 100 hPa for the chemical-transport models participating in this assessment.

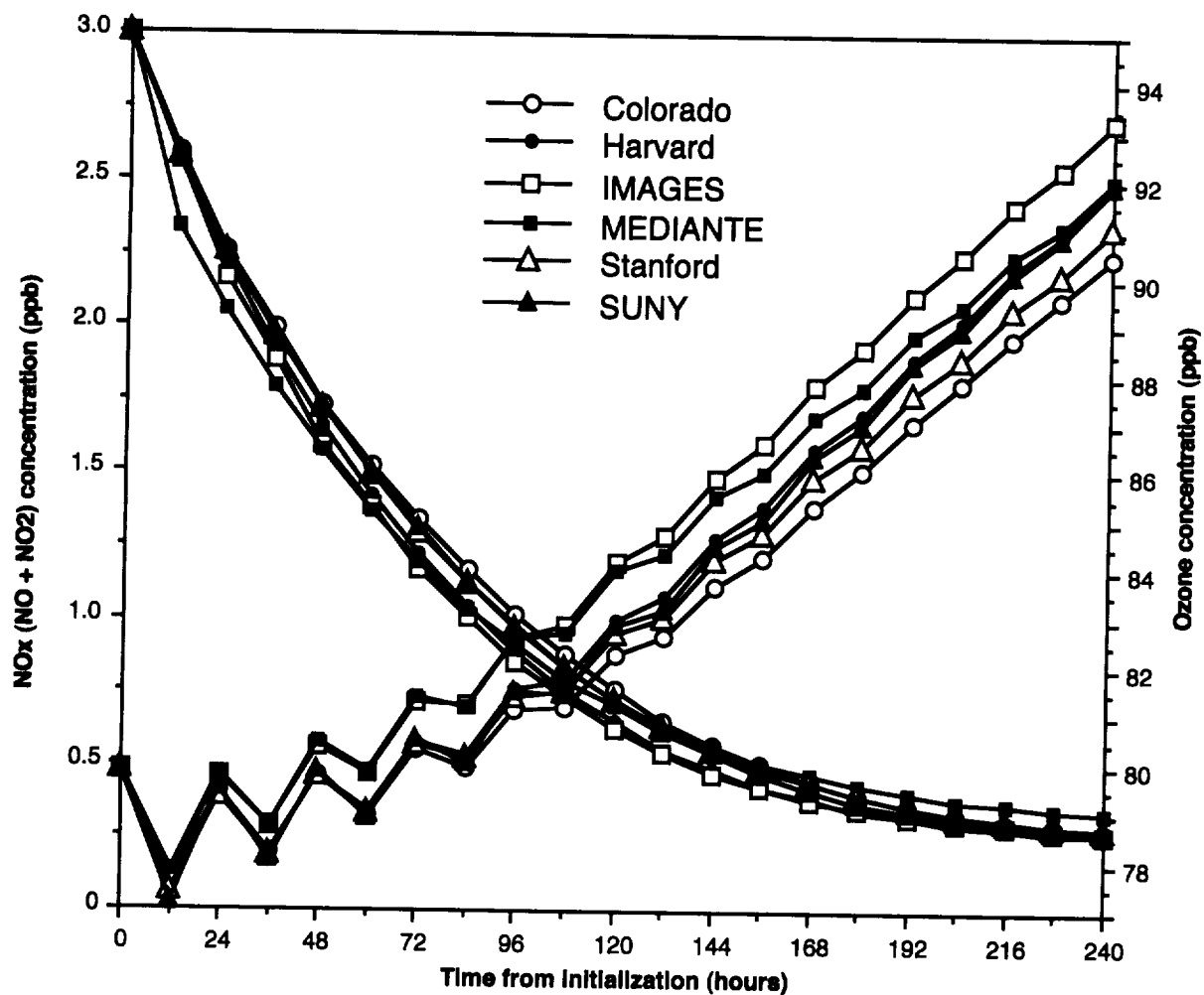


**Figure 4-2.** Calculated time evolution of concentrations of ozone and  $\text{NO}_x$  during 10 days following initialization with identical meteorological and chemical conditions. Simulations at 300 mbar, 235 K, 21 June, 40°N conditions. Initial ozone = 80 ppbv, CO = 100 ppbv, acetone = 0.5 ppbv, and  $\text{H}_2\text{O}$  = 100 ppmv. All reactive nitrogen initially present as NO.

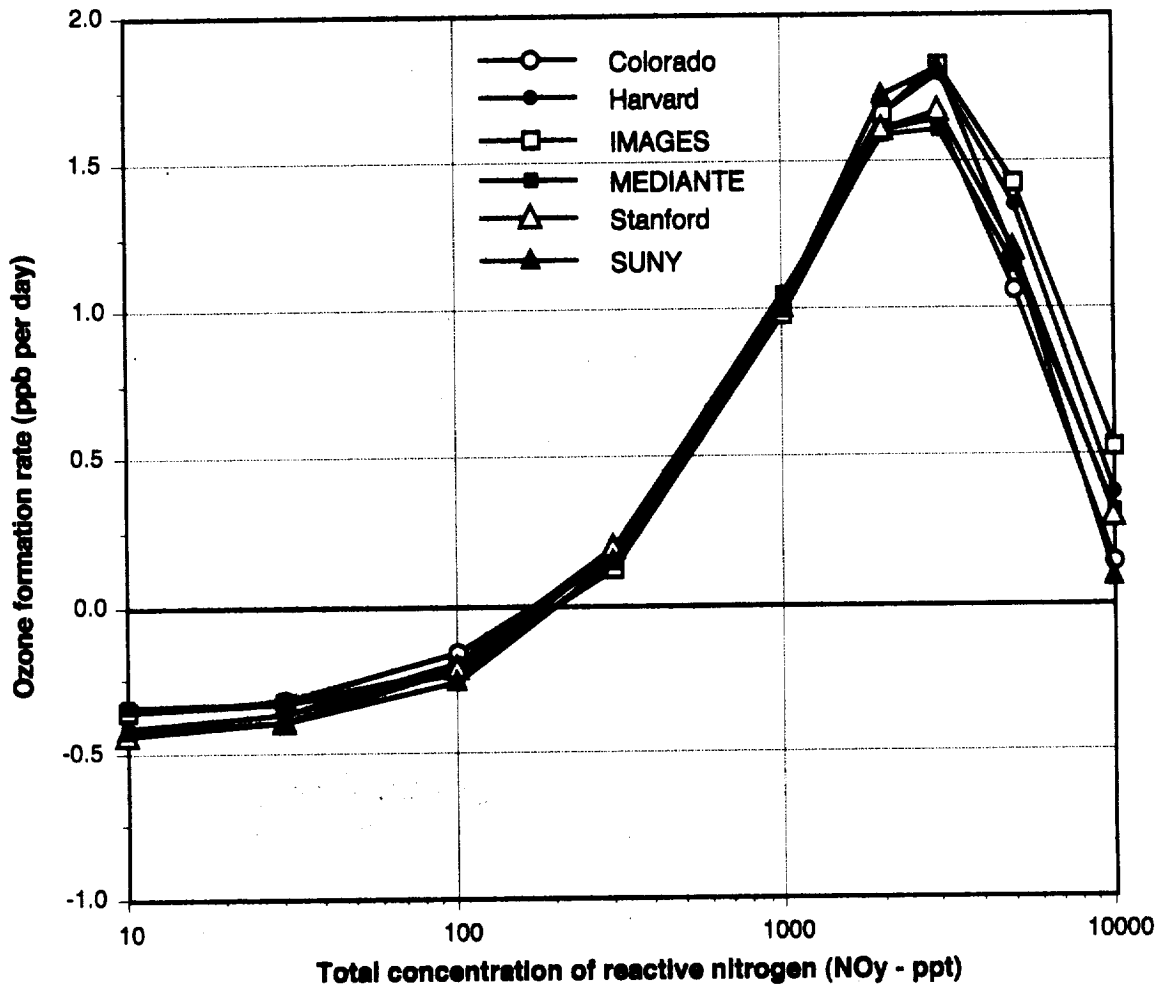


**Figure 4-3.** Ozone formation rate calculated for upper tropospheric conditions by various atmospheric chemical reaction mechanisms vs. total concentration of reactive nitrogen. Formation rates averaged during last five days of a 10-day integration from identical initial conditions.

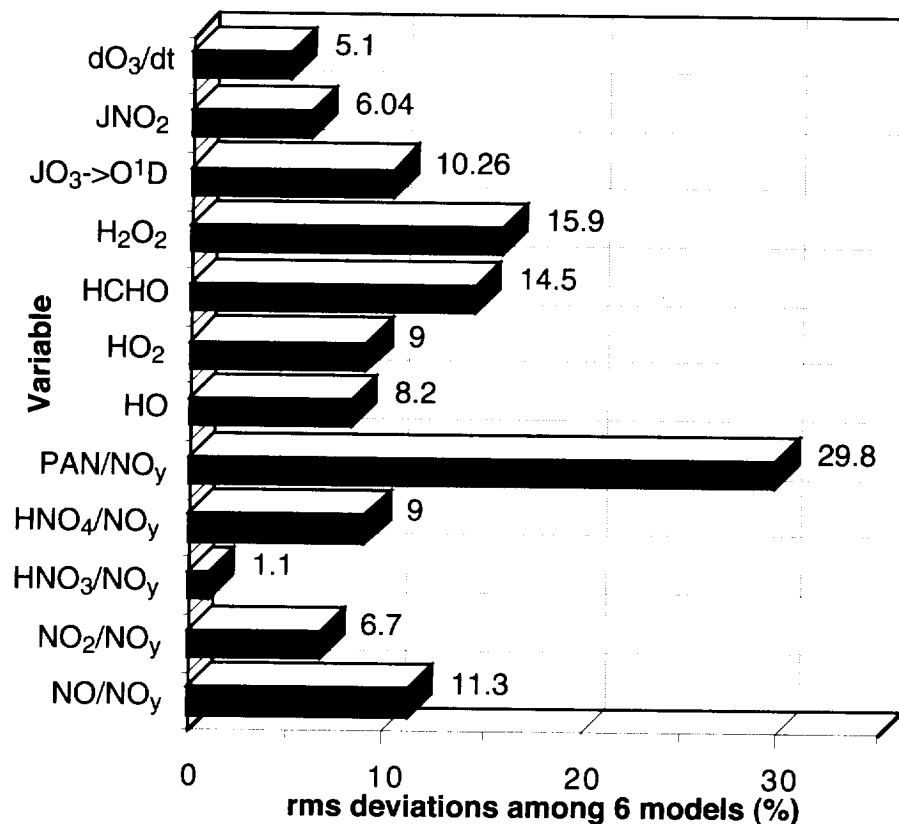


**Figure 4-4.** Root mean square deviation, relative to mean, expressed as percent for a number of model parameters after 10-day integration at [NO<sub>y</sub>] = 3 ppbv. All variables correspond to outputted concentrations except dO<sub>3</sub>/dt which refers to ozone formation rate and JNO<sub>2</sub> and J(O<sub>3</sub> → O<sup>1</sup>D)) which refer to calculated photolysis rates.

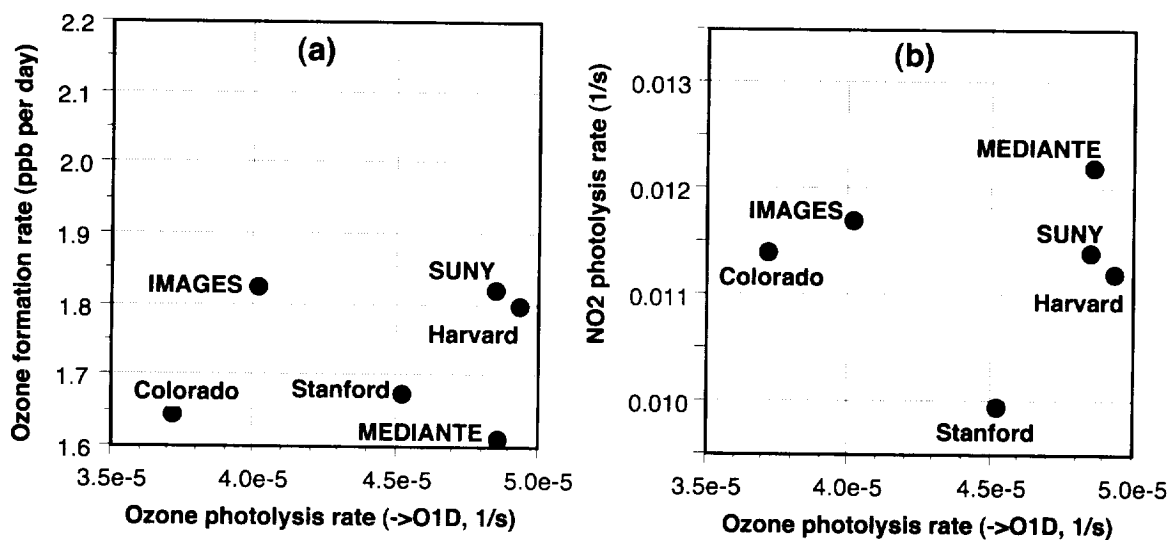


**Figure 4-5.** Correlation scatter diagram for (a) ozone formation rate and ozone photolysis rate, and for (b) NO<sub>2</sub> and ozone photolysis rate. Ozone formation rates compared at 3 ppbv NO<sub>y</sub>.

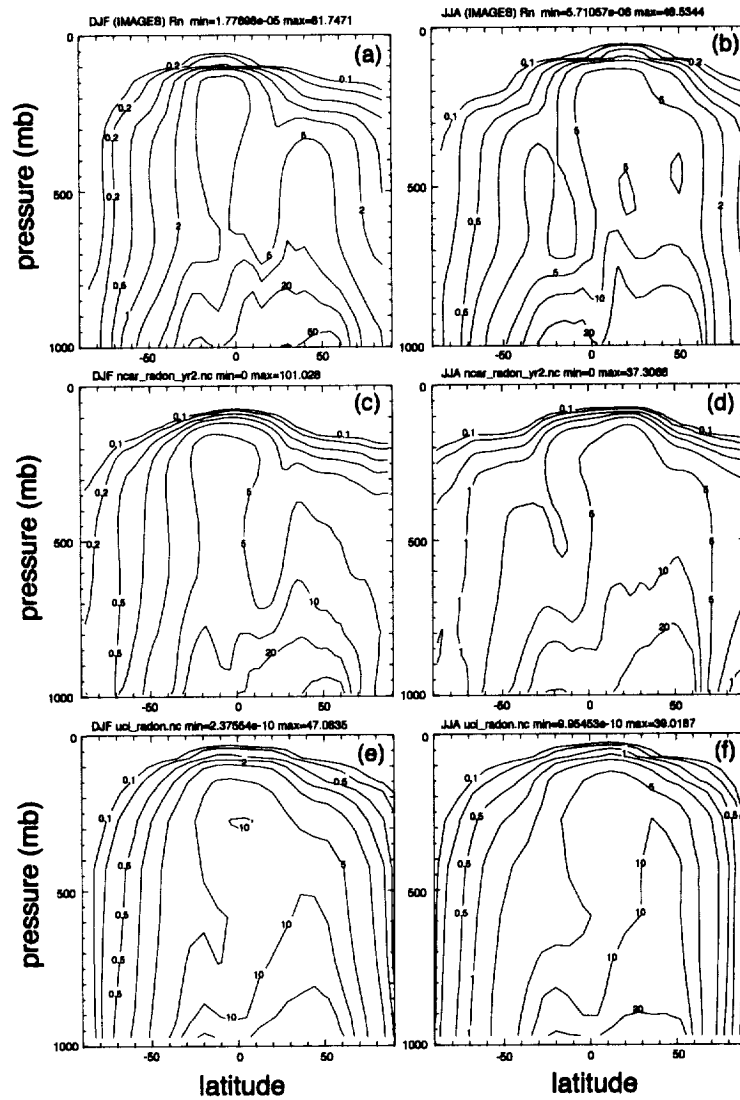


**Figure 4-6.** Zonally averaged monthly mean radon concentrations for the models. Top: IMAGES; Middle, GMI/CCM2; Bottom, GMI/UCI. Left panels are for DJF, right for JJA. Ordinate has units of pressure (mbar). Abscissa has units of degrees (latitude). Units are volume mixing ratio times  $10^{21}$ .

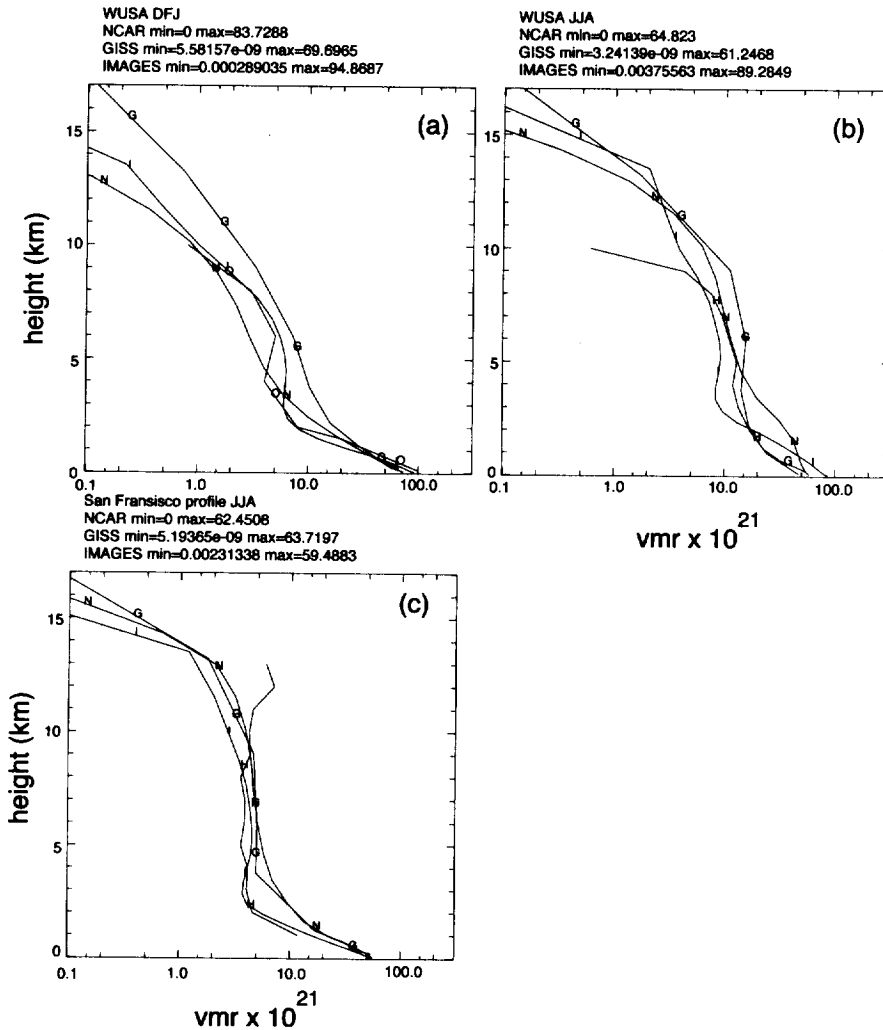


**Figure 4-7.** Seasonal profiles of models vs. observations of radon. Top left panel, Western US during DJF. Top Right Western US over JJA. Bottom Left. San Francisco Region during JJA. Ordinate has units of height (km). Units are volume mixing ratio times  $10^{21}$ . Lines Labeled "O" are composites of observations. Lines labeled "N", "U", and "I" are the GMI/CCM2, GMI/UCI and IMAGES models respectively.

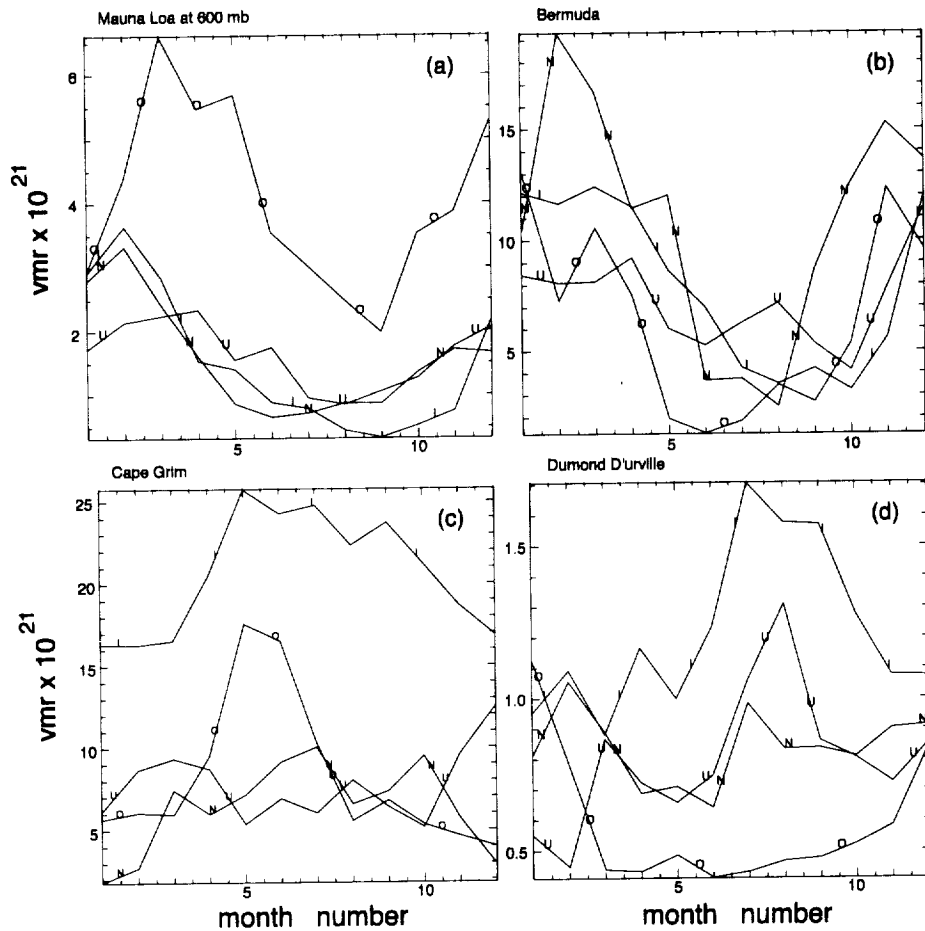


**Figure 4-8.** Time series of surface values for the models compared to observations of radon at various stations (month number vs. mixing ratio). Units are volume mixing ratio times  $10^{21}$ . Lines Labeled "O" are composites of observations. Lines labeled "N", "U", and "I" are the GMI/CCM2, GMI/UCI and IMAGES models respectively.

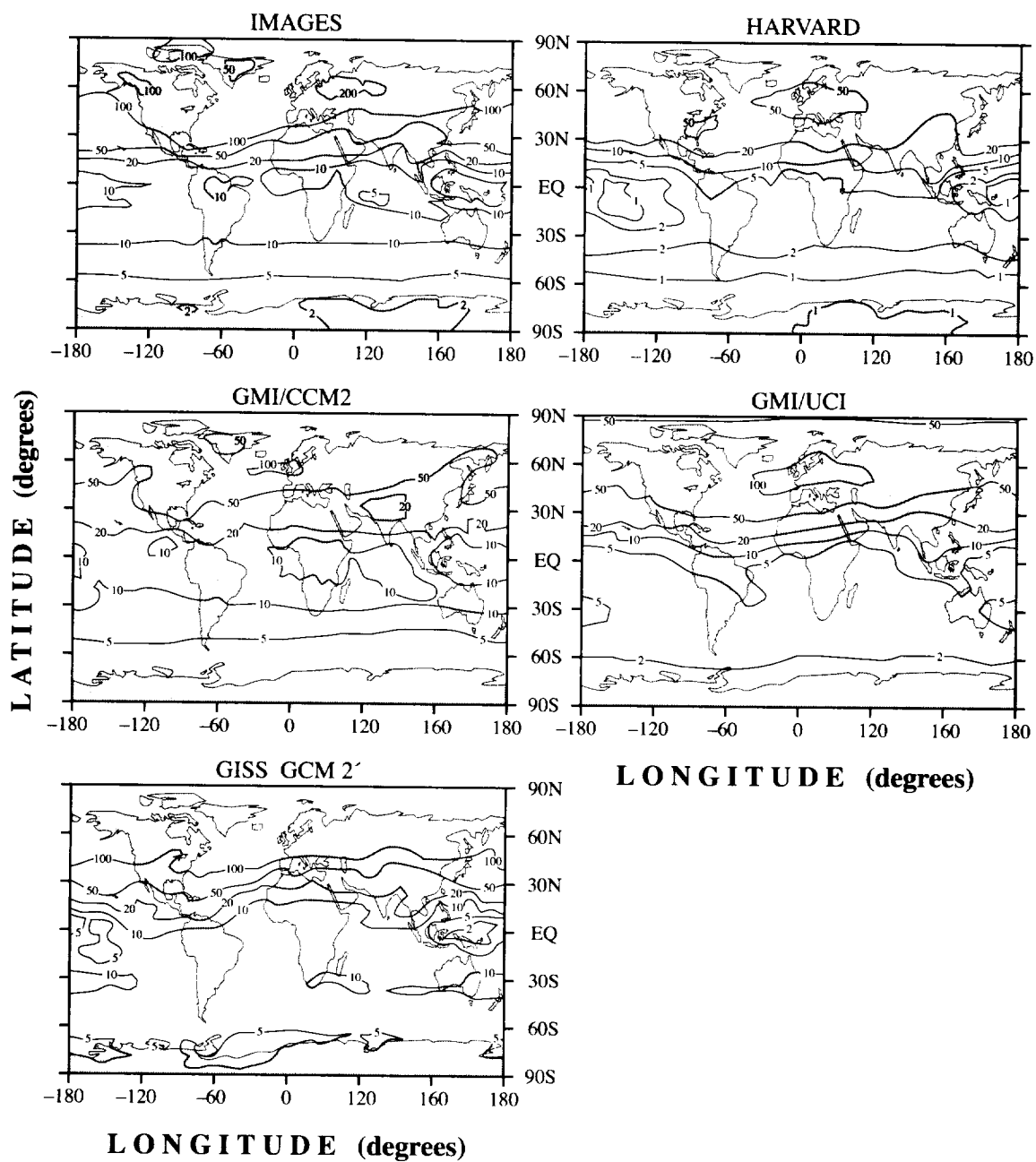


**Figure 4-9.** Simulated concentrations of aircraft  $\text{NO}_y$  (pptv) at 250 mbar in July.

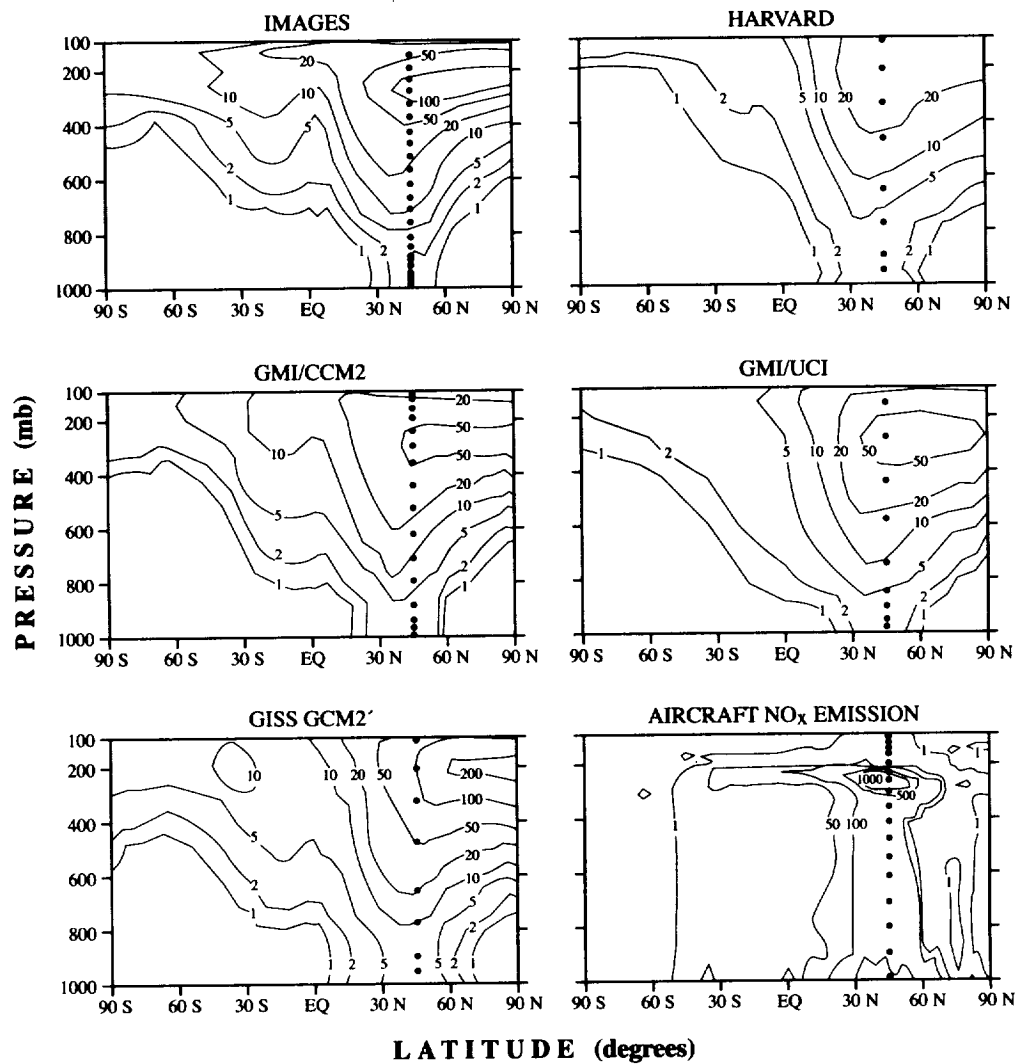


**Figure 4-10.** Simulated zonal mean concentrations of aircraft  $\text{NO}_y$  (pptv) as a function of latitude and altitude in July. The lower right-hand panel shows the emission inventory (molecules  $\text{cm}^{-3} \text{s}^{-1}$ ). The dots indicate the vertical resolution of the different models and of the emission inventory.

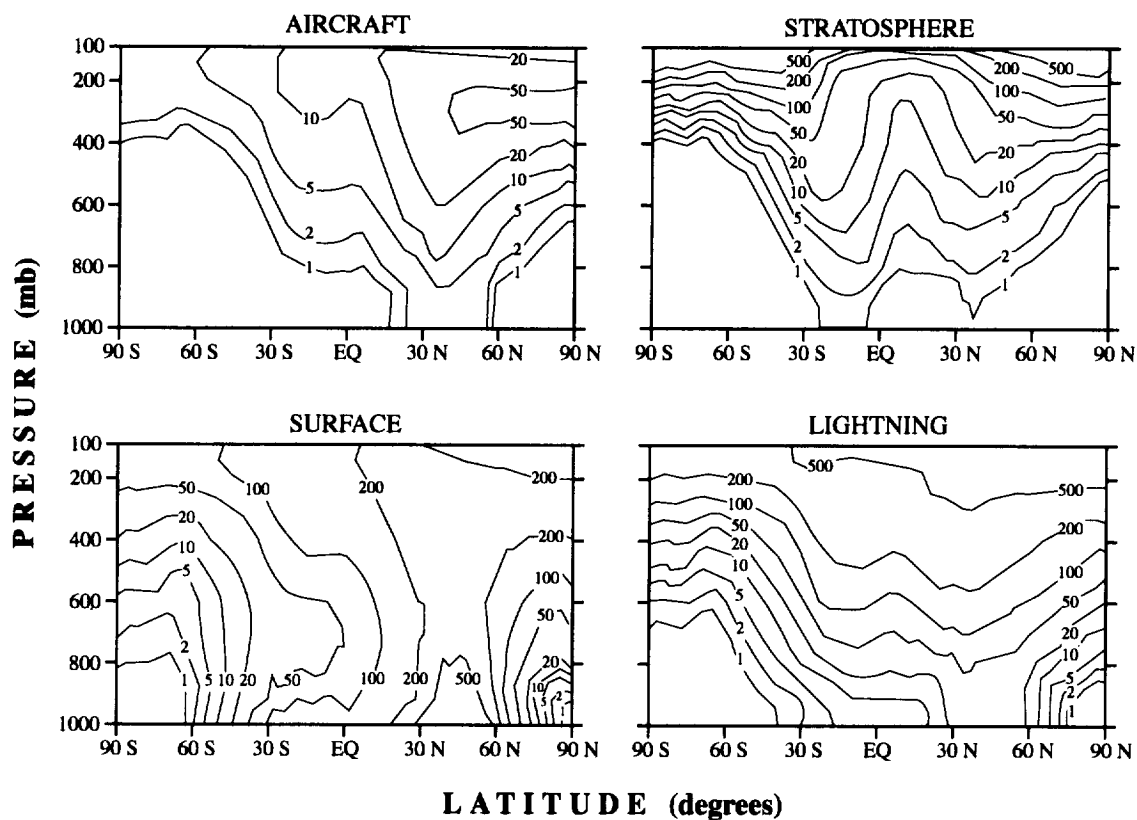


**Figure 4-11.** Simulated zonal mean concentrations of  $\text{NO}_y$  (pptv) contributed by individual sources in the GMI/CCM2 model in July.

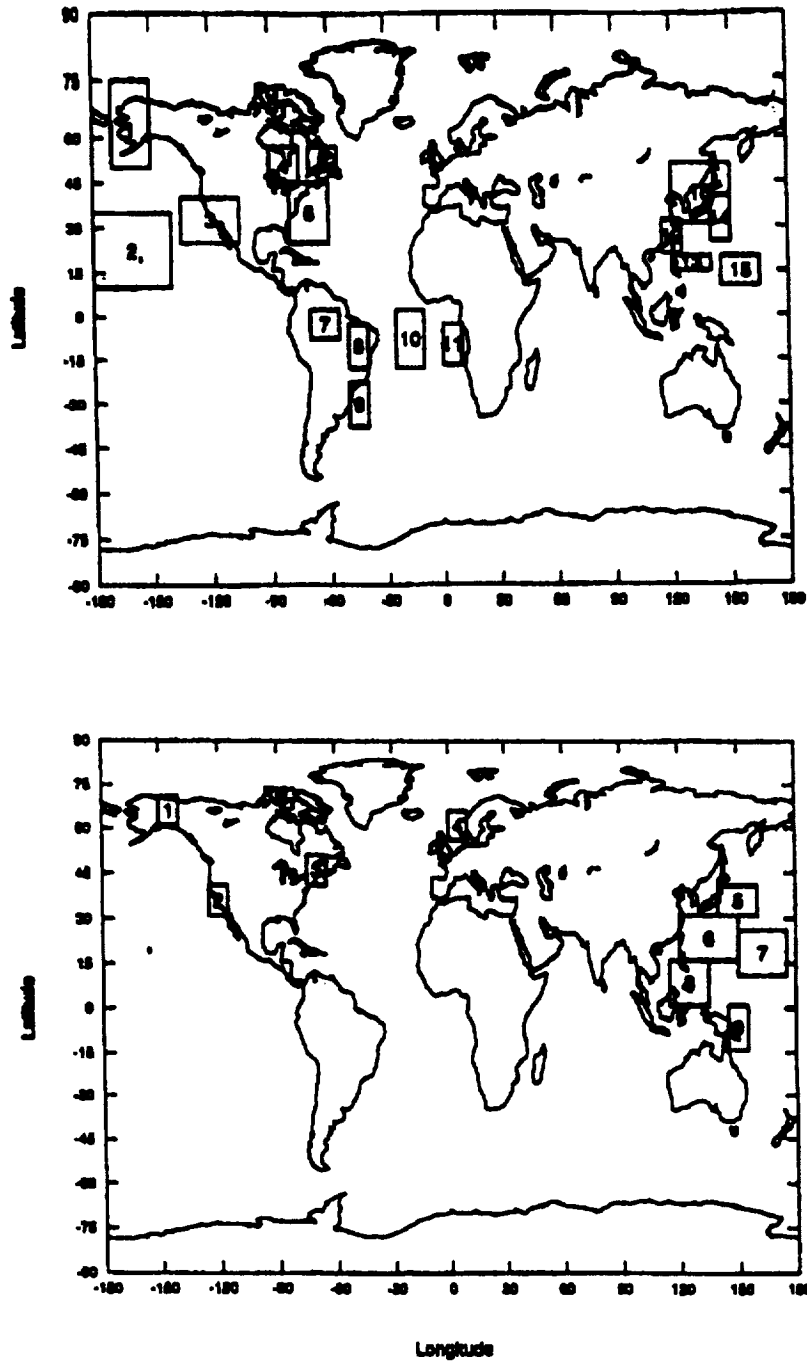


**Figure 4-12.** Regions for which vertical profiles were derived for model evaluation. Data for NO, HNO<sub>3</sub>, and PAN were provided by J. Bradshaw as averages values for grid boxes of 5° in latitude and longitude, and 1 km in altitude, derived from (top) the 'NH summer' (June-October) NASA/GTE missions and (bottom) the 'NH winter' AASE-II and PEM West-B aircraft campaigns. These data were further averaged over the regions shown in the figure to form profiles to compare with the data. The regions were selected based on the availability of observations and the spatial patterns apparent in the data for NO.

Daytime NO/PAN/HNO<sub>3</sub> regional profiles

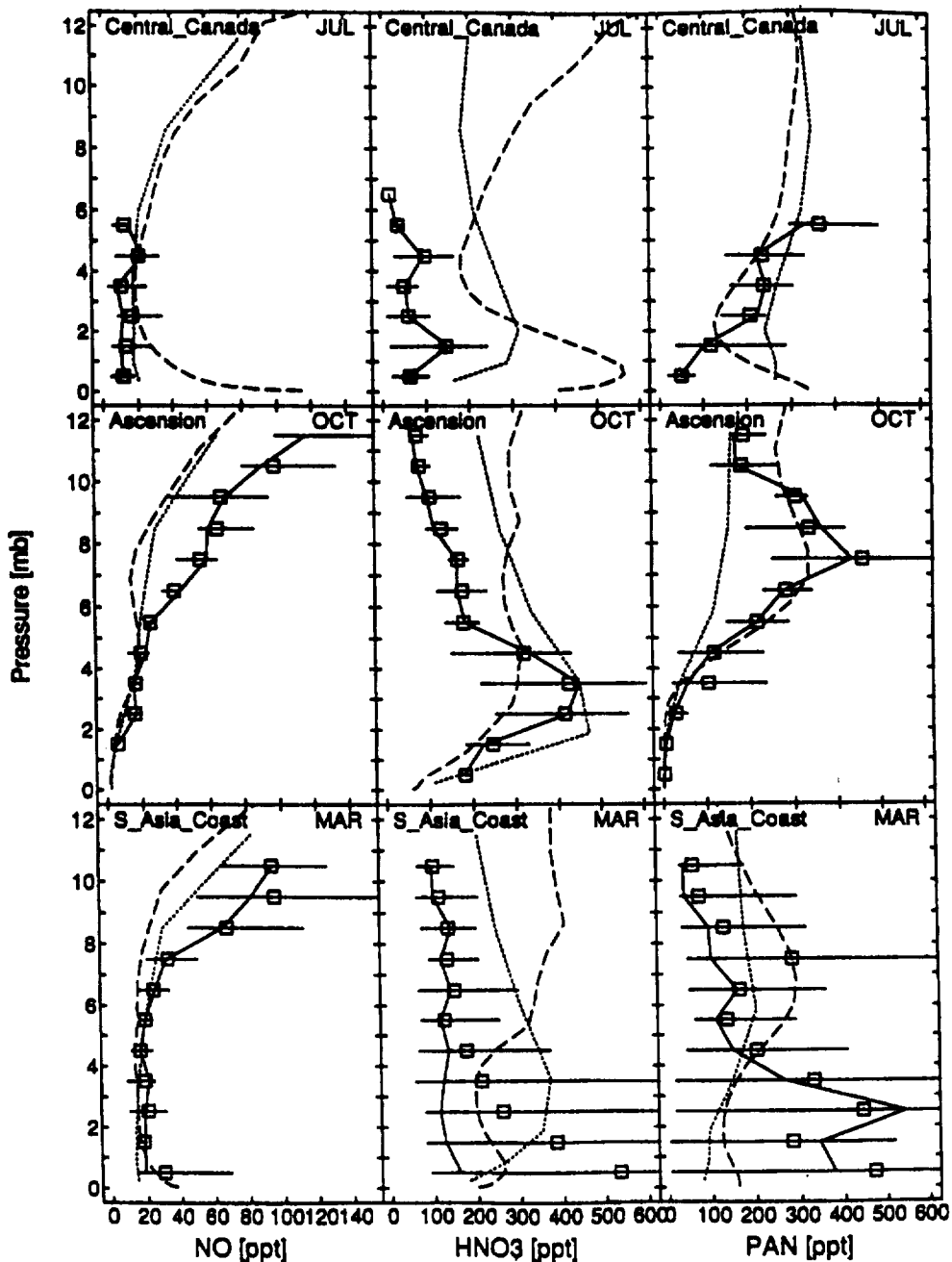
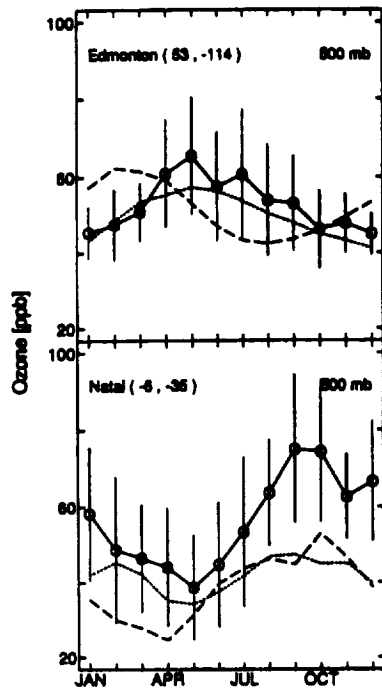


**Figure 4-13.** Vertical profiles for NO, HNO<sub>3</sub>, and PAN, for three selected regions from Figure 4-12. For each region, the solid lines show the median vertical profiles derived from the 5° x 5° averages, the squares show the mean for each region, and the horizontal lines show the range of the 5° x 5° averages. The results from IMAGES are given by the dashed lines, and the results of the Harvard model by the dotted lines, for the month in which the observations were made. The model results for NO are noontime values.

(a)



(b)

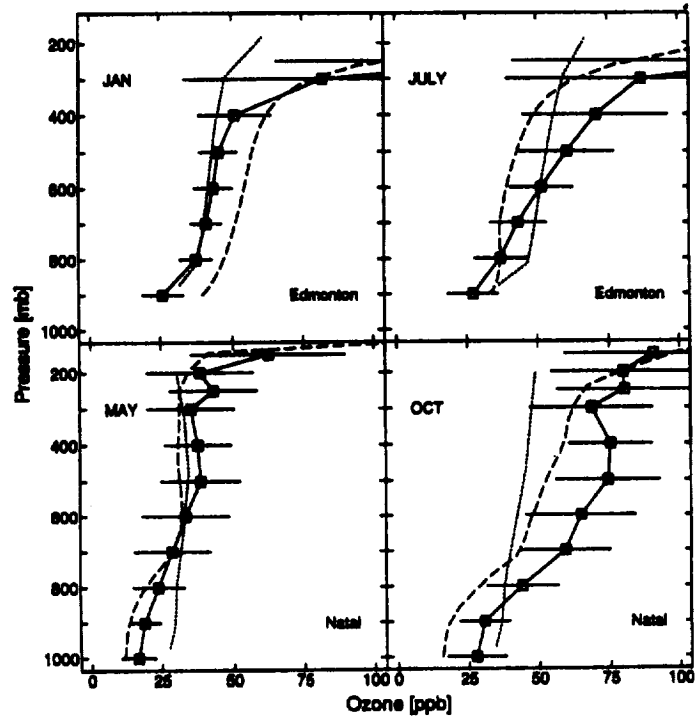


**Figure 4-14.** (a) Seasonal cycle of ozone at 500 mbar for Edmonton, Canada, and Natal, Brazil. The circles are means for 14 years of data, and the vertical lines show one standard deviation based on the individual measurements for each calendar month [Logan, personal communication]. The results from IMAGES are given by the dashed lines, and the results of the Harvard model by the dotted lines, for the grid box containing the station. (b) Vertical profiles for ozone for Edmonton in January and July, and for Natal in May and October, for the data in (a). Model results as in (a).

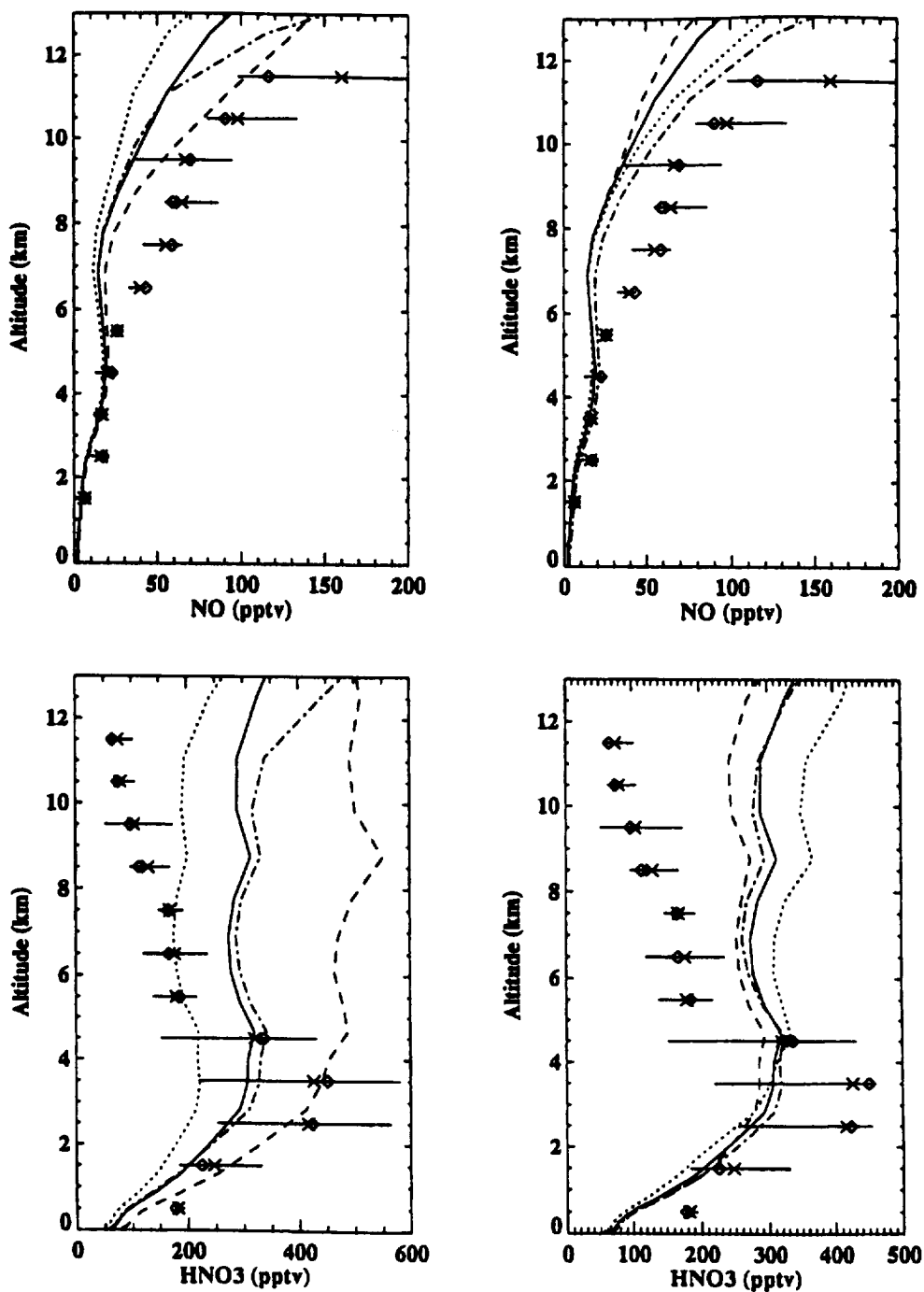


**Figure 4-15.** Comparison of model-derived profiles of NO and HNO<sub>3</sub> from IMAGES sensitivity calculations with observations at Ascension Island. Data is shown in terms of mean (crosses) and median (diamonds) values and one standard deviation of range. The left panels show model profiles for the baseline run (Case 1, solid line), lightning = 2 Tg (Case 3A, dotted line), lightning = 10 Tg (Case 3B, dashed line), and lightning = Price & Rind (Case 3C, dash-dotted line). The right panels show the baseline run (Case 1, solid line), reduced convection (Case 4A, dotted line), enhanced convection (Case 4B, dashed line), and JHNO<sub>3</sub>\*3 (Case 7, dash-dotted line).

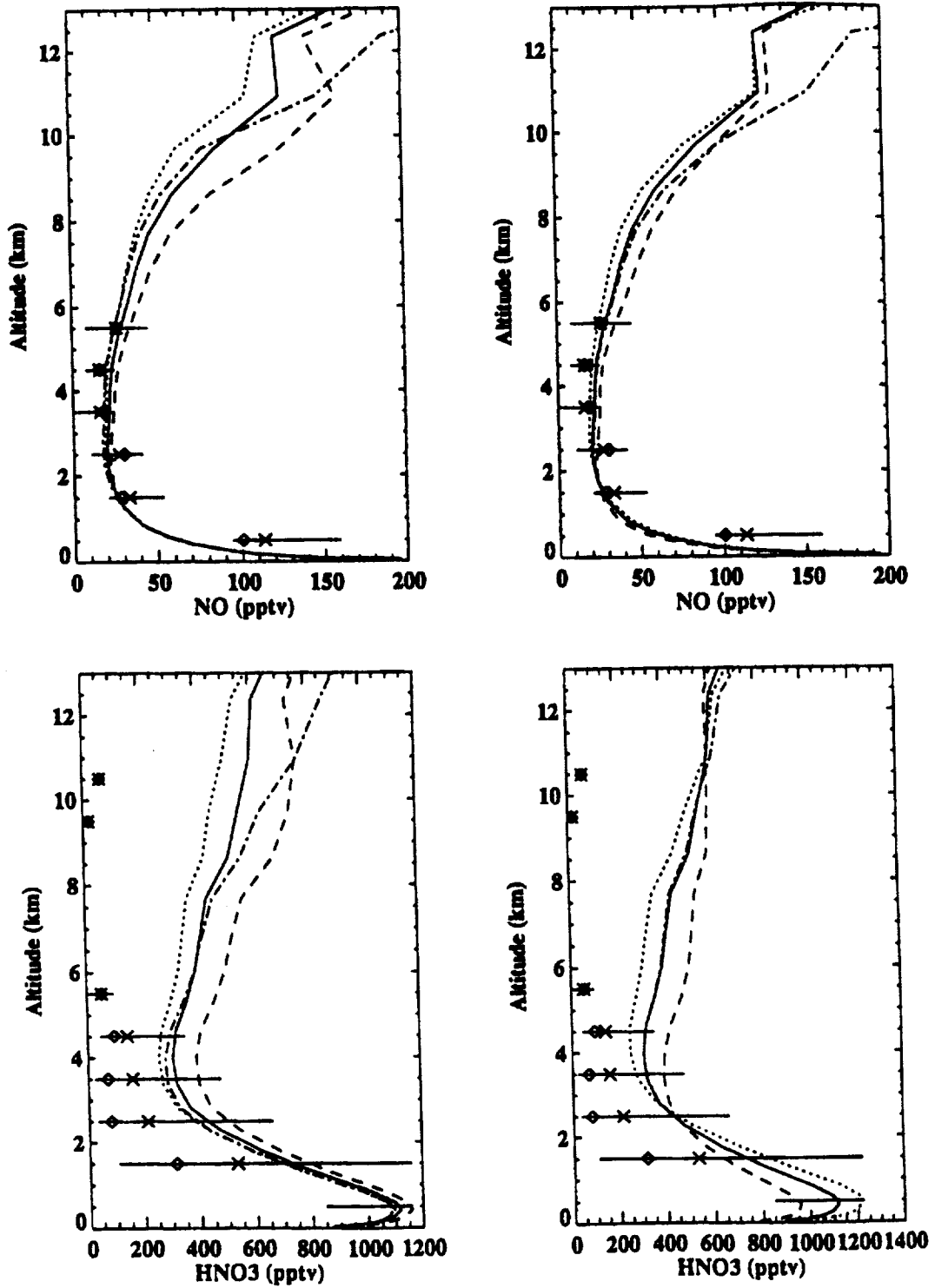
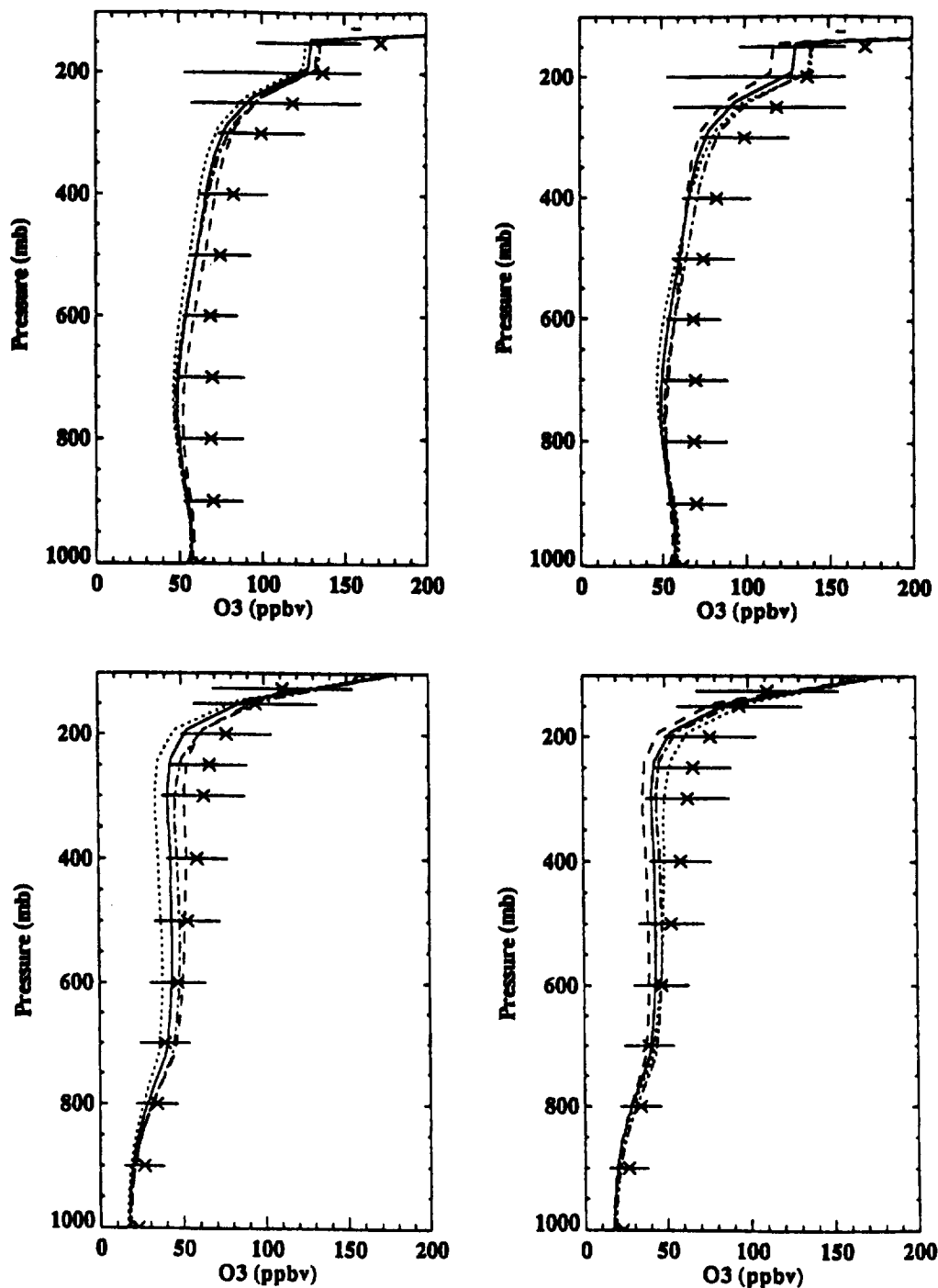
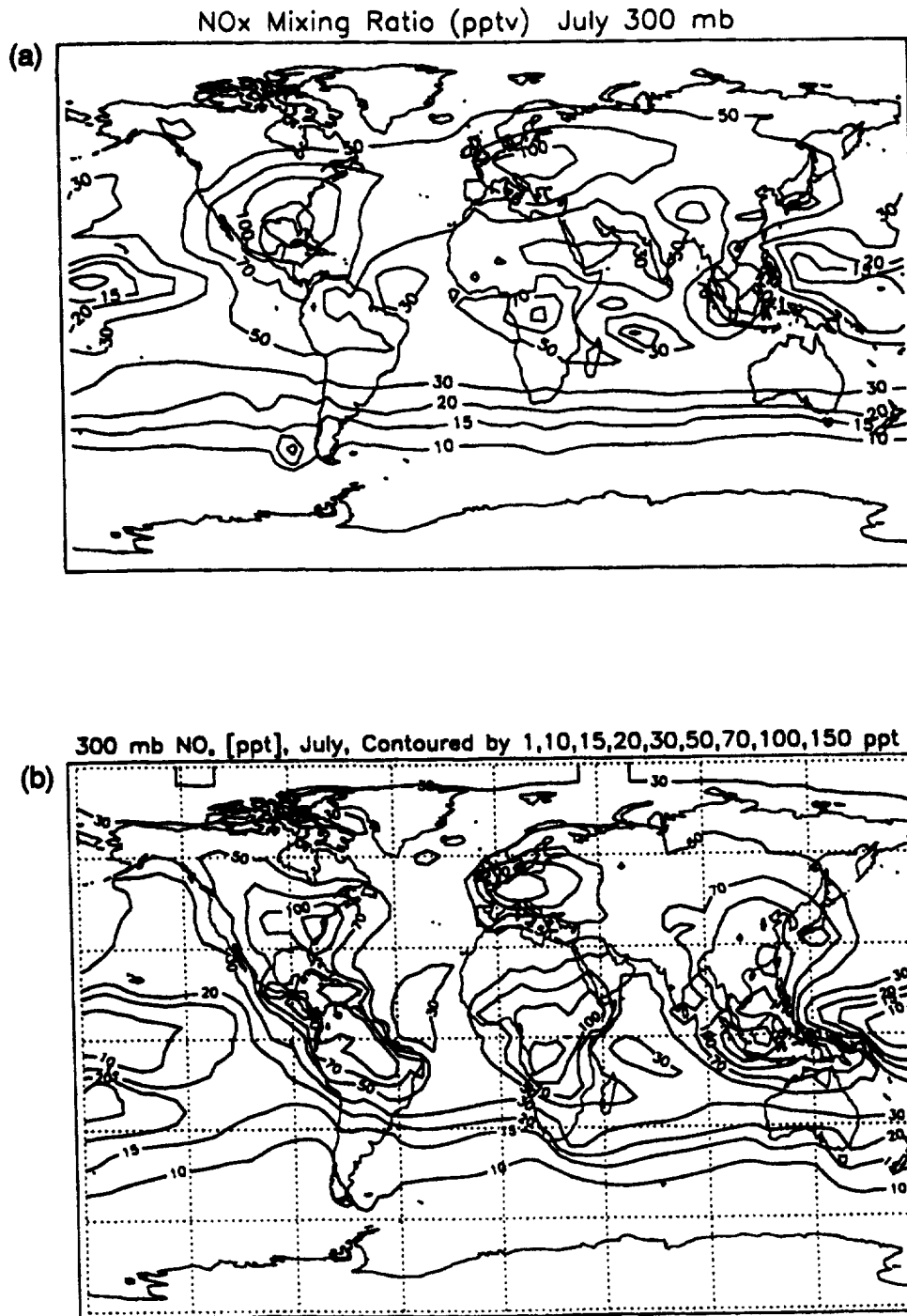


Figure 4-16. Same as Figure 4-15 except comparison with observations of NO and HNO<sub>3</sub> in eastern US (Wallops Island).



**Figure 4-17.** Comparison of model-derived profiles of ozone from IMAGES sensitivity calculations with observations at Wallops Island (top panels) and Natal (bottom panels) for July. The left panels show model profiles for the baseline run (Case 1, solid line), lightning = 2 Tg (Case 3A, dotted line), lightning = 10 Tg (Case 3B, dashed line), and lightning = Price & Rind (Case 3C, dash-dotted line). The right panels show the baseline run (Case 1, solid line), reduced convection (Case 4A, dotted line), enhanced convection (Case 4B, dashed line), and JHNO<sub>3</sub>\*3 (Case 7, dash-dotted line).



**Figure 4-18.** Model derived NO<sub>x</sub> mixing ratios (in pptv) for July at 300 mbar corresponding to sensitivity calculation Case 2 using 1992 aircraft emissions. (a) IMAGES; (b) Harvard-GISS. Note: the tropopause outside of the tropics in the Harvard model is too high, implying that 300 mbar is always in tropospheric air.

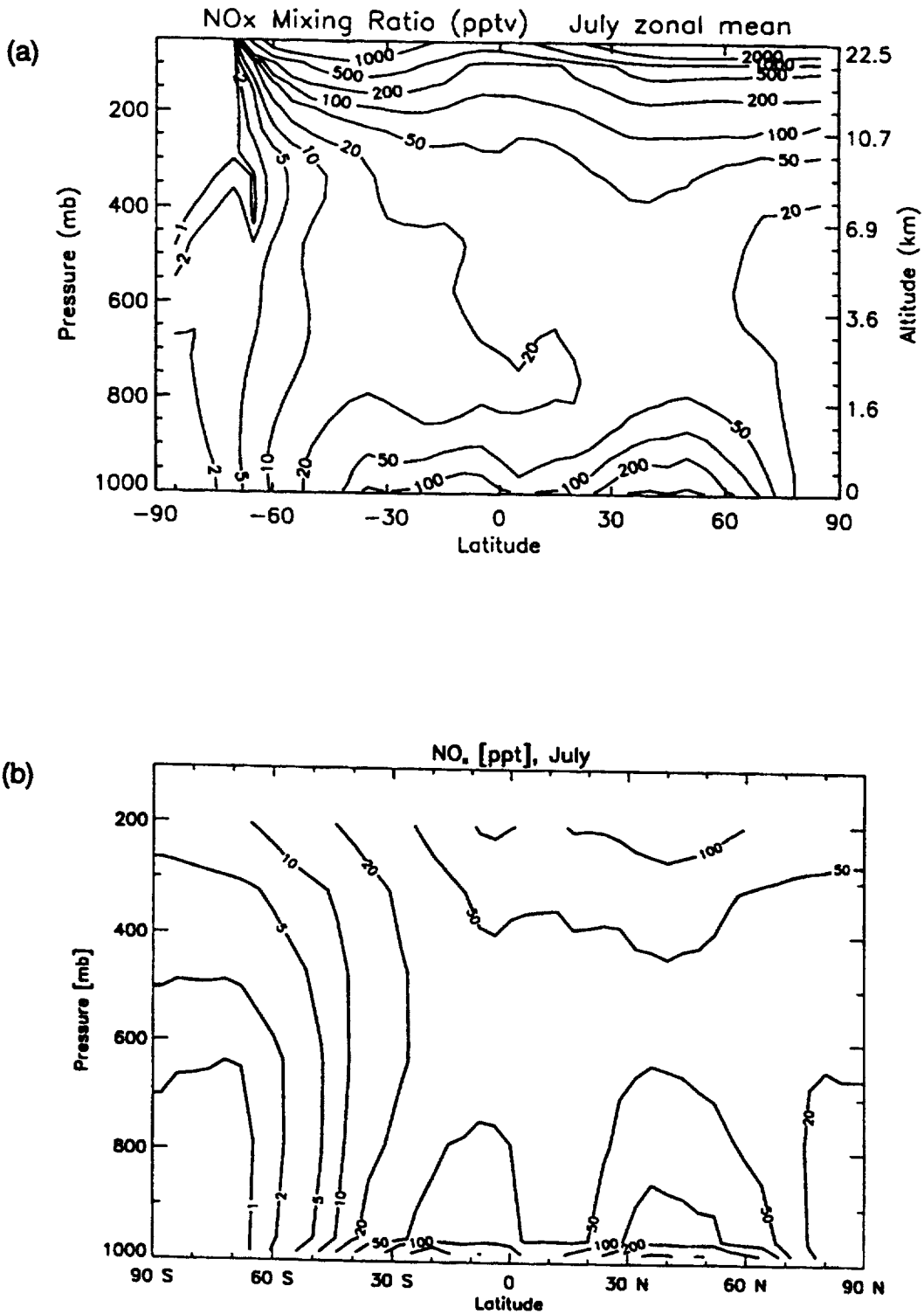


**Figure 4-19.** Zonally-averaged model derived NO<sub>x</sub> mixing ratios (in pptv) for July corresponding to sensitivity calculation Case 2 using 1992 aircraft emissions. (a) IMAGES; (b) Harvard-GISS. Note: the tropopause outside of the tropics in the Harvard model is too high, causing air below 200 mb to always be in the troposphere.

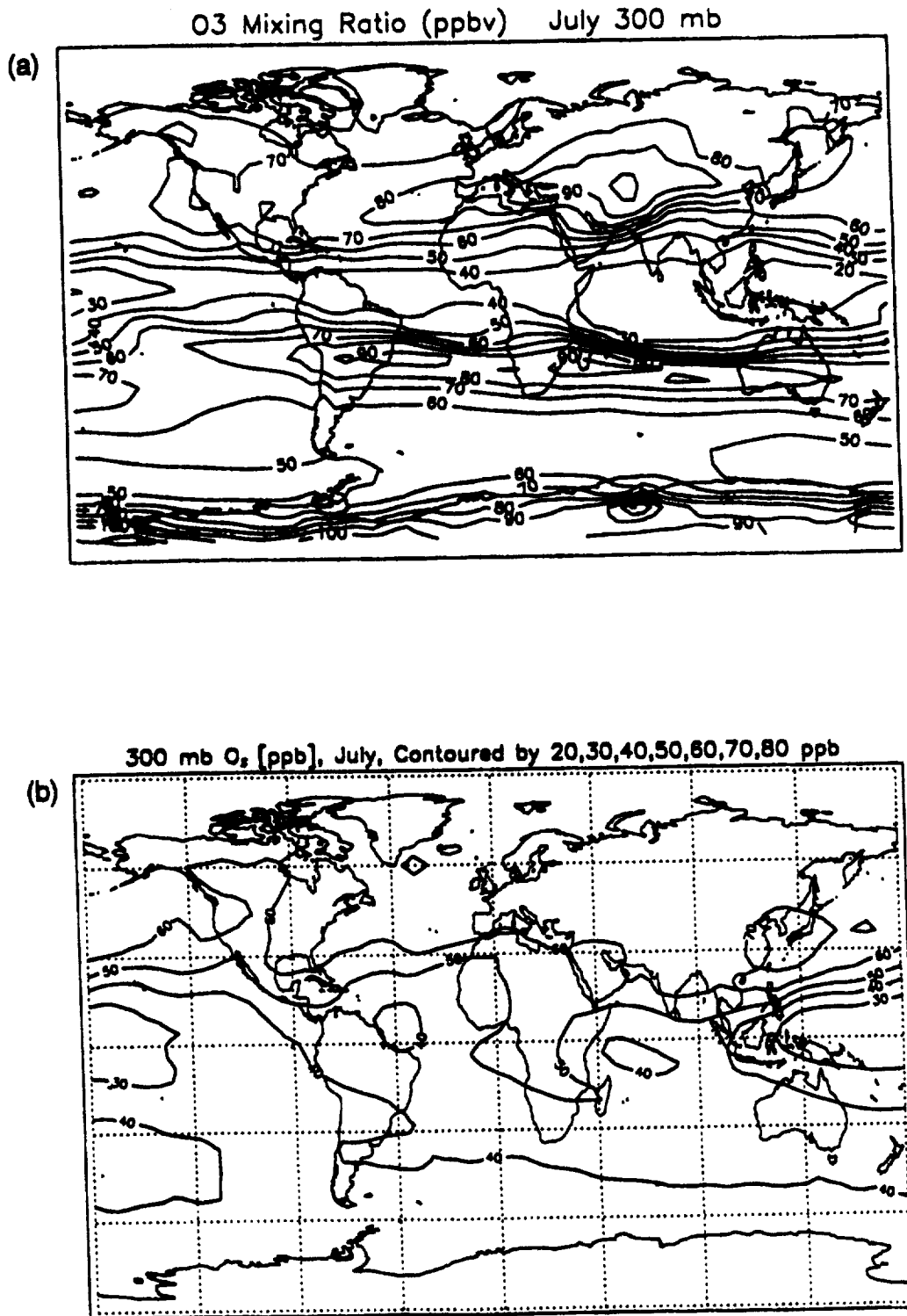


**Figure 4-20.** Model derived ozone mixing ratios (in ppbv) for July at 300 mbar corresponding to sensitivity calculation Case 2 using 1992 aircraft emissions. (a) IMAGES; (b) Harvard-GISS. Note: the tropopause outside of the tropics in the Harvard model is too high, implying that 300 mbar is always in tropospheric air.

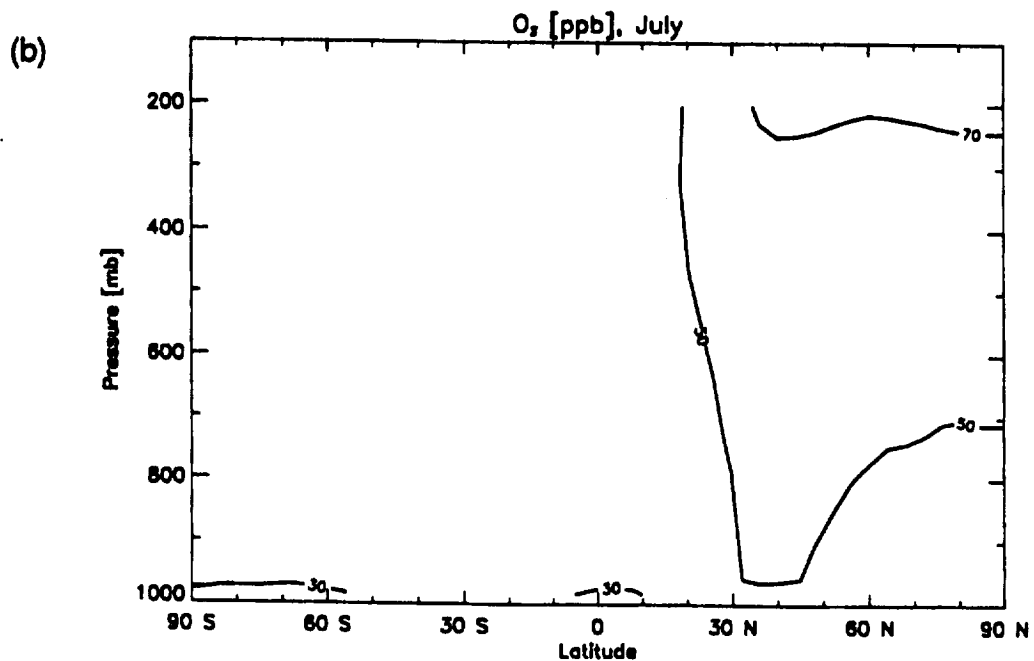
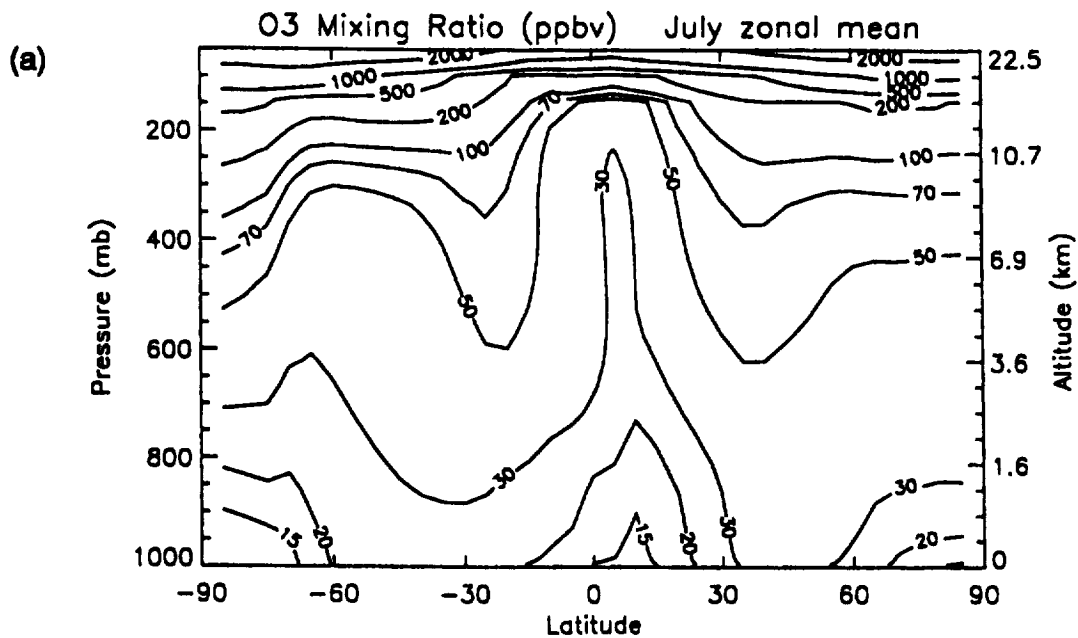


**Figure 4-21.** Zonally-averaged model derived ozone mixing ratios (in ppbv) for July corresponding to sensitivity calculation Case 2 using 1992 aircraft emissions. (a) IMAGES; (b) Harvard-GISS. Note: the tropopause outside of the tropics in the Harvard model is too high, causing air below 200 mb altitude to be always in the troposphere.

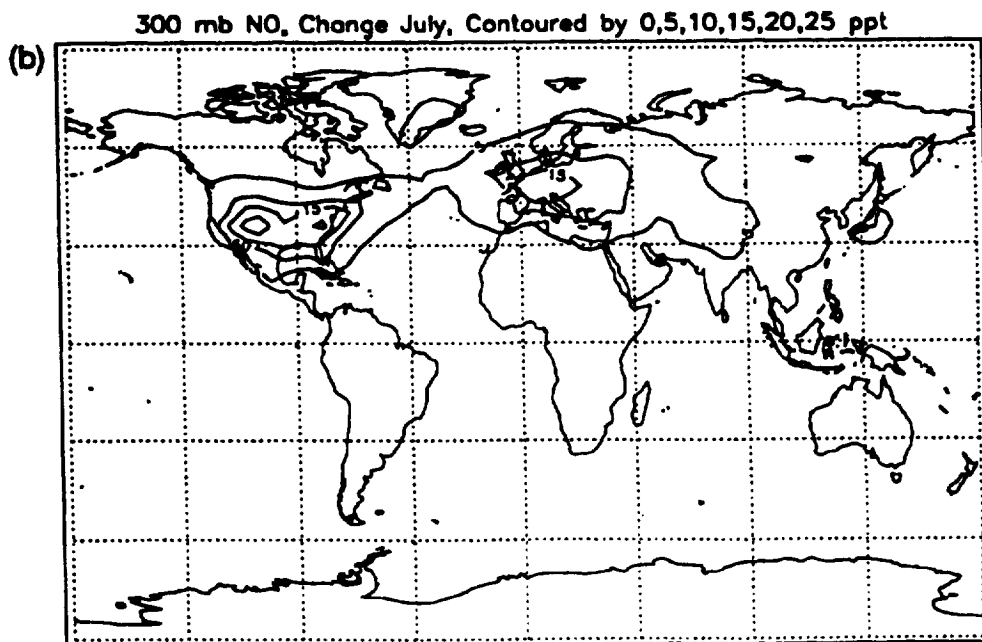
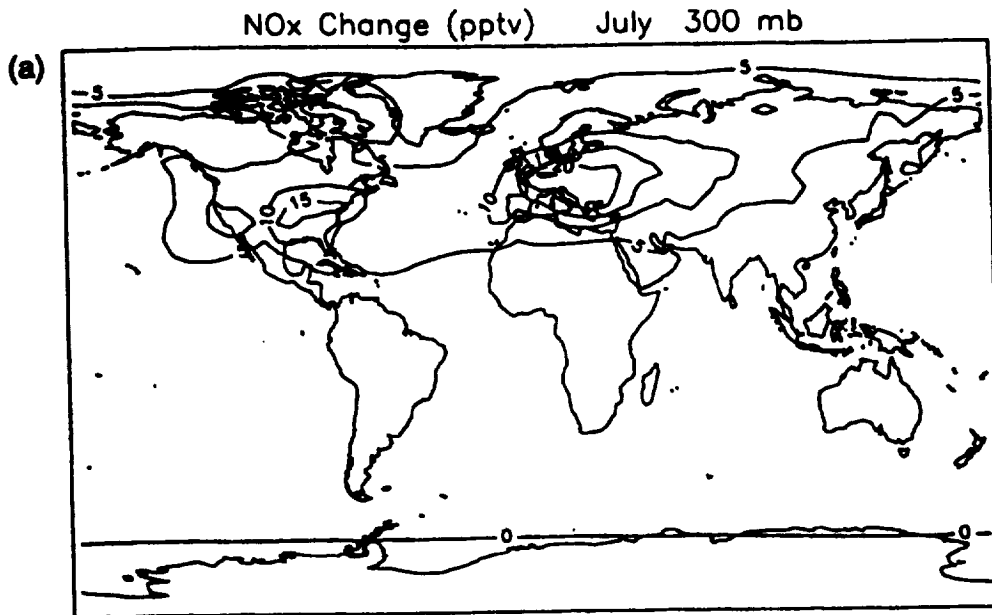


**Figure 4-22.** Contours of calculated changes in NO<sub>x</sub> at 300 mbar for July due to 1992 aircraft emissions (Case 2, relative to atmosphere with no aircraft) as determined by: (a) IMAGES; (b) Harvard-GISS. Units are pptv. Note: the tropopause outside of the tropics in the Harvard model is too high, implying that 300 is always in tropospheric air.

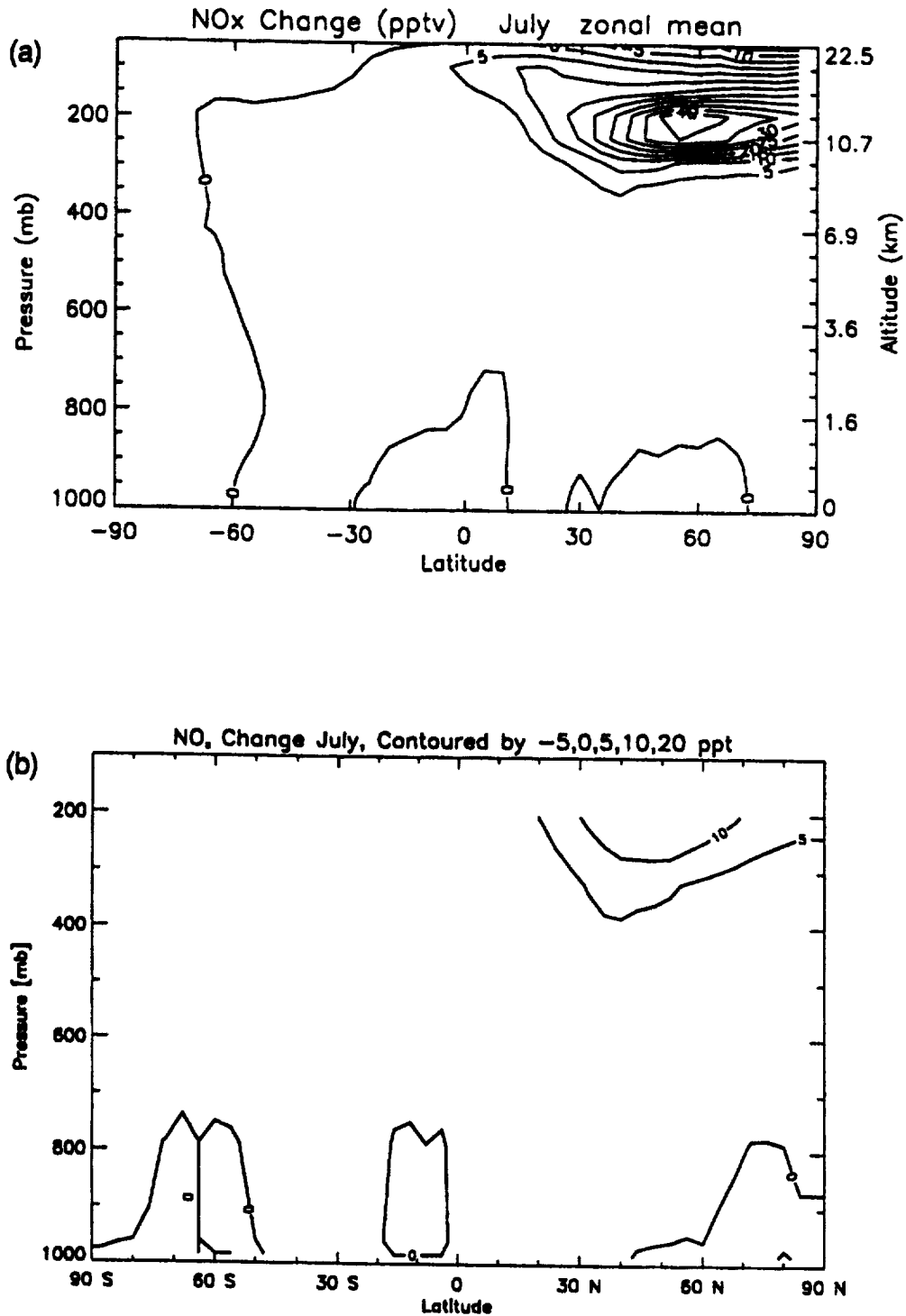


**Figure 4-23.** Zonally-averaged calculated changes in  $\text{NO}_x$  for July due to 1992 aircraft emissions (Case 2) as determined by: (a) IMAGES; (b) Harvard-GISS. Units are pptv. Note: the tropopause outside of the tropics in the Harvard model is too high, implying that 200 mbar and altitudes below are always in tropospheric air.

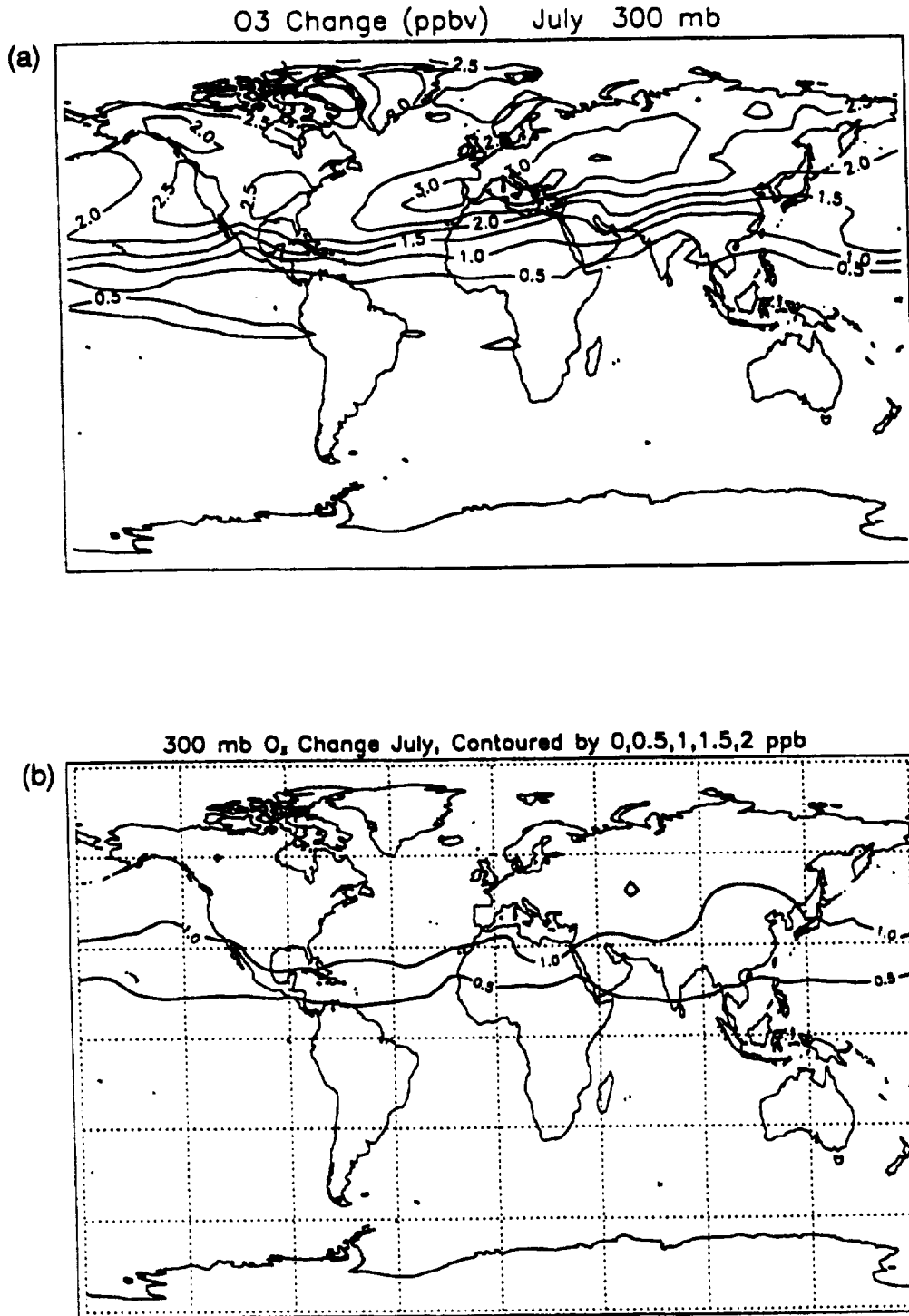


**Figure 4-24.** Contours of calculated changes in ozone at 300 mbar for July due to 1992 aircraft emissions (Case 2, relative to atmosphere with no aircraft) as determined by: (a) IMAGES; (b) Harvard-GISS. Units are ppbv. Note: the tropopause outside of the tropics in the Harvard model is too high, implying that 300 mbar is always in tropospheric air.

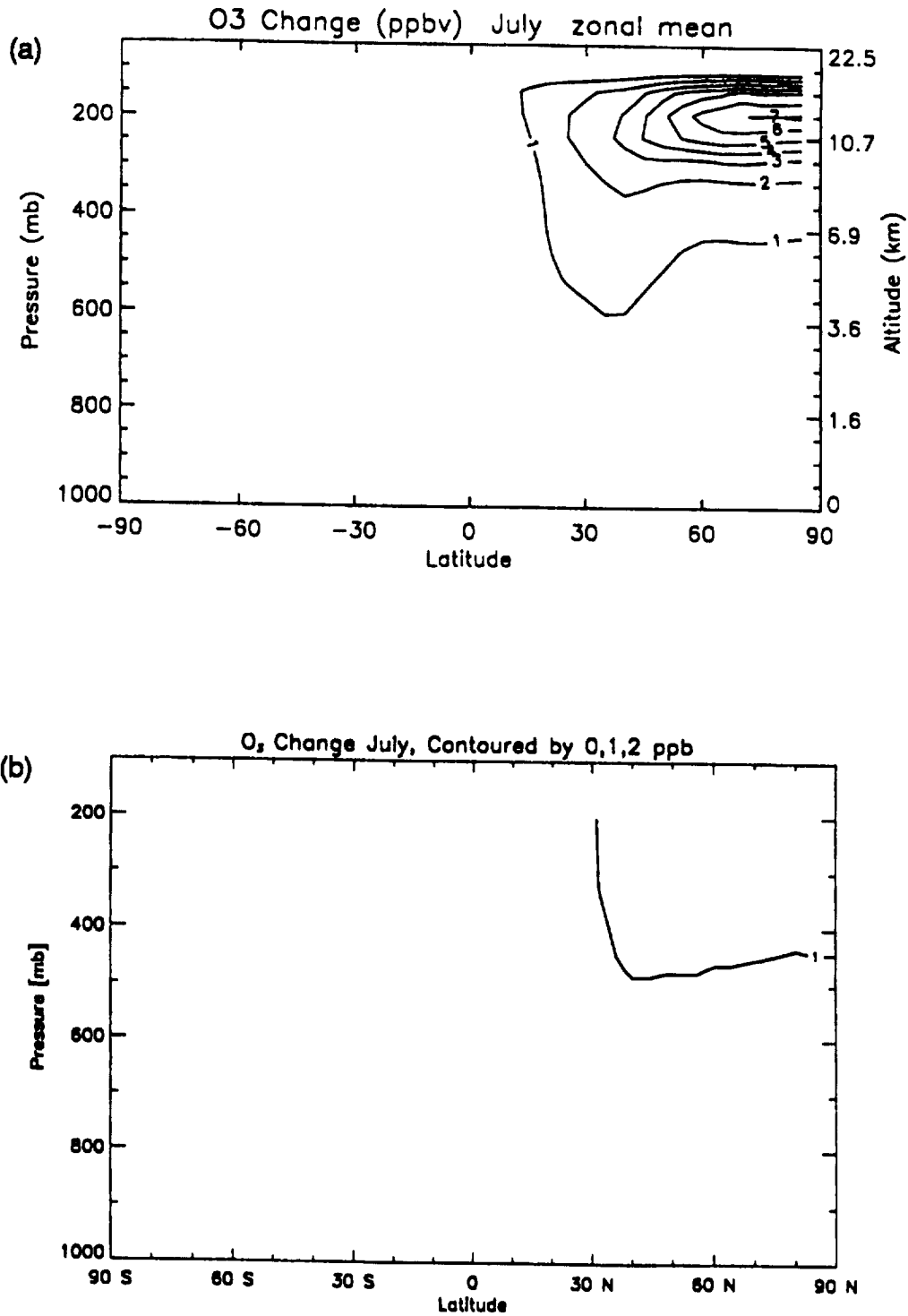


**Figure 4-25.** Zonally-averaged calculated changes in ozone for July due to 1992 aircraft emissions (Case 2, relative to atmosphere with no aircraft) as determined by: (a) IMAGES; (b) Harvard-GISS. Units are ppbv. Note: the tropopause outside of the tropics in the Harvard model is too high, implying that 200 mbar and altitudes below are always in tropospheric air.

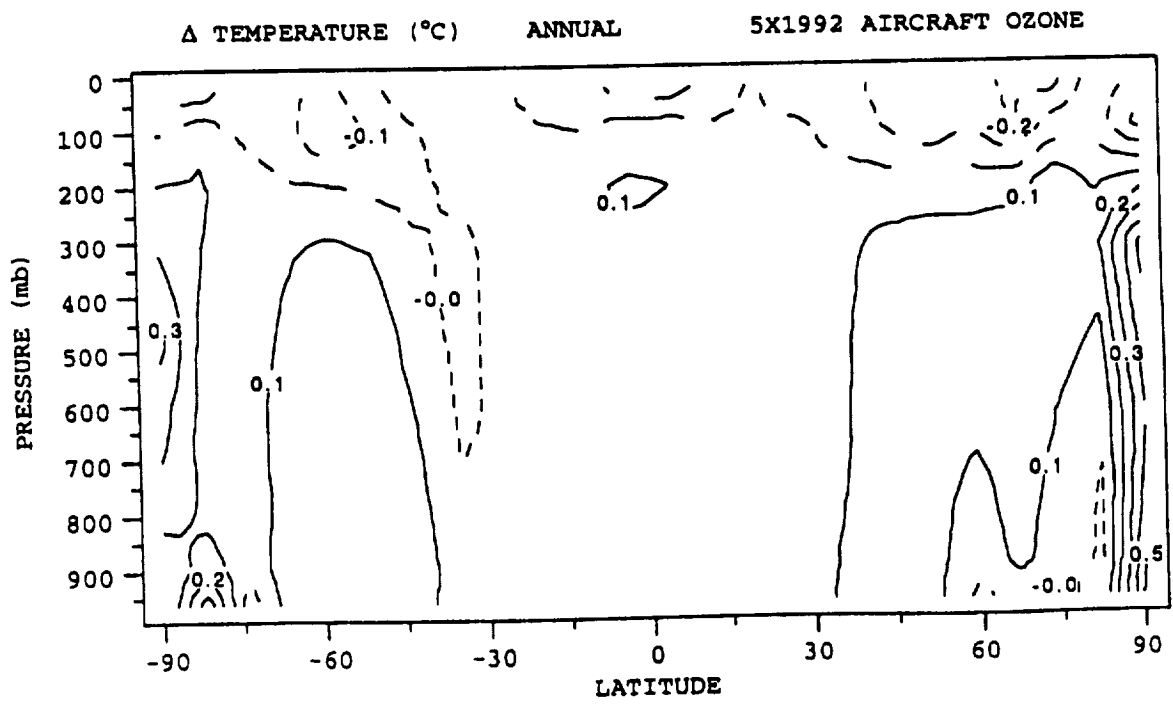
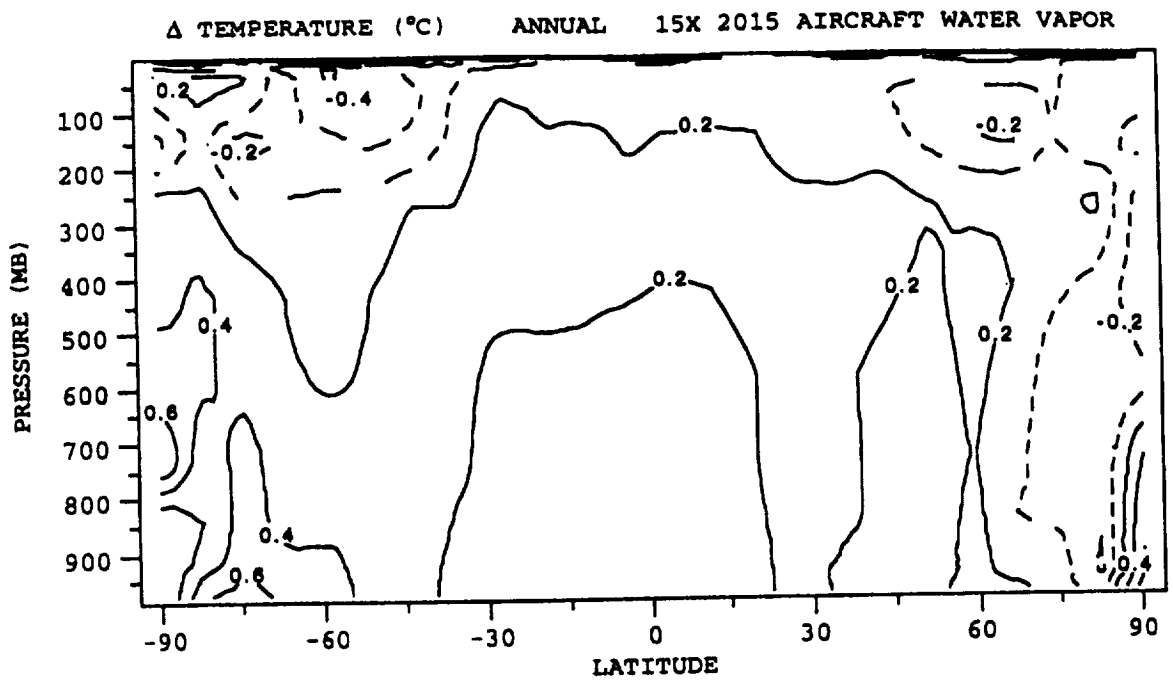


**Figure 4-26.** Annual average temperature change in the GISS GCM resulting from exaggerated aircraft forcings: 15 x 2015 water vapor release (top); 5 x 1992 aircraft emissions effect on ozone (bottom).

## 5. SUMMARY AND CONCLUSIONS

### 5.1 Summary

This report is the first in a planned series of SASS project assessments of the atmospheric impacts of present and future fleets of subsonic aircraft. The focus of these assessments is on cruise emissions of subsonic aircraft and their effects on the Earth's total column abundance of ozone and its climate. In addition to documenting advances in the scientific understanding of aircraft atmospheric effects resulting from project activities, the assessments seek to provide an adequate scientific basis for policy and technology decisions. Determination of assessment adequacy is difficult, but clearly reduction of uncertainties to levels at or below the predicted magnitudes of the impacts is required.

The results of this assessment for the current subsonic fleet (i.e., 1992 fleet) are summarized in Table 5-1. At this stage in the scientific effort most of the assessment results are qualitative in nature. A few of the aircraft effects are sufficiently well understood to be amenable to realistic model simulations. Quantitative estimates for those cases are listed in the table along with associated uncertainty estimates. In the table, ozone changes are given in terms of the total atmospheric column in order to be comparable to predictions for supersonic aircraft operation and chlorofluorocarbon release. Total column ozone changes are approximately an order of magnitude less than tropospheric column changes given in Table 4-5, reflecting the substantially smaller amount of ozone residing in the troposphere as compared to the stratosphere.

The effect of the current subsonic aircraft fleet on column ozone is estimated to be of similar magnitude, but of opposite sign to the predicted effects of a future supersonic aircraft fleet [Stolarski *et al.*, 1995]. Uncertainties are large, relative to the estimated magnitudes of the ozone effects, for both of the studied aircraft fleets.

Climate impacts are subdivided into direct and indirect "forcings" of the radiative flux at the top of the troposphere. Direct effects involve absorption or reflection of radiation by contrails and other exhaust species of interest. Indirect effects refer to the radiative properties of molecules or particles that are derived from, or modified by, exhaust species of interest (e.g., effects of soot, sulfur oxides, and water vapor on existing or future cirrus clouds). The sign of a particular radiative forcing indicates the direction of the expected system thermal response. Positive and negative forcings are associated with surface warming and cooling, respectively. Radiative forcings are calculated for steady-state distributions resulting from continued aircraft operation except in the case of the long-lived gas CO<sub>2</sub>, where results are given for a single year (i.e., 1992) of emission and for the sum total of emissions over the last 30 years.

As evidenced from Table 5-1, the indirect impact of current aircraft emissions of NO<sub>x</sub> on climate, through changes in ozone, is comparable to the direct, accumulated, effect of the past 30 years of aircraft CO<sub>2</sub> emissions, albeit with great uncertainty attached to the NO<sub>x</sub> effect. Both emissions lead to global warming, but the calculated degrees of warming are within the variability of the model. Qualitatively, the model studies of ozone change are consistent with those reported by AERONOX [Schumann, 1995] and show greatest sensitivity to uncertainties in the magnitude of the lightning source of NO<sub>x</sub> and in the identification of relevant heterogeneous and non-methane hydrocarbon chemistry. Assuming that the sensitivity studies have captured the range of uncertainties in our understanding of critical atmospheric processes, then the range of calculated

ozone changes shown in table 4.5a (approximately a factor of 3) serves as a first-order estimate of the overall predictive uncertainty. Deficiencies in model parameterizations also contribute to the overall predictive uncertainty. While these deficiencies are largely unquantified at present, the limited number of inter-model comparisons performed for this assessment suggest that variations in model construction contribute an additional factor of 1.5 to 2 to the predictive uncertainty.

In view of the large uncertainty associated with ozone calculations for the current subsonic fleet, it is premature to attempt quantitative predictions of ozone impacts resulting from future fleet scenarios. Some qualitative insight into potential future impacts is gained from a sensitivity study of the effect of 5 times the 1992 emissions. The results of this exercise indicate that in regions of low background  $\text{NO}_x$ , such as the Southern Hemisphere, ozone increases scale proportionately with aircraft  $\text{NO}_x$  emissions. However, in regions of high background  $\text{NO}_x$ , such as the Northern Hemisphere, the proportionality between ozone increases and  $\text{NO}_x$  emissions is somewhat less than in the low- $\text{NO}_x$  background regions. This behavior is consistent with the current understanding of the competition between ozone production and loss processes (refer to Section 3.2.2.1), although we note that there is substantial quantitative uncertainty regarding the competition between processes.

An approximate three-fold increase in air traffic (two-fold increase in  $\text{NO}_x$  emissions) relative to today is anticipated by the year 2015. Traffic growth is likely to be greater in the low- $\text{NO}_x$  background Asian Pacific region than in the North American or European regions. Combining this growth pattern with the above-mentioned model sensitivity results leads us to expect that global ozone, and the associated radiative forcing, will increase essentially linearly with the 2015 aircraft fleet size. Accordingly, a two-fold increase in aircraft  $\text{NO}_x$  emissions, as is anticipated by the year 2015, should result in an approximate doubling of the ozone (+ 0.2%) and associated radiative forcing (+ 0.02  $\text{W m}^{-2}$ ) changes due to aircraft.

Climate impacts due to cloud particle formation from aircraft water, sulfur, and soot emissions are judged to be potentially significant but remain unquantified at this time. Correlated increases in observed high cloud frequency and jet fuel usage suggest a significant climate connection and results from several model sensitivity studies indicate that increased cloud cover may impact climate to a greater extent than aircraft-induced ozone changes. However, there is a great deal of uncertainty regarding both the magnitude and sign of the radiative forcing associated with contrail and cirrus cloud increases. Existing global climate models have difficulty incorporating cloud microphysical details and an adequate observational database has not yet been compiled with which to test the simplifying parameterizations employed in the GCMs.

The effects of soot and sulfur on cirrus cloud and contrail microphysics are not well understood at present. Recent field measurements have discovered that volatile particle emissions from some commercial aircraft are 3 to 30 times greater than predicted by plume and wake models. Given this discrepancy and its implied lack of understanding of the nucleation mechanism, any attempt to estimate the number of aircraft-derived particles capable of acting as IN or CCN is highly speculative.

## 5.2 Recommendations

Aircraft emissions of CO<sub>2</sub>, NO<sub>x</sub>, and particles (i.e., water, sulfur, soot combinations) have been identified in this assessment as having potential environmental significance. In contrast to CO<sub>2</sub>, NO<sub>x</sub> impacts are only partially quantified and particle impacts are mostly unquantified. During the next few years emphasis should be placed on reducing the uncertainty associated with ozone changes due to NO<sub>x</sub> emissions and on deriving quantitative estimates of climate impacts of particle emissions. The former effort requires additional information on the sources of upper tropospheric NO<sub>x</sub> in areas of heavy aircraft traffic, such as over continental Europe, continental United States, the North Atlantic, or the Pacific. In obtaining this information, methodologies must be developed to differentiate between aircraft, continental surface, lightning, and stratospheric sources of NO<sub>x</sub>.

Model treatments of ozone chemistry and transport must be significantly improved to render confident numerical predictions. In addition to assimilating further information of NO<sub>x</sub> source strengths and distributions, future models must possess vertical resolutions of at least 1 km in the upper troposphere to successfully resolve the important chemical and radiative processes. The model sensitivities to heterogeneous and background NMHC chemistry must be explored with an aim toward developing a satisfactory set of input reactions. In developing the input reaction set, a number of potentially important NMHC, aqueous phase, and gas-surface reactions need to be characterized in the laboratory. In addition, observational data on the composition and distribution of tropospheric aerosols are required.

Assessment of the climate impacts of particles will most benefit from increased understandings of the mechanisms of particle formation in aircraft plumes, the tendency of aircraft generated particles to act as CCN and IN, and the microphysical characteristics of contrails and cirrus clouds. Collection and analysis of appropriate field data, as is being done in the SUCCESS and POLINAT missions, is paramount. These data should be complemented by laboratory studies of post-combustion phenomena, including heterogeneous processes, since the laboratory techniques offer greater control of the experimental variables. Comparisons of field data to model predictions made using the results of laboratory studies will increase our understanding of the speciation within the distribution between the gas-phase and condensed-phase for the major emissions (e.g., NO<sub>x</sub> and SO<sub>x</sub>). Additional characterization of engine exhaust, particularly of SO<sub>x</sub> oxidation products and of particle emissions, is required to define the initial state of aircraft exhaust emissions.

Relating particle microphysical characteristics to differences in cloud and contrail radiative properties is also required in order to quantify climate impacts of aircraft operation. Improved characterizations of cloud and contrail radiative properties must be accompanied by efforts to improve GCM parameterizations of these features.

Assessment of the climatic impact of aircraft emissions (with the exception of CO<sub>2</sub>) must deal explicitly with the heterogeneity of the perturbations and associated radiative forcing of the climate. The radiative impact of the anticipated ozone increases and high-cloud modifications occurs primarily in the upper troposphere of the northern mid-latitudes, and appears to exert a fundamentally different climate forcing than equivalent changes in the well mixed greenhouse gases such as CO<sub>2</sub> and CH<sub>4</sub>. The simple concept of Global Warming Potential may not be adequate to compare the aircraft effects with those of CO<sub>2</sub> and a new approach to indexing climate perturbations may need to be found.

**Table 5-1.** Summary of estimated atmospheric impacts of current subsonic aircraft emissions.

Emittant	Impact	Impact Estimate (Global Ave.)	Absolute Uncertainty Estimate
NO <sub>x</sub>	O <sub>3</sub> Column	+ 0.1% (+0.3% ave. over 30°-60°N)	±0.5%, NO <sub>x</sub> sources poorly quantified
	Direct Radiative Forcing	+0.001 W m <sup>-2</sup>	small
	Indirect Rad. Forcing	+ 0.01 W m <sup>-2</sup>	±0.05 W m <sup>-2</sup> , NO <sub>x</sub> sources poorly quantified
CO <sub>2</sub>	O <sub>3</sub> Column	negligible	small
	Direct Radiative Forcing	+0.0003 W m <sup>-2</sup> (+0.0067 W m <sup>-2</sup> over last 30 yr.)	±0.0001 W m <sup>-2</sup> , mainly due to model uncertainties
H <sub>2</sub> O	O <sub>3</sub> Column	small	large, depends on PSC details
	Direct Radiative Forcing (due to contrails)	significant, sign uncertain	large, radiative transfer properties of contrails poorly known
	Indirect Rad. Forcing	potentially significant	moderate, depends on involvement in PSC/O <sub>3</sub> processes and/or in plume processes that result in CCN and IN
Sulfur	O <sub>3</sub> Column	small	large, sources inadequately defined, size distribution poorly known
	Direct Radiative Forcing	+0.0001 W m <sup>-2</sup>	moderate, sources inadequately defined, size distribution poorly known
	Indirect Rad. Forcing	potentially significant	large, interaction with aircraft soot and role as CCN/IN poorly defined
Soot	O <sub>3</sub> Column	small	small
	Direct Radiative Forcing	+ 0.003 W m <sup>-2</sup>	moderate, size distribution and single particle albedo uncertain
	Indirect Rad. Forcing	unknown	large, depends on # that are coated with sulfur and act as CCN or IN
Hydrocarbons	O <sub>3</sub> Column	small	small
	Direct Radiative Forcing	negligible	small
	Indirect Rad. Forcing	negligible	small
CO	O <sub>3</sub>	small	small
	Direct Radiative Forcing	negligible	small
	Indirect Rad. Forcing	negligible	small

## 6. REFERENCES

- Allen, D. J., R. Rood, and R. Hudson, Three-dimensional radon 222 calculations using assimilated meteorological data and a convective mixing algorithm, *J. Geophys. Res.*, *101*, 6871-6881, 1996.
- Andreae, M. O., Editor, Climatic effects of changing atmospheric aerosol levels, in *World Survey of Climatology, Volume 16: Future Climates of the World*, A. Henderson-Sellers, 1995.
- Andreae, M. O., Emissions of trace gases and aerosols from Southern African savanna fires, in *Fire in Southern African Savannas: Ecological and Atmospheric Perspectives*, M. O. Andreae, J. G. Goldammer, J. A. Lindesay, and B. van Wilgen, Editors, University of Witwatersrand Press, Johannesburg, South Africa, in preparation, 1996.
- Anthony, S. E., R. T. Tisdale, R. D. Disselkamp, M. A. Wilson, M. A. Tolbert, and J. C. Wilson, FTIR studies of low temperature sulfuric acid aerosols, *Geophys. Res. Lett.*, *22*, 1105-1108, 1995.
- Anthony, S. E., T. B. Onasch, R. T. Tisdale, R. S. Disselkamp, M. A. Tolbert, and J. C. Wilson, Laboratory studies of ternary H<sub>2</sub>SO<sub>4</sub>/HNO<sub>3</sub>/H<sub>2</sub>O particles: Implications for polar stratospheric cloud formation, submitted to *J. Geophys. Res.*, 1996.
- Arnold, F., J. Scheid, T. Stilp, H. Schlager, and M. E. Reinhardt, Measurements of jet aircraft emissions at cruise altitudes, I: The odd-nitrogen gases NO, NO<sub>2</sub>, HNO<sub>2</sub>, and HNO<sub>3</sub>, *Geophys. Res. Lett.*, *19*, 2421-2424, 1992.
- ASTM, 1996 *Annual Book of ASTM Standards, Volume 05.01*, Standard specification for aviation turbine fuels, D 1655-95a, American Society for Testing and Materials, 549-552, 1996.
- Atkinson, R. A., D. L. Baulch, R. A. Cox, R. F. Hampson, Jr., J. A. Kerr, and J. Troe, Evaluated kinetic and photochemical data for atmospheric chemistry, Supplement IV, IUPAC subcommittee on gas kinetic data evaluation for atmospheric chemistry, *J. Phys. Chem.*, *21*, 1125-1571, 1992.
- Austin, J., N., N. Butchart, and K. P. Shine, Possibility of an Arctic ozone hole in a doubled-CO<sub>2</sub> climate, *Nature*, *360*, 221-225, 1992.
- Balkanski, Y. J., D. J. Jacob, G. M. Gardner, W. M. Graustein, and K. K. Turekian, Transport and residence times of continental aerosols inferred from a global 3-dimensional simulation of <sup>210</sup>Pb, *J. Geophys. Res.*, *98*, 20573-20586, 1993.
- Bao, Z. C., and J. R. Barker, Temperature and ionic strength effects on some reactions involving sulfate radical: SO<sub>4</sub>-(aq), *J. Phys. Chem.*, in press, 1996.
- Balashov, B., and A. Smith, ICAO analyses trends in fuel consumption by world's airlines, *ICAO Journal*, 18-21, 1992.

- Baughcum, S. L., D. M. Chan, S. M. Happenny, S. C. Henderson, P. S. Hertel, T. Higman, D. R. Maggiora, and C. A. Oncina, Emissions scenarios development: Scheduled 1990 and projected 2015 subsonic, Mach 2.0 and Mach 2.4 aircraft, in *The Atmospheric Effects of Stratospheric Aircraft: A Third Program Report*, NASA Reference Publication 1313, 89-131, 1993a.
- Baughcum, S. L., M. Metwally, R. K. Seals, and D. J. Wuebbles, Emissions scenarios development: Completed scenarios database, Subchapter 3-4, in *The Atmospheric Effects of Stratospheric Aircraft: A Third Program Report*, NASA Reference Publication 1313, 185-208, 1993b.
- Baughcum, S. L., S. C. Henderson, P. S. Hertel, D. R. Maggiora, and C. A. Oncina, *Stratospheric Emissions Effects Database Development*, NASA CR-4592, 1994.
- Baughcum, S. L., Subsonic aircraft emissions inventories, in *Atmospheric Effects of Aviation: First Report of the Subsonic Assessment Project*, NASA Reference Publication 1385, 15-29, 1996a.
- Baughcum, S. L., *Aircraft Emissions Deposited in the Stratosphere and within the Arctic Polar Vortex*, NASA CR-4714, 1996b.
- Baughcum, S. L., T. G. Tritz, S. C. Henderson, and D. C. Pickett, *Scheduled Civil Aircraft Emission Inventories for 1992: Database Development and Analysis*, NASA CR-4700, 1996a.
- Baughcum, S. L., S. C. Henderson, and T. G. Tritz, *Scheduled Civil Aircraft Emission Inventories for 1976 and 1984: Database Development and Analysis*, NASA CR-4722, 1996b.
- Beck, J., C. Reeves, F. de Leeuw, and S. Penkett, The effect of aircraft emissions on tropospheric ozone in the Northern Hemisphere, *Atm. Env.*, 26A, 17-19, 1992.
- Benkovitz, C. M., J. Dignon, J. Pacyna, T. Scholtz, L. Tarrasn, E. Voldner, and T. E. Graedel, Global gridded inventories of anthropogenic emissions of sulfur and nitrogen, *J. Geophys. Res.*, in press, 1996.
- Beyer, K. D., S. W. Seago, H. Y. Chang, and M. J. Molina, Composition and freezing of aqueous H<sub>2</sub>SO<sub>4</sub>/HNO<sub>3</sub> solutions under polar stratospheric conditions, *Geophys. Res. Lett.*, 21, 871-874, 1994.
- Blake, D. F., and K. Kato, Latitudinal distribution of black carbon soot in the upper troposphere and lower stratosphere, *J. Geophys. Res.*, 100, D4, 7195-7202, 1995.
- Boeing Commercial Airplane Group, *1996 Current Market Outlook*, 1996.
- Boer, G. J., K. Arpe, M. Blackburn, M. Déqué, W. L. Gates, T. L. Hart, H. le Trent, E. Roeckner, D. A. Sheinin, I. Simmonds, R. N. B. Smith, T. Tokioka, T. T. Wetherald, and D. Williamson, Some results from an intercomparison of the climates simulated by 14 atmospheric general circulation models, *J. Geophys. Res.*, 97, 12771-12786, 1992.
- Bradshaw, J. *et al.*, On the lightning sources of tropospheric NO<sub>x</sub>, *J. Geophys. Res.*, in preparation, 1996.

- Brasseur, G. P., C. Granier, and S. Walters, Future changes in stratospheric ozone and the role of heterogeneous chemistry, *Nature*, 348, 626-628, 1990.
- Brasseur, G. P., J.-F. Müller, and C. Granier, Atmospheric impact of NO<sub>x</sub> emissions by subsonic aircraft: A three dimensional study, *J. Geophys. Res.*, 101, 1423-1428, 1996.
- Brown, R. C., R. C. Miake-Lye, M. R. Anderson, C. E. Kolb, and T. J. Resch, Aerosol dynamics in near field aircraft plumes, submitted to *J. Geophys. Res.*, 1995.
- Busen, R., and U. Schumann, Visible contrail formation from fuels with different sulfur contents, *Geophys. Res. Lett.*, 22, 1357-1360, 1995.
- Carleton, K. L., D. M. Sonnenfroh, W. T. Rawlins, B. E. Wyslouzil, and S. Arnold, Freezing behavior of single sulfuric acid aerosols suspended in a quadrupole trap, submitted to *J. Geophys. Res.*, 1996.
- Cess, R. D. *et al.*, Uncertainties in carbon dioxide radiative forcing in atmospheric general circulation models, *Science*, 262, 1252-1255, 1993.
- Chang, J., R. Brost, I. Isaksen, S. Madronich, P. Middleton, W. R. Stockwell, and C. Walcek, A three-dimensional Eulerian acid deposition model: Physical concepts and formulation, *J. Geophys. Res.*, 92, 14681-14700, 1987.
- Changnon, S. A., Midwestern cloud, sunshine and temperature trends since 1901: Possible evidence of jet contrail effects, *J. Appl. Meteor.*, 20, 496-508, 1981.
- Chin, M., D. J. Jacob, G. M. Gardner, M. S. Forman-Fowler, and P. A. Spiro, and D. L. Savoie, A global three-dimensional model of tropospheric sulfate, *J. Geophys. Res.*, in press, 1996.
- Clarke, A. D., Atmospheric nuclei in the Pacific midtroposphere: Their nature, concentration, and evolution, *J. Geophys. Res.*, 98, 20633-20647, 1993.
- Considine, D. B., P. S. Connell, D. E. Kinnison, C. H. Jackman, X. X. Tie, G. Pitari, L. Ricciardulli, G. Visconti, and D. J. Wuebbles, Intercomparison of the effects of PSC parameterizations on 2D model predictions of HSCT impact, *AGU 1996 Spring Meeting Abstracts*, Supplement to EOS, 1996.
- Cooke, W. F., and J. J. N. Wilson, A global black carbon aerosol model, *J. Geophys. Res.*, 101, 19395-19409, 1996.
- Cooper, P. L., and J. P. D. Abbatt, Heterogeneous interactions of OH and HO<sub>2</sub> radicals with surfaces characteristic of atmospheric particulate matter, *J. Phys. Chem.*, 100, 2249-2254, 1996.
- Costen, R. C., G. M. Tennille, and J. S. Levine, Cloud pumping in a one-dimensional model, *J. Geophys. Res.*, 93, 15941-15954, 1988.
- Crosley, D. R., NO<sub>y</sub> blue ribbon panel, *J. Geophys. Res.*, 101, 2049-2052, 1996.
- Crutzen, P. J., The role of NO and NO<sub>2</sub> in the chemistry of the troposphere and stratosphere, *Ann. Rev. Earth Planet. Sci.*, 7, 443-472, 1979.
- Danilin, M. Y., A. Ebel, H. Elbern, and H. Petry, Evolution of the concentrations of trace species in an aircraft plume: Trajectory study, *J. Geophys. Res.*, 99, 18951-18972, 1994.

- Davis, D, J. Crawford, G. Chen, W. Chameides, S. Liu, J. Bradshaw, S. Sandholm, G. Sachse, G. Gregory, B. Anderson, J. Barrick, A. Bachmeier, E. Browell, D. Blake, F. Rowland, Y. Kondo, H. Singh, R. Talbot, B. Heikes, J. Collins, J. Rodriguez, J. Merrill, and R. Newell, An assessment of the photochemical O<sub>3</sub> tendency in the western North Pacific as inferred from GTE/PEM-West (A) observations during fall 1991, *J. Geophys. Res.*, *101*, 2111-2134, 1996.
- Dentener, F. J., and P. J. Crutzen, Reaction of N<sub>2</sub>O<sub>5</sub> on tropospheric aerosols: Impact on the global distributions of NO<sub>x</sub>, O<sub>3</sub>, and OH, *J. Geophys. Res.*, *98*, 7149-7163, 1993.
- DeMore, W. B., S. P. Sander, D. M. Golden, R. F. Hampson, M. J. Kurylo, C. J. Howard, A. R. Ravishankara, C. E. Kolb, and M. J. Molina, *Chemical kinetics and photochemical data for use in stratospheric modeling*, JPL Publication 94-26, Pasadena, CA, 1994.
- De Rudder, A., N. Larsen, X. X. Tie, G. P. Brasseur, and C. Granier, Model study of polar stratospheric clouds and their effect on stratospheric ozone, 1: Model description, *J. Geophys. Res.*, *101*, 12567-12574, 1996.
- Dignon, J., J. E. Penner, C. S. Atherton, and J. J. Walton, Atmospheric reactive nitrogen: A model study of natural and anthropogenic sources and the role of microbial soil emissions, *Proceedings of CHEMRAWN VII World Conference on Atmospheric Chemistry*, 1992.
- Disselkamp, R. S., S. E. Anthony, A. J. Prenni, R. B. Onasch, and M. A. Tolbert, Crystallization kinetics of nitric acid dihydrate aerosols, *J. Phys. Chem.*, *100*, 9127-9137, 1996.
- DOE, *International Energy Annual 1993*, DOE/EIA-0219(93), Department of Energy, 1995.
- Donahue, N. M., M. K. Dubey, R. Mohrschlatdt, K. L. Demerjian, and J. G. Anderson, A high pressure flow study of the reaction NO<sub>2</sub> + OH → HONO<sub>2</sub> in nitrogen, submitted to *J. Geophys. Res.*, 1996.
- Douglas Aircraft Company, *Outlook for Commercial Aircraft, 1994-2013*, 1995.
- Douglass, A. R., R. B. Rood, C. J. Weaver, M. C. Cerniglia, K. F. Brueske, Implications of three-dimensional tracer studies for two-dimensional assessments of the impact of supersonic aircraft on stratospheric ozone, *J. Geophys. Res.*, *98*, 8949-8963, 1993.
- Dye, J. E., D. Baumgardner, B. W. Gandrud, S. R. Kawa, K. K. Kelly, M. Loewenstein, G. V. Ferry, K. R. Chan, and B. L. Gary, Particle size distributions in Arctic polar stratospheric clouds, growth and freezing of sulfuric acid droplets, and implications for cloud formation, *J. Geophys. Res.*, *97*, 8015-8034, 1992.
- Emmons, L. K., M. A. Carroll, D. A. Haughlustaine, G. P. Brasseur, C. Atherton, J. Penner, S. Sillman, H. Levy II, F. Rohrer, W. M. F. Wauben, P. F. J. van Velthoven, Y. Wang, D. J. Jacob, P. Bakwin, R. Dickerson, B. Doddridge, C. Gerbig, R. Honrath, G. Hubler, D. Jaffe, Y. Kondo, J. W. Munger, A. Torres, and A. Volz-Thomas, Climatologies of NO<sub>x</sub> and NO<sub>y</sub>: A comparison of data and models, submitted to *Atmos. Environ.*, 1996.
- Exner, M., H. Herrmann, and R. Zellner, Laser-based studies of reactions of the nitrate radical in aqueous solution, *Ber. Bunsen Ges. Phys. Chem.*, *96*, 470-485, 1992.

- Fahey, D. W., E. R. Keim, E. L. Woodbridge, R. S. Gao, K. A. Boering, B. C. Daube, S. C. Wofsy, R. P. Lohmann, E. J. Hints, A. E. Dessler, C. R. Webster, R. D. May, C. A. Brock, J. C. Wilson, R. C. Miake-Lye, R. C. Brown, J. M. Rodriguez, M. Lowenstein, M. H. Proffitt, R. M. Stimpfle, S. W. Bowen, and K. R. Chan, *In situ* observations in aircraft exhaust plumes in the lower stratosphere at mid-latitudes, *J. Geophys. Res.*, *100*, 3065-3074, 1995a.
- Fahey, D. W., E. R. Keim, K. A. Boering, C. A. Brock, J. C. Wilson, S. Anthony, T. F. Hanisco, P. O. Wennberg, R. C. Miake-Lye, R. J. Salawitch, N. Louisnard, E. L. Woodridge, R. S. Gao, S. G. Donnelly, R. C. Wamsley, L. A. Del Negro, B. S. Daube, S. C. Wofsy, C. R. Webster, R. D. May, K. K. Kelly, M. Loewenstein, J. R. Podolske, and K. R. Chan, Emission measurements of the Concorde supersonic aircraft in the lower stratosphere, *Science*, *270*, 70-74, 1995b.
- Franzblau, E., and C. J. Popp, Nitrogen oxides produced from lightning, *J. Geophys. Res.*, *94*, 11089-11104, 1989.
- Gao W., and M. L. Wesely, Modeling gaseous dry deposition over regional scales with satellite observations, I: Model development, *Atmos. Environ.*, *29*, 727-737, 1995.
- Gery, M. W., G. Z. Whitten, J. P. Killus, and M. C. Dodge, A photochemical kinetics mechanism for urban and regional scale computer modeling, *J. Geophys. Res.*, *94*, 12925-12956, 1989.
- Giorgi, F., and W. L. Chameides, Rainout lifetimes of highly soluble aerosols as inferred from simulations with a general circulation model, *J. Geophys. Res.*, *91*, 14367-14376, 1986.
- Goldstein, A. H., S. C. Wofsy, and C. M. Spivakovsky, Seasonal variations of nonmethane hydrocarbons in rural New England: Constraints on OH concentrations in northern mid-latitudes, *J. Geophys. Res.*, *100*, 21023-21033, 1995.
- Guenther, A., *et al.*, A global model of natural volatile organic compound emissions, *J. Geophys. Res.*, *100*, 8873-8892, 1995.
- Granier, C., W.-M. Hao, G. Brasseur, and J.-F. Müller, Land use practices and biomass burning: Impact on the chemical composition of the atmosphere, *Proceedings of the Chapman Conference on Biomass Burning and Global Change*, J. Levine, Editor, accepted for publication, 1996.
- Haagen-Smit, A. J., Chemistry and physiology of Los Angeles smog, *Indust. Eng. Chem.*, *44*, 1342-1346, 1951.
- Hack, J., Parameterization of moist convection in the NCAR community climate model, CCM2, *J. Geophys. Res.*, *99*, 5551-5568, 1994.
- Hadaller, O. J., and A. M. Momeny, *The Characteristics of Future Fuels*, Boeing publication D6-54940, 1989.
- Hadaller, O. J., and A. M. Momeny, Characteristics of Future Aviation Fuels, Chapter 10, in *Transportation and Global Climate Change*, D. L. Greene and D. J. Santini, Editors, American Council for an Energy-Efficient Economy, Washington, DC, 1993.
- Hagen, D. E., M. B. Trueblood, and P. D. Whitefield, A field sampling of jet exhaust aerosols, *Part. Sci. Tech.*, *10*, 53-63, 1992.

- Hagen, D. E., P. D. Whitefield, and M. B. Trueblood, Particulate characterization in the near field of commercial transport aircraft exhaust plumes using the UMR-MASS, *Proceedings of the International Scientific Colloquium on the Impact of Emissions from Aircraft and Spacecraft upon the Atmosphere*, Koln, Germany, 1994.
- Hagen, D. E., P. D. Whitefield, and H. Schlager, Particulate emissions in the exhaust plume for commercial jet aircraft under cruise conditions, *J. Geophys. Res.*, *101*, 19551-19558, 1996.
- Hagen, D. E., and P. D. Whitefield, Particulate characterization in the near field of commercial transport aircraft exhaust plumes using the UMR-MASS, part 1, *J. Geophys. Res.*, in press, 1996.
- Hameed, S., O. G. Paidoussis, and R. W. Stewart, Implications of natural sources for the latitude gradient of NO<sub>y</sub> in the unpolluted troposphere, *Geophys. Res. Lett.*, *8*, 591-594, 1981.
- Hameed, S., and J. Dignon, Changes in the geographical distributions of global emissions of NO<sub>x</sub> and SO<sub>x</sub> from fossil-fuel combustion between 1966 and 1980, *Atmos. Envir.*, *22*, 441-449, 1988.
- Hansen, J., D. Johnson, A. Lacis, S. Lebedeff, P. Lee, D. Rind, and G. Russell, Climate impact of increasing atmospheric carbon dioxide, *Science*, *213*, 957, 1981.
- Hansen, J., G. Russell, D. Rind, P. Stone, A. Lacis, S. Lebedeff, R. Ruedy, and L. Travis, Efficient 3-dimensional global models for climate studies - Model-I, Model-II, *Mon. Wea. Rev.*, *111*, 609-662, 1983.
- Hansen, J., A. Lacis, D. Rind, G. Russell, P. Stone, I. Fung, R. Ruedy, and J. Lerner, Climate sensitivity: Analysis of feedback mechanisms, in *Climate Processes and Climate Sensitivity*, J. Hansen and T. Takahashi, Editors, Geophysical Monograph 29, American Geophysical Union, Washington, DC, 130-163, 1984.
- Hansen, J., M. Sato, A. Lacis, and R. Ruedy, Climate impact of ozone change, in *Proceedings of IPCC Hamburg meeting*, 1993.
- Hanson, D. R., J. B. Burkholder, C. J. Howard, and A. R. Ravishankara, Measurement of OH and HO<sub>2</sub> radical uptake coefficients on water and sulfuric acid surfaces, *J. Phys. Chem.*, *96*, 4979-4985, 1992.
- Hao, W. M., M. H. Liu, and P. J. Crutzen, Estimates of annual and regional releases of CO<sub>2</sub> and other trace gases to the atmosphere from fires in the tropics, based on FAO statistics from the period 1975-1980, presented at *Third International Symposium on Fire Ecology*, Freiburg University, Germany, 1989.
- Hauglustaine, D. A., C. Granier, G. P. Brasseur, and G. Megie, Impact of present aircraft emissions on nitrogen oxides on tropospheric ozone and climate forcing, *Geophys. Res. Lett.*, *21*, 2031-2034, 1994.
- Hofmann, D. J., Twenty years of balloon-borne tropospheric aerosol measurements at Laramie, Wyoming, *J. Geophys. Res.*, *98*, 12753-12766, 1993.
- Hoinka, K. P., M. E. Reinhardt, and W. Metz, North Atlantic air traffic within the lower stratosphere: cruising times and corresponding emissions, *J. Geophys. Res.*, *98*, 23113-23131, 1993.

- Holtslag, A. A. M., and B. A. Bouville, Local versus non-local boundary layer diffusion in a global climate model, *J. Clim.*, *6*, 1825-1842, 1993.
- Howard, R. P., Editor, *Experimental Characterization of Gas Turbine Emissions at Simulated Flight Altitude Conditions*, AEDC-TR-96-3, 1996.
- Hu, J. H., D. Czizco, and J. Abbatt, Reaction probabilities for N<sub>2</sub>O<sub>5</sub> hydrolysis on sulfuric acid and ammonium sulfate aerosols at room temperature, to be submitted to *J. Phys. Chem.*, 1996.
- Hudson, J. G., J. Hallett, and C. F. Rogers, Field and laboratory measurements of cloud-forming properties of combustion aerosols, *J. Geophys. Res.*, *96*, 10847-10859, 1991.
- Hudson, J. G., and A. D. Clarke, Aerosol and cloud condensation nuclei measurements in the Kuwaiti plume, *J. Geophys. Res.*, *97*, 14533-14536, 1992.
- Huebert, B. J., and A. L. Lazrus, Bulk composition of aerosols in the remote troposphere, *J. Geophys. Res.*, *85*, 7337-7344, 1980.
- Hurst, D. F., D. W. T. Griffith, J. N. Carras, D. J. Williams, and P. J. Fraser, Measurements of trace gases emitted by Australian savanna fires during 1990 dry season, *J. Atmos. Chem.*, *18*, 33-56, 1994.
- ICAO, *ICAO Engine Exhaust Emissions Databank, First Edition-1995*, ICAO Doc. 9646-AN/943, International Civil Aviation Organization, 1995.
- ICAO CAEP WG3, *Report of the Emissions Inventory Sub-Group*, Bonn, Germany, 1995.
- Intergovernmental Panel on Climate Change (IPCC), *Climate Change, The IPCC Scientific Assessment*, J. T. Houghton, C. J. Jenkins and J. Ephraums, Editors, Cambridge University Press, Cambridge, UK, 1990.
- Intergovernmental Panel on Climate Change (IPCC), *Climate Change 1992*. J. T. Houghton, B. A. Callander, and S. K. Varney, Editors, Cambridge University Press, Cambridge, UK, 1992.
- Intergovernmental Panel on Climate Change (IPCC), *Climate Change 1994*, J. T. Houghton, L. G. Meira Filho, J. Bruce, H. Lee, B. A. Callander, E. Haites, N. Harris, and K. Maskell, Editors, Cambridge University Press, Cambridge, UK, 1994.
- Intergovernmental Panel on Climate Change (IPCC), *Climate Change 1995*, J. T. Houghton, L. G. Meira Filho, B. A. Callander, N. Harris, A. Kattenberg, and K. Maskell, Editors, Cambridge University Press, Cambridge, UK, 1996.
- Iraci, L. T., A. M. Middlebrook, and M. A. Tolbert, Laboratory studies of the formation of polar stratospheric clouds: Nitric acid condensation on thin sulfuric acid films, *J. Geophys. Res.*, *100*, 20969-20977, 1995.
- Jackman, C. H., Effects of energetic particles on minor constituents of the middle atmosphere, *J. Geomag. Geoelectr.*, *43*, 637-646, 1991.
- Jackman, C. H., Energetic particle influences on NO<sub>y</sub> and ozone in the middle atmosphere, in *Interactions Between Global Climate Subsystems, The Legacy of Hann*, Geophysical Monograph 75, IUGG, Volume 15, 1993.

- Jacob, D. J., M. J. Prather, S. C. Wofsy, and M. B. McElroy, Atmospheric distribution of  $^{85}\text{Kr}$  simulated with a general circulation model, *J. Geophys. Res.*, *92*, 6614-6626, 1987.
- Jacob, D. J., J. A. Logan, R. M. Yevich, G. M. Gardner, C. M. Spivakovsky, S. C. Wofsy, J. W. Munger, S. Sillman, M. J. Prather, M. O. Rodgers, H. Westberg, and P. R. Zimmerman, Simulation of summertime ozone over North America, *J. Geophys. Res.*, *98*, 14797-14816, 1993.
- Jacob, D. J., M. J. Prather, P. J. Rasch, R.-L. Shia, Y. J. Balkanski, S. R. Beagley, D. J. Bergmann, W. T. Blackshear, M. Brown, M. Chiba, M. P. Chipperfield, J. de Grandpre, J. E. Dignon, J. Feichter, C. Genthon, W. L. Grose, P. S. Kasibhatla, I. Kohler, M. A. Kritz, K. Law, J. E. Penner, M. Ramonet, C. E. Reeves, D. A. Rotman, D. Z. Stockwell, P. F. J. Van Velthoven, G. Verver, O. Wild, H. Yang, and P. Zimmermann, Intercomparison of global atmospheric transport models using  $^{222}\text{Rn}$  and other short-lived tracers, *J. Geophys. Res.*, in press, 1996a.
- Jacob, D. J., B. G. Heikes, S.-M. Fan, J. A. Logan, D. L. Mauzerall, J. D. Bradshaw, H. B. Singh, G. L. Gregory, R. W. Talbot, D. R. Blake, and G. W. Sachse, The origin of ozone and  $\text{NO}_x$  in the tropical troposphere: A photochemical analysis of aircraft observations over the South Atlantic Basin, *J. Geophys. Res.*, in press, 1996b.
- Johnson, C., J. Henshaw, and G. McInnes, Impact of aircraft and surface emissions of nitrogen oxides on tropospheric ozone and global warming, *Nature*, *355*, 69-71, 1992.
- Jones, A. E., K. S. Law, and J. A. Pyle, Subsonic aircraft and ozone trends, *J. Atmos. Chem.*, *23*, 89-105, 1996.
- Kärcher, B., A trajectory box model for aircraft exhaust plumes, *J. Geophys. Res.*, *100*, 18835-18844, 1995.
- Kärcher, B., Th. Peter, U. M. Biermann, and U. Schumann, The initial composition of jet condensation trails, *J. Atm. Sci.*, *53*, 3066-3083, 1996.
- Kasibhatla, P. S., H. Levy, W. J. Moxim, and W. L. Chameides, The relative impact of stratospheric photochemical production on tropospheric  $\text{NO}_y$  levels - a model study, *J. Geophys. Res.*, *96*, 18631-18646, 1991.
- Kasibhatla, P. S.,  $\text{NO}_y$  from subsonic aircraft emissions: a global three-dimensional model study, *Geophys. Res. Lett.*, *20*, 1707-1710, 1993.
- Kley, D., H. Geiss, and V. A. Mohnen, Tropospheric ozone at elevated sites and precursor emissions in the United States and Europe, *Atmos. Envir.*, *28*, 149-158, 1994.
- Ko, M. K. W., N. D. Sze, and D. K. Weisenstein, Use of satellite data to constrain the model-calculated atmospheric lifetime for  $\text{N}_2\text{O}$ : Implications for other gases, *J. Geophys. Res.*, *96*, 7547-7552, 1991.
- Koop T., U. M. Biermann, W. Raber, B. P. Luo, P. J. Crutzen, and Th. Peter, Do stratospheric aerosol droplets freeze above the ice frost point?, *Geophys. Res. Lett.*, *22*, 917-920, 1995.
- Kumar, P. P., G. Manohar, and S. Kandalgaonkar, Global distribution of nitric oxide produced by lightning and its seasonal variation, *J. Geophys. Res.*, *100*, 11203-11208, 1995.

- Landau, Z. H., M. Metwally, R. Van Alstyne, and C. A. Ward, *Jet Aircraft Engine Exhaust Emissions Database Development -- Year 1990 and 2015 Scenarios*, NASA CR-4613, 1994.
- Lary, D. J., R. Toumi, A. M. Lee, M. Newchurch, M. Pirre, and J. B. Renard, Carbon aerosols and atmospheric photochemistry, *J. Geophys. Res.*, in press, 1997.
- Laursen, K. K., P. V. Hobbs, L. F. Radke, and R. A. Rasmussen, Some trace gas emissions from North American biomass fires with an assessment of regional and global fluxes from biomass burning, *J. Geophys. Res.*, *97*, 20687-20701, 1992.
- Lawrence, M. G., W. L. Chameides, P. S. Kasibhatla, H. Levy II, and W. Moxim, Lightning and atmospheric chemistry: *The Rate of Atmospheric NO Production, Handbook of Atmospheric Electrodynamics, 1*, H. Volland, Editor, 189-202, CRC Press, Boca Raton, FL, 1995.
- Lee, S. H., M. Le Dilosquer, H. M. Pasaribu, M. J. Rycroft, and R. Singh, Some consideration of engine emissions from subsonic aircraft at cruise altitudes, in *Impact Emissions from Aircraft and Spacecraft Upon the Atmosphere*, U. Schumann and D. Wurzel, Editors, DLR, Koln, Germany, 76-81, 1994.
- Levy II, H., and W. J. Moxim, Simulated global distribution and deposition of reactive nitrogen emitted by fossil fuel combustion, *Tellus*, *41*, 256-271, 1989.
- Levy II, H., W. J. Moxim, P. S. Kasibhatla, and J. A. Logan, The global impact of biomass burning on tropospheric reactive nitrogen in *Global Biomass Burning: Atmospheric, Climatic, and Biospheric Implications*, J. S. Levine, Editor, 363-369, MIT Press, Cambridge, MA 1991.
- Levy II, H., W. J. Moxim, and P. S. Kasibhatla, A global three-dimensional time-dependent lightning source of NO<sub>x</sub>, *J. Geophys. Res.*, *000*, in press, 1996.
- Lewellen, D. C., and W. S. Lewellen, Large-eddy simulations of the vortex-pair breakup in aircraft wakes, *American Institute of Aeronautics and Astronautics Journal*, in press, 1996.
- Li, Z., R. R. Friedl, S. B. Moore, and S. P. Sander, Interaction of peroxyacetic acid with solid H<sub>2</sub>O-ice, *J. Geophys. Res.*, *101*, 6795-6802, 1996.
- Liaw, Y. P., D. L. Sisterson, and N. L. Miller, Comparison of field, laboratory, and theoretical estimates of global nitrogen-fixation by lightning, *J. Geophys. Res.*, *95*, 22489-22494, 1990.
- Lilienfeld, H. V., P. D. Whitefield, and D. Hagen, *Ground Testing of Emissions from Aircraft Exhaust*, AIAA-95-0110, 1995.
- Lilienfeld, H. V., P. D. Whitefield, and D. E. Hagen, Soot Emissions from Jet Aircraft, Paper ICAS-96-4.1.3, *Proceedings of the 20th Congress of the International Council of the Aeronautical Sciences*, Sorrento, Italy, 8-13 September, 1996.
- Limaye, S., S. Ackerman, P. Frye, M. Isa, H. Ali, A. Wright, and A. Rango, Satellite monitoring of smoke from the Kuwaiti oil fires, *J. Geophys. Res.*, *97*, 14551-14564, 1992.
- Liou, K. N., S. C. Ou, and G. Koenig, An investigation of the climatic effect of contrail cirrus, in *Air Traffic and the Environment: Background, Tendencies, and Potential Global Atmospheric Effects*, U. Schumann, Editor, Springer-Verlag, New York, 154-169, 1990.

- Liou, K. N., J. L. Lee, S. C. Ou, Q. Fu, and Y. Takano, Ice-cloud microphysics, radiative-transfer and large-scale cloud processes, *Meteor. Atm.*, 46, 41-50, 1991.
- Liousse, C., J. E. Penner, C. Chuang, J. J. Walton, H. Edelman, and H. Cachier, A global three-dimensional model study of carbonaceous aerosols, *J. Geophys. Res.*, 101, 19411-19432, 1996.
- Liu, S. C., J. R. McAfee, and R. Cicerone, Radon 222 and tropospheric vertical transport, *J. Geophys. Res.*, 89, 7291-7297, 1984.
- Lobert, J. M., D. H. Scharffe, W.-M. Hao, T. A. Kuhlbusch, R. Seuwen, P. Warneck, and P. J. Crutzen, Experimental evaluation of biomass burning emissions: Nitrogen and carbon compounds, in *Global Biomass Burning: Atmospheric, Climatic and Biospheric Implications*, J. S. Levine, Editor, MIT Press, Cambridge, MA, 1991.
- Logan, J. A., M. J. Prather, S. C. Wofsy, and M. B. McElroy, Tropospheric chemistry: A global perspective, *J. Geophys. Res.*, 86, 7210-7254, 1981.
- Logan, J. A., Tropospheric ozone: Seasonal behavior, trends, and anthropogenic influences, *J. Geophys. Res.*, 85, 10463-10482, 1985.
- Logan, J. A., Trends in the vertical distribution of ozone: An analysis of ozonesonde data, *J. Geophys. Res.*, 99, 25553-25587, 1994.
- Lyon, T. F., W. J. Dodds, and D. W. Bahr, *Determination of the Effects of Ambient Conditions on CFM56 Aircraft Engine Emissions*, EPA-460/3-79/011, National Technical Information Service, Springfield, VA, 1979.
- Lyon, T. F., W. J. Dodds, and D. W. Bahr, *Determination of Pollutant Emissions Characteristics of General Electric CF6-6 and CF6-50 Model Engines*, FAA-EE-80-27, National Technical Information Service, Springfield, VA, 1980.
- Machta, L., and T. Carpenter, Trends in high cloudiness at Denver and Salt Lake City: Man's impact on the climate, W. H. Mathews, W. W. Kellogg, and G. D. Robinson, Editors, MIT Press, Cambridge, MA, 410-415, 1971.
- McCormick, M. P., R. E. Veiga, and W. P. Chu, Stratospheric ozone profile and total ozone trends derived from the SAGE I and SAGE II data, *Geophys. Res. Lett.*, 19, 269-272, 1992.
- McInnes, G., and C. T. Walker, *The Global Distribution of Aircraft Air Pollutant Emissions*, Warren Spring Laboratory Report LR 872, 1992.
- Metwally, M., *Jet Aircraft Engine Emissions Database Development--1992 Military, Charter, and Nonscheduled Traffic*, NASA CR-4684, 1995.
- Miake-Lye, R. C., M. Martinez-Sanchez, R. C. Brown, and C. E. Kolb, Plume and wake dynamics, mixing, and chemistry behind a high speed civil transport aircraft, *J. Aircraft*, 30, 467-479, 1993.
- Miake-Lye, R. C., M. Martinez-Sanchez, R. C. Brown, and C. E. Kolb, Calculations of condensation and chemistry in an aircraft contrail, in *Impact of Emissions from Aircraft and Spacecraft upon the Atmosphere*, Proceedings of an International Scientific Colloquium, Koln, Germany, April 18-20, 1994, U. Schumann and D. Wurzel, Editors, 106-112, 1994.

- Michelsen, H. A., R. J. Salawitch, P. O. Wennberg, and J. G. Anderson, Production of O<sup>1</sup>D from photolysis of O<sub>3</sub>, *Geophys. Res. Lett.*, *21*, 2227-2230, 1994.
- Middleton, P., W. R. Stockwell, and W. P. L. Carter, Aggregation and analysis of volatile organic compound emissions for regional modeling, *Atmos. Environ.*, *24A*, 1107-1133, 1990.
- Miller, A. J., G. C. Tao, G. C. Reinsel, D. Wuebbles, and L. Bishop, Comparisons of observed ozone trends in the stratosphere through examination of Umkehr and balloon ozonesonde data, *J. Geophys. Res.*, *100*, 11209-11217, 1995.
- Minnis, P., J. K. Ayers, and S. P. Weaver, Surface based observations of contrail occurrence frequency over the U.S. April 1993 - April 1994, NASA reference paper, submitted, 1996a.
- Minnis, P., J. K. Ayers, and D. R. Doellung, Contrails over the U.S. and their potential impact on the radiation budget, *Proc. Impact of Aircraft Emissions upon the Atmosphere International Coll.*, Paris, France, October 15-18, 1996b.
- Moxim, W. J., H. Levy II, and P. S. Kasibhatla, Simulated global tropospheric PAN: Its transport and impact on NO<sub>x</sub>, *J. Geophys. Res.*, *101*, 12621-12638, 1996.
- Müller, J.-F., Geographical distribution and seasonal variation of surface sources and deposition velocities of atmospheric trace gases, *J. Geophys. Res.*, *97*, 3787-3804, 1992.
- Müller, J.-F., and G. Brasseur, IMAGES: A three-dimensional chemical transport model of the global troposphere, *J. Geophys. Res.*, *100*, 16445-16490, 1995.
- Nance, J. D., P. V. Hobbs, and L. R. Radke, Airborne measurements of gases and particles from an Alaskan wildfire, *J. Geophys. Res.*, *98*, 14873-14882, 1993.
- Oltmans, S. J., and H. Levy II, Surface ozone measurements from a global network, *Atmos. Environ.* *28*, 9-24, 1994.
- Ou, S.-C., and K. N. Liou, Ice microphysics and climatic temperature feedback, *Atmos. Res.*, *35*, 127-138, 1995.
- Palikonda, R., P. Minnis, L. Nguyen, D. P. Garber, W. L. Smith, Jr., and D. F. Young, Remote sensing of contrails and aircraft altered cirrus, *Proc. Impact of Aircraft Emissions upon the Atmosphere International Coll.*, Paris, France, October 15-18, 1996.
- Paulson, S. E., and J. H. Seinfeld, Development and evaluation of a photooxidation mechanism for isoprene, *J. Geophys. Res.*, *97*, 20703-20715, 1992.
- Penner, J. E., C. S. Atherton, J. Dignon, S. J. Ghan, and J. J. Walton, Tropospheric nitrogen - a 3-dimensional study of sources, distributions, and deposition, *J. Geophys. Res.*, *96*, 959-990, 1991.
- Pham, M., J.-F. Müller, G. Brasseur, C. Granier, and G. Megie, A three-dimensional study of the tropospheric sulfur cycle, *J. Geophys. Res.*, *100*, 26061-26092, 1995.
- Pham, M., J.-F. Müller, G. Brasseur, C. Granier, and G. Megie, A 3D model study of the global sulfur cycle: Contributions of anthropogenic and biogenic sources, *Atm. Environ.*, *30*, 1815-1822, 1996.
- Piccot, S. D., J. J. Watson, and J. W. Jones, A global inventory of volatile organic compound emissions from anthropogenic sources, *J. Geophys. Res.*, *97*, 9897-9912, 1992.

- Pickering, K. E., Y. Wang, W.-K. Tao, and C. Price, The vertical distribution of NO<sub>x</sub> produced by lightning, manuscript in preparation, 1996.
- Pitari, G., V. Rizi, L. Ricciardulli, and G. Visconti, High speed civil transport impact: Role of sulfate, nitric acid trihydrate, and ice aerosols studied with a two-dimensional model including aerosol physics, *J. Geophys. Res.*, *98*, 23141-23164, 1993.
- Pitchford M., J. G. Hudson, and J. Hallett, Size and critical supersaturation for condensation of jet engine exhaust particles, *J. Geophys. Res.*, *96*, 20787-20793, 1991.
- Ponater, M., S. Brinkop, R. Sausen and U. Schumann, Simulating the Global Atmospheric Response to Aircraft Water Vapour Emissions and Contrails - A First Approach Using a GCM, *Ann. Geophys.*, *14*, 941-960, 1996.
- Prather, M. J., Numerical advection by conservation of second-order moments, *J. Geophys. Res.*, *91*, 6671-6681, 1986.
- Prather, M. J., M. B. McElroy, S. C. Wofsy, G. Russell, and D. Rind, Chemistry of the global troposphere: Fluorocarbons as tracers of air motion, *J. Geophys. Res.*, *92*, 6579-6613, 1987.
- Prather, M. J., and H. L. Wesoky, Editors, *The Atmospheric Effects of Stratospheric Aircraft: A First Program Report*, NASA Reference Publication 1272, Washington, DC, 1992.
- Price, C., and D. Rind, A simple lightning parameterization for calculating global lightning distributions, *J. Geophys. Res.*, *97*, 9919-9933, 1992a.
- Price, C., and D. Rind, Simulating global lightning frequencies using observed satellite cloud data, *Proceedings of the Ninth International Conference on Atmospheric Electricity*, St. Petersburg, Russia, ICAE, 327-330, 1992b.
- Price, C., and D. Rind, What determines the cloud-to-ground fraction in thunderstorms?, *Geophys. Res. Lett.*, *20*, 463-466, 1993.
- Price, C., and D. Rind, Modeling global lightning distributions in a general circulation model, *Mon. Wea. Rev.*, *122*, 1930-1939, 1994.
- Price, C., M. Prather, and J. Penner, NO<sub>x</sub> from lightning, Part I: Global distribution based on lightning physics, *J. Geophys. Res.*, in press, 1996.
- Prinn, R. G., R. F. Weiss, B. R. Miller, J. Huang, F. N. Alyea, D. M. Cunnold, P. J. Fraser, D. E. Hartley, and P. G. Simmonds, Atmospheric trends and lifetime of CH<sub>3</sub>CCl<sub>3</sub> and global OH concentrations, *Science*, *269*, 187-192, 1995.
- Pueschel, R. F., D. F. Blake, K. G. Snetsinger, A. D. A. Hansen, S. Verma, and K. Kato, Black carbon (soot) aerosol in the lower stratosphere and upper troposphere, *Geophys. Res. Lett.*, *19*, 1659-1662, 1992.
- Pueschel, R. F., J. M. Livingston, B. V. Ferry, and T. E. DeFelice, Aerosol abundances and optical characteristics in the Pacific basin free troposphere, *Atmos. Env.*, *28*, 951-960, 1994.
- Quackenbush, T. R., M. E. Teske, and A. J. Bilanin, Computation of wake/exhaust mixing downstream of advanced transport aircraft, American Institute of Aeronautics and Astronautics (AIAA) 24th Fluid Dynamics Conference, Orlando, FL, 6-9 July 1993.

- Ramaroson, R., and G. Brasseur, MEDIANTE: A chemical transport model of the atmosphere, Part I: Simulation of stratospheric composition, in preparation.
- Rasch, P. J., and D. Williamson, Computational aspects of moisture transport in global models of the atmosphere, *Q. J. R Meteorol. Soc.*, *116*, 1071-1090, 1990.
- Rasch, P. J., X. X. Tie, B. A. Boville, and D. L. Williamson, A 3-dimensional transport model for the middle atmosphere, *J. Geophys. Res.*, *99*, 999-1017, 1994.
- Rasch, P., H. Feichter, K. Law, N. Mahowald, J. Penner, *et al.*, An assessment of scavenging and deposition processes in global models; results from the WCRP Cambridge workshop of 1995, manuscript in preparation, 1996.
- Reiner, Th., and F. Arnold, Laboratory flow reactor measurements of the reaction  $\text{SO}_3 + \text{H}_2\text{O} + \text{M} \rightarrow \text{H}_2\text{SO}_4 + \text{M}$ : Implications for gaseous  $\text{H}_2\text{SO}_4$  and aerosol formation in the plumes of jet aircraft, *Geophys. Res. Lett.*, *20*, 2659-2662, 1993.
- Rickey, J. E., *The Effect of Altitude Conditions on the Particle Emissions of a J85-GE-5L Turbojet Engine*, NASA TM-106669, 1995.
- Ridley, B. J. Walega, J. E. Dye, and F. E. Grahek, Distribution of NO, NO<sub>x</sub>, NO<sub>y</sub>, and O<sub>3</sub> to 12 km altitude during the summer monsoon season over New Mexico, *J. Geophys. Res.*, *99*, 25519-25534, 1994.
- Rind, D., The doubled CO<sub>2</sub> climate: Impact of the sea surface temperature gradient, *J. Atmos. Sci.*, *44*, 3235-3268, 1987.
- Rind, D., R. Suozzo, N. K. Balachandran, A. Lacis, and G. L. Russell, The GISS global climate/middle atmosphere model, Part I: Model structure and climatology, *J. Atmos. Sci.*, *45*, 329-370, 1988.
- Rind, D., Drying out of the tropics, *New Scientist*, *146*, 36-40, 1995.
- Rind, D., and P. Lonergan, Modeled impacts of stratospheric ozone and water vapor perturbations with implications for high-speed civil transport aircraft, *J. Geophys. Res.*, *100*, 7381-7396, 1995.
- Rind, D., P. Lonergan, and K. Shah, The climatic effect of water vapor release in the upper troposphere, *J. Geophys. Res.*, in review, 1996.
- Rind, D., and J. Lerner, Use of online tracers as a diagnostic-tool in general circulation model development, 1: Horizontal and vertical transport in the troposphere, *J. Geophys. Res.*, *101*, 12667-12683, 1996.
- Roberts, J. M., Reactive odd nitrogen (NO<sub>y</sub>) in the atmosphere, in *Composition Chemistry and Climate of the Atmosphere*, H. Singh, Editor, VNR, New York, 1995.
- Rodhe, H., Precipitation scavenging and tropospheric mixing, in *Precipitation Scavenging, Dry Deposition, and Resuspension*, H. R. Pruppacher, Editor, 719-729, Elsevier, New York, 1983.
- Rogaski, C. A., D. M. Golden, and L. R. Williams, Laboratory measurements of H<sub>2</sub>O uptake on amorphous carbon: Effects of chemical treatment with NO<sub>2</sub>, SO<sub>2</sub>, H<sub>2</sub>SO<sub>4</sub>, and HNO<sub>3</sub>, to be submitted to *Geophys. Res. Lett.*, 1996a.

- Rogaski, C. A., D. M. Golden, and L. R. Williams, Heterogeneous chemistry of  $\text{HNO}_3$  on model soot surfaces, to be submitted to *J. Phys. Chem.*, 1996b.
- Rossow, W. B., and R. A. Schiffer, ISCCP cloud data products, *Bull. Am. Meteorol. Soc.*, 72, 2-20, 1991.
- SAE, *Aircraft Gas Turbine Exhaust Smoke Measurement*, SAE ARP1179, Society of Automotive Engineers, Revision B, 1991.
- Sassen, K., and G. C. Dodd, Haze particle nucleation simulations in cirrus clouds and applications for numerical and lidar studies, *J. Atmos. Sci.*, 46, 3005-3014, 1989.
- Sassen, K., Corona-producing cirrus cloud properties derived from polarization lidar, *Appl. Optics*, 30, 3421-3428, 1991.
- Sausen, R., W. J. Collins, C. Johnson, H. Kelder, R. Kingdon, I. Köhler, A. G. Kraabøl, A. Kraus, C. Marizy, R. Ramarosan, F. Rohrer, M. P. Scheele, D. Stevenson, F. Stordal, A. Strand, P. F. J. van Velthoven, and W. M. F. Wauben, Global atmosphere model simulations, in *The Impact of  $\text{NO}_x$  Emissions from Aircraft upon the Atmosphere at Flight Altitudes 8-15 km (AERONOX)*, U. Schumann, Editor, EC-DLR Publication on Research Related to Aeronautics and Environment, 1995.
- Scheel, H. E., E. G. Brunke, and W. Seiler, Trace gas measurements at the monitoring station Cape Point, South-Africa, between 1978 and 1988, *J. Atmos. Ch.*, 11, 197-210, 1990.
- Schubert, S., C.-K. Park, C.-Y. Wu, W. Higgins, Y. Kondratyev, A. Molod, L. Takacs, M. Seablom, and R. Rood, *A Multi-Year Assimilation with the GEOS-1 System: Overview and Results*, NASA Technical Memorandum 104606, Vol. 6, Technical Report Series on Global Modeling and Data Assimilation, M. Suarez, Editor, 1995.
- Schulte, P., and H. Schlager, In-flight measurements of cruise altitude nitric oxide emission indices of commercial jet aircraft, *Geophys. Res. Lett.*, 23, 165-168, 1996.
- Schulte, P., H. Schlager, U. Schumann, S. L. Baughcum, and F. Deidewig,  $\text{NO}_x$  emission indices of subsonic wide-bodied jet aircraft at cruise altitude: *In situ* measurements and predictions, submitted to *J. Geophys. Res.*, 1996.
- Schumann, U., On the effect of emissions from aircraft engines on the state of the atmosphere. *Ann. Geophys.*, 12, 365-384, 1994.
- Schumann, U., Editor, *AERONOX - The Impact of  $\text{NO}_x$  Emissions from Aircraft upon the Atmosphere at Flight Altitudes 8-15 km*, Report EUR 16209 EN, European Commission DG XII and DLR Cologne, 1995.
- Schumann, U., Editor, *Pollution from Aircraft Emissions in the North Atlantic Flight Corridor (POLINAT)*, Report EUR 16978 EN, Office for Official Publication of the European Communities, Luxembourg, 1996.
- Schumann, U., J. Ström, R. Busen, R. Baumann, K. Gierens, M. Krautstrunk, F. P. Schröder, and J. Stingl, *In situ* observations of particles in jet aircraft exhausts and contrails for different sulfur-containing fuels, *J. Geophys. Res.*, 101, 6853-6869, 1996.

- Shah, K., D. Rind, and P. Lonergan, Aircraft and doubled CO<sub>2</sub> impacts on GCMAM and MSU stratospheric and tropospheric temperatures, abstract presented at Spring AGU, manuscript in preparation, 1996.
- Sheridan, P. J., C. A. Brock, and J. C. Wilson, Aerosol particles in the upper troposphere and lower stratosphere: Elemental composition and morphology of individual particles in northern midlatitudes, *Geophys. Res. Lett.*, *21*, 2587-2590, 1994.
- Singh, H. B., Reactive nitrogen in the troposphere, *Environ. Sci. and Tech.*, *21*, 320-327, 1987.
- Singh, H. B., and P. L. Hanst, Peroxyacetyl nitrate (PAN) in the unpolluted atmosphere: An important reservoir for nitrogen oxides, *Geophys. Res. Lett.*, *8*, 941-944, 1981.
- Singh, H., D. Herlth, R. Kolyer, L. Salas, J. Bradshaw, S. Sandholm, D. Davis, J. Crawford, Y. Kondo, M. Koike, R. Talbot, G. Gregory, G. Sachse, E. Browell, D. Blake, F. Rowland, R. Newell, J. Merrill, B. Heikes, S. Liu, P. Crutzen, and M. Kanakidou, Reactive nitrogen and ozone relationships over the western Pacific: Distribution, partitioning and sources, *J. Geophys. Res.*, *101*, 1793-1809, 1996.
- Smolarkiewicz, P., and P. Rasch, Monotone advection on the sphere: An Eulerian versus semi-Lagrangian approach, *J. Atmos. Sci.*, *48*, 793-810, 1991.
- Spicer, C. W., M. W. Holdren, D. L. Smith, D. P. Hughes, and M. D. Smith, Chemical composition of exhaust from aircraft turbine engines, *J. Eng. Gas Turbines Power*, *114*, 111-117, 1992.
- Spicer, C. W., M. W. Holdren, R. M. Higgin, and T. F. Lyon, Chemical composition and photochemical reactivity of exhaust from aircraft turbine engines, *Ann. Geophys.*, *12*, 944-955, 1994.
- Spivakovsky, C. M., R. Yevich, J. A. Logan, S. C. Wofsy, M. B. McElroy, and M. J. Prather, Tropospheric OH in a three-dimensional chemical trace model: An assessment based on observations of CH<sub>3</sub>CCl<sub>3</sub>, *J. Geophys. Res.*, *95*, 18441-18472, 1990a.
- Spivakovsky, C. M., S. C. Wofsy, and M. J. Prather, A numerical method for parameterization of atmospheric chemistry: Computation of tropospheric OH, *J. Geophys. Res.*, *95*, 18433-18440, 1990b.
- Starr, D. O'C., and S. K. Cox, Cirrus clouds, Part II: Numerical experiments on the formation and maintenance of cirrus, *J. Atmos. Sci.*, *42*, 2682-2694, 1985.
- Stephens, G. L., S. Tsay, P. W. Stackhouse, Jr., and P. J. Flatau, The relevance of the microphysical and radiative properties of cirrus clouds to climate and climate feedback, *J. Atmos. Sci.*, *47*, 1742-1753, 1990.
- Stockwell, W. R., P. Middleton, J. S. Chang, and X. Tang, The second generation regional acid deposition model chemical mechanism for regional air quality modeling, *J. Geophys. Res.*, *95*, 16343-16367, 1990.
- Stolarski, R. S., and H. L. Wesoky, Editors, *The Atmospheric Effects of Stratospheric Aircraft: A Third Program Report*, NASA Reference Publication 1313, Washington, DC, 1993.
- Stolarski, R. S., S. L. Baughcum, W. H. Brune, A. R. Douglass, D. W. Fahey, R. R. Friedl, S. C. Liu, R. A. Plumb, L. R. Poole, H. L. Wesoky, and D. R. Worsnop, 1995 *Scientific*

- Assessment of the Atmospheric Effects of Stratospheric Aircraft*, NASA Reference Publication 1381, Washington, DC, 1995.
- Tabor, K. L., L. Gutzwiller, and M. J. Rossi, The heterogeneous interaction of NO<sub>2</sub> with amorphous carbon, *Geophys. Res. Lett.*, *20*, 1431-1434, 1993.
- Takano, Y., K. N. Liou, and P. Minnis, The effects of small ice crystals on cirrus radiative properties, *J. Atmos. Sci.*, *49*, 1487-1493, 1992.
- Tao, W.-K., and J. Simpson, The Goddard cumulus ensemble model, Part I: Model description, *Terres. Atmos. and Oceanic Sciences*, *4*, 35-71, 1993.
- Tarasick, D. W., D. I. Wardle, J. B. Kerr, J. J. Gellefleur, and J. Davies, Tropospheric ozone trends over Canada 1980 - 1993, *Geophys. Res. Lett.*, *22*, 409-412, 1995.
- Tenenbaum, J., Jet stream wind analysis: Comparisons with independent aircraft data over southwest Asia, *Wea. and Forecasting*, *6*, 320-326, 1991.
- Tenenbaum, J., Jet stream winds: Comparisons of aircraft observations with analysis, *Wea. and Forecasting*, *11*, 3188-197, 1996.
- Thompson, A., R. R. Friedl, and H. L. Wesoky, Editors, *Atmospheric Effects of Aviation: First Report of the Subsonic Assessment Project*, NASA Reference Publication 1385, Washington, DC, 1996.
- Tie, X. X., G. P. Brasseur, C. Granier, A. De Rudder, and N. Larsen, Model study of polar stratospheric clouds and their effect on stratospheric ozone, 2. Model results, *J. Geophys. Res.*, *101*, 12575-12584, 1996.
- Toon, O. B., and M. A. Tolbert, Spectroscopic evidence against nitric acid trihydrate in polar stratospheric clouds, *Nature*, *375*, 218-221, 1995.
- Turman, B. N., and B. C. Edgar, Global lightning distributions at dawn and dusk, *J. Geophys. Res.*, *87*, 1191-1206, 1982.
- Vedantham, A., and M. Oppenheimer, *Aircraft Emissions and the Global Atmosphere - Long-term Scenarios*, Environmental Defense Fund, 1994.
- Vitt, F. M., and C. H. Jackman, A comparison of sources of odd nitrogen production from 1974 through 1993 in the Earth's middle atmosphere as calculated using a two-dimensional model, *J. Geophys. Res.*, *101*, 6729-6739, 1996.
- Volz-Thomas, A., Trends in photo-oxidant concentrations, in *Photo-Oxidants: Precursors and Products*, *Proc. EUROTRAC Symp. 1992*, P. M. Borrell, P. Borrell, T. Cvitas, and W. Seiler, Editors, Acad. Publ., The Hague, The Netherlands, 59-64, 1993.
- Wahner, A., F. Rohrer, D. H. Ehhalt, B. Ridley, and E. Atlas, Global measurements of photochemically active compounds, in *Proceedings of 1st IGAC Scientific Conference: Global Atmospheric-Biospheric Chemistry*, Eilat, Israel, 205-222, 1994.
- Wang, P. H., G. S. Kent, M. P. McCormick, L. W. Thomason, and G. K. Yue, Retrieval analysis of aerosol-size distribution with simulated extinction measurements at SAGE-III wavelengths, *Appl. Optics*, *35*, 433-440, 1996.

- Wauben, W. M. F., P. F. J. van Velthoven, and H. Kelder, *Changes in tropospheric NO<sub>x</sub> and O<sub>3</sub> due to subsonic aircraft emissions*, KNMI, De Bilt, The Netherlands, 1995.
- Wege, K., H. Claude, and R. Hartmanngruber, Several results from the 20 years of ozone observations at Hohenpeissenberg, in *Ozone in the Atmosphere*, R. D. Bojkov and P. Fabian, Editors, A. Deepak Publishing, Hampton, Virginia, 109-112, 1989.
- Whitefield, P. D., M. B. Trueblood, and D. E. Hagen, Size and hydration characteristics of laboratory simulated jet engine combustion aerosols, *Part. Sci. and Tech.*, *11*, 25-36, 1993.
- Whitefield, P. D., D. E. Hagen, J. D. Paladino, and H. V. Lilenfeld, Aerosol emission indices from commercial transports at cruise altitudes, to be submitted to *Geophys. Res. Lett.*, 1996.
- WMO, *Scientific Assessment of Ozone Depletion: 1994*, World Meteorological Organization Global Ozone Research and Monitoring Project Report No. 37, 1995.
- Wormhoudt, J., M. S. Zahniser, D. D. Nelson, J. B. McManus, R. C. Miale-Lye, and C. E. Kolb, Infrared tunable diode laser measurements of nitrogen oxide species in an engine exhaust in *Optical Techniques in Fluid, Thermal, and Combustion Flows*, SPIE Proc. V2546, 552-561, 1996.
- Worsnop, D. R., L. E. Fox, M. S. Zahniser, and S. C. Wofsy, Vapor pressures of solid hydrates of nitric acid: Implications for polar stratospheric clouds, *Science*, *259*, 71-74, 1993.
- Wuebbles, D. J., and D. E. Kinnison, Sensitivity of Stratospheric ozone to present and possible future aircraft emissions, in *Air Traffic and the Environment - Background, Tendencies and Potential Global Atmospheric Effects*, U. Schumann, Editor, Springer-Verlag, Berlin, Heidelberg, 1990.
- Wuebbles, D. J., D. Maiden, R. K. Seals, Jr., S. L. Baughcum, M. Metwally, and A. Mortlock, Emissions Scenarios Development: Report of the Emissions Scenarios Committee, in *The Atmospheric Effects of Stratospheric Aircraft: A Third Program Report*, NASA Reference Publication 1313, R. S. Stolarski and H. L. Wesoky, Editors, 1993a.
- Wuebbles, D. J., S. L. Baughcum, M. Metwally, and R. K. Seals, Jr., Fleet operational scenarios, in *The Atmospheric Effects of Stratospheric Aircraft: Interim Assessment Report of the NASA High-Speed Research Program*, NASA Reference Publication 1333, 39-53, 1993b.
- Wyslouzil, B. E., K. L. Carleton, D. M. Sonnenfroh, W. T. Rawlins, and S. Arnold, Observations of hydration of single modified carbon aerosols, *Geophys. Res. Lett.*, *21*, 2107-2110, 1994.
- Yienger, J. J., and H. Levy II, Empirical model of global soil-biogenic NO<sub>x</sub> emissions, *J. Geophys. Res.*, *100*, 11447-11464, 1995.
- Zhang, R., M.-T. Leu, and L. F. Keyser, Heterogeneous chemistry of HONO on liquid sulfuric acid: A new mechanism of chlorine activation on stratospheric sulfate aerosols, *J. Phys. Chem.*, *100*, 339-395, 1996.
- Zhao, J., and R. P. Turco, Nucleation simulations in the wake of a jet aircraft in stratospheric flight, *J. Aerosol Sci.*, *26*, 779-795, 1995.
- Zheng, J., A. J. Weinheimer, B. A. Ridley, S. C. Liu, G. W. Sachse, B. E. Anderson, and J. E. Collins, Jr., An analysis of aircraft exhaust plumes from accidental encounters, *Geophys. Res. Lett.*, *21*, 2579-2582, 1994.



# APPENDICES

**A Authors, Contributors, and Reviewers**

**B Acronyms and Abbreviations**

**C Chemical Nomenclature and Formulae**





## Contributors and Reviewers

Jonathan P. Abbatt	University of Chicago
David F. Blake	NASA Ames Research Center
Donald R. Blake	University of California, Irvine
Guy P. Brasseur	National Center for Atmospheric Research
William H. Brune	Pennsylvania State University
David B. Considine	NASA Goddard Space Flight Center
David R. Crosley	SRI International
Anne R. Douglass	NASA Goddard Space Flight Center
Doug Dubois	Boeing Commercial Airplane Group
James E. Dye	National Center for Atmospheric Research
Anthony Fiorentino	United Technologies Pratt & Whitney
Marvin A. Geller	State University of New York, Stony Brook
Donald E. Hagen	University of Missouri, Rolla
James E. Hansen	NASA Goddard Institute for Space Studies
Stephen C. Henderson	Boeing Commercial Airplane Group
Matthew H. Hitchman	University of Wisconsin
Daniel J. Jacob	Harvard University
Paul Kang	Federal Aviation Administration
Jack A. Kaye	NASA Headquarters
Malcolm Ko	Atmospheric and Environmental Research, Inc.
Charles E. Kolb	Aerodyne Research, Inc.
Mark A. Kritz	State University of New York, Albany
Ming-Taun Leu	Jet Propulsion Laboratory
W. Steve Lewellen	West Virginia University
Harvey V. Lilienfeld	McDonnell Douglas Corporation
Patrick Minnis	NASA Langley Research Center
Alan Mortlock	McDonnell Douglas Corporation
Rebel Nichols	Boeing Commercial Airplane Group
Joyce E. Penner	University of Michigan
Kenneth E. Pickering	University of Maryland
James R. Podolske	NASA Ames Research Center
Michael J. Prather	University of California, Irvine
Brian A. Ridley	National Center for Atmospheric Research
Douglas Rotman	Lawrence Livermore National Laboratory
Kathryn Shah	NASA Goddard Institute for Space Studies
Richard S. Stolarski	NASA Goddard Space Flight Center
Joel Tenenbaum	State University of New York, Purchase
Anne M. Thompson	NASA Goddard Space Flight Center
Edward E. Uthe	SRI International
Paul Wennberg	Harvard University
Howard L. Wesoky	NASA Headquarters
Philip D. Whitefield	University of Missouri, Rolla
Martin F. Zabielski	United Technologies Research Center

## APPENDIX B

### ACRONYMS AND ABBREVIATIONS

---

1-D	one-dimensional (altitude)
2-D	two-dimensional (altitude and latitude)
3-D	three-dimensional (altitude, latitude, and longitude)
AEAP	Atmospheric Effects of Aviation Project
AEDC	Arnold Engineering Development Center
AERONOX	Impact of NO <sub>x</sub> Emissions from Aircraft upon the Atmosphere
ANCAT	Abatement of Nuisance Caused by Air Traffic
BCA	black carbon aerosol
CAEP	Committee on Aviation Environmental Protection (ICAO)
CART	Clouds and Radiation Testbed
CCM2	Community Climate Model-2
CCM3	Community Climate Model-3
CCN	cloud condensation nuclei (i.e., particles that will deliquesce or become liquid by absorbing moisture from the air at humidities with respect to water that are less than unity)
CFC	chlorofluorocarbon
CN	condensation nuclei (i.e., particles that will form droplets at high water supersaturation)
CTM	chemical transport model
DAO	Data Assimilation Office
DJF	December, January, February
DOE	Department of Energy
DOT	Department of Transportation
ECHAM	ECMWF model, Hamburg version
ECMWF	European Center for Medium Range Weather Forecast - UK
EI	emission index in g emittant/kg fuel

GCM	general circulation model
GCMAM	Global Climate Middle Atmosphere Model
GEIA	Global Emissions Inventories Activity
GFDL	Geophysical Fluid Dynamics Laboratory
Gg	gigagram (10 <sup>9</sup> grams)
GISS	Goddard Institute for Space Studies
GMI	Global Modeling Initiative
GOES	Geostationary Operational Environmental Satellite
GWP	global warming potential
HC	hydrocarbons
HSCT	high-speed civil transport
ICAO	International Civil Aviation Organization
IMAGES	Intermediate Model for the Annual and Global Evolution of Interactive Systems
IN	ice nuclei (i.e., particles on which vapor may be deposited directly in the solid phase)
IPCC	Intergovernmental Panel on Climate Change
IR	infrared
ISCCP	International Satellite Cloud Climatology Project
JJA	June, July, August
LS	lower stratosphere
LTO	landing and take-off
NASA	National Aeronautics and Space Administration
NCAR	National Center for Atmospheric Research
NH	Northern Hemisphere
nm	nanometer (10 <sup>-9</sup> meters)
NMC	National Meteorological Center
NMHC	non-methane hydrocarbon
nmi	nautical mile
NWS	National Weather Service
OAG	Official Airline Guide
OECD	
ONERA	Office National d'Etudes et de Recherches Aérospatiales

PDL	Polarization Diversity Lidar
PEM	Pacific Exploratory Mission
P(O <sub>3</sub> )	net rate of ozone production
POLINAT	Pollution from Aircraft Emissions in the North Atlantic Flight Corridor
ppbv	parts per billion by volume
PPM	piecewise parabolic method
ppmv	parts per million by volume
pptv	parts per trillion by volume
PSC	polar stratospheric cloud
RCM	radiative-convective model
SAE	Society of Automotive Engineers
SAGE	Stratospheric Aerosol and Gas Experiment
SASS	Subsonic Assessment
SH	Southern Hemisphere
SLC	Salt Lake City, Utah
STE	stratospheric-tropospheric exchange
STRAT	Stratospheric Tracers of Atmospheric Transport
SUCCESS	SUBsonic aircraft: Contrail Cloud Effects Special Study
TDL	tunable diode laser
Tg	teragram (10 <sup>12</sup> grams))
Tg N	teragram of nitrogen
TRACE-A	Transport and Atmospheric Chemistry near the Equator-Atlantic
UADP2	Upper Atmosphere Data Pilot - 2
UCI	University of California at Irvine
UKMO	United Kingdom Meteorological Office
USSR	Union of Soviet Socialist Republics
UT	upper troposphere
UV	ultraviolet
WCRP	World Climate Research Program
WG3	Working Group 3 (Emissions) of CAEP
WINDTEMP	Boeing computer code and database of climatological winds and temperatures on world air routes
WMO	World Meteorological Organization



## APPENDIX C

### CHEMICAL FORMULAE AND NOMENCLATURE

---

$C_2H_2$	acetylene
$C_3H_8$	propane
$C_n$	generic designation for species with n carbon atoms
CFC	chlorofluorocarbon
$CH_4$	methane
$Cl^-$	chlorine ion
$ClNO_3$	chlorine nitrate
CO	carbon monoxide
$CO_2$	carbon dioxide
HC	hydrocarbon
HCl	hydrogen chloride
HCN	hydrogen cyanide
$HNO_2$	nitrous acid
$HNO_3$	nitric acid
$HNO_4$	peroxynitric acid
$HO_2$	hydroperoxyl radical
$HO_x$	hydrogen oxides
$H_2O$	water
$H_2O_2$	hydrogen peroxide
HOCl	hypochlorous acid
$HSO_3^-$	bisulfate ion
$H_2SO_4$	sulfuric acid

NAT	nitric acid trihydrate
NMHC	nonmethane hydrocarbon
NO	nitric oxide
NO <sub>2</sub>	nitrogen dioxide
NO <sub>3</sub>	nitrogen trioxide
NO <sub>x</sub>	nitrogen oxides (NO + NO <sub>2</sub> )
NO <sub>y</sub>	reactive nitrogen (= NO + NO <sub>2</sub> + HNO <sub>3</sub> + 2N <sub>2</sub> O <sub>5</sub> + ClNO <sub>3</sub> + HNO <sub>4</sub> + PAN + ...)
NH <sub>3</sub>	ammonia
NH <sub>4</sub> <sup>+</sup>	ammonium ion
NH <sub>4</sub> HSO <sub>4</sub>	ammonium bisulfate
N <sub>2</sub> O	nitrous oxide
N <sub>2</sub> O <sub>5</sub>	dinitrogen pentoxide
O( <sup>1</sup> D)	atomic oxygen (first excited state)
O( <sup>3</sup> P)	atomic oxygen (ground state)
O <sub>2</sub>	molecular oxygen
O <sub>3</sub>	ozone
OH	hydroxyl radical
OH <sup>-</sup>	hydronium ion
O <sub>x</sub>	odd oxygen [O <sub>3</sub> + O( <sup>1</sup> D) + O( <sup>3</sup> P)]
PAN	peroxyacetyl nitrate (CH <sub>3</sub> CO <sub>3</sub> NO <sub>2</sub> )
Rn	radon
<sup>222</sup> Rn	radon-222
RO <sub>2</sub>	organic peroxy radical
RNO <sub>3</sub>	alkyl nitrate
RNO <sub>4</sub>	alkyl peroxy nitrate
RCO <sub>3</sub> NO <sub>2</sub>	acyl peroxy nitrate
SO <sub>2</sub>	sulfur dioxide
SO <sub>3</sub>	sulfur trioxide
SO <sub>4</sub> <sup>2-</sup>	sulfate ion
SO <sub>x</sub>	sulfur oxides







**REPORT DOCUMENTATION PAGE**Form Approved  
OMB No. 0704-0188

Public reporting burden for this collection of information is estimated to average 1 hour per response, including the time for reviewing instructions, searching existing data sources, gathering and maintaining the data needed, and completing and reviewing the collection of information. Send comments regarding this burden estimate or any other aspect of this collection of information, including suggestions for reducing this burden, to Washington Headquarters Services, Directorate for Information Operations and Reports, 1215 Jefferson Davis Highway, Suite 1204, Arlington, VA 22202-4302, and to the Office of Management and Budget, Paperwork Reduction Project (0704-0188), Washington, DC 20503.

**1. AGENCY USE ONLY (Leave blank)****2. REPORT DATE**  
May 1997**3. REPORT TYPE AND DATES COVERED**  
Reference Publication**4. TITLE AND SUBTITLE**Atmospheric Effects of Subsonic Aircraft: Interim Assessment  
Report of the Advanced Subsonic Technology Program**5. FUNDING NUMBERS**ARTOP UPN 538  
Code 916**6. AUTHOR(S)**

Randall R. Friedl, Editor

**7. PERFORMING ORGANIZATION NAME(S) AND ADDRESS (ES)**Goddard Space Flight Center  
Greenbelt, Maryland 20771**8. PERFORMING ORGANIZATION  
REPORT NUMBER**

97B00048

**9. SPONSORING / MONITORING AGENCY NAME(S) AND ADDRESS (ES)**National Aeronautics and Space Administration  
Washington, DC 20546-0001**10. SPONSORING / MONITORING  
AGENCY REPORT NUMBER**

NASA RP-1400

**11. SUPPLEMENTARY NOTES**

Friedl: NASA HQ, Washington, D.C. (Currently at JPL, Pasadena, California).

**12a. DISTRIBUTION / AVAILABILITY STATEMENT**Unclassified - Unlimited  
Subject Category 45

Availability: NASA CASI (301) 621-0390.

**12b. DISTRIBUTION CODE****13. ABSTRACT (Maximum 200 words)**

This first interim assessment of the subsonic assessment (SASS) project attempts to summarize concisely the status of our knowledge concerning the impacts of present and future subsonic aircraft fleets. It also highlights the major areas of scientific uncertainty, through review of existing databases and model-based sensitivity studies. In view of the need for substantial improvements in both model formulations and experimental databases, this interim assessment cannot provide confident numerical predictions of aviation impacts. However, a number of quantitative estimates are presented, which provide some guidance to policy makers.

**14. SUBJECT TERMS**

Subsonic assessment; quantitative estimates; emissions; inventory; methodology; contrails.

**15. NUMBER OF PAGES**

168

**16. PRICE CODE****17. SECURITY CLASSIFICATION  
OF REPORT**

Unclassified

**18. SECURITY CLASSIFICATION  
OF THIS PAGE**

Unclassified

**19. SECURITY CLASSIFICATION  
OF ABSTRACT**

Unclassified

**20. LIMITATION OF ABSTRACT**

UL